Accelerated Alkali-Silica Reaction and Corrosion of Reinforcing Steel in Concrete: Application on Dry Casks

A Dissertation

Presented to

the Faculty of the Department of Civil Engineering

University of Houston

In Partial Fulfillment

Of the Requirements for the Degree

Doctor of Philosophy

In Civil Engineering

by

Arezou Attar

August 2016

Accelerated Alkali-Silica Reaction and Corrosion of Reinforcing Steel in Concrete: Application on Dry Casks

Arezou Attar

Approved:

Chair of the Committee
Bora Gencturk, Assistant Professor,
Civil and Environmental Engineering

Committee Members:

Kaspar J. Willam, Distinguished Professor,
Civil and Environmental Engineering

Cumaraswamy Vipulanandan, Professor,
Civil and Environmental Engineering

James K. Meen, Research Associate Professor,
Department of Chemistry

Debora Rodrigues, Assistant Professor,
Civil and Environmental Engineering
Environmental Engineering

Suresh K. Khator, Associate Dean,
Cullen College of Engineering

Roberto Ballarini, Professor,
Chair of Department in Civil and Environmental Engineering

ACKNOWLEDGEMENT

I am extremely grateful to Dr. Gencturk, who gave me the opportunity to work on this research project, for his guidance, support and patience throughout my studies at the University of Houston. I also would like to thank my committee members, Dr. Willam, Dr. Vipu, Dr. Meen, and Dr. Tekin, for their valuable comments and advice.

I am also indebted to the continuous love, support and encouragement from my parents and my brother during the past years, which otherwise, would not have made this journal possible.

I would like to thank the sponsors of this project, the United States Department of Energy through the Nuclear Energy University Program, Contract No. 00128931.

Finally, I would like to thank and recognize the help of my colleagues in different stages of preparing and casting the concrete specimens.

Accelerated Alkali-Silica Reaction and Corrosion of Reinforcing Steel in Concrete: Application on Dry Casks

An Abstract

of a

Dissertation

Presented to

the Faculty of the Department of Civil Engineering

University of Houston

In Partial Fulfillment

Of the Requirements for the Degree

Doctor of Philosophy

In Civil Engineering

by

Arezou Attar

August 2016

ABSTRACT

The durability is one of the main reasons making concrete the most abundantly consumed material in the world after water. However, severe exposure conditions and improper or low quality mixture designs can cause physical and chemical changes in concrete which lead to deterioration and premature failure of the structure. This process is called aging. Two of the main aging mechanisms in reinforced concrete structures are corrosion and alkali-silica reaction (ASR). These two processes occur very slowly and to assess them in a short period of time, they need to be accelerated. Furthermore, these mechanisms are dependent on the geometry and boundary conditions of the structure. Therefore, research on these aging mechanisms is structure specific and depends on the scale of observation. This study proposes a method through addition of chemicals to the concrete mixture for accelerating aging that is applicable to both small- and large- specimens. The aging is accelerated through addition of sodium hydroxide to accelerate ASR and calcium chloride to the mixture to accelerate corrosion. The effect of the addition of these chemicals on both physical and mechanical properties of concrete was investigated through a series of destructive and non-destructive testing at the materials and structural levels. The results indicate that the addition of sodium hydroxide to the concrete mix, combined with the use of reactive aggregate and no fly ash, considerably accelerates ASR and crack propagation on the surface of the specimens. Similarly, the addition of calcium chloride effectively accelerates corrosion. To investigate the validity of the proposed approach at the structural level, a vertical concrete dry cask for storage of nuclear waste was chosen as the case study. In this case study, three 1/3-scale dry casks were subjected to accelerated ASR and corrosion with the addition of chemicals to the mixture and their effect was measured over eighteen months. Furthermore, the service life of the scaled down casks was estimated

considering the real life conditions. This approach is expected to help researchers to better understand the long term behavior of reinforced concrete dry casks.

TABLE OF CONTENTS

LIST OF FIGURES

LIST OF TABLES

LIST OF ABBREVIATIONS

AAR: Alkali Aggregate Reaction

AASHTO: American Association of State Highway and Transportation Officials

ACI: American Concrete Institute

ACR: Alkali Carbonate Reaction

ASR: Alkali-Silica Reaction

ASSR: Alkali Silicate/Silica Reaction

ASTM: American Society for Testing and Materials

C_3A: Tricalcium Aluminate ($Ca_3Al_2O_3$)

C_3S: Tricalcium Silicate (Ca_3SiO_5)

C_2S: Dicalcium Silicate (Ca_2SiO_4)

COD: Crack Opening Displacement

C-S-H: Calcium Silicate Hydrate ($CaO.2SiO_2.4H_2O$)

DCSS: Dry Cask Storage Systems

EDX: Energy Dispersive X-ray

JCI: Japanese Concrete Institute

NRC: Nuclear Regulatory Commission

NPP: Nuclear Power Plants

OD: Oven Dry

PVC: Polyvinyl Chloride

RC: reinforced concrete

RCPT: Rapid Chloride Penetration Test

RH: Relative Humidity

SCC: Self Consolidating Concrete

SSD: Saturated Surface Dry

SEM: Scanning Electron Microscopy

SNF: spent nuclear fuel

TSC: Test Shipping Cask

UPV: Ultrasonic Pulse Velocity

UV: Ultra Violate

w/c: water-cement ratio

1. INTRODUCTION

1.1 Research Significance

Aging in reinforced concrete (RC) structures occurs due to a combination of physical, thermal, chemical and mechanical effects. The aging mechanisms may include cracking due to temperature variations, creep and shrinkage, alkali-silica reactivity (ASR or also known as alkali-aggregate reaction) of concrete and corrosion of reinforcing bars (rebar). These effects may result in lower mechanical resistance and failure to meet serviceability or strength criteria in RC structures. This study focuses on two main degradation mechanisms in reinforced concrete structures, namely ASR and corrosion. The aging-induced deterioration due to these mechanisms and others may result in a failure to meet serviceability or strength requirements of the structure. However, these processes usually occur very slowly and one needs accelerated tests to observe significant levels of aging within the limits of a typical research study. Furthermore, the distress in the structure is not only a material property but it is also strongly influenced by structural configuration such as the geometry, boundary conditions and reinforcement ratios. This research is motivated by the fact that most techniques adopted in the laboratory for accelerated aging are applicable to small specimens for material level studies, techniques such as immersion in solutions, passing an electrical current through rebar and subjecting in specimens to high temperature. However, these methods are not applicable to large-scale structures, i.e., the structural level. Therefore, there is a need for further research on accelerated aging of ASR and corrosion of RC structures at the structural scale. For the structural level investigation in this study, dry cask storage systems (DCSS) were studied. DCSS are widely used worldwide for storage of spent nuclear fuel (SNF). Particularly in the United States, other than the SNF pools, DCSS are the only means for storage of SNF. The DCSS are licensed in the

United States for an initial 20 years (with a possible extension of 40 years). The absence of a long-term (or permanent) storage facility has brought up concerns regarding the long-term performance of DCSS, which may now have to be used for extended durations reaching over 100 years. The DCSS with an exposed vertical concrete overpack account for approximately 50% of the DCSS inventory in the United States.

The emphasis of this study is on the impact of chemical additives, namely the addition of NaOH and $CaCl_2$ to accelerate ASR and corrosion, on the physical and mechanical properties of the resulting concrete at the material level as well as on the structural level using three 1/3-scale specimens fabricated from DCSS models.

1.2 Objectives and Organization of the Dissertation

The main objective of this study is to understand and expand the knowledge on the aging effect on the reinforced concrete structures in the long term with emphasis on ASR and corrosion. To achieve this objective, it was decided to accelerate the aging process and investigate the effect on mechanical and physical properties of concrete at both the material and structural levels. The aging was accelerated with addition of chemicals to the concrete and by placing the specimens outdoors without subjecting them to extreme conditions such as high temperature and relative humidity or by passing current. Additionally, this study investigates the suitability of artificially mixing chemicals into concrete as a method to accelerate aging of the concrete structures.

Chapter 1 provides the introduction, overview, problem statement, objectives, and scope of work.

Chapter 2 presents a background on the two main aging effects, ASR and corrosion, and explains the existing techniques for accelerating these two effects for material and structural level studies. It also provides information on the methods to predict the service life of structures affected by corrosion.

Chapter 3 describes the properties of materials used in this study such as cement, fly ash, aggregates, and rebar. It also provides the testing plan for different concrete mixtures prepared and cast at both material and structural level.

Chapter 4 describes the test results obtained through different testing on fresh concrete, such as setting time and density, as well as physical and mechanical properties of concrete obtained through a series of destructive tests such as chloride penetration, density and compression and split tensile strength of hardened concrete. Properties such as surface resistivity, ultra-sonic pulse velocity (UPV), and crack maps of concrete were also measured using non-destructive tests.

Chapter 5 briefly describes the selection and geometric properties of the scaled down casks. It also provides the results of monitoring of the control and age-accelerated casks through half-cell potential, UPV and monitoring the crack propagation due to corrosion of rebar and ASR during the aging process. Further in this section, the service life of the corrosion-accelerated casks prepared inside the lab is compared with the scaled down cask in the real conditions at three nuclear stations in US.

Finally, Chapter 6 provides the concluding remarks of the work presented in this thesis.

2. BACKGROUND

2.1 Introduction

Concrete deterioration occurs during the life of the structure because of the combination of various physical, thermal, chemical, structural, biological or mechanical processes. This time-dependent deterioration on concrete is called aging.

The changes in a concrete mixture start with cement hydration and continue with the crystallization of amorphous constituents and reactions between cement, paste, aggregate and reinforcing steel. Concrete may also deteriorate because of its interaction with the environment and exhibit distress due to shrinkage, creep, corrosion of reinforcing steel and alkali-silica reactivity (ASR) of aggregates. The aging of concrete structures may continue to the point that the structure cannot meet its functional and performance requirement any longer. Certain properties such as hardness, toughness, compressive strength, tensile strength, shear or modulus of elasticity may increase over time as shown in Figure 1(a) as concrete matures, while other properties such as porosity, permeability and diffusivity decrease, as seen in Figure 1(b). However, when aging and degradation occurs, the mechanical properties decrease over time as shown in Figure 2 (Pinto et al., 2002).

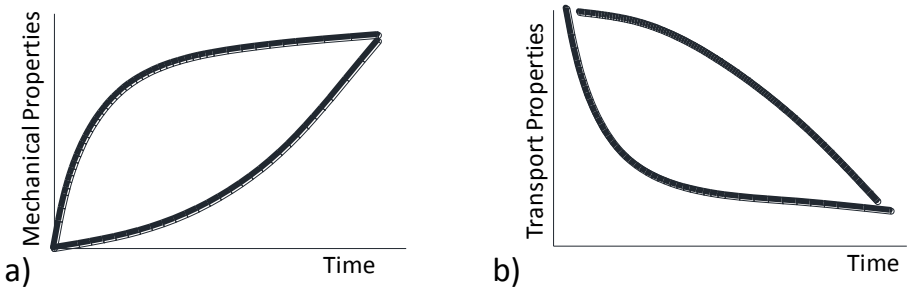

Figure 1.(a) schematic development of mechanical properties over time (b) schematic development of transport properties over time (Pinto et al., 2002)

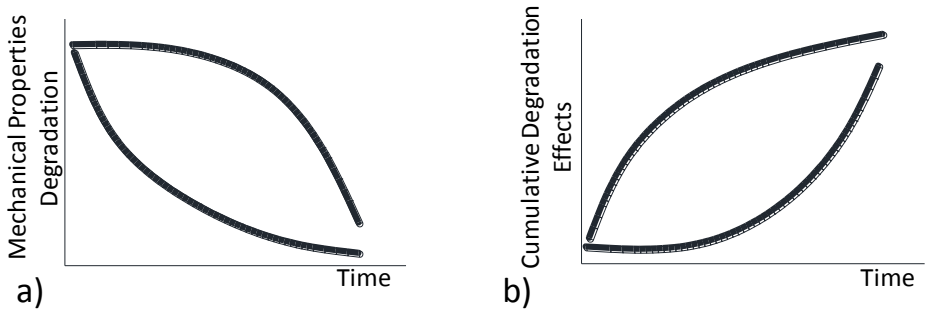

Figure 2 (a) schematic degradation of mechanical properties over time (b) schematic of cumulative effect of degradation in terms of depth of penetration, crack intensity, etc. (Pinto et al., 2002)

These mechanisms affect concrete and steel, as well as their interface properties, and reduce structural performance under mechanical loading. In this study, two aging effects, ASR and corrosion, were studied; these effects are further explained in the following sections (Sections 2.2 and 2.3).

2.2 ASR

Three forms of alkali aggregate reaction (AAR) depending on the type of involved minerals, have been identified in the literature: alkali carbonate reaction (ACR), alkali silica reaction (ASR) and slow/late expanding alkali silicate/silica reaction (ASSR). ACR is the reaction between carbonate aggregate particles and the cement paste of Portland and cement concrete/mortar. ASR is a disruptive reaction within concrete and ASSR is associated with the expansion of coarse aggregate (Charlwood, 1994). ASR is considered as the most common form of AAR compared to ACR and ASSR and therefore is the focus of this study. ASR is a pathogenic reaction in cement composites (Mladenovic et al., 2009) and is one of the most common damage mechanisms in concrete structures. Necessary elements for initiation of this reaction are reactive silica, sufficient alkali and sufficient moisture. Pesavento and Gawin (2012) explained ASR as the reaction of the hydroxyl ion (OH^-) of the alkalies (sodium and potassium) from hydraulic cement

or other sources with the silanol groups (Si-O) and breaking of the siloxane bonds. Pan et al. (2012) expressed this reaction

$$\text{Si-O-Si} \equiv +Na^{+} \text{ (or } K^{+}) + OH^{-} \rightarrow \equiv \text{Si-O-Na (or K)} + \text{H-O-Si} \equiv, \quad (1)$$

where the silonal groups react with hydroxyl ions and produce a weak acid on the surface of the aggregate. This silicic acid immediately reacts with further hydroxyl ions and liberates more water according to (Pan et al., 2012)

$$\equiv \text{Si-O-H} + Na^{+} \text{ (or } K^{+}) + OH^{-} \rightarrow \equiv \text{Si-O-Na (or K)} + H_2O, \quad (2)$$

where the cations of the pore solution are attracted to Si-O- molecules and bind to form Si-O-Na, which comprises the alkali-silica gel. Na^{+}, K^{+} and Ca_2^{+} diffuse into the gel in sufficient numbers to balance the negatively charged groups. After reaching the saturation point, a gel consisting of silica, alkalis, water and other ions is created. The reactions are shown below (Farny and Kosmatka, 1997; Bahadure and Naik, 2013)

$$SiO_2 + 2NaOH + H2O \rightarrow Na_2SiO_3.2H_2O, \quad (3)$$
$$SiO_2 + 2KOH + H2O \rightarrow K_2SiO_3.2H_2O, \text{ and} \quad (4)$$
$$SiO_2 + Ca(OH)_2 \rightarrow CaO.SiO_2.H_2O.2H_2O. \quad (5)$$

In this process, alkalis from the cement or from an external source (sodium, potassium or calcium) penetrate into the siliceous particle and react with free silica present in the aggregate, thus forming alkali hydroxide and loosening the lattice structure; see Figure 3 (Sarkar et al., 2004). The product of this reaction is a hydrophilic alkali-silica gel, which has a high tendency to absorb water from its environment such as pore solution, and expand. Since the gel is surrounding mortar, an osmotic pressure is generated by the swelling. When the pressure from this gel exceeds the tensile strength of concrete, cracks occur to relieve the pressure; more water migrates inside the concrete, and the gel swells even more (ACI Committee 221, 1998). This cracking may eventually cause the failure of the concrete (Anantharaman, 2008). According

to previous studies, gel can be formed at different relative humidities, although for it to swell, relative humidity (RH) must be higher than 80% (Figg, 1983; Ferraris, 1995). Temperature can also influence the speed of this reaction; however, it cannot be easily interpreted, since higher temperature causes not only quicker reaction but also reduced viscosity of the gel, which can make the gel enter the concrete pores with a reduction of its expansive potential (Pignatelli, 2012). Idorn (1993) studied various available reactive aggregates and their reaction patterns. It was found that concrete usually cracks in a 3- or 4-pronged star pattern at each reacted aggregate. This pattern is enough to relieve the pressure and accommodate the resulting volume increase (Farny and Kosmatka, 1997). The width of alkali-silica macro-cracks at the exposed surface of concrete element is usually between 0.1 mm to over 10 mm. The ASR effect on properties of concrete becomes significant after cracks become visible on the surface of the concrete. This effect reduces compressive inelastic secant stiffness (and hence the resonant frequency), flexural and tensile strength, and Young's modulus of concrete (Fan and Hanson, 1998b; Jones and Clark, 1998; Monette and Gardner, 2002; Attoh-Okine and Atique, 2006). However, the influence of ASR on compressive strength is unclear because of contradictory results obtained by different researchers (Okine, 2006). Aside from the reduction of most of the properties of concrete, ASR was also found to increase the shear capacity of reinforced beams (Ahmed et al., 1998; Attoh-Okine and Atique, 2006).

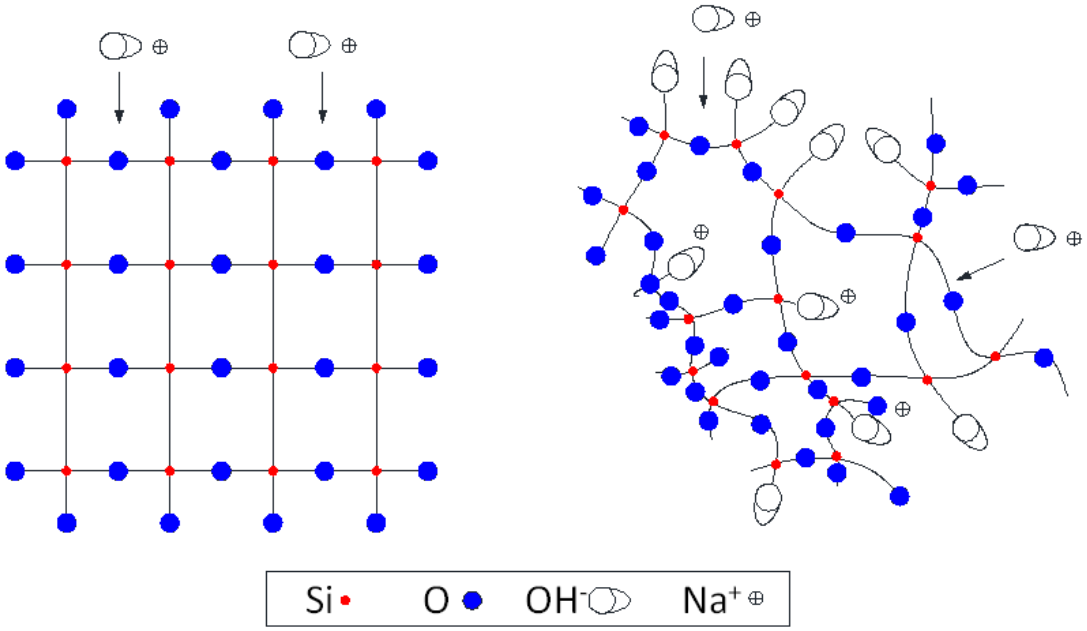

Figure 3 Schematic representation of the attack of alkaline solutions on silica, (a) well crystallized silica (b) poorly crystallized silica (reprinted from Sarkar et al. (2004))

Typical symptoms of ASR that can be seen on concrete structures are shown in Figure 4.

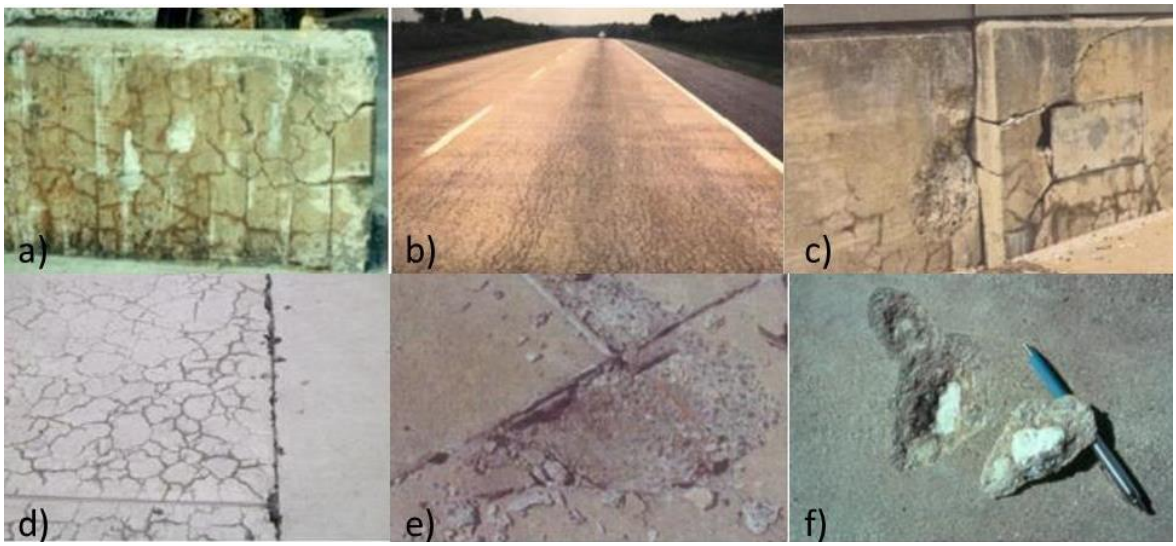

Figure 4 (a) random (map or pattern) cracking (b) preferred alignment of cracks (c) misalignment of adjacent sections (d) extrusion of joint sealant (e) crushing of concrete at joints (f) pop-out over reactive aggregate (FHWA, 2013)

2.2.1 Silica Contribution to the Reaction

The siliceous aggregate used in concrete mixtures may be natural or artificial siliceous glass, which possibly consist of a variety of silicon dioxide or hydrous silica. The contribution of the silica to the ASR is a function of the type, form, degree of crystallization and solubility of these compounds in the aggregate. Silica minerals in aggregates are generally stable in crystalline form and they are reactive if amorphous. The crystalline silicate structure is formed by the repetition of the silicon tetrahedron in an oriented three-dimensional space by linking of the tetrahedra by shared oxygen atoms at the common corner. The amorphous silicate structures are formed by a combination of the silicon tetrahedron; in this form, tetrahedra are arranged in a random three-dimensional space (Prezzi et al., 1992). The poorly crystallized aggregate presents a large surface area for reaction and has many lattice defects (Poole, 1992). It is often recommended to use the non-reactive aggregate in concrete mixture; however, usually this is not a practical solution for the regular concrete mixture, since the aggregate available close to the field is being used, which might contain reactive silica.

2.2.2 Alkali Contribution to the Reaction

Concrete mixture contains soluble alkali salts such as sodium (in the form of sodium oxide, Na_2O) and potassium (in the form of potassium oxide, K_2O) and perhaps extended to rubidium and caesium (Figg, 1983). These salts are mostly available from the Portland cement as a primary source, supplementary cementing materials, pozzolana, aggregate, chemical admixtures, and external sources such as seawater and deicing salt or wash water. Liu and Tam (2002) summarize these reaction as shown in Table 1. Based on previous studies, an ASR reaction is unlikely when the alkali amount is below 0.6 percent Na_2O_{eq} (Folliard et al., 2003).

Table 1 Possible Sources of Alkali in Concrete (Liu and Tam, 2002)

Cement	Major source and contains alkaline oxides (Na_2O and K_2O)
Pozzolana	Pozzolana is a common cementitious material. The siliceous or aluminous materials contained in pozzolana may react with lime (CaO) at ambient temperature to form cementitious compounds. Alkali is then released during the process
Aggregate	Feldspar, mica, glassy rock and glass in aggregate may release alkali in concrete. Marine sand may contain traces of sodium chloride which, if not washed thoroughly, can introduce significant amount of alkali in concrete
Admixture	Admixture (e.g. accelerators, retarders, water reduces, super-plasticizers and air entraining agents) may contain sodium and potassium compounds which can increase the alkali content of concrete
De-icing salts	In cold areas, the use of de-icing salts containing sodium ions may increase the alkali content of concrete
External sources	Soils containing alkali may also increase the alkali content of the concrete that comes into contact with them

2.2.3 Testing Methods For Potential Reactivity of Aggregate and Concrete Mixture

There are different test methods for evaluating the reactivity of aggregates. These tests may be categorized as petrographic methods, chemical methods, the mortar bar method and concrete prism methods. A summary of these tests is shown in Table 2 (Farny and Kosmatka, 1997). The limitations of a few of these standards are mentioned in Table 3. In this study, ASTM C1260 (2007b) and ASTM C1293 (2008b) are chosen to test the reactivity of fine and coarse aggregate, respectively. These tests are being used all over the world and are capable of detecting numerous reactive aggregates. However, it should be noted that there are always differences between the laboratory specimens and cores taken from structures. To accelerate ASR, submerging in water with the presence of alkali in a hot and humid environment is generally used. In contrast, a structural member is cast and cured in its formwork for a period of days. After stripping and de-propping, the concrete surface is exposed to the atmosphere and usually dries, causing surface shrinkage (Blight and Alexander, 2011).

The comparison of different expansion conditions are shown in Figure 5. In this graph Blight and Alexander (2011) compared the results of expansion in two sets of measurement

(laboratory concrete prisms and cores taken from aged structure) and in two different conditions of expansion (free and restrained). The difference between laboratory specimens and cores were, firstly, the size and, second, the temperature; prisms were maintained at 38˚C while the cores stored at 23˚C. Higher free expansion, almost 9 times higher, of laboratory concrete is due to its smaller size which causes a shorter seepage path for taking up water. The effect of size can be seen clearly in free expansion of a 10 mm thick slab which swells more rapidly than the concrete core. An applied stress restraining the swell reduces the expansion in both cases (Blight and Alexander, 2011).

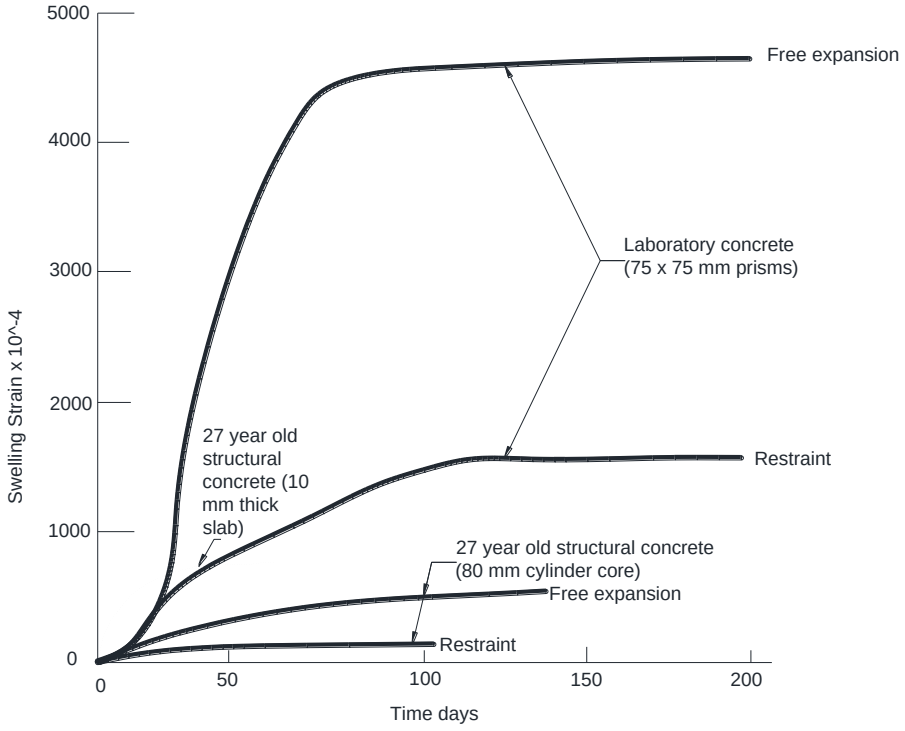

Figure 5 Comparison of free and partly restrained swelling of laboratory prisms and 27 year old cores of concrete placed in a nominally 100% RH atmosphere (Blight and Alexander, 2011)

Table 2 Test Methods for Alkali Silica Reactivity

Test name	Purpose	Method	Type of test	Type of sample	Duration of test	Measurement
ASTM C856 (2014a) (AASHTO T 299 (2004))	to identify products of ASR in hardened concrete	Petrographic	Staining of a freshly exposed concrete surface and viewing under UV light	Different sample size	Immediate results	Intensity of fluorescence
ASTM C295 (2012a)	Examination of samples representative of materials to determine their performance	Petrographic	Visual and SEM/XRD	Different sample size	Short	Particle shape, size, texture, color, mineral composition and physical condition
RILEM TC 191-ARR1 (2003)	Examination of samples test to identifies rock types and minerals that might react with hydroxyl ions from the concrete pore solution	Petrographic	Microscopical examination, separation technique and point counting	Thin section 50 x 30 mm	Short	Particle shape, size, texture, type, mineral composition and physical condition
ASTM C289 (2007a)	Potential reactivity of an aggregate with alkalis in Portland cement concrete	Chemical	Sample reacted with alkaline solution at 80˚C	Three 25-gram samples of crushed and sieved aggregate	24 hours	Drop in alkalinity and amount of silica solubilized
ASTM C227 (2010d)	Determination of the susceptibility of cement-aggregate combinations to expansive reactions involving hydroxyl ions associated with the alkalis	Mortar bar	Mortar bars stored over water at 37.8˚C and high RH	At least 4 mortar bars of standard dimensions 25 x 25 x 285 mm	First measurement at 14 days, then 1,2,3,4,6,9, and 12 months, and every 6 months after that	Length change

Table 2 (continued) Test Methods for Alkali Silica Reactivity

Test name	Purpose	Method	Type of test	Type of sample	Duration of test	Measurement
ASTM C1260 (2007b) (AASHTO T 303 (1996)) (CSA A23.2-25A (2014))	To test the potential of deleterious alkali-silica reaction of aggregate in mortar bars	Mortar bar	Mortar bars stored in alkaline solution at 80˚C	At least 3 mortar bars of standard dimension	16 days	Length change
ASTM C1567 (2013c)	To test the potential of deleterious alkali-silica reaction of aggregate in mortar bars with hydraulic cement, pozzolans and ground granulated blast furnace slag	Mortar bar	Mortar bars stored in alkaline solution at 80˚C	At least 3 mortar bars of standard dimension	16 days	Length change
ASTM C342 (1997a)	To determine the potential ASR expansion of cement-aggregate combinations	Mortar bar	Mortar bars stored in alkaline solution at 23˚C	At least 3 mortar bars of standard dimension	52 weeks	Length change
RILEM TC 191-ARR2 (2000)	To test the potential of deleterious alkali-silica reaction of aggregate in mortar bars	Mortar bar	Mortar bars stored in alkaline solution at 80˚C	3 mortar bars of standard dimension	16 days	Length change
CRD C662-10 (2010)	To test the potential of deleterious alkali-silica reaction of aggregate in mortar bars	Mortar bar	Mortar bars stored in alkaline solution at 80˚C	3 mortar bars of standard dimension	30 days	Length change

Table 2 (continued) Test Methods for Alkali Silica Reactivity

Test name	Purpose	Method	Type of test	Type of sample	Duration of test	Measurement
EB-70 (2005)	To test the potential of deleterious alkali-silica reaction of aggregate in mortar bars	Mortar bar	Mortar bars stored in KAc deicer solution at 80˚C	3 mortar bars of standard dimension	16 days	Length change
NT-Build 295 (1985)	To test the potential of deleterious alkali-silica reaction of given sand in mortar bars	Mortar bar	Mortar bars stored in NaCl solution at 50˚C	3 mortar bars of 40 x 40 x 160 mm dimension	8 weeks	Length change
ASTM C 1293 (2008b) (CSA A 23.2-14A (2014))	To determine the potential ASR expansion of cement-aggregate combinations	Concrete prism	Concrete prisms stored over water at 38˚C	3 prisms per cement-aggregate combination of standard dimension 75 x 75 x 285 mm	First measurement at 7 days, then 28 and 56 days, then 3,6,9, and 12 months, and every 6 months after that	Length change
RILEM TC 191-ARR3 (2000)	To determine the potential ASR expansion of cement-aggregate combinations	Concrete Pprism	Concrete prisms stored over water at 38˚C	3 prisms per cement-aggregate combination of standard dimension 75 x 75 x 285 mm	First measurement at 7 days, 2, 4, 13, 26, and 52 weeks after mixing	Length change

Table 3 Limitation of Test Methods for Alkali-Silica Reactivity

Test Name	Limitations
ASTM C295 (2012a)	Need an experienced operator
ASTM C289 (2007a)	• Cannot identify slowly reactive aggregate • Underestimate the amount of dissolved silica • Falsely diagnose the aggregate reactivity (Stark, 1994; Zollinger et al., 2009) • Poor performance due to crushing the aggregate (Fournier and Bérubé, 1993)
ASTM C227 (2010d)	• Long term test • Not suitable for slowly reactive aggregate (Fournier and Bérubé, 1993) • Presence of wick promote leaching of alkalis and reduce the expansion which cause aggregate pass as innocuous (Folliard et al., 2004)
ASTM C1260 (2007b)	Severe test condition for some aggregates such as greywackes (Touma, 2000; Zollinger et al., 2009)
ASTM 1567 (2013c)	Ponding largely influence the alkalinity of the pore solution (Shafaatian et al., 2013)
EB-70 (2005)	• Not suitable for moderately and slowly reactive aggregate • Cannot adequately characterize aggregate (Rangaraju and Olek, 2011)
NT-build 295 (1985)	• Only suitable for fine aggregate • Driver of the reaction is NaCl and not alkali hydroxide, therefore the composition of Portland cement is important (Latifee, 2013)
ASTM C1293 (2008b)	• Long term test • Underestimate the extent of the reaction (Zollinger et al., 2009) • Alkali can potentially leach out if the prism due to convective air currents and results in less expansion (Folliard et al., 2004; Folliard et al., 2006)

2.3 Corrosion

Corrosion in steel not only causes loss of steel cross-sectional area, but also the growth of the oxide and rust leads to the cracking and spalling of the concrete surface (Broomfield, 1997). In fewer cases corrosion may cause hydrogen embrittlement, which leads to a brittle failure of the reinforcement (Bertolini et al., 2013). These problems have a negative effect on the aesthetic of the structures, and when they get more severe, they reduce the serviceability and safety of the concrete structures. A cost study estimated the direct cost of corrosion damage in the US as $276 billion – approximately 3.1% of the nation's gross domestic product (Koch et al., 2002).

As fresh concrete is placed around the steel in reinforced concrete structures, the mix solution penetrates through the rust pores on the steel and forms hydrated calcium ferrite ($4.CaO.Fe_2O_3.13H_2O$). Additionally, a thin passive layer of iron and calcium hydroxides [$Fe(OH)_2$ and $Ca(OH)_2$] with thicknesses from 1 nm to 100 nm are formed. These products in the vicinity of the steel raise the pH of the concrete pore solution to about 13 (CEFRACOR, 2014). This layer is a dense and impenetrable film. When the pH of concrete becomes less than 11.5, it indicates that the pore solution is becoming acidified and the passive layer will degrade (Holder, 1999). In the presence of chloride ions or due to carbonation, the alkalinity of the concrete will reduce to pH levels of 9 (Bargaheiser and Butalia, 2007) and 8 (Parrott, 1987), respectively. The passive layer will be damaged and corrosion will start. Ricker (1994) categorized corrosion, based on the morphology of the damage, in eight different groups: general corrosion, pitting corrosion, crevice corrosion, intergranular corrosion, environmentally induced fracture, dealloying, galvanic corrosion, and erosion corrosion. The mechanism of corrosion that is of relevance to this study is due to chloride, which is described in more detail below.

As mentioned above, concrete is alkaline in nature with a pore solution pH of 12-13 that naturally creates a protective environment for the embedded steel. This means it contains microscopic pores with high concentration of soluble calcium, sodium and potassium oxides (Broomfield, 1997). However, the presence of chloride can damage the protective layer formed and start the corrosion of rebar. This process reduces the cross-sectional area of the rebar and the load bearing capacity of the structure. If corrosion reaches a certain level, it also reduces the bond strength (Almusallam et al., 1996), and degrades the reliability of the adjacent concrete (Jaffer and Hansson, 2009). Two mechanisms of chloride-induced corrosion exist: (1) microcell corrosion, when active corrosion and the corresponding cathodic half-cell reaction take place at adjacent parts of the same metal, and (2) macrocell corrosion, when the actively corroding bar is

coupled to another passive bar (Hansson et al., 1985). These mechanisms are shown in Figure 6. The initiation of corrosion needs an anode for oxidation reaction, a cathode for reduction of oxygen, an electrical connector to carry the electron charge and an electrolyte to carry the ionic charge; all these conditions should exist for this reaction to take place (Holder, 1999). Moreover, the temperature and RH also have an effect on the corrosion. Below freezing point, the pore water will freeze and stop the corrosion. Additionally, tests indicate that the corrosion rate is maximum when the RH is around 90-95% (Tuutti, 1982). When concrete is completely saturated, oxygen starvation slows down the corrosion (Broomfield, 1997) .The chloride-induced corrosion process is described in the following equations (Bentur et al., 1997):

$$Fe^{2+}+2Cl^{-}\rightarrow FeCl_{2,} \quad (6)$$

$$Fe\rightarrow Fe^{2+}+2e^{-}, \quad (7)$$

$$1/2O_2+H_2O+2e^{-}\rightarrow 2OH^{-}, \quad (8)$$

$$FeCl_2+2\ H_2O\rightarrow Fe(OH)_2+HCl, \quad (9)$$

$$Fe^{2+}+2OH^{-}\rightarrow Fe(OH)_2, \text{ and} \quad (10)$$

$$2Fe(OH)_2+1/2O_2+H_2O\rightarrow Fe(OH)_3\rightarrow Fe_2O_3.3H_2O. \quad (11)$$

In these reactions when chloride ion reaches to the rebar, it activates the surface of the bar to form an anode; two electrons released in this reaction must be consumed elsewhere to preserve electrical neutrality (Broomfield, 1997). Therefore, the stable passivized surface film acts as a cathode, and the decomposition of the passive layer starts. After oxidation of the steel, hydroxide forms that leads to corrosion where ferrous hydroxide becomes ferric hydroxide and then hydrated ferric oxide (rust). This reaction happens during a time period in the service life of structure and different factors can alter the rate of corrosion. In Figure 7, curve 1 shows regular corrosion due to ion penetration or carbonation induced corrosion; however, if a crack is induced on the surface of the concrete, the initiation period will decrease and follow curve 2 (Jung et al., 2003). The initial period shows depassivation and is the time required for the protective layer of the alkaline hydrated cement matrix to be destroyed. The second slope shows the propagation

phase, the time when corrosion products form and apply enough stress to the surrounding concrete that the concrete cracks. The limitation is reached when the reliability of the structure is impaired (Schiessl, 1988).

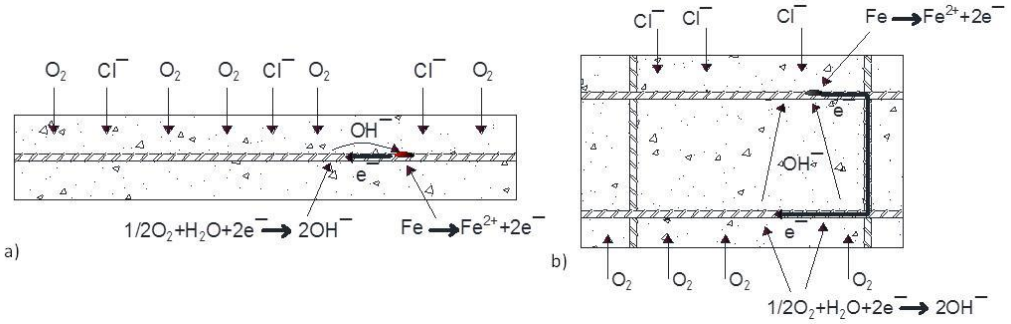

Figure 6 (a) microcell corrosion, (b) macrocell corrosion (Hansson et al., 1985)

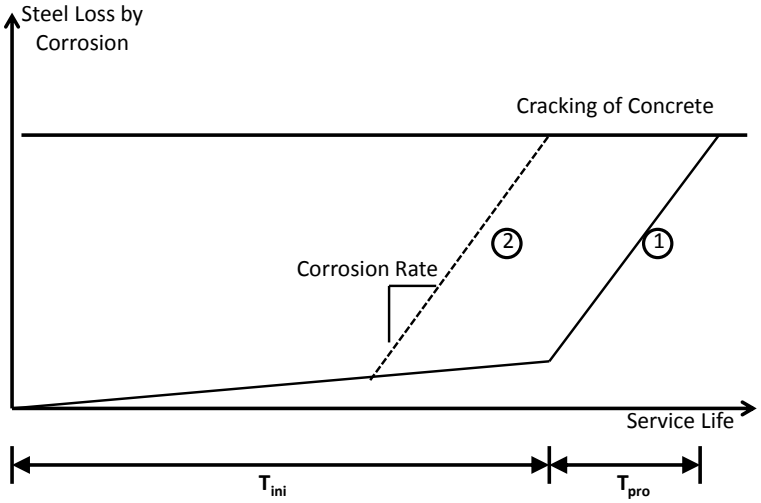

Figure 7 Steel corrosion according to time [reprinted from Jung et al. (2003)]

Furthermore, the presence of chloride ion in the concrete changes the chemical composition of the cement paste (Brown and Doerr, 2000). It can have a positive effect, such as reduction in bleeding of concrete (Lamond and Pielert, 2006), and accelerate some of the concrete properties at early age, but this cannot be sustained in the long term. The concrete will show higher deterioration compared to the sound concrete (Abalaka and Babalaga, 2011). Increasing the percentage of chloride in concrete or in curing medium causes mechanical properties of concrete such as strength and dynamic modulus to deteriorate. This process also increases other damaging

reactions such as carbonation (Lee et al., 2000; Darwin et al., 2007; Sutter et al., 2008; Abd El-Salam et al., 2012; Kim et al., 2013; Shi et al., 2014). The chloride binding happens in two different forms: chemically by chloride and the hydration product reacting together or physically by the chloride ion being absorbed on the surface of the hydration product (Schiessl, 1988). These bindings are associated with the formation of complex salts in the mixture containing $CaCl_2$, $Ca(OH)_2$ and/or $CaCO_3$ (Chatterji, 1978). The common example of a chemical bond of chloride with C-S-H (calcium silicate hydrate, the main product of hydration) or tricalcium aluminate ($3CaO.Al_2O_3$) results in formation of Friedel's salt ($3CaO.Al_2O_3.CaCl_2.10H_2O$) or, when the chloride ion amount is high, the chloride analogue of ettringite ($C_3A.3CaCl_2.30H_2O$) might also formed. These bindings also change the chemical composition of C-S-H by removing calcium. These reactions can briefly be explained as the reaction of aluminate and ferrite phases with calcium chloride and formation of hydrous analogues to the sulphate phases ($C_3(A,F).3CaCl_2.30H_2O$ and $C_3A.CaCl_2.10H_2O$). In the presence of calcium chloride, the reaction of C_3A and brownmillerite ($Ca_2(Al,Fe)_2O_5$) with gypsum ($CaSO_4.2H_2O$) is significantly accelerated. Ettringite is formed initially, and after consumption of SO_4^{2-} ions, Friedel's salt is produced. The transition of ettringite to AFm (i.e. Alumina, ferric oxide, monosulphate, an important phase in hydration and which has a formula of $3CaO.(Al,Fe)_2O_3.CaSO_4.nH_2O$ with simplified crystalline hydrates) begins only after the consumption of $CaCl_2$ (Kurdowski, 2004, 2014). The concrete containing chloride also has coarser pore structure and a greater total porosity than regular concrete (Hansson et al., 1985). These changes in the chemical composition decrease the overall strength of the concrete (Wang et al., 2006).

Chloride ions may be present in the mixture due to three reasons: intentional or unintentional addition into the fresh mix and ingress from outside in the hardened state:

- *Addition of chloride in the fresh mix.* Concrete may be contaminated with chloride because of using seawater or brackish water. Portland cement may also contain a small amount of chloride. Or chlorides may be added deliberately as inorganic accelerators; this method was widely used until the mid-1970s (Broomfield, 1997). Similarly, other additives in concrete such as ground granulated blast furnace slag may have significant chloride content (Neville, 1995). This case can causes immediate corrosion reactions (Schiessl, 1988). To reduce the effects of chloride in concrete, different standards recommended different limits on the chloride content. For example, BS 8110 (2005) and EN 206 (2000) permit a chloride ion concentration of 0.2%-0.4% by mass of binder for reinforced concrete. ACI 318 (2011) permits 0.15% water-soluble chloride by weight of cement; ACI 222 (2001) limits this amount to 0.2%.
- *Ingress of chlorides.* Chloride ions may also ingress from outside. This is mostly of a concern for structures that are located in or close to a marine environment because of sea salt spray or sea water wetting. Or in cold regions, structures are subjected to deicing salt such as NaCl, $CaCl_2$ and $MgCl_2$ where the cycles of wetting and drying repeat with different concentrations of ions. The penetration of chloride mainly occurs due to a diffusion process by capillary suction and absorption (Neville, 1995). This penetration depends on six main parameters in concrete mixtures: the composition of the cement, the amount of cement per m^3, the composition and compaction of the concrete, the curing conditions of the concrete and the environmental conditions of the concrete (Schiessl, 1988).
- *Chemical changes due to fire in a concrete structure.* Polyvinyl Chloride (PVC) is one of the common materials used in structures and has high chlorine content. When temperature increases above 80-90˚C, PVC starts to decompose and liberates gaseous hydrochloric

acid (HCl). This gaseous HCl can dissolve in water and penetrate deeper sections of concrete structures and can cause corrosion in reinforced concrete (Kropp and Hisldorf, 1995).

A different standard method is available to measure the chloride penetration rate inside the concrete, as shown in Table 4. The limitations of these tests are summarized in Table 5. There are different types of tests for corrosion rate, such as electrochemical tests, cabinet tests, immersion tests, high-temperature and high-pressure corrosion tests, placing the specimens in seawater, freshwater, soil or subjecting to high temperature. There are different standard tests which are related to each type of corrosion testing and environment. Table 6 shows some of these methods for measuring corrosion in the RC structures.

Table 4 Test Methods for Chloride Penetration Rate

Test Name	Purpose	Type of test	Type of sample	Duration of test	Measurement
AASHTO T259 (1980)	Evaluate ingress of chloride into concrete	Ponding the sample in 3% sodium chloride solution	Slab with minimum thickness of 90±15mm	90 days	Acid-soluble chloride concentration at different depths
ASTM C1543 (2010b)	Determines the penetration of chloride ion into concrete	Ponding the sample in 3% sodium chloride solution	Slab with minimum thickness of 90±15mm	90 days, 6 and 12 months and 12 months interval	Acid-soluble chloride concentration at different depths
NT-Build 443 (Bulk Diffusion Test) (1995)	Determine the penetration parameter	Water saturating and ponding the specimen in NaCl solution	Cylinder with least dimension of 75x100mm	At least 35 days	Total chloride concentration at different depths
AASHTO T277 (2011a) (ASTM C1202 (2012a))	Determination of the electrical conductance of concrete	Passing electrical current through sample	50±3mm thick slices of 100mm diameter cores or cylinders	6 hours	Total charge

Table 4 (continued) Test Methods for Chloride Penetration Rate

Test Name	Purpose	Type of test	Type of sample	Duration of test	Measurement
NT-Build 492 (CTH Test) (1999)	Determination of the chloride migration coefficient in cement based materials	Passing electrical current through vacuum saturated specimen	50±3mm thick slices of 100mm diameter cores or cylinders	6 hours	Temperature and depth of penetration
ASTM C1585 (Sorptivity) (2013d)	Determine the rate of absorption of water by measuring the increase in the mass of a specimen	Ponding the specimen in water	50±5mm thick slices of 100mm diameter cores or cylinders	At least 15 days	Weight of specimens

Table 5 Limitation of Test Methods for Chloride Penetration Rate

Test Name	Limitations
AASHTO T259 (1980)	• Initial sorption effect due to drying the specimens for 28 days • Exposure condition causes chloride drawn into concrete through mechanism other than pure diffusion (Stanish et al., 1997)
NT-Build 443 (1995)	• Longer ponding period for high quality concrete
AASHTO T277 (2011 (ASTM C1202 (2012a))	• Low precision, the difference in one lab can be close to 42% and in multilaboratory is 51%, that can lead to loss of confidence in the test results (ASTM, 2012g) • Current passed is related to all ions not only chloride ions • Measurement made before steady-state migration • High voltage, increase the temperature, temperature increase is higher in the poor quality control which cause higher voltage pass and show the concrete ion penetrability higher than the actual amount (Stanish et al., 1997)
ASTM C1585 (2013d)	• Evaluating the surface of concrete, not the bulk properties of it • The test is useful for very shallow steel not the typical of steel in RC structures (Stanish et al., 1997) • Only possible after completely drying out the specimens

Table 6 Test Methods for Corrosion Rate

Test Name	Purpose	Type of Test	Type of Sample	Duration of Test	Measurement
RILEM TC 154-EMC (2004)	assess the rate of degradation of concrete structures	Non-destructive testing	RC structures	Short	Free corrosion potential or half-cell potential
ASTM G1 (2011a)	evaluating the corrosion by mass loss	Cleaning the specimens in acid solution	Reinforcement bar	Short	Mass loss

Table 7 Limitation of Test Methods for Chloride Penetration Rate

Test Name	Limitations
RILEM TC 154-EMC (2004)	• The method can only predict the corrosion of the closer layer of reinforcement facing the counter electrode • It does not provide information on corrosion rate
ASTM G1 (2011a)	• corrosion rate obtained from this test for the highly localized such as in pitting or crevice corrosion may be misleading

2.4 Accelerated Aging

To predict the structural behavior in the long term, there are different methods available. The first method is the performance history of a structure, which is based on the performance of a full-scale structure under normal conditions and during the long exposure time. This method is precise but very conservative. The second method is by monitoring the performance of a prototype in extreme outdoor conditions; similar to the first method, this method can take a long time until a severe degradation is observed. The third method is accelerated aging in the laboratory, in which one or more degradation factors are set to a higher level than normal (Martin, 1985). ASTM E632-82 (1996) defines accelerated aging tests as ones in which the degradation of building materials is intentionally accelerated over the conditions expected in service. In other words, if the aging process of concrete and its degradation accelerates by means of different chemical or physical processes, it is called accelerated aging. This specific exposure

condition provokes the degradation reaction more rapidly than would normally happen in the service environment. In this testing method, it is assumed that the accelerated sample behaves the same way as an in-service structure works and a control specimen can measure the small changes in properties due to acceleration (Pommersheim and Clifton, 1985). Proper identification of degradation mechanisms is important in extrapolating test results obtained through this method and predicting service life of a structure. It should be noted that there are some limitation in accelerated tests, which Pommersheim (1985) summarized as follows: methods for correlating laboratory results with in-service results are rarely provided; provisions are usually not made for taking different applications into account; the concrete specimens tested in the laboratory have substantially different configurations compared to real-life structures; the factors affecting service life and the degradation mechanics are complex, not well understood and difficult to quantify; sensitive detection methods are needed since changes may be small under normal conditions; results may be extrapolated, often for exposure periods hundreds or thousands of times longer than normally feasible. It is important to remember that acceleration can change the mechanism and the performance does not correlate well with the real structure. Regardless of all the limitations, the accelerated testing method is usually the best alternate solution compared to waiting for the structure to age through the regular process over several decades.

The following methods are used individually or sometimes together to accelerate aging of concrete due to ASR and corrosion:

- Creating a corrosion cell with or without impressed current through the rebar
- Adding chemicals to the mixture
- Subjecting to high temperatures

- Subjecting to high humidity and wet-dry cycles
- Subjecting to high levels of chemical solutions

There are different studies on the acceleration of alkali-silica reactivity in the lab and mostly two methods are being used. In the first method, ASR was accelerated by immersing the specimens inside the alkaline solutions at different temperatures (Parsons and Insley, 1944; Harrisson et al., 1987; Fournier and Bérubé, 1993; Gillott and Soles, 1993; Mukhopadhyay et al., 2009). In some other cases, a high-alkali content cement was also used (Stanton, 1943b; Jones and Tarleton, 1958a; Davis and Oberholster, 1988). The other method that is frequently used is adding sodium hydroxide or other alkali hydroxide to the mixing water and concrete paste and keeping the specimens at different temperatures (Diamond and Ong, 1994; Smaoui et al., 2005; Poole, 2007; Temuujin et al., 2009; Garci Juenger and Jennings, 2011; Nuruddin et al., 2011; Bahadure and Naik, 2013; Gao et al., 2013; Kupwade-Patil and Allouche, 2013; Memon et al., 2013). A short summary of these studies is provided in Table 8. Adding NaOH to the mixing water mostly increases the pH in pore solution, and mixing it to the concrete paste increases the internal alkali content of the mixture (Poole, 2007). Immersing in solution is a practical approach for small specimens in a laboratory environment. However, for real-size structures, immersion is not easily achievable and the second method is more desirable.

Some studies investigated the effect of fly ash and its type on ASR (Shehata and Thomas, 2000; Thomas et al., 2011). Fly ash in the concrete mix reduces the ASR gel expansion (Nagataki et al., 1991; Blackwell et al., 1992). This reduction is due to three different mechanisms: dilatation of the cement alkalis by mixing the cement with a fly ash, low availability of calcium to react with the expansive gel, and lower permeability to water and low diffusivity of alkalis from outside (Detwiler, 1997; Shehata and Thomas, 2000; Thomas et al., 2011).

Table 8 Previous Studies on Accelerating Alkali-Silica Reactivity (ASR)

References	Procedure
Stanton (1943b)	Using high-alkali content cement, Immersing in 0.5M NaOH, 0.5M KOH and $Ca(OH)_2$ solutions. In different temperatures form 25 to 90 ˚C
Parsons and Insley (1944)	Immersing in 10% NaOH, 10%KOH, 10% K_2SO_4 and $Ca(OH)_2$ solutions
Jones and Tarleton (1958a)	High-alkali cement. Immersing in 20g/litre NaOH, 20g/litre KOH, $Ca(OH)_2$ solutions
Gillott and Soles (1993)	Immersed in 2M NaOH at 38 ˚C
Davis and Oberholster (1988)	High-alkali cement. Immersing in 1M NaOH, 1M KOH at 80 ˚C
Harrisson et al. (1987)	Acceleration on opal stones. Immersing the specimens in 1M KOH
Fournier and Bérubé (1993)	Immersing in 1M NaOH at 38 ˚C
Diamond and Ong (1994)	Low alkali and normal alkali cement used in testing. To low alkali cement mixture NaOH, KOH or LiOH added in a way that total Na_2O reach 1%, 1.4%, 1.8% and 2.2% by weight of cement added to the mixture. Keep at 100% RH and 38 ˚C; w/c: 0.485
Bérubé and Frenette (1994)	1.0M NaOH or 1M NaCl or Water at two temperature of 38˚C and 80 ˚C; w/c: 0.55
Ferraris (1995)	High-alkali cement. Immersing specimens in 1M NaOH at 80 ˚C or 100% RH and 20˚C; w/c: 0.3, 0.4, 0.5, 0.6
Smaoui et al. (2005)	Low and high alkali concrete (3.52 kg/m^3 NaOH added to the mix for high alkali concrete). Specimens kept at 100% RH and 23 ˚C; w/c: 0.41
Poole (2007)	Changing the alkali content of cement to 0.85% by adding dilute solution of NaOH; w/c: 0.4, 0.44, 0.5, 0.55, 0.68
Temuujin et al. (2009)	14.0M NaOH added to the mixture
Mukhopadhyay et al. (2005; 2009)	Immersing aggregate at 0.25M, 0.5M and 1.0M NaOH solutions at 60 ˚C, 70 ˚C and 80 ˚C temperature; w/c: 0.4, 0.47, 0.49, 0.6, 0.7
Nuruddin et al. (2011)	8.0, 10.0, 12.0, 14.0M NaOH added to the mixture
Al-Bakri et al. (2011)	6.0, 8.0, 10.0, 12.0, 14.0 and 16.0M NaOH added to the mixture
Garci Juenger and Jennings (2011)	1.0M NaOH added to the mixture of cement paste at 20˚C; w/c: 0.45
Memon et al. (2013)	Mixture of NaOH and Na_2O solution used as activator. NaOH concentration used is 6.0, 8.0, 10.0, 12.0 and 14.0M
Kupwade-Patil and Allouche (2013)	A blend of sodium silicate and 14M sodium hydroxide used in specimens. The specimens immersed in 1M NaOH at 80 ˚C

Table 8 (continued) Previous Studies on Accelerating Alkali-Silica Reactivity (ASR)

References	Procedure
Gao et al. (2013)	Mortar specimens, NaOH add to the mix to be the same as NaOH in ponding solution. Immersing specimens in 1M NaOH at 60 ˚C w/c: 0.5
Bahadure and Naik (2013)	Adding NaOH to the concrete mixture for concentration of 1.0, 2.0, 3.0 and 4.0M; w/c: 0.5, 0.54, 0.58, 0.63

For accelerating corrosion, in most studies, a corrosion cell is created and the corrosion is driven by passing a direct current through the reinforcement. To create the corrosion cell, a wet sponge (Jung et al., 2003; Hansson et al., 2006; Ortega et al., 2011; Silva, 2013) or direct immersion inside a saline solution was adopted (Okba et al., 1997; Shayanfar and Ghalehnovi, 2007; Johnson, 2010; Yu et al., 2010). Passing current is an effective approach for accelerating corrosion; however, it comes with various challenges for real-size structures related to creating the electrochemical cell and achieving uniform corrosion in reinforcement distributed throughout the structure. Adding salts directly to the mixture is another method that was used previously and showed good results in accelerating corrosion (Jang et al., 1995; Al-Attar and Abdul-Kareem, 2011). The effect of adding different salts such as KCl, NaCl and $CaCl_2$ to the concrete mixture with different percentages from 0 to 2.0% chloride by weight of cement on the corrosion of rebar has been studied. Researchers looked at the pH, electrical conductivity and corrosion rate in concrete containing these salts. Some studies also looked at the values of chloride to hydroxyl concentration. The importance of this value is that when it exceeds 0.6, the chloride ion starts to break down the passive layer; this amount is approximately equal to a concentration of 0.4% chloride by weight of cement if chloride salts are cast into concrete and 0.2% if they diffuse into it (Hausmann, 1967; Broomfield, 2007). This ratio is related to the pH of the pore water and the amount of chloride in the pore water (Holder, 1999).

Diamond (1986) studied the effect of adding $CaCl_2$ and NaCl to concrete mixtures and measured the values of Cl^-/OH^- in the pore solution. No difference was observed between $CaCl_2$ and NaCl. However Pruckner and Gjørv (2004) showed that adding NaCl to the mix as a source of chloride results in a higher pH and lower Cl^-/OH^- ratio compared with $CaCl_2$. There have been other studies that made similar investigations and came to the conclusion that the corrosive effect of NaCl is significantly less than that of $CaCl_2$ (Helmuth et al., 1993; Jang et al., 1995; Pakshir and Esmaili, 1998; Pruckner and Gjørv, 2004; Kelestemur and Yildiz, 2006). They also found that concrete containing calcium chloride has more open pore structures and lower pH compared to the other salts (Hansson et al., 1985). However, the impacts of this approach on various properties of the concrete mixture have not been studied in detail before. The summary of some of these studies and the amount of chloride used in the concrete are shown in Table 9.

Table 9 Chloride Additive to the Concrete

References	Additive	Dosage	w/c
Hansson, Frølund, and Markussen (1985)	KCl	0%, 0.5%, 1 .0% and 2.0% by weight of cement	-
	NaCl		
	$CaCl_2$		
Diamond (1986)	$CaCl_2$	0.05%, 0.2%, 0.5%, 1%, 1.5% and 2.0% by weight of cement	0.5
	NaCl	0.21%, 0.52% and 1.05% by weight of cement	
Helmuth et al (1993)	$CaCl_2$	0.5%, 1.0% and 2.0% by weight of cement	0.5
	NaCl	0.5%, 1.0% and 2.0% by weight of cement	
Jang et al (1995)	Deicing salts NaCl	1.0% and 2.0% by weight of cement	
Pakshir and Esmaili (1998)	$CaCl_2$	0.1%, 0.5%, 1.0% and 2.0% by weight of water	0.56
	NaCl	0.1%, 0.5%, 1.0% and 2.0% by weight of water	
Pruckner and Gjorv (2004)	$CaCl_2$	0.25 and 0.75 mol/kg cement	0.5
	NaCl	0.5 and 1.5 mol/kg cement	
Kelestemur and Yildiz (2006)	NaCl	1.0%, 2.0% and 3.0% by weight of water	0.53
			0.69

Table 9 (continued) Chloride Additive to the Concrete

References	Additive	Dosage	w/c
Wang et al (2006)	$CaCl_2$	9.5% and 37.5% by weight	0.48
	NaCl	13.3% and 26.5% by weight	
Al-Attar et al (2011)	NaCl	0.8% by weight of cement	0.33
			0.45
El-Salam et al (2012)	NaCl	1.0%, 5.0% and 10% by weight of cement	0.46
Anacta (2013)	NaCl	10.0%, 20.0% and 30.0% by weight of water	0.4

There have been a handful of studies in the literature on accelerated aging of structural members for ASR and corrosion (Folliard et al., 2006; Deschenes et al., 2009; Talley et al., 2016). However, in almost all of these studies aging was accelerated through application of heat and/or higher exposure to chemicals from the environment. These techniques are not easily applicable at the structural scale; therefore, in this thesis, to accelerate aging due to ASR and corrosion, the addition of alkalis and chloride was investigated as a practical method at the structural scale.

2.5 Correlating Field Conditions to Accelerated Aging

Here, existing analytical models to predict the service life of structures are described. These models are used later to correlate the rate of accelerated deterioration under laboratory conditions to the rate of actual deterioration in the field.

2.5.1 Service Life of Concrete Structures under Chloride Attack

The prediction of the service life of a structure is important for estimating the life cycle cost decision, determining the risks and liabilities and predicting the time to failure. ASTM E632-82 (1996) defines the service life of the structure as the period of the time after installation during which all properties exceed the minimum acceptable values when routinely maintained. To be able to predict the service life, some information from the actual building is needed, such as

performance and main deterioration reasons in the structure. Here we chose corrosion as the main effect. By the time the earliest visible signs of corrosion become apparent on the concrete, the structure may be severely damaged; therefore, it is important to be able to predict the service life of the concrete structures. Predicting the service life of a reinforced concrete structure is a complex task because of the large influence of the environmental conditions and concrete properties. Furthermore, the tolerated extent of damage may vary with the intended use of the structure and can affect the service life prediction (Lopez et al., 1993). There are different method to predict the service life such as the time crack appears on the surface, area loss of rebars and using time shift method. The latter is mostly used to predict the age of concrete when changes in the concrete changes the degree of hydration over a time and is mostly used to predict the creep over time. Therefore, first two method was chose for this study.

To predict the service life of the structures, it is important to study the factors that affect the degradation process in concrete, here chloride ion ingress as well as corrosion. At least ten factors may influence the corrosion rate (SINTEF, 2008):

- Temperature: the rate of corrosion increases with an increase in the ambient temperature; however, at high temperature, around 40°C, the corrosion rate decreases due to lack of oxygen. In addition to the temperature itself, thermal capacity and thermal conductivity of concrete also play important roles.
- Supply of oxygen to the pore water in contact with the cathodic area of the steel surface: the rate of this supply is dependent on concrete porosity, the degree of moisture content in these pores, the concrete cover thickness, and temperature. When the concrete porosity is high and the concrete cover is low, the rate of oxygen supply increases.

- RH in the concrete pores: a corrosion reaction and movement of chloride ions can only proceed in liquid water; therefore, if the pores dry out, the electrochemical reaction stops. Furthermore, the percentage of concrete RH has an effect on oxygen supply and electrical resistivity of the concrete. This parameter can be defined as a humidity diffusion coefficient in concrete.
- Concentration of dissolved chloride ions in the pore water in contact with the anodic areas of the steel surface: when the concentration of chloride ion in concrete reach the threshold value, the corrosion can start.
- The chloride binding capacity of concrete and chloride diffusion coefficient of concrete also affect chloride transport and initiation of corrosion. The former can be defined based on cement and mix properties such as particle size distribution in cement, type of cement, gypsum content, water-cement ratio, aggregate and air content.
- Alkalinity, or the concentration of OH^- ions in the pore water in contact with the steel surface: the alkalinity or pH of concrete can affect the corrosion rate in three ways. The corrosion cell potential increases with decreasing pH. Also, the pH increases the dissolution of chemically bound chloride as well as increasing the concentration ratio of $[Cl^-]/[OH^-]$.
- Electrical resistivity of the concrete: low resistivity favors migration of ions and development of corrosion pits.
- Galvanic interactions between different parts of the steel reinforcement: the galvanic macrocell action increases as the electrochemical potentials difference increases between the anodic and cathodic areas.

- Effect of the oxide (rust) layer formation on corrosion rate: the corrosion rate is highest at the beginning of an exposure, but with accumulation of protective corrosion products on the metal surface, it reduces.

There are different models available to predict the service life and corrosion process in structures. It should be noted that in the modeling procedures, there is always some limitation with regard to the complexity of the reaction, as the models do not consider all relevant factors. For these reasons, it is customary to make various assumptions and rely on empirical formulations.

2.5.1.1 Diffusion of chloride ions

The first stage in deterioration of concrete through corrosion is that chloride ions diffuse through concrete toward rebar. The length of this stage may vary greatly from one reinforced concrete to another, depending on many factors such as thickness of the concrete cover, the permeability of concrete, and the environmental conditions. In general this stage is the longest stage during the life span of concrete structures (Suwito and Xi, 2003). Chloride ions are transported in solution through the porous concrete cover in various processes. The diffusion process is modeled by solving the one dimensional equation for Fick's second law of diffusion:

$$\frac{\partial C}{\partial t} = D_e \left(\frac{\partial^2 C}{\partial x^2} \right), \tag{12}$$

where, C is chloride ion concentration, t is time and D_e is the diffusion coefficient. In this model, the diffusion coefficient was considered constant. The well-known analytical solution for this equation is

$$C(x,t) = C_i + (C_s - C_i)\,\mathrm{erf}\left(\frac{x}{\sqrt{4tD_e}} \right), \tag{13}$$

where *C(x,t)* is the chloride concentration inside the concrete (mass %), C_s is the surface chloride concentration (mass %), C_i is the initial chloride concentration measured on the concrete (mass %), *x* is the depth below the exposed surface (m), D_e is the effective chloride transport coefficient (m^2/sec), *t* is the exposure time (sec) and *erf* is the error function. Based on this equation the corrosion initiation time can be estimated as follows:

$$T_i = \frac{{x_{cr}}^2}{4D_e}\left[\mathrm{erf}^{-1}\left(\frac{C_s - C_{cr}}{C_s - C_i}\right)\right],^{-2} \quad (14)$$

where, x_{cr} is concrete cover depth, D_e is the effective chloride transport coefficient (m^2/sec), C_s is the surface chloride concentration (mass %), C_i is the initial chloride concentration measured on the concrete (mass %), and C_{cr} is the threshold chloride content. In this model, the chloride content of the exposed concrete surface is constant.

2.5.1.2 Corrosion of reinforcement and crack initiation

The time to crack initiation is the time needed from the corrosion initiation until sufficient corrosion product (rust) is generated to produce cracking on the concrete. Different studies developed mathematical models for prediction of this time.

Beaton and Stratfull (1963) proposed an empirical model which later became the Stratfull formula:

$$T_{cr} = \frac{10^{0.0442C_0}C_0^{0.717}C^{1.22}1011}{K_0^{0.42}W_m^{1.17}}, \quad (15)$$

where, *Tcr* is years to cracking of concrete, C_0 is sacks of cement per cubic yard of concrete, *C* is concrete cover (in), K_0 is the chloride concentration of water (ppm),and W_m is the mixing water in percent of concrete volume. Later, Clear and Hay (1976), modified the Stratfull formula to the following:

$$T_{cr} = \frac{129C^{1.22}}{K_0^{0.42}P}, \tag{16}$$

where, C is concrete cover (in), K_0 is the chloride concentration of water (ppm), and P is the water-cement ratio. The formula can also be rewritten as (Purvis et al., 1994)

$$T_{cr} = \left[\frac{2.695C^{1.22}t^{0.21}}{C_s^{0.42}P}\right]^{\frac{1}{1.21}}, \tag{17}$$

where, C is concrete cover (in), C_s is the surface chloride concentration (mass %), t is the time at which C_s was measured, and P is the water-cement ratio. Another empirical model was later proposed by Morinaga (1990) with the assumption that cracking of concrete happens when corrosion products on reinforcing steel reach to a certain level. The amount is divided by the instantaneous corrosion rate to get the time for cracking as

$$T_{cr} = \frac{0.602\left(1 + \frac{2C}{D_i}\right)^{0.85} D_i}{J_r}{}_r, \text{and} \tag{18}$$

$$J_r = \left(\frac{W}{F}\right) i_{corr}, \tag{19}$$

where, D_i is the diameter of steel bar (mm), C is the thickness of concrete cover (mm), i_{corr} is the corrosion current density (μA/cm^2), J_r is the instantaneous corrosion rate, W=27.925 g, and F is Faraday's constant (96487 Coulombs/mol).

The empirical models presented did not account for the mechanical properties of concrete which have significant effects on the time to corrosion cracking. Later, other researchers worked on mathematical models to account for more parameters. Some of these studies are discussed below.

Bažant (1979) proposed a physics-based model for prediction of corrosion of steel and times to corrosion cracking of concrete cover for marine structures. In this model, the basic assumption was that oxygen and chloride ion transport through concrete occur in one dimension and are

quasi-stationary. Also in this model, the volume expansion due to hydrated red rust, ($Fe(OH)_3$), was introduced as a prescribed displacement at the surface of the bars. This process causes an increase in diameter of the bars and applying stresses to the cover which led to cracking of the concrete cover. By combining all these assumptions, the time to cracking of concrete can estimated from the following:

$$\rho_r = \frac{\rho_{st}}{4}, \tag{20}$$

$$\rho_{cor} = \frac{\pi}{2}\left[\left(\frac{1}{\rho_r}\right) - \left(\frac{0.583}{\rho_{st}}\right)\right]^{-1}, \tag{21}$$

$$\delta_{pp} = \left(\frac{D_i(1+\varphi_c)}{E_c}\right)\left\{(1+\upsilon_c) + d^2\left[\frac{2}{S^2} + \frac{1}{4C(1+D_i)}\right]\right\}, \tag{22}$$

$$\Delta D = 2f_t\frac{C}{D_i}\delta_{pp}, \text{and} \tag{23}$$

$$T_{cr} = \rho_{cor}\frac{D_i\Delta D}{SJ_r}, \tag{24}$$

where, ρ_r is the mass density of $Fe(OH)_3$, ρ_{st} is the mass density of steel, φ_c is the creep coefficient (typically about 2.0), E_c is the elastic modulus of concrete, υ_c is the Poisson ratio of concrete, *C* is the thickness of concrete cover (mm), f_t is the tensile strength of concrete, D_i is the diameter of steel bar (mm), and *S* is the bar spacing. The critical value of ΔD here was brought for inclined cracks emanating from a single bar and for the conditions where the rebar spacing is less than $6D_i$. This model relates the time of cracking to corrosion rate, cover depth, spacing, and some properties of concrete such as tensile strength, Poisson's ratio, elastic modulus and creep coefficient.

Liu (1996) proposed a simplified methodology for characterizing the dynamic corrosion process based on chloride content, temperature, resistance of concrete, and corrosion time after initiation. In this model, three stages were considered: free expansion, stress initiation and cracking. Free expansion is related to the porous zone around the steel/concrete interface which gradually gets filled with the corrosion products and allows the free expansion of them. The next

stage is after the porous zone gets filled and corrosion products start to apply expansive pressure, and when this pressure exceeds the tensile strain of concrete, the crack initiates. The critical amount of rust and the time of cracking are defined as follows:

$$R_i = \frac{D_i + 2d_0}{2}, \quad R_0 = C + \frac{D_i + 2d_0}{2}, \tag{25}$$

$$W_{st} = \alpha . W_{crit}, \tag{26}$$

$$k_p = 2.59 \times 10^{-6} \left(\frac{1}{\alpha}\right) \pi D_i i_{corr}, \tag{27}$$

$$E_{ef} = \frac{E_c}{1 + \varphi_c}, \tag{28}$$

$$W_{crit} = \rho_{rust} \left(\pi \left[\frac{C f_t}{E_{cf}} \left(\frac{R_i^2 + R_0^2}{R_0^2 - R_i^2} + \upsilon_c \right) + d_0 \right] D_i + \frac{W_{st}}{\rho_{st}} \right), \text{and} \tag{29}$$

$$T_{cr} = \frac{W_{crit}^2}{2k_p}, \tag{30}$$

where D_i is the diameter of the steel bar (mm), *C* is the thickness of concrete cover (mm), ρ_{rust} is the mass density of rust, d_0 is the thickness of the porous zone, W_{st} is the mass of corroded steel, α is the molecular weight of steel or corrosion products, φ_c is the creep coefficient (typically about 2.0), E_c is the elastic modulus of concrete, ρ_{rust} is the mass density of rust, and f_t is the tensile strength of steel.

Bhargava et al (2006) in their analytical model followed similar assumptions to Bažant and Liu. The solutions presented considering a simple two-zone model for the cover concrete, crack and uncracked zone. The time until cracking can be found from the following equations when R_c is equal to R_0,

$$\begin{aligned} u_c = d_c \big(& E_{ef1}[(1 - \upsilon_{c2})R_c^2 + (1 + \upsilon_{c2})R_0^2][2R_i R_c] \big) \\ & / \Big(E_{ef1}[(1 - \upsilon_{c2})R_c^2 + (1 + \upsilon_{c2})R_0^2] \big[(1 + \upsilon_{c1})R_c^2 \\ & + (1 - \upsilon_{c2})R_i^2 \big] - E_{ef2} \big(R_c^2 - R_i^2 \big)(R_c^2 - R_0^2)(1 - \upsilon_{c1}^2) \Big) \end{aligned} \tag{31}$$

$$R_c = \sqrt{\frac{1}{\left[\frac{f_t(1+\upsilon_{c2})}{E_{ef2}\left\{\frac{(1+\upsilon_{c2})u_c R_c R_0^2}{(1+\upsilon_{c2})R_0^2+(1-\upsilon_{c2})R_c^2}\right\}} - \frac{1}{R_0^2}\right]}}, \quad (32)$$

$$\rho_{rust} = \frac{\rho_{st}}{\alpha\alpha_1}, \quad (33)$$

$$D_2 = \frac{2(R_i + d_c)}{1 - \frac{d_c}{R_i}\left\{\frac{E_{ef1}(1-\upsilon_s)}{E_s\left(\frac{R_0^2+R_i^2}{R_0^2-R_i^2}+\upsilon_{c1}\right)}\right\}}, \quad (34)$$

$$\alpha_1 = 10.60138 - 12.67876\alpha + 1.50424\alpha^2, \quad (35)$$

$$W_r = \frac{\pi}{4}\rho_{rust}\alpha_1\left[\frac{D_2^2 - D_i^3}{\alpha_1 - 1}\right], \quad (36)$$

$$k_p = A_p \pi D_i i_{corr}, \text{and} \quad (37)$$

$$T_{cr} = \frac{W_r^2}{2k_p} \quad (38)$$

where, R_c is the radius of the crack front, R_0 is the outer radius of a thick concrete cylinder, u_c is the radial displacement at R_c, υ_c is the Poisson ratio of concrete, D_i is the diameter of the steel bar (mm), E_{ef} is the effective modulus of elasticity of concrete, *C* is the thickness of concrete cover (mm), d_0 is the thickness of the porous zone, W_{st} is the mass of corroded steel, α is the molecular weight of steel or corrosion products, φ_c is the creep coefficient (typically about 2.0), E_c is the elastic modulus of concrete, ρ_{rust} is the mass density of rust, f_t is the tensile strength of steel, E_s is the Young modulus of steel, α_1 is the volume expansion ratio for the expansive corrosion products, i_{corr} is the annual mean corrosion rate, i_{corr} is the corrosion current density (μA/cm^2), and A_p is constant.

Maaddawy (2007) presented a mathematical model to predict the time from corrosion to cracking. The concrete ring is assumed to crack when the tensile stresses in the circumferential direction at every part of the ring have reached the tensile strength of concrete. The time of cracking can be found from the following equation:

$$D' = D + 2d_0, \tag{39}$$

$$\psi = \frac{D'^2}{2C}(C + D'), \text{and} \tag{40}$$

$$T_{cr} = \left[\frac{7117.5(D + 2d_0)(1 + \upsilon_c + \psi)}{iE_{ef}}\right]\left[\frac{2cf_{ct}}{D} + \frac{2\delta_0 E_{ef}}{(1 + \upsilon_c + \psi)(D + 2d_0)}\right], \tag{41}$$

where D_i is the diameter of steel bar (mm), d_0 is the thickness of porous zone, *C* is the thickness of concrete cover (mm), υ_c is the Poisson ratio of concrete, E_{ef} is the effective modulus of elasticity of concrete, i is the current density, f_{ct} is the tensile strength of concrete, ψ is the factor that depends in D_i, C and d_0.

2.5.2 Area Loss

Once the protective layer on the rebar becomes damaged, the corrosion will start and the rust starts developing around the rebar. This process dissolves the reinforcement and causes the loss of rebar area. To measure this parameter, Thoft-Christensen (1996), proposed a simple method based on the rate of corrosion:

$$D(t) = D_i - i_{corr}.(t - T_i), \text{and} \tag{42}$$

$$A(t) = \begin{cases} nD_i^2\dfrac{\pi}{4} & for\ t \le T_i \\ n[D(t)]^2\dfrac{\pi}{4} & for\ T_i \le t \le T_i + D_i/i_{corr}, \\ 0 & t \ge T_i + D_i/i_{corr} \end{cases} \tag{43}$$

where, D_i is the diameter of steel bar (mm), i_{corr} is the corrosion current density (μA/cm2), A(t) is the area of reinforcement bars at the time t years, and n is the number of reinforcement bars. In this model it is considered that all the bars in the structure have similar diameter. For the general case Enright and Frangopol (1998) suggested the following equations:

$$D_j(t) = \begin{cases} D_{j0} & for\ t \le T_{i_j} \\ D_{j0} - i_{corr}\left(t - T_{i_j}\right) & for\ T_{i_j} \le t \le T_{i_j} + D_{j0}/i_{corr}, \text{and} \\ 0 & t \ge T_{i_j} + D_{j0}/i_{corr} \end{cases} \tag{44}$$

$$A(t) = \frac{\pi}{4}\sum_{j=1}^{n}\left[D_j(t)\right]^2, \tag{45}$$

where, D_{j0} is the diameter of steel bar (mm), and i_{corr} is the corrosion current density (μA/cm^2). Comparing this area loss between the estimated actual situation and that observed in accelerated aging tests of this study, the rate of accelerated aging may be established.

2.5.3 Corrosion Rate

Corrosion current density is related to the transport of electrical charges inside concrete and this number may vary greatly between 10^{-2} to 10^2 μA/cm^2 (SINTEF, 2008). This parameter is related to environmental conditions such as temperature and humidity, exposure time and chloride content (see Section 2.5.1). It has a strong effect on predicting the time of cracking and area loss as mentioned in Sections 2.5.1.2 and 2.5.2. There are different methods to measure the corrosion rate in the structure such as weight loss and electrochemical tests (polarization resistance technique). Weight loss can be measured through gravimetric methods that involve cleaning the corroded rebar in an acidic solution. Using Faraday's law of electrochemical equivalence, the corrosion rate in terms of the amount of steel dissolving and forming hydroxide/oxide may be calculated from the electric current as follows

$$m = \frac{i.t.a}{n.F}, \tag{46}$$

where, *m* is the mass of iron per area dissolved at the anode (g/m^2), *t* is time (s), *a* is the atomic mass of iron (55.8 g/mol), *n* is the number of electrons liberated in the anodic reaction, *F* is Faraday's constant (96487 C/mol), and *i* is the electric current density (A/m^2). If the mass density of iron is taken as 7.87 kg/dm^3, Faraday's law can be rewritten as

$$V_{corr} = 0.0116 i_{corr}, \tag{47}$$

where, V_{corr} is the corrosion rate (mm/year), and i_{corr} is corrosion current density (μA/cm^2). This relationship can be used to connect the gravimetric results to corrosion current density.

Two popular methods for measuring the polarization resistance are linear polarization resistance (LPR) and galvanostatic pulse. There are different models proposed to predict the corrosion rate based on experimental results. Most of these methods involve some constant parameter such as RH and temperature. Therefore, the results can be compared only if the specimens were tested under similar conditions. Liu (1996) proposed a model which contains temperature, concrete ohmic resistance, chloride content and exposure time versus corrosion rate based on almost 3000 measurements from 7 series of chloride-contaminated specimens and using multiple non-linear regression models. The regression results presented as follows:

$$i_{corr} = \frac{1}{1.08}\ln^{-1}\left(7.89 + 0.7771\ln 1.69C_{cl} - \frac{3006}{T} - 0.000116R_c + 2.24t^{-0.215}\right), \quad (48)$$

where, i_{corr} is the corrosion rate (μA/cm^2), C_{cl} is chloride content (kg/m^3), T is the temperature at the depth of steel surface (in degree Kelvin), R_c is resistivity of concrete (Ohm) and t is corrosion time (year). Although this model considers a rather large number of parameters, it has been calibrated through a limited number of cases.

2.6 Dry Cask Storage Systems (DCSS)

As the application of this project on real size structures, a dry cask storage system for nuclear waste was considered.

Dry cask storage systems (DCSS) were initially designed as interim storage of nuclear waste (Rigby, 2010). However, due to uncertainty in long-term storage, these dry storages are the only option currently in the United States (Attar et al., 2016).

In the United States, there are currently over 1,850 dry cask storage systems (DCSS) in 34 states at 75 sites (Howard and Akker, 2014; U.S. NRC, 2015). Over the next few decades, spent nuclear fuel (SNF), in increasing amounts, will have to be transferred from the pools to DCSS. If

the SNF production rate stays the same, by the time the last operating reactor is decommissioned in 2055, there will be approximately 140,000 metric tons of waste in DCSS (U.S. GAO, 2012); see Figure 8. This will increase the number of DCSS to 9,300.

The initial licensing term approved by the U.S. Nuclear Regulatory Commission (NRC) for dry storage is 20 years, which may be extended another 40 years (NEI, 2014; U.S. NRC, 2016). However, in the absence of a permanent storage facility, these casks might be used for longer periods. Therefore, it is important to understand the long-term performance of DCSS, particularly, the impacts of material aging. The majority of commercial spent fuel is stored in concrete storage casks or modules. As of 2012, 60.6% of casks had an exposed reinforced concrete (RC) overpack. Therefore, this study focused on DCSS with an exposed RC overpack. Out of all DCSS with an exposed RC overpack, 62.84% are in a horizontal and 37.26% are in a vertical configuration (Lambert et al., 2012; Leduc, 2012).

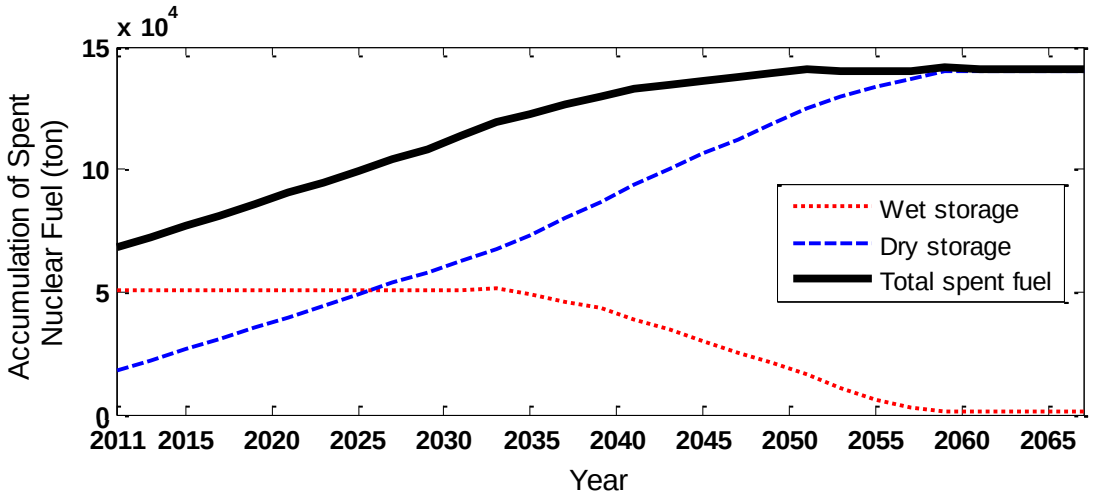

Figure 8 Trends in accumulation of spent nuclear fuel in the United States (U.S. GAO, 2012)

In this study, we focused on a vertical configuration for its higher vulnerability to other events such as tip-over impact in the case of a hazard and investigate the effect of ASR and corrosion on a 1/3 scale model through series of non-destructive testing.

3. EXPERIMENTAL PROGRAM FOR MATERIAL LEVEL TESTING

3.1 Materials Used in Research Project

Fine and Coarse Aggregates

In order to deliberately accelerate ASR for laboratory trials, a reactive fine aggregate (silica sand from the Brazos River near Houston, TX) was used. The coarse aggregate was regular and non-reactive. The gradations of coarse and fine aggregates are presented in Figure 9 (see also Table A 1 and Table A 2 in the appendix).

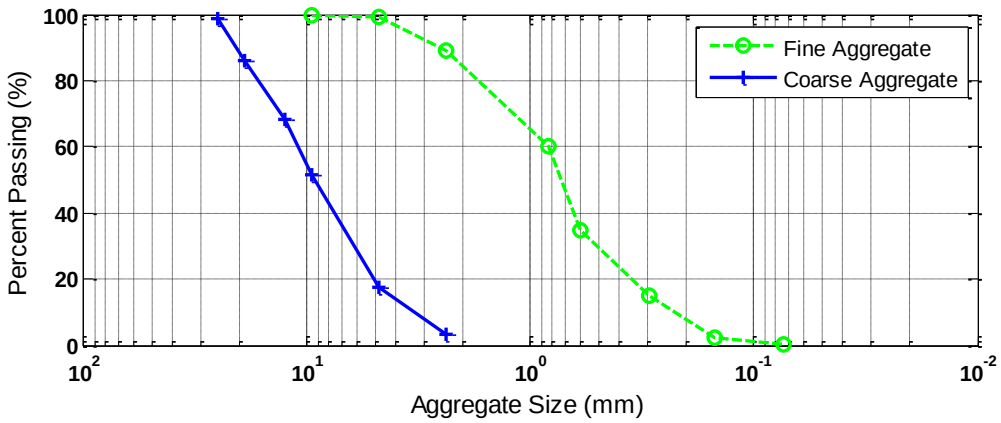

Figure 9 Gradations of aggregate used in preparing concrete specimens

For certain tests on hardened concrete, it is necessary to know the density, relative density and absorption of fine and coarse aggregate. Therefore these properties are measured based on ASTM C127-12 (2012e) and ASTM C128-12 (2012f) for coarse and fine aggregate, respectively. The results of these tests are shown in Table 10 (in this table OD represents the oven dry condition and SSD represents saturated surface dry).

Table 10 Density of Fine and Coarse Aggregate

Aggregate	Relative density (OD)	Relative density (SSD)	Density (OD) kg/m^3	Density (SSD) kg/m^3	Apparent density
Fine	2.40	2.42	2394.96	2409.42	2430.18
Coarse	1.62	1.64	1619.61	1635.08	1645.13

Potential alkali reactivity of fine aggregate

A mortar bar test was performed on two different mixes. One of the mixes was prepared following the recommendations of ASTM C1260 (2007) to measure the potential for deleterious ASR of fine aggregate. The other set was prepared with the same mix proportions but with the addition of 4% Cl^- by weight of cement (the same amount as for the other $CaCl_2$ specimens). The dimensions of the specimen are shown in Figure 10. Note that the reactivity of fine aggregate is tested here and these specimens were not prepared during the main casting but at a later date using the same mixture ingredients. Figure 11 and Figure 12 show the expansion of these two mixes up to 90 days.

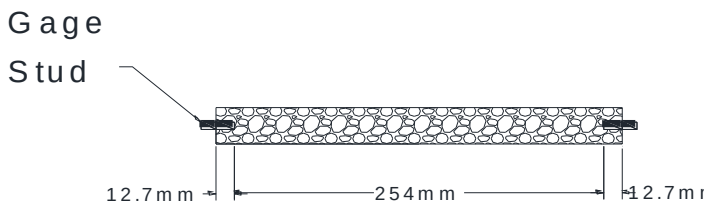

Figure 10 Specimen dimension for ASR expansion tests (ASTM C1260 (2007b)

At 14 days, if the expansion is less than 0.1%, the aggregate is characterized as non-reactive. On the other hand, when the expansion is over 0.2%, it means that the aggregate is reactive. If expansion falls between 0.1% and 0.2%, the test is inconclusive regarding the reactivity of the aggregate. From Figure 11, it is seen that the expansion is about 0.202% which shows that the aggregates are reactive. A comparison of the results indicates that the mortar mix with 4% Cl^- by weight of cement slightly reduces the expansion.

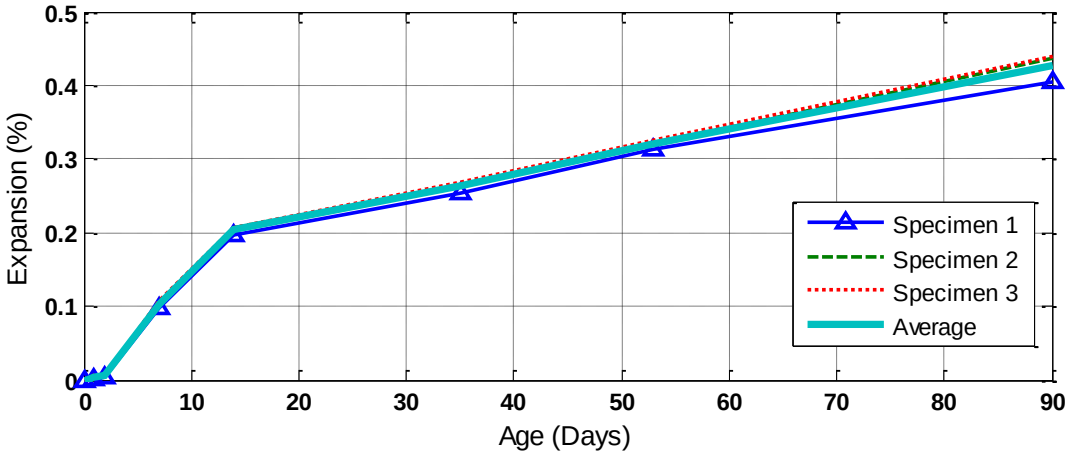

Figure 11 Expansion of regular mortar mix

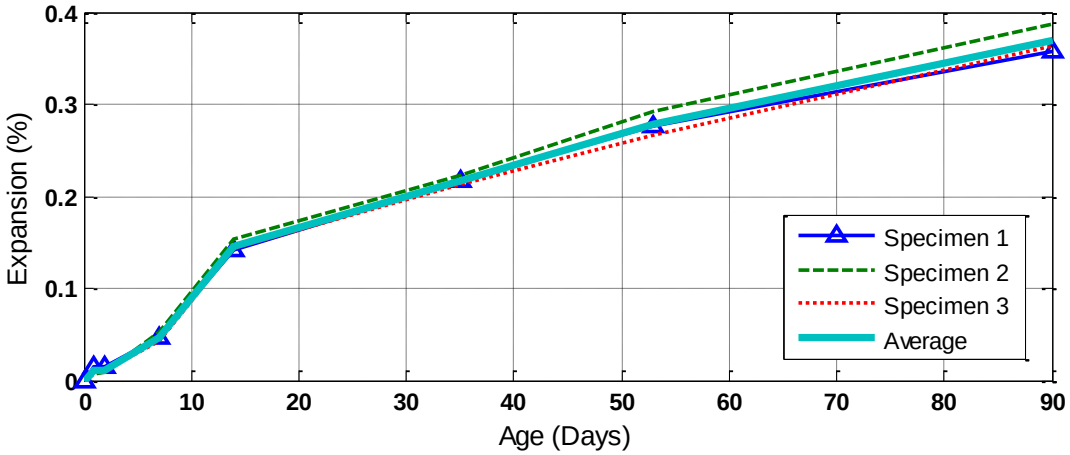

Figure 12 Expansion of regular mortar mix with 4% Cl^-

Potential alkali reactivity of coarse aggregate

The reactivity of coarse aggregate was also measured using the proposed accelerated concrete prism method (used in Guebec) (Berube and Fournier, 1993) by increasing the temperature to 80 °C and immersing the specimens in 1N NaOH. However, it should be noted that this test procedure is too severe compared to the method presented in ASTM C1293 (2008b) for finding the reactivity of coarse aggregate in long-term testing.. The limit suggested for this test was 0.04% at 4 weeks. Since the reactivity of coarse aggregate was intended to be measured, non-reactive fine aggregate was used in the specimens' preparation. Figure 13 shows the dimensions of

specimen prepared for this test. The results of this test are shown in Figure 14. According to the result, shown in Figure 14, the coarse aggregate were not reactive.

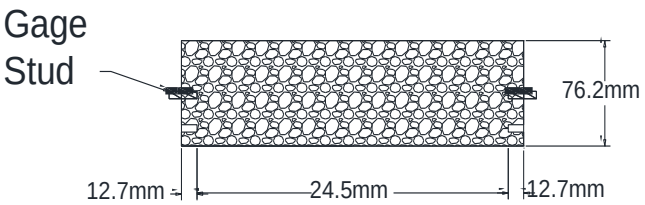

Figure 13 Specimen dimension for ASR expansion tests (ASTM C1293(2008b))

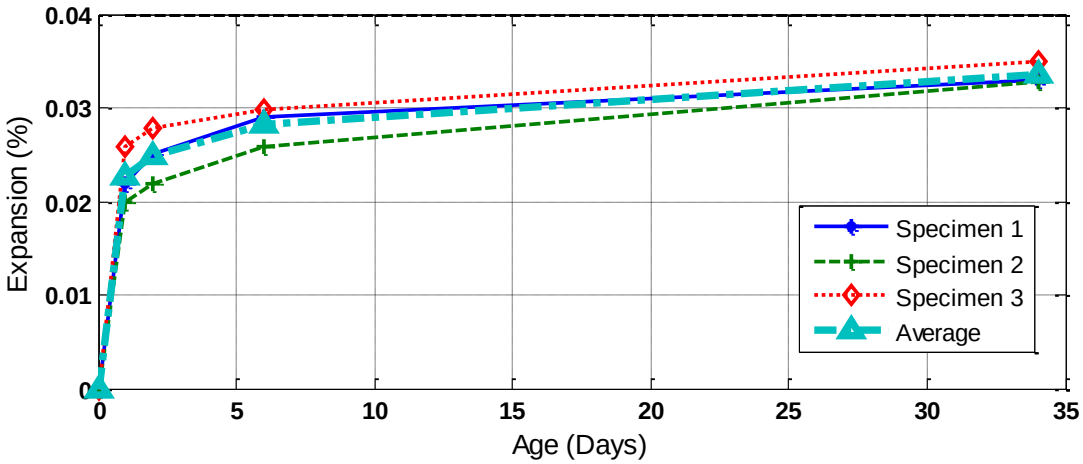

Figure 14 Expansion of regular mortar mix

Portland Cement

Based on ASTM C150 (2012c), there are ten types of Portland cement, I through V, air-entraining type IA, IIA, IIIA, and moderate heat of hydration II(MH), II(MH)A. In this study, type I/II Portland cement was used, which satisfies requirements for both Type I and Type II. In this cement, the strength requirements meet those for Type I, and composition requirements meet those for Type II. The chemical composition of the cement is given in Table 11. Physical properties of the cement reported by the manufacturer are provided in Table 12. The cement was tested based on ASTM C150 (2012c).The Na_2O equivalent in weight percent of cement was 0.49.

Table 11 Chemical Composition of Cement

Compound	Oxide (%)							Potential Compounds (%)		
	SiO_2	Al_2O_3	Fe_2O_3	CaO	MgO	SO_3	Na_2O_{eq}	C_3S	C_2S	C_3A
Percentage	21.11	4.43	3.87	63.96	1.54	2.48	0.49	58	17	5

Table 12 Physical and Mechanical Property Test Results on Cement

Physical Item	Spec. Limit	Test Result
Air content of mortar (volume %)	12 max	9
Fineness (cm^2/g) (Air permeability)	2800 min	3993
# 325 Fineness, % pass	Not Applicable	97
Autoclave expansion (%)	0.80 max	-0.01
Compressive strength (MPa)		
1 Day	Not Applicable	13.5
3 Days	12.0	22.0
7 Days	19.0	32.4
28 Days	Not Applicable	Not Applicable
Setting time (minutes) (Vicat)		
Initial	Not less than 45	84
Final	Not more than 375	210
False set (%)	Not Applicable	Not Applicable

Fly Ash

Fly ash is the finely divided residue that results from the process of combustion of ground or powdered coal. Fly ash is classified in three different types: Class N, Class F, and Class C. Class N fly ash is from raw or calcined natural pozzolans; Class F is produced from burning anthracite or bituminous coal; and Class C is produced from burning lignite or subbituminous coal. For this study, Class F fly ash was used. The chemical composition of fly ash is shown in Table 13. The Na_2O equivalent in fly ash was 0.84 weight percent. Physical properties of fly ash as reported by the manufacturer are provided in Table 14. The fly ash was tested based on ASTM C618 (2012b).

Table 13 Chemical Component of FlyAsh

Compound	SiO_2	Al_2O_3	Fe_2O_3	CaO	MgO	SO_3	Na_2O	K_2O	Na_2O_{eq}
Percentage	58.21	24.06	4.13	8.12	1.96	0.29	0.2	0.97	0.84

Table 14 Physical Property Test Results on Fly Ash

Physical Tests	Results	ASTM C618 (2012b) Class F/C	AASHTO M 295 (2011b) Class F/C
Moisture Content, %	0.01	3.0 max.	3.0 max.
Loss on Ignition, %	0.44	6.0 max.	5.0 max.
Amount Retained on No. 325 Sieve, %	30.72	34 max.	34 max.
Specific Gravity	2.22		
Autoclave Soundness, %	-0.03	0.8 max.	0.8 max.
Strength Activity Index with Portland Cement at 7 days, % of Control	75	75 min.	75 min.
Strength Activity Index with Portland Cement at 28 days, % of Control	87.2	75 min.	75 min.
Water Required, % of Control	96.7	105 max.	105 max.
Loose Bulk Density, kg/m^3	1081.2		

Chemical Admixtures

Chemical admixtures are the ingredients in concrete that help enhance the properties of hardened concrete during the process of preparation and mixing, transportation, placement and curing. Different types of these admixtures are used based on the necessary function for the concrete mixture: water-reducing admixtures, retarding admixtures, accelerating admixtures, superplasticizers, corrosion inhibition admixtures, workability enhancement, etc. For the self-consolidated mixture prepared for this study, two types of admixtures are used, MasterGlenium as superplasticizer and MasterPozzolith as normal plasticizer; both also have water-reducing function. The latter was used to control the setting time.

- *MasterGlenuim*

For the self-consolidated concrete mixture, MasterGlenium 7500 was used as the water-reducing admixture; it is added to the mix with a delayed addition to obtain its optimum water reduction.

- *MasterPozzolith*

Another water-reducing admixture used in the mixture that helps to make a more uniform and predictable mixture is MasterPozzolith 200. This normal plasticizer was added to the mix with a delayed addition similar to the MasterGlenium but it was dispensed separately.

Reinforcing Bars

In the design of the main cask, threaded rebar #19 is used, and #10 bar size conforms to the reinforcing bar size in the final scaled cask design. Therefore, tensile testing is performed on #10 and #19 rebar based on ASTM A370 (2012h) to characterize the stress-strain behavior. The results are shown in Figure 15 and Figure 16 for #10 and #19 rebar, respectively. The yield strengths of #10 and #19 rebar were found as 551.4 and 429.5 MPa, respectively. Other properties of the rebar are provided in Table 15.

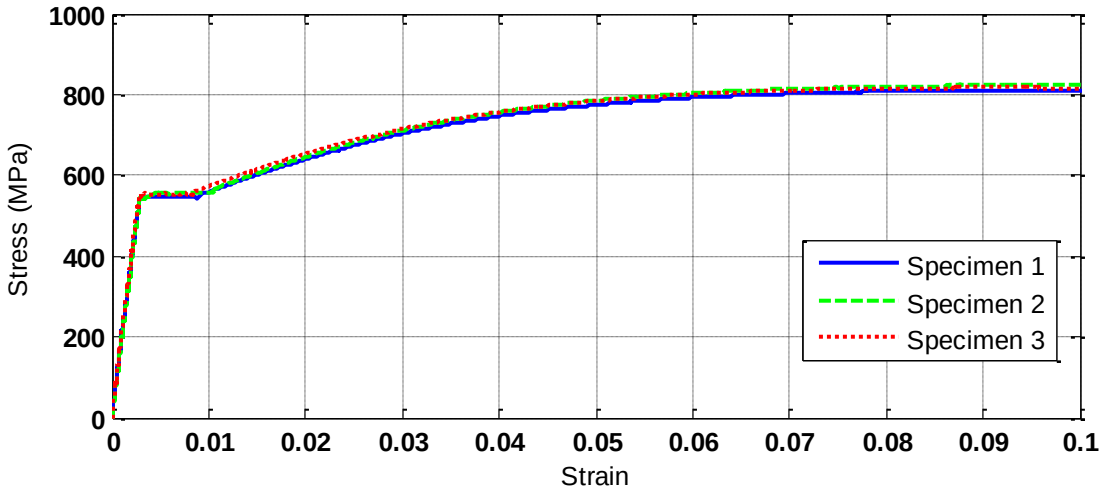

Figure 15 Tensile stress-strain behavior of #10 rebar

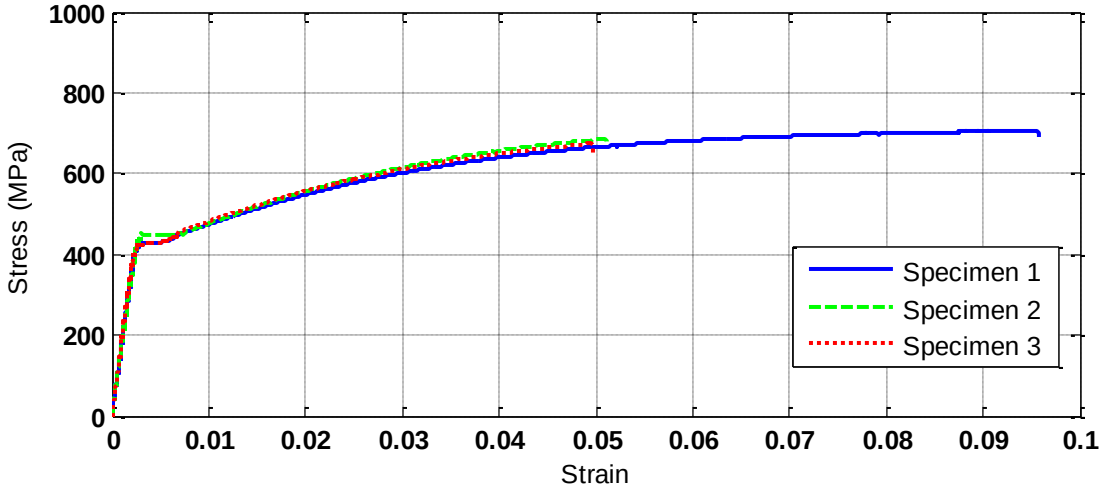

Figure 16 Tensile stress-strain behavior of #19 rebar

Table 15 Properties of Rebar

Rebar Size	Yield Stress (MPa)	Ultimate Stress (MPa)	Modulus of Elasticity (GPa)
#10	551.41	817.66	190.98
#19	429.54	728.78	175.37

3.2 Design of Concrete Mixtures

To understand the effects of NaOH and $CaCl_2$ on the fresh and hardened properties of concrete (such as slump, which is an indicator of workability of concrete, setting time and compressive strength), and to choose the maximum practical mixing amounts before the complete set of specimens was prepared, four different mixtures were studied. The first mix was prepared as a control without any additional $CaCl_2$ or NaOH. Sodium hydroxide was added to the second mix and the other two mixtures were prepared by adding calcium chloride. Table 16 shows the mixed proportions.

As explained above, using fly ash replacement of cement is one of the most effective ways to reduce ASR in concrete. Therefore, based on a literature review (Stanton, 1943a; Jones and Tarleton, 1958b; Ferraris, 1995; Smaoui et al., 2005; Bahadure and Naik, 2013), to get a higher expansion rate in a shorter period, fly ash was omitted from the second mix and 0.8% NaOH by weight of cement as an extra alkaline was added to the mixtures. To accelerate corrosion,

additional chloride ions (Cl^-) as $CaCl_2$ flakes were added in mixtures three and four, amounting to 4% and 7%, respectively, by weight of concrete. It should be noted that the amount of water for these mixes was adjusted based on the moisture content of coarse and fine aggregates. The percentage of evaporable moisture in a sample of aggregate was determined by drying both surface moisture and moisture in the pores based on ASTM C566 (2013f). The results of this test are provided in Table 17. Two tests were performed for each of the fine and coarse aggregates to obtain the results shown in Table 17.

Table 16 Proportions of the Concrete Mixtures

Material	Unit	Mixture 1	Mixture 2	Mixture 3	Mixture 4
Cement (~0.57% alkali content)	kg	12.84	37.70	12.84	12.84
Type F Fly Ash	kg	4.26	0.00	4.26	4.26
3/8" Pea Gravel (~0.3% expansion)	kg	48.67	48.67	48.67	48.67
Sand River (~0.3% expansion)	kg	43.09	43.09	43.09	43.09
Water	kg	5.72	5.72	5.72	5.72
Admix #1 (Pozzolith 200N)	ml	45.84	45.84	45.84	45.84
Admix #2 (Glenium 7500N)	ml	91.97	91.97	91.97	91.97
Additional Alkali (NaOH)	kg	-	0.15	-	-
Additional Chloride (CaCl2)	kg	-	-	0.78	1.36

Table 17 Moisture Contents of the Aggregates

Aggregate	Mass of original sample (g)	Mass of dried sample (g)	Moisture content (%)
Pea Gravel #1	828	804	2.99
Pea Gravel #2	884	860	2.79
Sand #1	427	403	5.96
Sand #2	417	390	5.84

Figure 17 shows different tests performed on the fresh concrete. The results of these tests for the four mixes are shown in Table 18. Adding chemicals especially calcium chloride, noticeably reduced the workability of the concrete. Adding 7% chloride by weight of concrete resulted in a slump of zero for this mix. The added chemicals considerably changed the setting time of the concrete as well. The effect of calcium chloride was substantially more than that of sodium

hydroxide; in particular mixture no. 4 set in about 15 minutes, which was considered unacceptable.

Figure 17 Tests on fresh concrete: (a) mix temperature (b) slump (c) sieving the concrete for setting time test

Table 18 Fresh and Hardened Properties of the Concrete Mixtures

Mix No.	Ambient Temp. (˚F)	Fresh Concrete		
		Mix Temp. (˚F)	Slump (mm)	Setting Time (min)
1	24	24.4	254	285
2	23	24.4	190.5	240
3	25.5	24.4	203.2	180
4	27.6	29.4	0	15

A compression test was performed on 101.6 x 203.2 mm cylinders at ages of 1, 7 and 28 days. The results of these tests are provided in Figure 18. As mentioned above, the last mix set in 15 min; therefore, no testing for hardened properties was performed for mixture no. 4. Based on these findings, 4% chloride by weight of cement was deemed suitable for the accelerated corrosion mixture design and mixture no. 2 was used to accelerate ASR. Furthermore, the results indicate that addition of chloride higher than 4% will reduce the workability in setting time to an unacceptable level. Therefore, for the second phase, to better understand the effect of the addition of these chemicals, different amounts between 0% to 4% chloride by weight of cement and 0% to 0.8% sodium hydroxide by weight of cement were chosen.

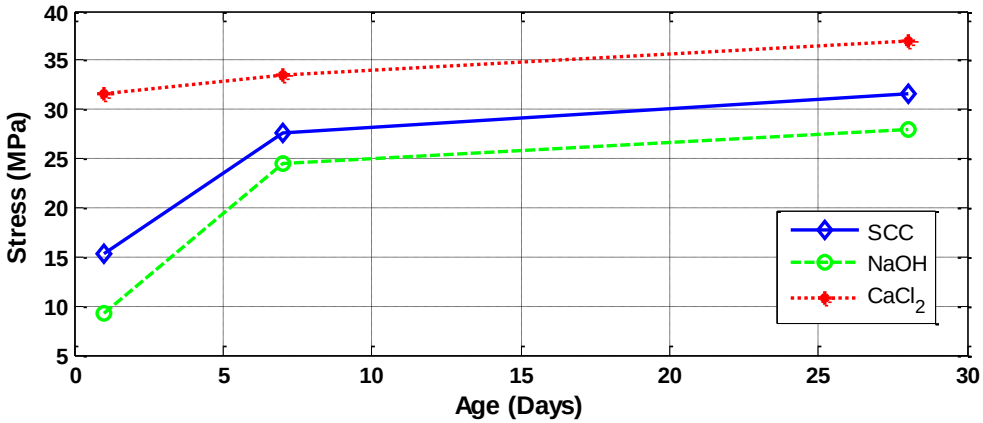

Figure 18 Compressive strength of concrete mixtures

3.2.1 Preparation of Test Specimens

Once the molds and test setups were prepared, the first phase of the project proceeded and the specimens were cast alongside the three scaled physical models of the casks with the mixtures designed as mentioned in previous sections; see Figure 19. The curing of the specimens for seven days is shown in Figure 20. The number of specimens prepared during the casting of the three concrete mixtures is shown in Table 19.

Figure 19 Casting of the concrete specimens

Figure 20 Sealed curing of the concrete specimens for the first seven days

Table 19 Number of Concrete Specimens, First Phase

Specimen Type	Specimen Size (mm)	SCC	NaOH-8	$CaCl_2$-4
Cylinder	101.6 x 203.2	65	65	50
Cylinder	76.2 x 152.4	26	28	21
Beam	101.6 x 101.6 x 355.6	30	33	31
Bond test specimen with #10 reinforcement, unconfined	152.4 x 152.4 x 152.4	7	9	8
Bond test specimen with #19 reinforcement, unconfined	152.4 x 152.4 x 152.4	8	8	8
Lollipop with #10 reinforcement	76.2 x 254	4	8	8
Lollipop with #19 reinforcement	127 x 254	3	8	9

The second phase of the project was performed on 8 other mixtures with different amounts of NaOH and $CaCl_2$. The first four were prepared with 0%, 0.2%, 0.4% and 0.8% of NaOH by weight of cement and the second four were prepared with 0%, 1%, 2% and 4% of chloride ion by weight of cement. The concrete mixtures of these concrete are shown in Table 20. In this table Admix #1 is Pozzolith 200N and Admix #2 is Glenium 7500N. These series of specimens were kept inside the lab for their first 28 days then were moved to the outside environment to go through the environmental cycles of temperature and humidity. Figure 21 shows some steps of the concrete preparation in the second phase of the project.

The naming of these mixtures in the texts are as follows: NaOH-0, NaOH-2, NaOH-4 and NaOH-8 for mixture with 0%, 0.2%, 0.4% and 0.8% of NaOH by weight of cement, respectively. Similarly, for $CaCl_2$ mixtures, $CaCl_2$-0, $CaCl_2$-1, $CaCl_2$-2, $CaCl_2$-4 were used for mixtures with addition of 0%, 1%, 2% and 4% chloride ion into the mixture, respectively. The number of specimens prepared in this phase is shown in Table 21. Between phases 1 and 2, a total of 880 specimens were prepared for this study.

Table 20 Properties of the Concrete Mixtures

Material	Unit	NaOH-0	NaOH-1	NaOH-2	NaOH-4	$CaCl_2$-0	$CaCl_2$-1	$CaCl_2$-2	$CaCl_2$-4
Cement	kg/m^3	431.55	431.55	431.55	431.55	323.80	323.80	323.80	323.80
Fly Ash	kg/m^3	-	-	-	-	107.55	107.55	107.55	107.55
Pea Gravel	kg/m^3	1227.54	1227.54	1227.54	1227.54	1227.54	1227.54	1227.54	1227.54
Sand River	kg/m^3	1086.99	1086.99	1086.99	1086.99	1086.99	1086.99	1086.99	1086.99
Water	kg/m^3	213.10	213.10	213.10	213.10	213.10	213.10	213.10	213.10
Admix #1*	ml/m^3	1155	1155	1155	1155	1155	1155	1155	1155
Admix #2**	ml/m^3	2320	2320	2320	2320	2320	2320	2320	2320
Add. NaOH	kg/m^3	-	0.92	1.84	3.67	-	-	-	-
Add. $CaCl_2$	kg/m^3	-	-	-	-	-	4.92	9.84	19.68

Figure 21 Casting of concrete specimens for second phase

Table 21 Number of Concrete Specimens, First Phase

Specimen Size	NaOH-0	NaOH-1	NaOH-2	NaOH-4	$CaCl_2$-0	$CaCl_2$-1	$CaCl_2$-2	$CaCl_2$-4
Cylinder 101.6 x 203.2 mm	36	39*	39*	39*	36	39*	39*	39*
Cylinder 76.2 x 152.4 mm	2	2	2	2	2	2	2	2
Beam 101.6 x 101.6 x 355.6 mm	6	6	6	6	6	6	6	6
Lollipop 76.2 x 254 mm with #10 reinforcement	-	-	-	-	6	6	6	6

* Three specimens cast as control mixture before adding chemicals to the mixtures

3.3 Testing Plan for First Phase of Specimens

As mentioned previously, three different concrete mixtures are considered. The first mixture is regular SCC (control) following the requirements of temperature and radiation shielding for dry casks as obtained from the literature as it relates to the case study application. The second mixture accelerates the alkali-silica reaction (ASR). This is achieved by increasing the alkalinity of the concrete mixture through sodium hydroxide (NaOH) addition and by replacing the aggregates with reactive ones. The third mixture design is a corrosive mixture, which is achieved by adding chloride ions (in the form of $CaCl_2$) to the fresh concrete. The specimens from these mixtures were prepared along with the casks. The details about the casks are provided in section 5. To plan the material testing, a comprehensive list of properties related to reinforced concrete is prepared as shown in Table 22. Among these properties, a selection was made considering the available knowledge in the literature and the objectives of this research. The selected properties to be measured are shown in bold font.

Table 22 Concrete Properties for Material Testing

Category	Property
Mix Properties	Aggregate content, mixing water content, water-to-cement ratio
Fresh Concrete	**Density, setting time, slump**, filling ability, passing ability, segregation resistance, air content
Mechanical	**Static elastic modulus, static Poisson's ratio**, dynamic elastic modulus, dynamic Poisson's ratio, **tensile strength**, **compressive strength**, flexural strength, tensile ductility, compressive ductility, fracture energy, creep function, shrinkage function, shear strength, dynamic shear modulus, bond strength, slip behavior
Physical	Concrete cover, air Content, acidity, **density**, **porosity**, **chemical composition (SEM/EDS), chloride content**, sorptivity, **absorption**, carbonation, leaching, pH, **cracking,** honeycombing, moisture content, sulfate resistance
Thermal	Conductivity, diffusivity, capacity, expansion/contraction
Transport	Chloride diffusivity
Other	Alkali silica reactivity, alkali carbonation reaction, corrosion potential, elongation

Material testing is mainly based on American Society for Testing and Materials (ASTM), Japanese Concrete Institute (JCI) and some European standardized tests. These tests are performed on fresh and hardened concrete. For fresh concrete setting time, horizontal free flow and density of concrete are measured. Tests for hardened concrete are density, absorption, and void (physical properties); compressive, splitting tensile, flexural, and bond strength, and fracture energy (mechanical properties); chloride penetration rate, and ASR mortar bar expansion (other properties). Furthermore, SEM/EDX measurement is performed on the concrete samples to see the effect of these changes on concrete matrix with time. The test plans are shown in Table 23.

Table 23 Test Plan for Concrete Mixtures

Temperature (ºC)	Room Temperature
Standards/ References	ASTM C39 (2012d), ASTM C496 (2011b), ASTM C78 (2010c), ASTM C1260 (2007b), ASTM C1293 (2008b), ASTM C642 (2013b), ASTM G1-03 (2011a), NT-build 208 (1996), NT-build 443(1995), JCI-S-001 (2003), ASTM C1723 (2010a)
Specimen type	Cylinders for compressive and split tensile strength (101.6 x 203.2 mm)
	Cylinders for density, absorption and void (76.2 x 152.4 mm)
	Un-notched prisms for flexural strength (101.6 x 101.6 x 355.6 mm)
	Notched prisms for fracture energy (101.6 x 101.6 x 355.6 mm) Notch depth is 30% of the prism depth ±5 mm. Note: Molds for un-notched prisms are used here. Notches are made with a concrete saw.
	Chloride penetration specimens (for SCC and NaOH mixes) Diameter at least 75 mm and not more than 3 times the maximum aggregate size, and length should be minimum 100 mm for Nordtest
	Lollipop specimen for mass loss measurement 76.2x 254 mm cylinder, having #10 bar in the middle 127x 254 mm cylinder, having #19 bar in the middle
	Mortar-bar specimen for ASR (for SCC and $CaCl_2$ mixes only) 25.4 x 25.4 x 285.75 mm prisms having 254 mm gauge length for reactivity of fine aggregate 76.2 x 76.2 x 285.75 mm prisms, having 254 mm gauge length for reactivity of coarse aggregate
Property measured	Compressive strength, splitting tensile strength, flexural strength, fracture energy, bond strength , chloride permeability, alkali reactivity, density, absorption and void, pH
Test ages	Compressive and splitting tensile strength tests: 1, 3, 7 and 28 days, 6 and 12 **Other tests:** 28 days, 6 and 12 months

3.4 Testing Plan for Second Phase of Specimens

To test the effect of different amounts of NaOH and $CaCl_2$ on the concrete mixture and determine the optimum amounts of chemicals to add for accelerating the aging process in the concrete structures additional specimens were prepared. Four different mixtures with 0%, 0.2%, 0.4% and 0.8% NaOH by weight of cement were considered. The fly ash was removed from these mixes and replaced with cement in order to accelerate the alkali-silica reactions. Four other mixtures with 0%, 1%, 2% and 4% chloride ion by weight of cement have also been prepared. Table 24 shows the testing program for NaOH and $CaCl_2$ mixtures.

Table 24 Test Plan for Concrete Mixtures Containing Different Levels of NaOH and $CaCl_2$

	NaOH	$CaCl_2$
Standards/ References	ASTM C39 (2012d), ASTM C496 (2011b) (2011), ASTM C78 (2010c), ASTM C469 (2014b), ASTM C805 (2013e)	ASTM C39 (2012d), ASTM C496 (2011b), ASTM C78 (2010c), ASTM C469 (2014b), ASTM G1-03 (2011a), ASTM C805 (2013e)
Specimen type	Cylinders for compressive and split tensile strength (101.6 x 203.2 mm)	
	Cylinders for density, absorption and void (76.2 x 152.4 mm)	
	Un-notched prisms for flexural strength and measuring the length change (101.6 x 101.6 x 355.6 mm)	
	Rapid chloride penetration specimens Cutting 50.8 mm height of 101.6 x 203.2 mm Cylinders	Lollipop specimen for mass loss and half-cell potential measurement 76.2 x 254 mm cylinder, having #3 bar in the middle
Property measured	Compressive strength, splitting tensile strength, flexural strength, static modulus of elasticity, static Poisson's ratio, rapid chloride permeability, density, absorption and void, UPV, surface resistivity, length change	Compressive strength, splitting tensile strength, flexural strength, static modulus of elasticity, static Poisson's ratio, rapid chloride permeability, density, absorption and void, UPV, surface resistivity, half-cell potential, corrosion (mass loss)
Test ages	**Flexural test:** 28 days and 6 months Density, absorption and void: 28 days **Other tests:** 7 and 28 days, 3 and 6months	
Specimen number	A minimum of 3 specimens will be tested at each age and for each test	

3.5 Testing Plan for Already Aged Specimens Obtained from a Research Nuclear Reactor

TRIGA (Training, Research, Isotopes, and General Atomics) is a class of small reactors which are designed and built for scientific institutions and universities. Specimens from the thirty-eight-year-old research reactor TRIGA MARK II, located inside a building at the campus of University of Illinois at Urbana Champaign (UIUC), which was decommissioned in 2012, were secured for testing and analysis in this study. Specimens 203 mm in diameter and 457 mm in length were obtained. These specimens were used for material characterization at the University of Houston (UH). All the samples were shipped to UH from UIUC.

Figure 22 Picture of the biological shielding wall of the decommissioned UIUC TRIGA reactor. Numbered holes show the locations from where the concrete samples have been taken. Cylindrical shaped samples in front of the holes (right panel) can also be seen

Figure 23 Picture of the seven samples

The testing plan considered for these specimens is presented in Table 25. To be able to perform mechanical testing on these concrete samples it is required to drill smaller cores taken from the TRIGA Reactor.

Table 25 Test Plan for TRIGA Specimens

Standards/ References	ASTM C39-12 (2012d), ASTM C496-11 (2011b), ASTM C642-13 (2013b), NT-build 208 (1996), NT-build 443 (1995), SEM test
Specimen type	***Cylinders*** (Diameter: max [3.7", at least two times the nominal maximum size of the coarse aggregate]. Length: between 1.9 to 2.1 of diameter)
	Chloride Penetration Specimens Diameter at least 75 mm and not more than 3 times maximum aggregate size and length should be minimum 100 mm for ***Nordtest*** (NT-build, 1995)
Property measured	Compressive strength, splitting tensile strength, chloride amount, chloride permeability, alkali reactivity, density, absorption and void, carbonation depth

3.6 Outdoor Exposure Site

The site of reinforced concrete structures has a great influence on the curing and aging. In particular, climate and exposure conditions are important. Climate can be defined as the large-scale conditions concerning temperature, wind, precipitation, etc. The climate can be studied in three different scales: regional climate, local climate, and near surface and surface climate. It was decided that after the concrete specimens were prepared and completed the curing process, the

specimens would be stored in an outside environment at the University of Houston structural lab (South Park Annex) in Houston, Texas. The location of the lab is shown in Figure 24.

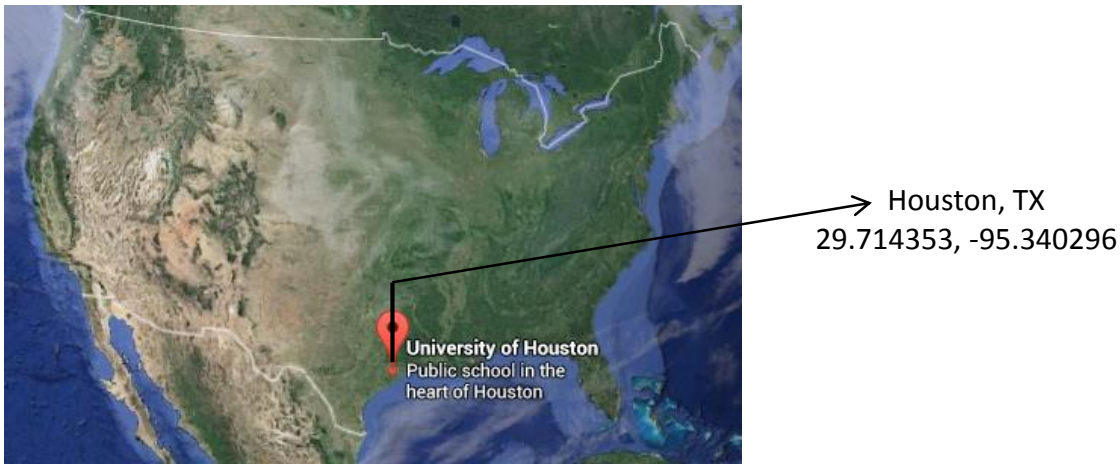

Figure 24 Specimen storage location (Google, 2015)

Weather averages of Houston as a regional climate based on averaging the climate data from 1981 to 2010, are shown in Table 26.

Table 26 Houston Weather Averages (NOAA, 2016)

Average annual high temperature	26.5 ˚C
Average annual low temperature	15.5 ˚C
Average temperature	21 ˚C
Average annual precipitation – rainfall	1264 mm

To study the effect of climate more closely, near surface climate was measured. To determine the temperature and relative humidity conditions near or on a surface, the sensor for these measurements is placed less than 10 m away from the specimens and the data were continuously recorded during the time. These data are shown in Figure 25.

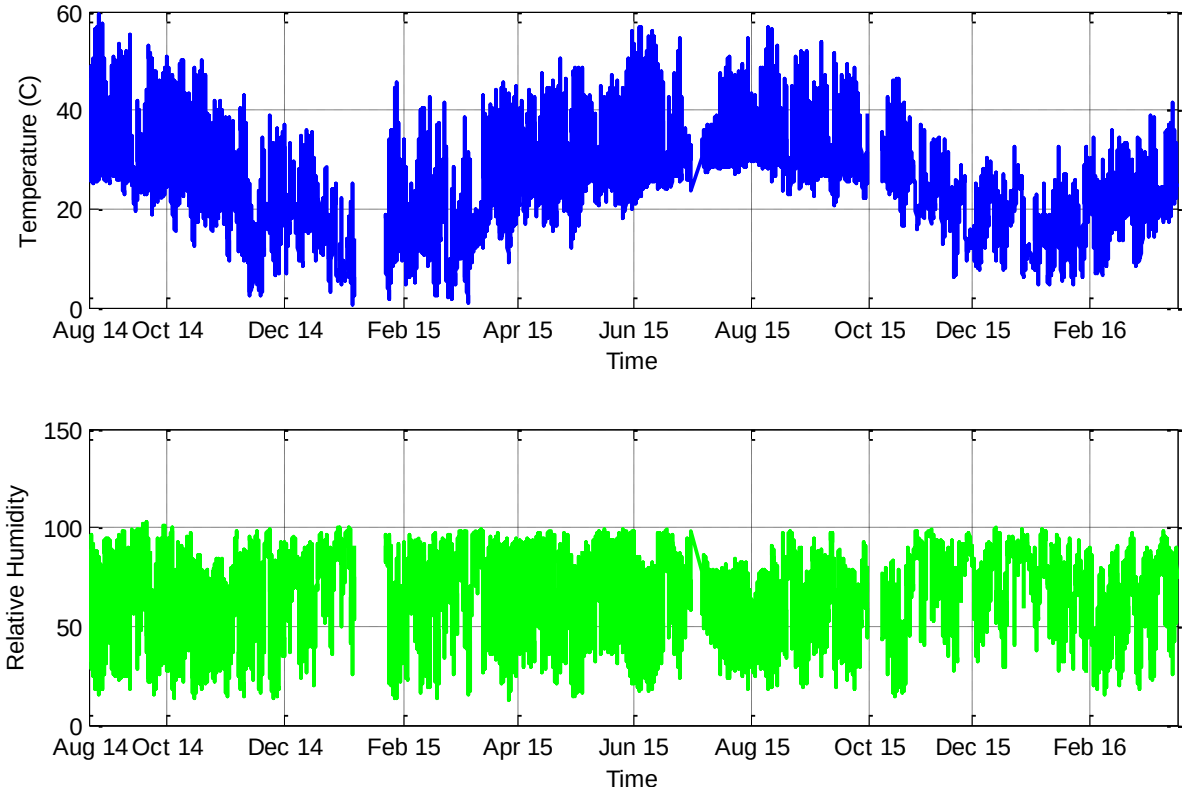

Figure 25 Ambient temperature and relative humidity

4. MATERIAL LEVEL TEST RESULTS

4.1 Fresh Properties of Concrete

Addition of different amounts of sodium hydroxide and calcium chloride affects the fresh properties of concrete such as setting time, density and slump. These are discussed in this section.

4.1.1 Setting time

The degree of stiffening of a mixture is measured based on ASTM C403 (2008a) and using the penetration resistance apparatus shown in Figure 26. After the concrete is mixed, it is sieved through the 4.75 mm sieve; thereafter, the mortar obtained is mixed thoroughly and placed inside a cylindrical container with a size of 76.2 x 76.2 mm. Prior to making a penetration test, the bleeding is removed using a pipette. The force for penetrating the needle 25 mm into the mortar is measured every hour.

Figure 26 penetration resistance apparatus

Calcium chloride is one of the inorganic accelerators that is being used in the construction of concrete structures to decrease the setting time (or increase the hardening rate). In this study, addition of 4% chloride in the concrete mixture decreases the setting time from 285 minutes to 180 minutes, which is about 37% reduction. The results of addition of $CaCl_2$ and NaOH to the

mixtures and their effect on setting time are shown in Table 27. It was seen that the setting time decreased substantially for the $CaCl_2$ mixture. The effect of NaOH on the setting time was less drastic. Different studies investigated the effect of alkali on these two properties (Hewlett, 2004; Allahverdi and Ghorbani, 2006; Memon et al., 2013). Their results indicate the reduction in setting time of concrete is in accordance with the results of this study.

Table 27 Setting Time of Fresh Concrete, Phase 1

Mix	Setting Time (min)
SCC_PH1	285
NaOH-8_PH1	240
$CaCl_2$-4_PH1	180

4.1.2 Density

The density measurements on fresh concrete based on ASTM C1611 (2009b) and using a gravimetric method were performed; see Figure 27. The results are provided in Table 28, Table 29 and Table 30. The density of fresh concrete in all mixtures is approximately the same and these chemicals do not have a significant effect on density.

Figure 27 Measuring the density of fresh concrete

Table 28 Density of Fresh Concrete, Phase 1

Mix	Average Density (g/cm^3)
SCC_PH1	2.325
NaOH-8_PH1	2.319
$CaCl_2$-4_PH1	2.347

Table 29 Density of Fresh Concrete, NaOH Mixtures, Phase 2

Mix	Average Density (g/cm^3)
NaOH-0_PH2	2.36
NaOH-2_PH2	2.41
NaOH-4_PH2	2.42
NaOH-8_PH2	2.38

Table 30 Density of Fresh Concrete, $CaCl_2$ Mixtures, Phase 2

Mix	Average Density (g/cm^3)
$CaCl_2$_0_PH2	2.31
$CaCl_2$_1_PH2	2.36
$CaCl_2$_2_PH2	2.33
$CaCl_2$_4_PH2	2.30

4.1.3 Horizontal free flow (slump)

A horizontal free flow test is performed on fresh concrete and passing abilities of the concrete mixtures were measured based on ASTM C1688 (2013a). This test measures the behavior of a compacted inverted cone of concrete under gravity as shown in Figure 28.

Figure 28 Slump test

The results are also provided in Table 31, Table 32 and Table 33. The slump was found to be very similar in each series of the mixtures. However, the addition of chloride, especially when the chloride amount is in higher concentration decreased the workability and slump of the concrete mixture. The difference between the measured slump for each series and in different phases is due to the differences in the volumes of the mix in each phase. The volume of concrete in the first phase was 3 yd^3 and this volume for the second phase for each mix was about 3.5 ft^3. Furthermore, different temperatures at the time of pouring concrete and casting the specimens is another source of difference.

Table 31 Slump Test Results, Phase 1

Mix	Average Slump (mm)
SCC_PH1	271.8
NaOH-8_PH1	228.6
$CaCl_2$-4_PH1	275.1

Table 32 Slump Test Results, NaOH Mixtures, Phase 2

Mix	Average Slump (mm)
NaOH-0_PH2	19.1
NaOH-2_PH2	25.4
NaOH-4_PH2	25.4
NaOH-8_PH2	25.4

Table 33 Slump Test Results, $CaCl_2$ Mixtures, Phase 2

Mix	Average Slump (mm)
$CaCl_2$_0_PH2	254.0
$CaCl_2$_1_PH2	254.0
$CaCl_2$_2_PH2	215.9
$CaCl_2$_4_PH2	203.2

4.1.4 Curing temperature

The temperature inside the concrete was measured from the casting time using the k-type thermocouple. Adding calcium chloride to the mixture slightly increased maximum hydration temperature in comparison to SCC, from 60.71°C to 63.95°C, in the first phase. The sodium hydroxide slightly decreases the hydration temperature and which was 59.21°C.

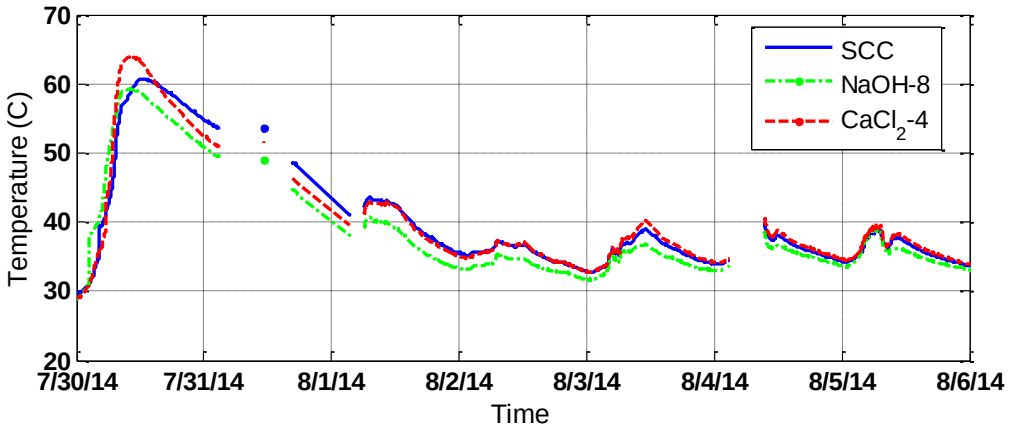

Figure 29 Effect of NaOH and $CaCl_2$ on the hydration temperature, phase 1

4.2 Physical Properties of Hardened Concrete

4.2.1 Density, absorption and void

Density, absorption and voids in hardened concrete are measured according to ASTM C642 (2013b) and based on the conversion between mass and volume. The weight of concrete is measured under different conditions: after drying in an oven for more than 24 hours at a temperature of 110˚C, after immersing in water until it is completely saturated, after boiling in water for 5 hours, and finally when immersed inside water and hanging with a wire to determine the apparent mass. Boiling and immersion of concrete is shown in Figure 30. After determining the mass of concrete specimens in these procedures, bulk density and absorption in different conditions as well as void space were calculated using the following equations

$$Absorption\ after\ immresion, \% = \frac{B - A}{A} \times 100, \tag{49}$$

$$Absorption\ after\ immersion\ and\ boiling, \% = \frac{C - A}{A} \times 100, \tag{50}$$

$$Bulk\ density, dry = \left(\frac{A}{C - D}\right)\rho = g_1, \tag{51}$$

$$Bulk\ density\ after\ immersion = \left(\frac{B}{C - D}\right)\rho, \tag{52}$$

$$Bulk\ density\ after\ immersion\ and\ boiling = \left(\frac{C}{C - D}\right)\rho, \tag{53}$$

$$Apparent\ density = \left(\frac{A}{A - D}\right)\rho = g_2, \text{and} \tag{54}$$

$$Volume\ of\ permeable\ pore\ space(voids), \% = \frac{g_2 - g_1}{g_2} \times 100. \tag{55}$$

where, *A* is mass of the oven-dried sample in air (g), *B* is mass of the surface-dry sample in air after immersion (g), *C* is mass of the surface-dry sample in air after immersion and boiling (g), *D* is the apparent mass of sample in water after immersion and boiling (g), g_1 is the bulk density dry (Mg/m^3), g_2 is apparent density, (Mg/m^3), and ρ is the density of water (1 g/cm^3)

Figure 30 (a) Boiling the specimens in water (b) measuring the weight of the specimens immersed in water

Density, absorption and voids in hardened concrete of all 8 mixtures in the second phase were measured at 28 days; see Figure 31 and Figure 32 (see also Table A 7 to Table A 10 in the appendix). Different amounts of NaOH and $CaCl_2$ did not have significant effects on the density, void and absorption of the concrete mixture. These properties were also measured on the specimens of the first phase (SCC, NaOH-8 and $CaCl_2$-4 concrete mixtures) at three different ages of 28, 210 and 365 days. The average results of two measurements of each property are provided in Table 34 and Table 35 and it is clear that these properties do not vary substantially with time.

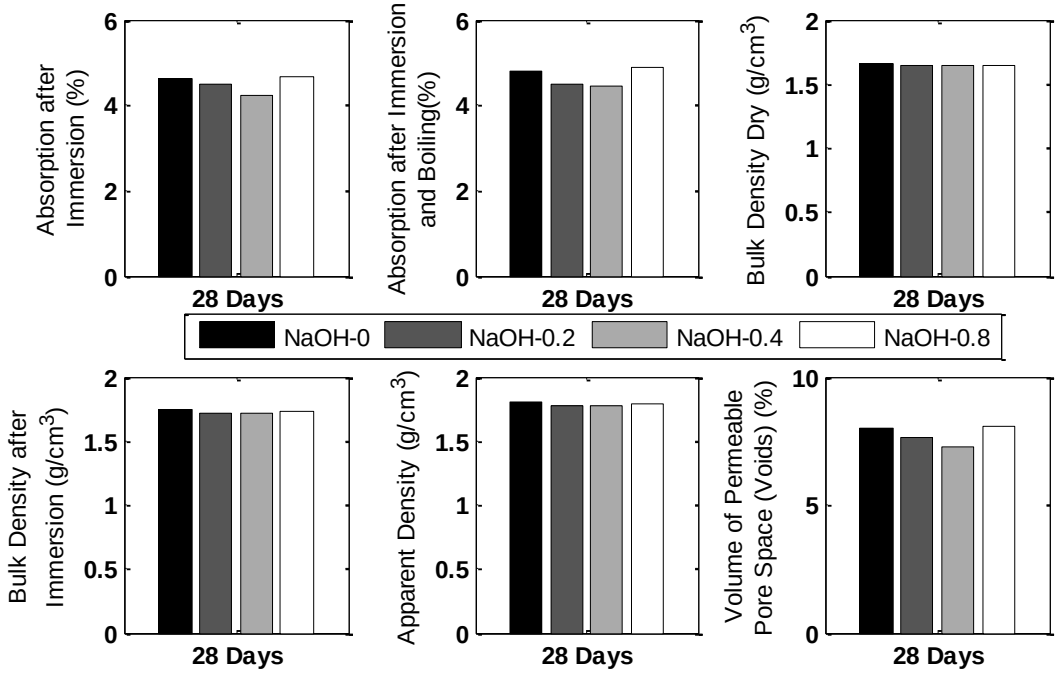

Figure 31. NaOH mixture density, void and absorption

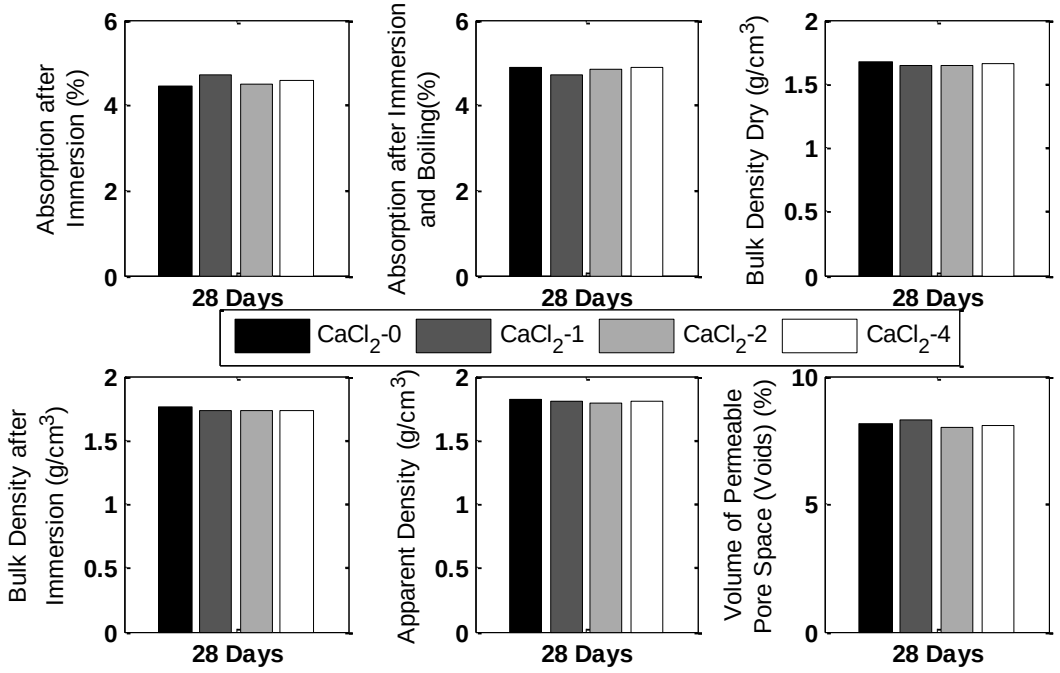

Figure 32 $CaCl_2$ mixture density, void and absorption

Table 34 Density of Hardened Concrete, Phase 1

Mix	Bulk Density, Dry (g/cm^3)			Bulk Density after Immersion (g/cm^3)			Apparent Density (g/cm^3)		
	28 day	210 day	365 day	28 day	210 day	365 day	28 day	210 day	365 day
SCC_PH1	1.66	1.68	1.65	1.76	1.78	1.75	1.85	1.87	1.83
NaOH-8_PH1	1.65	1.59	1.63	1.75	1.71	1.75	1.84	1.79	1.84
$CaCl_2$-4_PH1	1.65	1.63	1.63	1.76	1.76	1.74	1.85	1.87	1.84

Table 35 Absorption and Voids of Hardened Concrete, Phase 1

Mix	Absorption after Immersion (%)			Absorption after Immersion and Boiling (%)			Volume of permeable pore space (voids) (%)		
	28 day	210 day	365 day	28 day	210 day	365 day	28 day	210 day	365 day
SCC_PH1	5.5	5.6	5.4	6.0	6.2	5.9	10.0	10.4	9.7
NaOH-8_PH1	5.7	6.1	6.5	6.2	6.8	7.3	10.2	10.9	11.9
$CaCl_2$-4_PH1	6.5	6.7	6.6	6.8	7.5	7.2	11.1	12.3	11.6

These properties were also measured on already aged specimens of TRIGA reactors. The average density of aged specimens as the specimens received to the lab was found to be 2.71 g/cm^3. The results of gravimetrical measurement on these specimens are shown in Table 36 and Table 37. These properties, density, absorption and void, measured from the TRIGA reactor specimens are similar to the mixtures that were prepared in the lab.

Table 36 Density of TRIGA Specimens

No.	Bulk Density, Dry (g/cm^3)	Average	Bulk Density after Immersion (g/cm^3)	Average	Apparent Density (g/cm^3)	Average
1	1.50	1.49	1.60	1.58	1.66	1.64
2	1.49		1.58		1.64	
3	1.48		1.58		1.64	

Table 37 Absorption and Voids of TRIGA Specimens

No.	Absorption after Immersion (%)	Average	Absorption after Immersion and Boiling (%)	Average	Volume of permeable pore space (voids) (%)	Average
1	5.8	5.8	6.3	6.4	9.4	9.4
2	5.7		6.2		9.2	
3	5.9		6.6		9.8	

4.2.2 Chloride content

Chloride content tests were performed on all the mixtures in the first phase. Figure 33 shows various steps of the NT-build 208 (1996) test used for measuring the chloride content. Figure 33(a) shows the concrete powder obtained from cylinders made with different mixtures and kept inside the oven for two hours at 105˚C; in Figure 33(b) distilled water and nitric acid were added to the concrete powder to dissolve the chloride in the solution; the solution containing ions of chloride is added to an excess of silver nitrate. The chlorides precipitate as silver nitrate. Figure 33(c) shows the last step when the color of the solution changes to bright red when just enough silver nitrate and ammonium thiocyanate is added to the solution to titrate the Cl^-. In this reaction the excess of thiocyanate ions is indicated by the formation of a red iron(III)-complex. The amount of chlorides (Cl^-) is calculated according to the formula:

$$Weight - \%Cl^- = 3.545\frac{V_1N_1 - V_2N_2}{m} \quad (56)$$

where, V_1 is the added amount of silver nitrate solution (ml), N_1 is the normality of the silver nitrate solution, V_2 is the amount of ammonium thiocyanate solution added during the titration (ml), N_2 is the normality of ammonium thiocyanate solution and m is the weight of the sample (g).

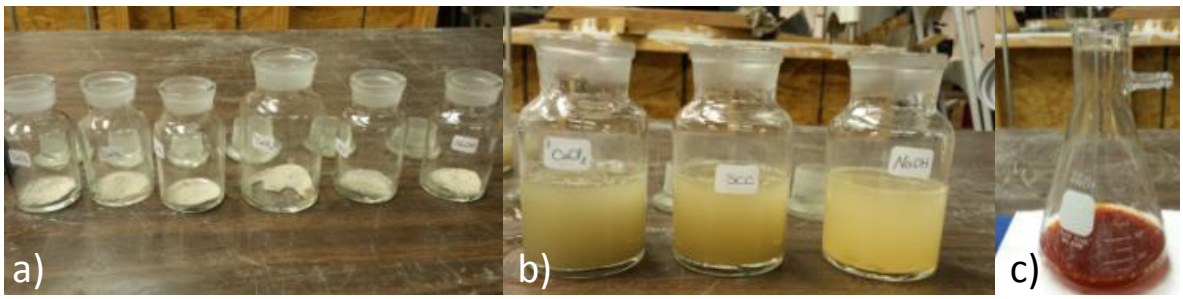

Figure 33 (a) concrete powder (b) concrete dissolved in solution (c) changing the color of solution because of indicator

The chloride content of each mixture from phase 1 is shown in Table 38. As expected, there was a negligible amount of chloride in SCC and NaOH-8 mixes and the amount of chloride in the $CaCl_2$-4 mixture was consistent with what was intended.

Table 38 Chloride Content of Concrete Mixtures, Phase 1

Mix	Percent Cl^-	Average weight percent Cl^- of the weight of concrete
SCC_PH1	0.0143	0.01
NaOH-8_PH1	0.0215	0.02
$CaCl_2$-4_PH1	0.6112	0.60
	0.5932	
	0.6069	
	0.6040	

4.2.3 Chloride penetration

Chloride ion penetration in concrete indirectly measures the permeability of concrete as a characteristic parameter of durability and its resistance to corrosion. The permeability of concrete and diffusion of the chloride ion is strongly influenced by the type of cement, and the type and proportions of blending materials such as fly ash (Roy et al., 1987). To measure this parameter NT build 443 (1995) is used. To perform this test, the concrete specimens should be at least 28 days old. After the concrete reaches this age, the specimen is cut in half and immersed in calcium hydroxide solution until it reaches a weight that does not change more than 0.1% within a 24 hour period. After that, three sides of the specimens are sealed with epoxy to create a 1-D diffusion case and the specimen is placed inside the NaCl solution for at least 35 days; the concrete powder was collected from different depths and the amount of chloride at is measured in these depths at desired ages. Figure 34(a) shows the specimens inside the $Ca(OH)_2$ solution and Figure 34 (b) shows them inside the NaCl solution.

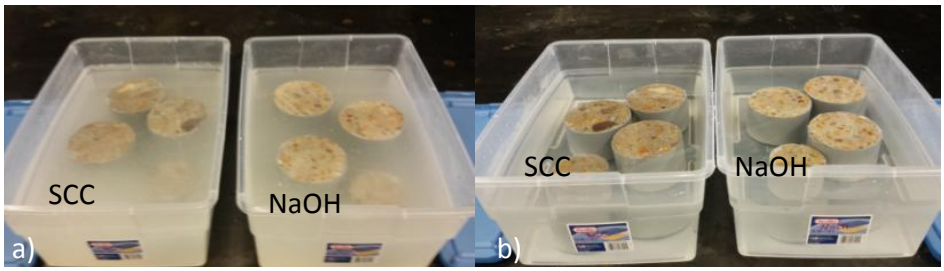

Figure 34 Concrete specimens in (a) $Ca(OH)_2$ solution (b) NaCl solution

After ponding the specimens, the general form of Fick's second law, as shown in equation (13), defined in Section 2.5.1.1, was used to calculate effective chloride transport coefficient and the boundary condition of the chloride profile at the exposed surface. It should be noted that chloride resistance of the concrete is presented in terms of effective chloride transport coefficient.

This bulk diffusivity test was performed on SCC and NaOH-8 mixtures from first phase, as well as on the already aged specimens of the TRIGA Reactor. The results of these tests are shown in Figure 35 and Figure 36. It is seen that for the concrete with fly ash and no NaOH addition (i.e., SCC mixture), the diffusivity is significantly lower than the mix without fly ash and 8% NaOH addition. This difference is attributed to the presence of NaOH but more importantly to the reduced diffusivity of the SCC mixture due to the presence of fly ash (Bilodeau and Malhotral, 1992; Naik et al., 1994; Naik et al., 1995). As shown in Table 39, the diffusivity of the SCC mixture remained more or less the same over time; while the diffusion increased by 30% at 365 days in comparison to 28 days measurement. Most of these changes was between 210 days 365 days. This increase is related to the increased interconnectivity of micro-cracks due to ASR gel expansion.

The average of effective chloride transport coefficient measured on aged TRIGA specimens was 3.85e-12 m^2/sec which was closer to the coefficient measured for the SCC mixture at 365 days.

Table 39 Average Effective Chloride Transport Coefficient, Phase 1

Mix	28 Days	210 Days	365 Days
	D_e (m^2/sec)	D_e (m^2/sec)	D_e (m^2/sec)
SCC_PH1	9.55E-12	1.09E-11	1.10E-11
NaOH-8_PH1	5.01E-11	5.10E-11	7.27E-11

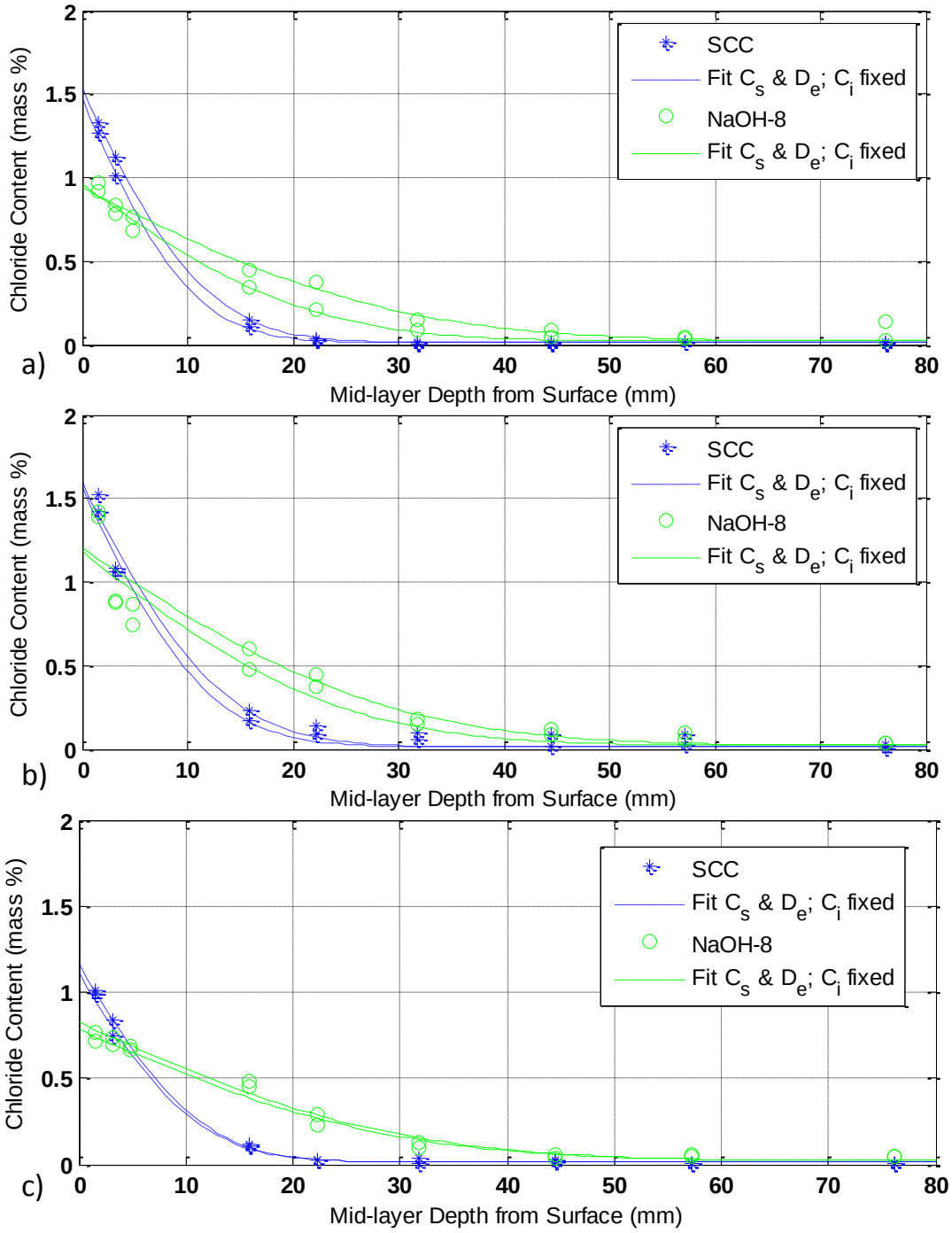

Figure 35 Accelerated chloride test on SCC and NaOH-8 concrete specimens at (a) 28 (b) 210 (c) 365 days

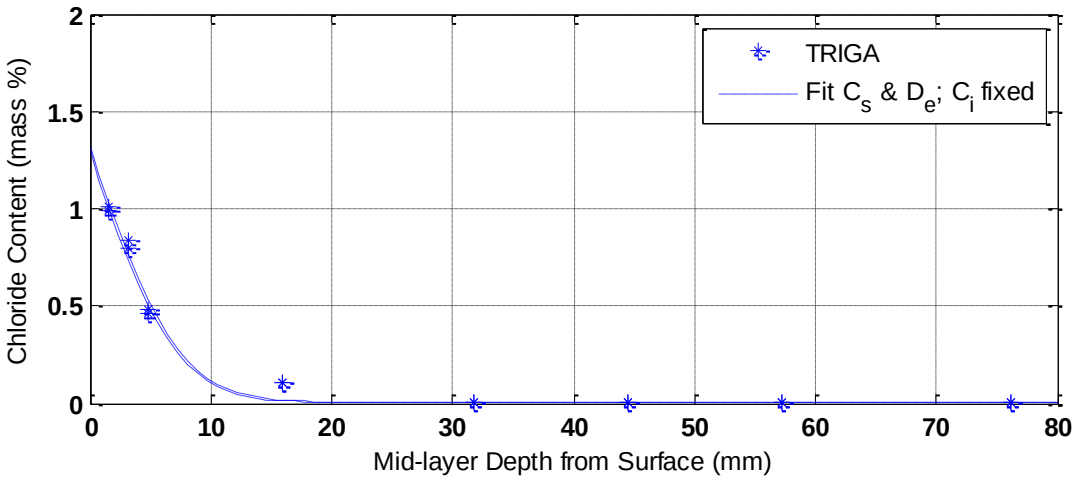

Figure 36 Chloride penetration test on TRIGA specimen

4.2.4 Rapid Chloride Penetration Test (RCPT)

Another test method that provides an indication of concrete resistance to the penetration of chloride ions is the rapid chloride penetration test. This test was performed based on ASTM C1202 (2012g) and it is similar to AASHTO T-277 (2011a). This test was performed on concrete specimens that were cut into 50 ± 3 mm slices from the top of a cylinder using a diamond saw. Thereafter, using a belt sander, sharp edges left from cutting and rough surfaces were cleared for the next step of applying epoxy. The 2 part Sikadur-32, Hi-Mod epoxy was applied on the side surface of specimens to completely cover the sides. As a next step, the specimens were placed inside vacuum desiccators for 3 hours to reduce the pressure to less than 50 mmHg. Then de-aerated water was added while the pump was still running for another hour. Then the pump was turned off and the specimens were left inside the desiccator for 18 ± 2 hrs. After these preparation steps were completed, the specimens were placed in cells filled with 3% NaCl and 0.3N NaOH solution. The results are presented in terms of ampere-seconds of charge passed through the specimens during a 6 hours period and was measured using the following equation

$$Q = 900(I_0 + 2I_{30} + 2I_{60} + \cdots + 2I_{300} + 2I_{330} + I_{360}), \quad (57)$$

where Q is the charge passed (ampere-seconds or coulombs), I_0 (amperes) is the current immediately after voltage is applied and I_t (amperes) is the current at t min after voltage is applied. The steps of specimen preparation are shown in Figure 37. The rapid chloride penetration device is shown in Figure 38.

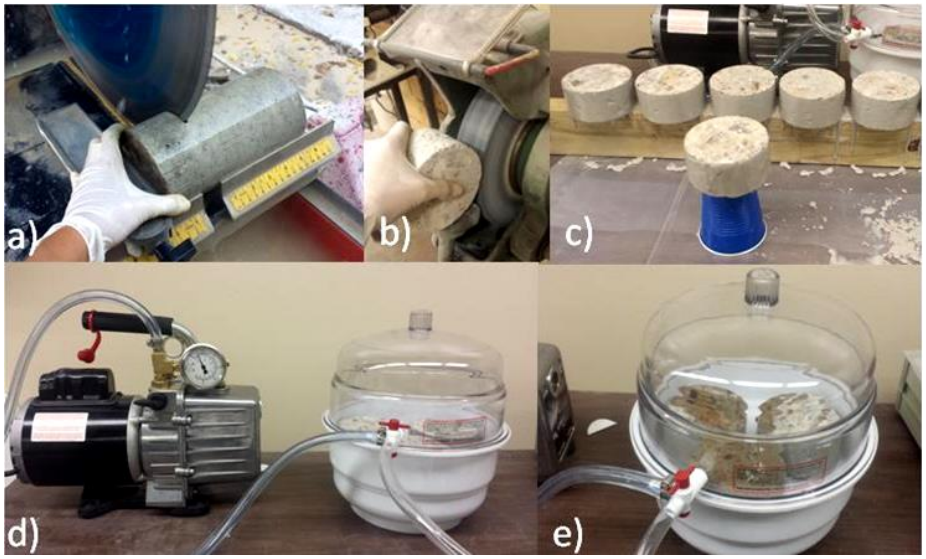

Figure 37 (a) Cutting concrete discs (b) sander to remove the burr and making ready to apply epoxy (c) applying epoxy on the side surface (d) vacuuming specimens in desiccators (e) adding de-aerated water while pump is running

Figure 38 Rapid chloride penetration device

Table 40 shows the qualitative indications of the chloride ion penetrability based on the measured value from this test method as it is present in ASTM C1202 (2011a).

Table 40 Chloride Ion Penetrability Based on Charge Passed (ASTM, 2012g)

Charge Passed (coulombs)	Chloride Ion Penetrability
> 4000	High
2000 – 4000	Moderate
1000 – 2000	Low
100 – 1000	Very Low
< 100	Negligible

The results of this test which was performed on NaOH mixtures at 28 and 180 days are shown in Table 41. The results indicate moderate chloride ion penetrability in all four mixtures. At 28 days, the charges passed are similar to each other. However, at 180 days, it is clear that increasing the sodium hydroxide decreases the chloride ion penetrability of the concrete slightly. It should be noted that the precision of this test is low and it allows the results to have a difference by 40% for each batch of concrete specimens tested by a single operated in a lab.

Table 41 Charge Passed in RCPT Test

Mix	Charge Passed (mA)		Charge Passed (mA)	
	28 Days		180 Days	
NaOH-0_PH2	3182	3239	3351	3368
	3296		3421	
NaOH-2_PH2	3354	3390	2984	3017
	3428		3050	
NaOH-4_PH2	3393	3326	2754	2845
	3259		2936	
NaOH-8_PH2	2942	3045	2845	2756
	3147		2667	

4.2.5 pH of concrete

Determining the pH is important since it is an indicator of corrosion or carbonation. The average pH of regular concrete is approximately 12; however, when it is carbonated, the pH reduces to about 8. Once pH falls below 10, the potential for corrosion increases. The pH of concrete is measured using a pH indicator paper as shown in Figure 39.

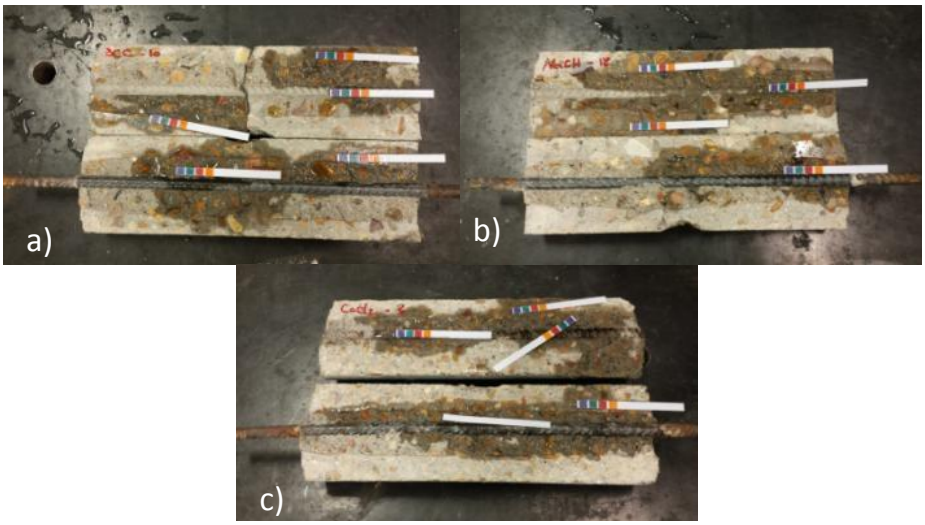

Figure 39 (a) pH of concrete in SCC specimen (b) pH of concrete in NaOH specimen (c) pH of concrete in $CaCl_2$ specimen

The results are shown in Table 42. The pH was measured at three different ages of 28, 210 and 365 days, and the results were similar. However, when the pH around the rebar is measured, a significant drop was observed in the presence of $CaCl_2$-4.

Table 42 pH of Concrete

Mix	pH of concrete	pH around the rebar
SCC_PH1	12	11
NaOH-8_PH1	12	11
$CaCl_2$-4_PH1	12	6

When calcium bearing phases present in the concrete are attacked by carbon dioxide of the air, conversion to calcium carbonate (i.e., carbonation) occurs. This chemical process lowers the pH of concrete to about 7, which is a value below the passivization threshold of steel. To determine the carbonation, there are different methods that can be used. The first method is visual inspection of the concrete and checking the discoloration of concrete, the second method is through optical microscope by detecting the presence of calcite crystals and absence of calcium hydroxide, ettringite and un-hydrated cement grains (Concrete-experts, 2016). The third method is using phenolphthalein. To determine the depth of carbonation, 0.2% solution of

phenolphthalein is sprayed on concrete as a pH indicator on a freshly cut or broken concrete sample. The depth can be estimated based on the change in the color of the specimen, as shown in Figure 40.

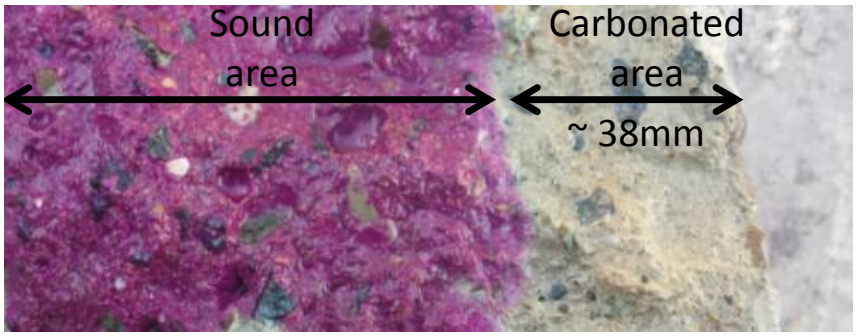

Figure 40 Determining the depth of carbonation

The TRIGA reactor was kept indoors and in controlled temperature and humidity; therefore, changes in these parameters had no effect on them similar to the regular reinforced concrete structure. However, the difference and main source of degradation in them was the high temperature and radiation from the core located in the center of reactor. Therefore, the measured carbonation shows the effect of the high temperature and radiation in the long term on the concrete properties of this type of reactor. Three concrete cores from the surface of the reactor were broken to have a fresh surface and carbonation was measured. The depth of carbonation from the surface was determined to be 38 mm. It should be noted that carbonation was not observed on the specimens prepared in the first and second phases.

4.2.6 SEM/EDS

To check the effect of aging on the composition of the NaOH concrete mixtures, SEM and EDS measurements were performed. The concrete cylinders were cut into half and a sample having a size of about 25.4 x 12.7 x 6.35 mm is extracted with a low speed diamond saw. The specimen is coated with a layer of platinum for SEM measurements and with carbon for EDS measurements;

see Figure 41. . The SEM imaging microscope used for this test is Leo 1530 Gemini and the EDS microscope used for compositional imaging is JEOL JSM.6330F; see Figure 42.

Figure 41 (a) Carbon coater, (b) platinum coater

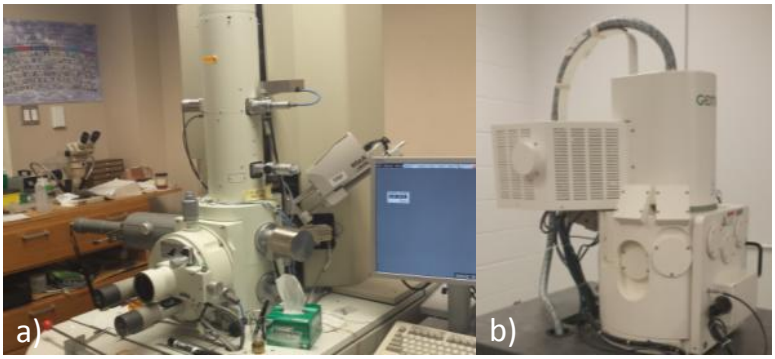

Figure 42 (a) JEOL JSM.6330F, (b) Leo 1530 Gemini

When specimens were inspected with scanning electron microscopy (SEM), cracks were found in both paste and aggregate on the specimens at an age of 6 months. Although the cracks were not completely filled with gel, EDS analysis of the crack shows the existence of alkali (Na^+ and K^+) in the crack. With increasing distance from the aggregate, the composition of the gel was found to be more similar to the calcium silicate hydrate with low alkali content and high calcium content. Figure 43 shows the crack on the aggregate and Figure 44 shows the element analysis of one of the points in the crack.

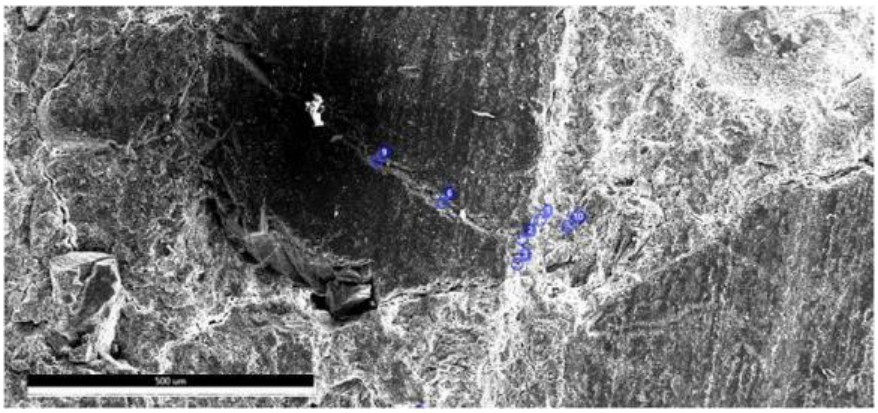

Figure 43 SEM/EDS micrograph of concrete from NaOH-8 Mixture Showing Crack in Aggregate and Paste

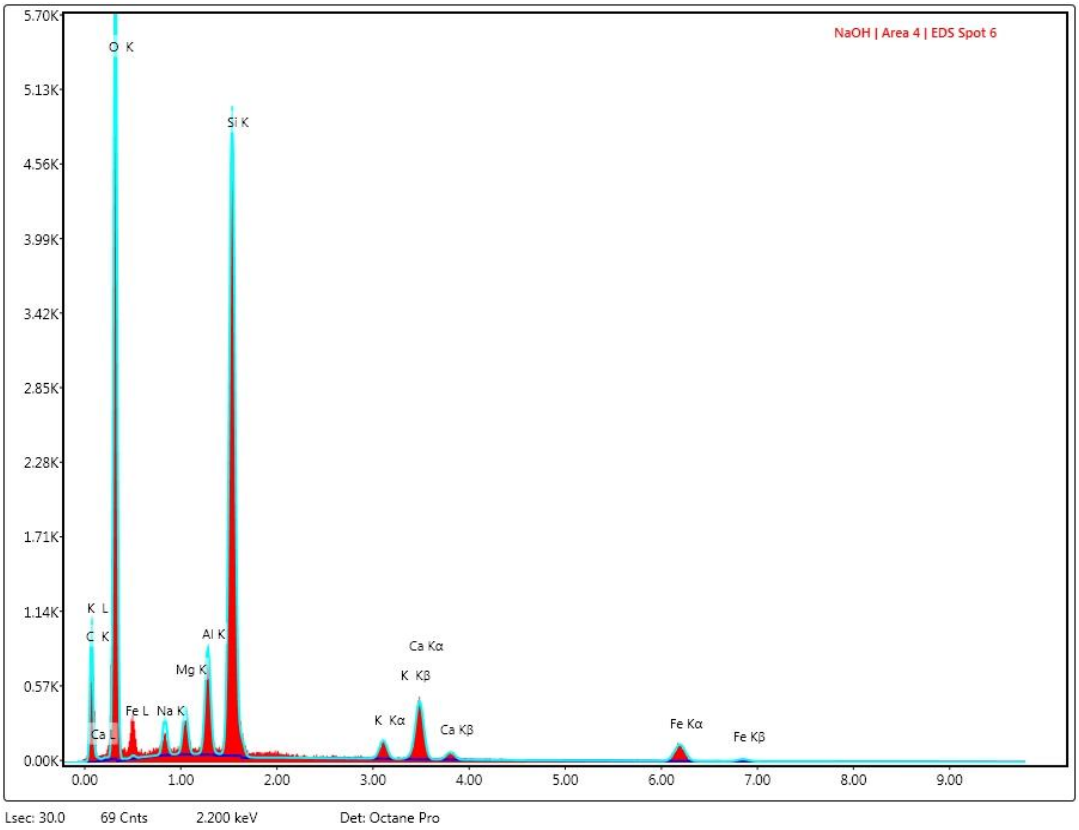

Figure 44 EDS analysis of the crack

4.3 Mechanical Properties of Concrete

Addition of sodium hydroxide (NaOH) to the mixture has an effect on the tensile and compressive strengths and the Young's modulus of concrete (Smaoui et al., 2005; Nuruddin et al., 2011; Bahadure and Naik, 2013). This effect becomes more critical when there is a high density of

cracks initially due to effects such as shrinkage, leading to softening of concrete (Brown, 2013). Addition of calcium chloride also has an effect on early strength gain of concrete. Intentionally adding chloride ions as well as ingress of chloride ions into the concrete structures may cause a series of chemical changes to the concrete matrix that could lead to a decreased strength of the concrete in the long term. To better understand these effects, the strengths of concrete (compression, splitting, tensile and flexural) were measured at different ages. Fracture energy of the mixtures with the highest amount of sodium hydroxide (NaOH-8) and calcium chloride ($CaCl_2$-4) in the first phase was measured at 210 days and compared with the SCC mixture.

4.3.1 Compressive strength

The compressive strength test was performed based on ASTM C39 (2012d). Stress and strain of the concrete during the compression test was measured using axial averaging extensometer. The test setup for the compression test is shown in Figure 45.

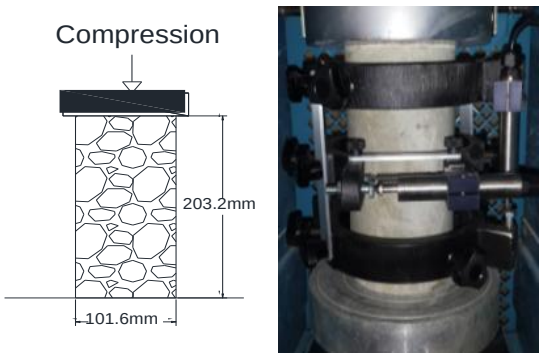

Figure 45 Compression test setup

The compressive strength of concrete measured at 1, 3, 7, 28, 210 and 365 days for the three concrete mixtures in the first phase and stress-strain was measured during the test (The complete results of measurements are in Figure A 1 through Figure A 6 in the appendix. Figure 46 shows the comparison of concrete strength for the different mixes at the five testing days. SCC and NaOH-8 from the first phase exhibited similar 1-day strength; however, a lower strength was yielded by

NaOH-8 for most of the testing time. In this phase $CaCl_2$-4 exhibited higher strength compared to the other two mixtures at the early age, which is due to increase in hydration in the concrete by calcium chloride. But in the long term and maturing concrete, SCC mixtures show higher strength. This result shows the harmful effects of a high percentage of chloride ion penetration and ASR in the long term.

For NaOH concrete mixtures in the second phase, the compressive strength was measured at 7, 28, 180 days, and for $CaCl_2$ concrete mixtures in the same phase, these measurements were performed at 7, 28, 90 and 180 days (see Figure A 7 to Figure A 22, also Table A 11 and Table A 12 in appendix). These results are compared at different ages as shown in Figure 47 for NaOH and $CaCl_2$ mixtures in the second phase. Before the chemicals were added to the mixtures, 3 cylinders were taken and compared at 28 days for consistency among the 8 mixtures. The results indicate the similarity of the mixtures prepared in each batch to each other and the mixtures prepared in first phase before mixing the chemicals. The complete test results appear in Figure A 23 and Figure A 24 in the appendix.

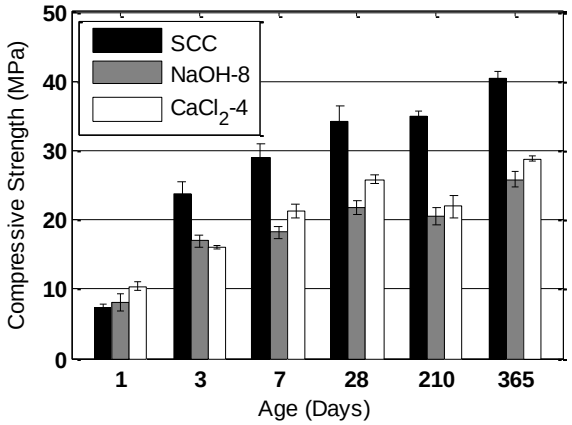

Figure 46 Concrete strength at different ages, phase 1

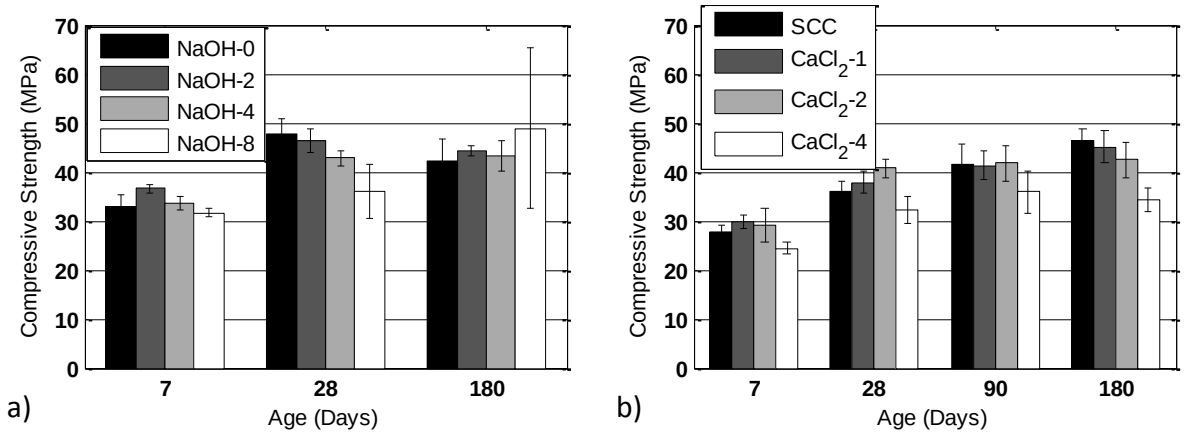

Figure 47 Strength at different ages, (a) NaOH concrete mixtures phase 2, (b) $CaCl_2$ concrete mixtures phase 2

From the results of testing in the second phase, it can be understood that addition of 0.2% sodium hydroxide to the mixture increases the strength of the concrete on the first day due to increased rate of hydration compared to the regular concrete. However, further addition (NaOH-4 and NaOH-8) was not beneficial in this regard. NaOH-4 yielded very similar 1-day strength as the control mixture, while NaOH-8 had slightly lower compressive strength. At 28 days, the control mixture with no NaOH had the highest strength and the strength was gradually lower at higher NaOH levels. At 180 days, NaOH-2 and NaOH-4 yielded slightly higher compressive strengths than the control. While, NaOH-8 resulted in a delayed strength gain and a considerable strength development was obtained at a later age. As a result, the highest compressive strength (which is 13% higher than that of NaOH-0) at 180 days was observed from NaOH-8. A drop in the strength of NaOH and NaOH-2 specimens were observed from 28 days to 180 days, which were within the intra-mixture variability at different ages. One of the reasons for difference in strength between the NaOH-0 and SCC mixtures is the replacement of 25% of the cement with fly ash in SCC mixtures, which reduces the strength of concrete. The reason for the difference in strengths of NaOH-8 specimens prepared in the first and second phases is potentially due to the differences in the water contents of these mixtures. A significantly larger volume of concrete, approximately 2000 liters was prepared for the first series and the accompanying material specimens, while only

100 liters of concrete was cast for each of the NaOH mixtures, which allowed a significantly better control of the mixture proportions in the latter.

Adding different amounts of calcium chloride to the concrete mixture resulted in different compressive strengths. It is seen that the addition of one or two percent chloride increases the early strength of concrete compared to SCC and $CaCl_2$-4 mixtures, however, at later ages, the strength gain of the mix without $CaCl_2$ is much higher than those of the other mixtures. The overall strength of $CaCl_2$-4 is the lowest among all mixtures.

Additionally, the results for specimens obtained from the TRIGA reactor are shown in Table 43 (see also Figure A 25 and Figure A 26 in the appendix). The results indicate that although concrete was located in environmentally harsh conditions due to high temperature and radiation the strength remained in the highly acceptable range. Unconfined compressive strength of concrete in nuclear power plants (NPP) is typically in the range of 13 MPa to 55 MPa, with 28 MPa being most common (Naus et al., 1996). Here compressive tests results show an average strength of 40.53 MPa, which is higher than the average concrete strength in NPP. Furthermore, the initial strength of concrete mixture can be estimated on the basis of this strength test. Concrete exposed to a temperature of 90 °C (similar to the NPP conditions) may lose up to 10% of its room temperature strength (Freskakis, 1979; Naus et al., 1996).

Table 43 Compressive Strength of TRIGA Specimens

Test	Compression Strength (MPa)	Average
TRIGA	43.7	40.5
	37.5	
	40.4	

4.3.2 Modulus of elasticity and Poisson's ratio

In the first phase, the modulus of elasticity was measured at the ages of 210 and 365 days. The results are shown in Figure 48 (see also Table A 13 in the appendix). The results of the test indicate that the modulus of elasticity in SCC and $CaCl_2$-4 mixture is similar at these two testing ages. However, for NaOH-8 mixture, this parameter decreased. This difference can be explained because of the increase in the density of cracks that leads to softening of concrete and decrease in the modulus of elasticity of it.

In the second phase, the modulus of elasticity for NaOH and $CaCl_2$ mixtures were also measured at these ages; they are shown in Figure 49 (see also Table A 14 and Table A 15 in appendix) It is clear that modulus of elasticity in NaOH mixtures at early ages does not show differences between different amounts of sodium hydroxide additive, however, looking at this property in specimens prepared along with the casks and at 270 and 365 days shows that adding 0.8% NaOH decreases the modulus of elasticity. This decrease is due to the increase in the crack density and softening of concrete. For $CaCl_2$ mixtures this property decreases with addition of the salts; for 1 and 2 percent the measurement is similar and higher than 4% $CaCl_2$ addition.

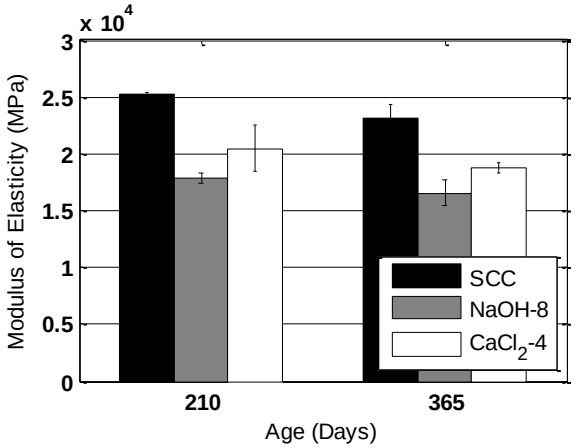

Figure 48 Modulus of elasticity of concrete mixtures, phase 1

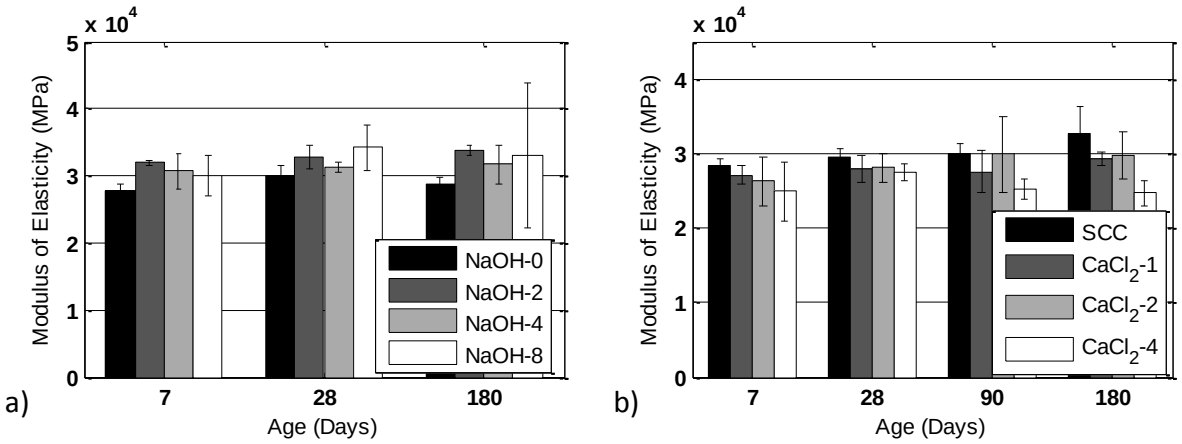

Figure 49 Modulus of elasticity (a) NaOH concrete mixture, phase 2 (b) $CaCl_2$ concrete mixture, phase 2

Poisson's ratio was also measured at the same time as the modulus of elasticity, at 210 and 365 days for first phase concrete mixtures. In the second phase, this property was measured at 7, 28 and 180 days for NaOH mixtures and at 7, 28, 90 and 180 days for $CaCl_2$ mixtures. The results are shown in Figure 50 and Figure 51 (see also Table A 16 to Table A 18 in the appendix). The results indicate the same trends as the modulus of elasticity.

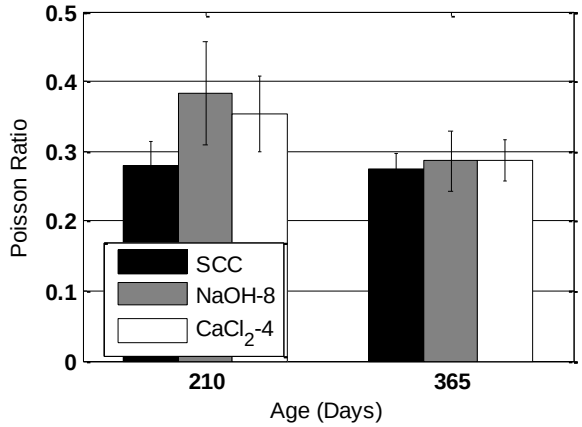

Figure 50 Poisson's ratio of concrete mixtures, phase 1

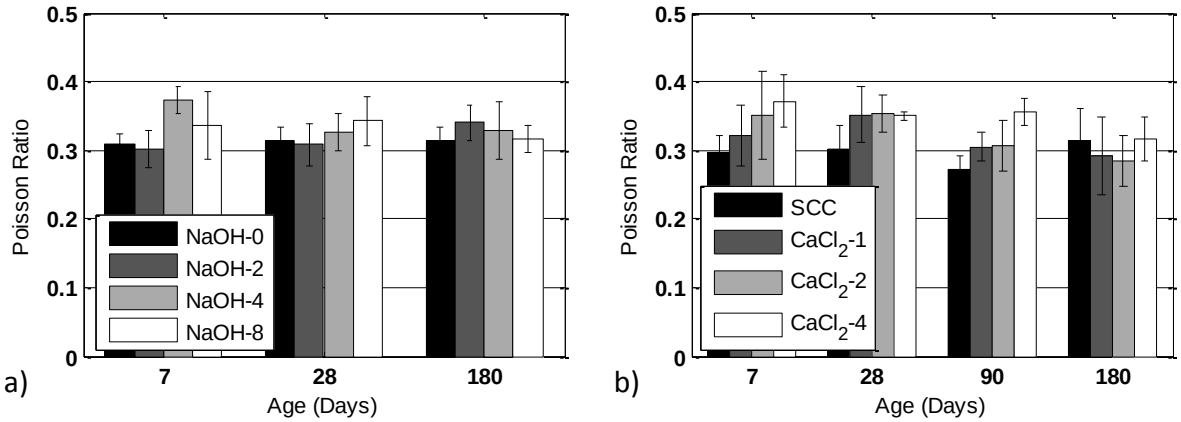

Figure 51 Poisson's ratio (a) NaOH concrete mixtures, phase 2 (b) $CaCl_2$ concrete mixtures, phase 2

The modulus of elasticity of TRIGA specimens are similar to those of the SCC mixture prepared in the first and second phase of this study. Similar to compressive strength, the original modulus of elasticity of the concrete in the TRIGA reactor can be estimated from the results obtained from the tests with considering 10% decrease in this property due to high temperature (Freskakis, 1979; Naus et al., 1996; Naus, 2007).

Poisson's ratio of concrete specimens from the TRIGA reactor concrete was also measured; see Table 43. This parameter was 25% higher than the SCC mixture in the first phase of this study. It has been hypothesized that changes in Poisson's ratio at the elevated temperature of NPP are very small and are about the same as at room temperature (Naus, 2010).

Table 44 Modulus of Elasticity and Poisson's Ratio of TRIGA Specimens

Test	MOE (MPa)	Average	Poisson's Ratio	Average
TRIGA	23516	24781	0.39	0.39
	27632		0.38	
	23195		0.41	

4.3.3 Splitting tensile strength

ACI 349 (2013) eliminated the splitting tensile strength requirement for nuclear structures; however, finding the splitting tensile strength for a structure that might have alkali silica reactions in the long term is important, since this property is sensitive to microcracking and decreases due

to this effect (Fan and Hanson, 1998a; Deschenes et al., 2009). Moreover, this test is important because of the tensile mode of failure of the concrete. The test is performed based on ASTM C496 (2011b). The test setup for the splitting tensile test is shown in Figure 52. Since the dimension of the upper and lower bearing face is less than the length of the cylinder, two steel plates having the dimensions 279.4 x 50.8 x 19.05 mm (L x W x H) were used. Plywood bearing strips 3.175 mm thick were also placed at the top and bottom between the specimen and the steel plates.

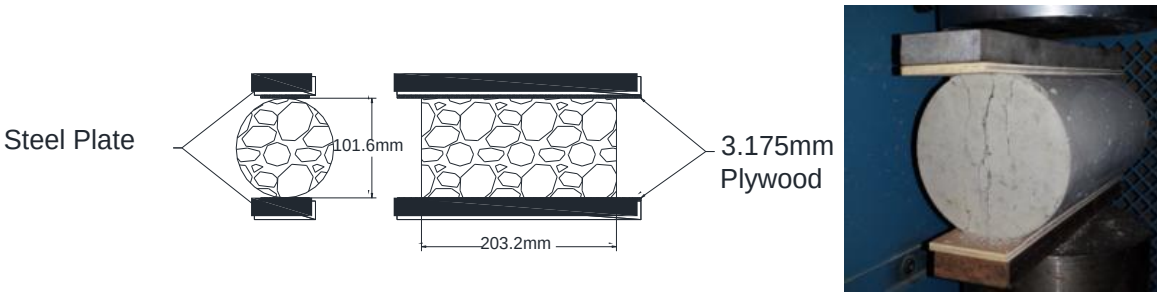

Figure 52 Splitting tensile test setup

The results of splitting tensile strength tests at 1, 3, 7, 28, 210 and 365 days for the three concrete mixtures of first phase are provided in Figure 53. The results show that the NaOH-8 mixture's strength is considerably less than that of SCC and after 28 days the strength was almost constant. The $CaCl_2$-4 mixture in this phase has lower strength than the NaOH-8 at an early age and higher strength that later ages and lower strength than SCC at all ages. The difference between $CaCl_2$ and NaOH addition at early age is due to the difference in hydration amount with the addition of chemicals. The results of splitting tensile tests for the NaOH and $CaCl_2$ concrete mixtures of the second phase are provided in Figure 54. The observations for split tensile strength were similar to those of the compressive strength tests in the NaOH mixtures of the second phase, a lower strength at early age and a delayed strength development. The 180 day strength of all the mixtures was similar, ranging from 4.54 MPa to 5.32 MPa. Again this difference between the NaOH-8 specimens for the first and second phases might be attributed to the differences in water content of the mixtures. The development of tensile strength of the concretes with

different levels of chloride shows a good agreement with that of compressive strength. The 7-day splitting tensile strengths of $CaCl_2$-1 and $CaCl_2$-2 mixtures were higher than that of SCC; however, the further addition of chloride (i.e., 4%) results in a significant decrease of early age strength. At 28 days, the splitting tensile strength of SCC mix was the highest, and $CaCl_2$-4 showed the lowest splitting tensile strength. But at 180 days, basically all are the same again.

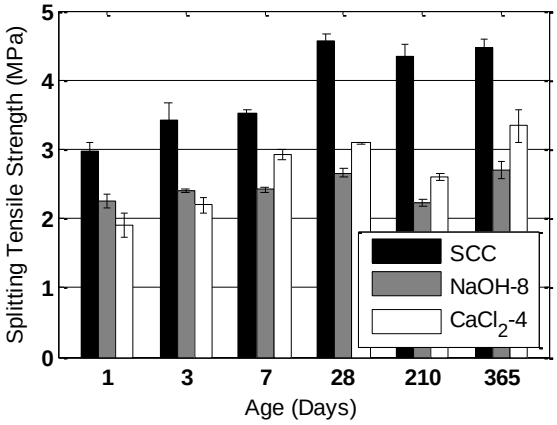

Figure 53 Split tensile test result at different ages, phase 1

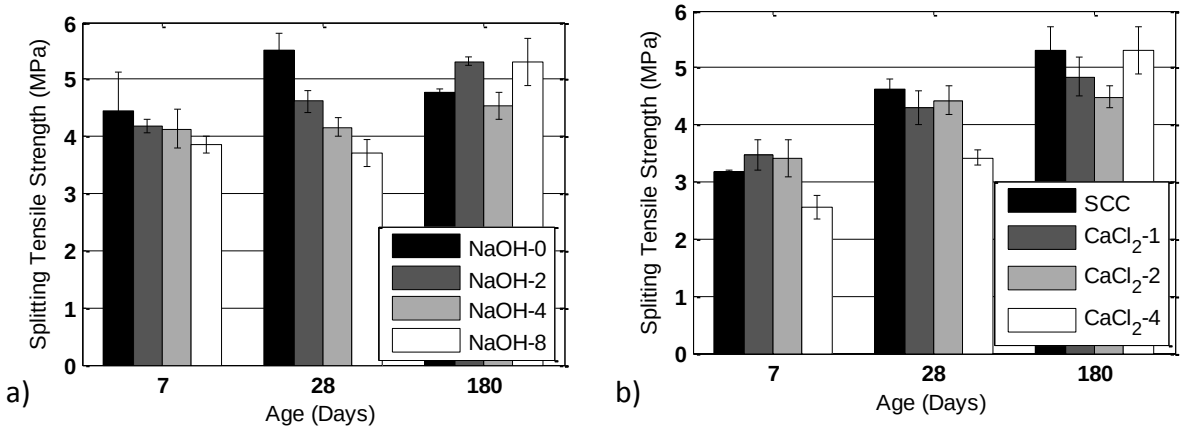

Figure 54 Split tensile test result at different ages, (a) NaOH concrete mixtures, phase 2, (b) $CaCl_2$ concrete mixtures, phase 2

The tensile strength of TRIGA reactor specimens was measured; see Table 45. In the high temperature of reactors and in the presence of nuclear radiation, there can be up to 5% reduction of splitting tensile strength (Naus, 2007). This strength is usually considered to be one-tenth to one-fifth of its compressive strength (Naus, 2007). The results of the tensile strength test confirm

that the tensile strength of the concrete is still in an acceptable range. The tensile strength of TRIGA reactor specimens are 15% less than SCC specimens prepared in the first phase. It is 27% and 13% higher than accelerated aged specimens for ASR and corrosion of first phase specimens, respectively.

Table 45 Tensile Strength of TRIGA Specimens

Test	Tensile Strength (MPa)	Average
TRIGA	3.96	3.74
	3.56	
	3.70	

4.3.4 Flexural strength

To find the flexural strength of concrete, there are two commonly used tests, 3-point and 4-point bending. In the latter, since the volume under stress is larger, the probability of finding a longer crack is higher and it yields a more accurate strength estimation (Nordson, 2014). Therefore, a 4-point bending test was chosen for measuring flexural strength. Figure 55 is showing the flexural test setup. The molds for both this test and the fracture energy test have dimensions of 101.6 x 101.6 x 355.6 mm.

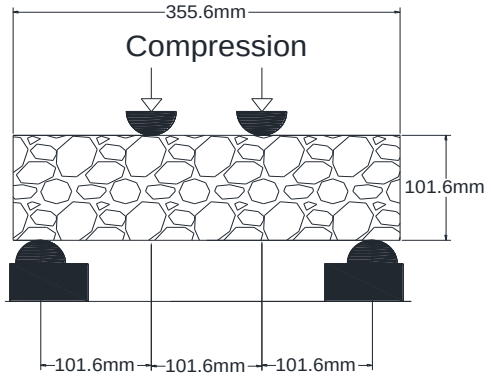

Figure 55 Flexural strength test setup

Knowing the dimensions of the specimens and the maximum load applied to the specimen during the flexural tests, the modulus of rupture can be found. Since all the fractures in the

specimens tested here initiate in the middle third of the span length, the modulus of rupture is calculated using the following equation:

$$R = \frac{PL}{bd^2}, \tag{58}$$

where *R* is modulus of rupture (MPa), *P* is maximum applied load (N), *L* is the span length (mm), *b* is the average width of specimen (mm) and *d* is the average depth of specimen (mm).

Flexural strength at the first phase was measured at three ages: 28, 365 and 455 days. The average results are provided in Figure 56; 6 beams were tested for each mixture at 28 days and 3 beams each at 365 and 455 days age (see Table A 19 in the appendix). The modulus of rupture of NaOH and $CaCl_2$ mixtures was obtained at 28 days and the results are provided in Figure 57.

At 28 days, the addition of sodium hydroxide reduced the modulus of rupture of the specimens and this reduction was greater in the mixture with 0.4% NaOH per weight of cement. For $CaCl_2$ mixtures the flexural strength increased with the addition of 2% chloride ion by weight of cement to the mixture which is due to acceleration in the hydration rate. However, increasing the amount of chloride ion, decreased strength noticeably, since high concentrations of $CaCl_2$ decrease the extent of cement hydration (Kishar et al., 2013). Overall, the SCC specimens has highest modulus of rupture, values for $CaCl_2$ specimens were lowest; and those for NaOH samples lowest.

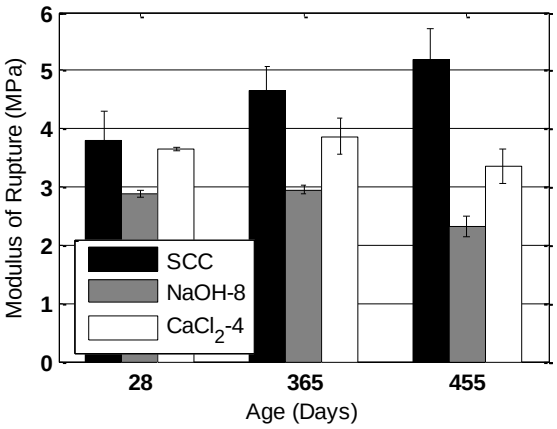

Figure 56 Modulus of rupture of concrete mixtures, phase 1

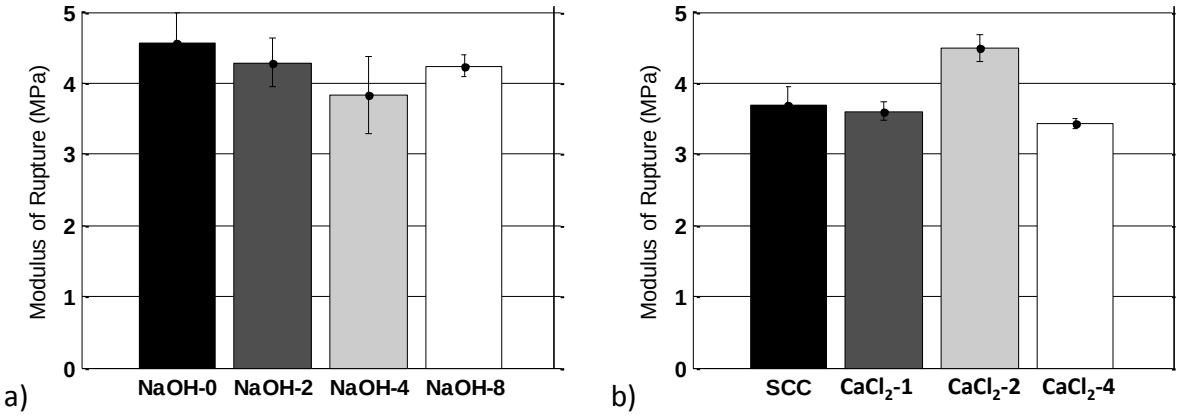

Figure 57 Modulus of rupture (a) NaOH concrete mixtures, phase 2 (b) $CaCl_2$ concrete mixtures, phase 2

4.3.5 Fracture energy

Fracture energy is one of the useful parameters for design with concrete and cementitious materials and it is needed for modeling the fracture behavior of the cohesive materials (FMC, 1985). Generally, concrete failure is due to cracks and cracking is preceded by formation of microcracks and their coalescence into macrocracks. The energy stored in concrete during this process is released at the time of fracture which is called fracture energy (Bassam et al., 2007). The fracture energy is related to the compressive strength and stiffness of concrete (Zhou et al., 1995; Rao and Prasad, 2002); therefore, when concrete ages this property will be affected. This test is performed based on JCI-S_001-2003 (2003), on the notched beam with dimensions of 101.6 x 101.6 x 304.8 mm. A notch with depth of 0.3D=30.54 mm (D is the depth of section) and width

of 5 mm was cut on the specimens; see Figure 58 As shown in Figure 58, in the fracture energy tests, the crack opening is measured with a crack-opening displacement (COD) gage, which is a strain gage-based extensometer. The fracture energy is calculated from the load versus COD relationship.

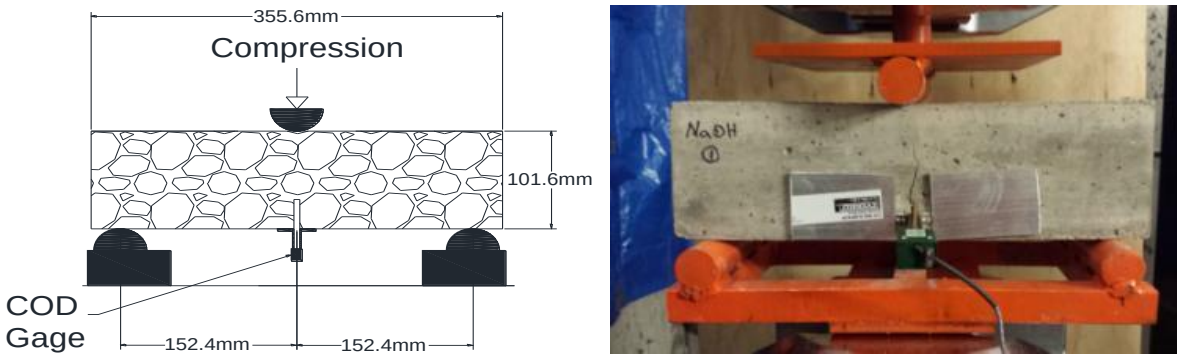

Figure 58 Fracture energy test

Fracture energy is calculated according to the following equation:

$$G_F = \frac{0.75W_0 + W_1}{A_{lig}} \text{ and} \tag{59}$$

$$W_1 = 0.75\left(\frac{S}{L}m\right)g.CMOD_c \tag{60}$$

where, G_F is fracture energy (MPa), W_0 is the area below the CMOD curve up to the rupture of specimen (N.mm), W_1 is the work done by the deadweight of the specimen (N.mm), m is the mass of specimen (kg), S is the loading span (mm), L is the total length of specimen (mm), g is gravitational acceleration (9.807m/s^2) and $CMOD_c$ is the crack mouth opening displacement at the time of rupture (mm).

Fracture energy was measured only at 210 days and on two specimens from each mixture as a measurement point to see the difference between the values of this property between the SCC and accelerated age concretes in the first phase of this study. From the crack opening versus load relationship shown in Figure 59 and the average of fracture energy measured from the reading shown in Table 46, it is clear that peak load in ASR accelerated specimens, i.e. the NaOH-8 mix,

were 30% less than the control mixture and the fracture energy measured from this test was 34% less. The peak in $CaCl_2$ mixture was 20% less than the SCC mixture, and the fracture energy was 16% lower.

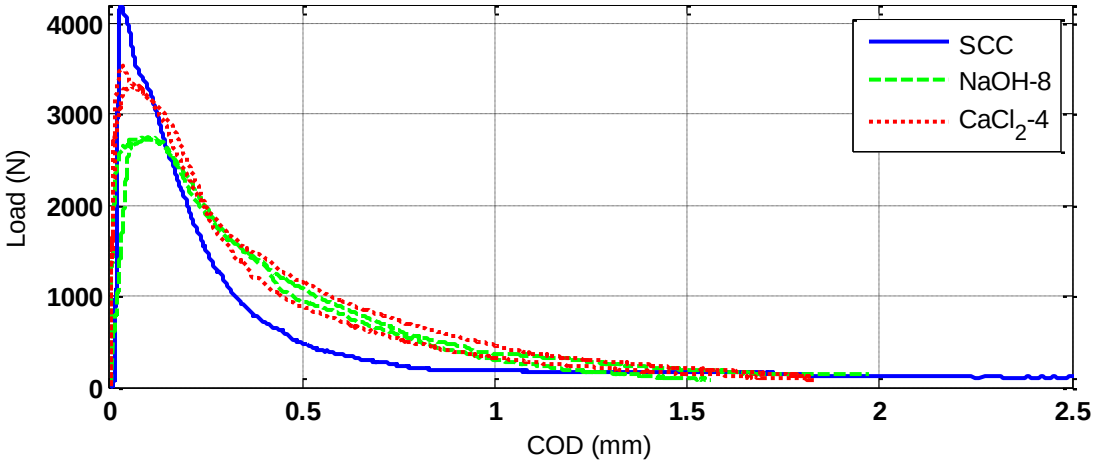

Figure 59 Crack opening versus load relationship of 3 different concrete mixtures

Table 46 Fracture Energy of Concrete Mixtures

Mix	G_f (N/mm)
SCC	0.44
NaOH-8	0.29
$CaCl_2$-4	0.37

4.3.6 Bond Strength

There are different variables affecting the bond between steel reinforcement and concrete. Nawy (2008) summarized the major factors as adhesion between the concrete and the reinforcing elements, the gripping effect resulting from the drying shrinkage of the surrounding concrete, the effect of concrete quality and strength in tension and compression, and mechanical anchorage effects of the ends of the bars through the development length, splicing, hooks and crossbars, in addition to diameter, shape and spacing of reinforcing. Since aging has a direct effect on some of these properties, it influences the bonds between concrete and rebar. Therefore, the pullout strength was measured on SCC, NaOH-8 and $CaCl_2$-4 specimens of the first phase. Cube specimens with 152.4 x 152.4 x 152.4 mm dimensions were prepared with #10 and #19 reinforcement, as

representative of the scaled down and prototype casks, respectively, from each mixture; see Figure 60. In this test, the development length for reinforcement is taken to be equal to four times the diameter of the rebar (development length for #10 and #19 rebar were 38.1 and 76.2 mm, respectively). The test was performed on unconfined concrete. The test setup for pullout test is shown in Figure 61.

It should be noted that this method does not represent realistic conditions, since the concrete around the loaded bar is under compression and the cover is quite large; however, it is one of the most widely used techniques aside from the beam-end type of testing for bond strength.

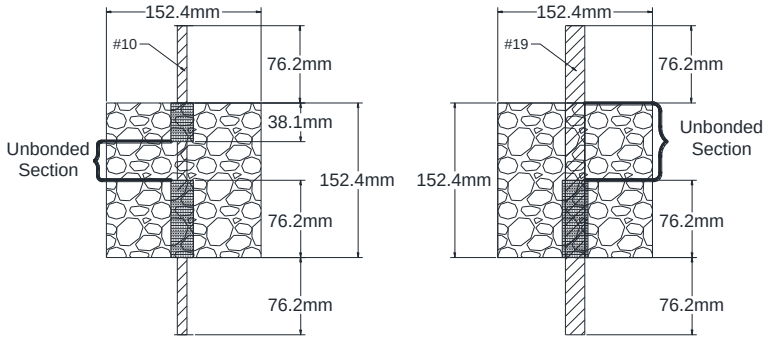

Figure 60 Dimensions of the pull-out test specimens

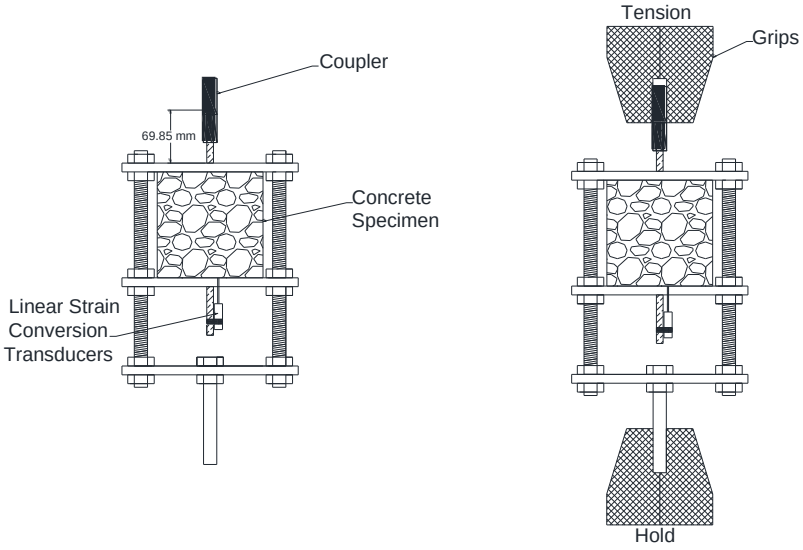

Figure 61 Pullout test setup

Knowing the maximum load before the complete pullout, the maximum bond strength can be calculated as:

$$\sigma_{b\_max} = \frac{P_{max}}{\pi d_b L_d}, \quad (61)$$

where P_{max} is maximum load applied on the specimen (N), d_b is the diameter of the rebar (mm), and L_d is the bond length (mm).

Bond strength was measured after 210 days on concrete specimens of the first phase. At this age, cracks had developed on the ASR accelerated specimens and corrosion products had developed on the rebars. The bond-slip relationships for these mixtures for #10 and #19 rebars are shown in Figure 62 and Figure 63, respectively. The average results of these tests on #10 and #19 rebars are shown in Figure 64 (see also Table A 22 and Table A 23). The results indicate higher bond strength for $CaCl_2$-4 mix with #10 rebars which was due to generation of corrosion products. At an early stage of corrosion, when the product increases to the certain point it increases the bond, but after this stage the bond decreases (Amleh and Ghosh, 2006). This corrosion product at early age overcomes the lower compression strength of this mix compared to SCC and causes the higher bond strength. For the same rebar size, NaOH-8 mixture shows the lowest bond strength. Increasing the rebar size to #19 clearly decreases the bond strength for all the mixtures. With this rebar size, the SCC mixtures showed the highest bond strength and NaOH-8 showed the lowest strength.

The failure mode in specimens with #19 rebar was brittle with splitting of the concrete surrounding the bar; see Figure 65. In the specimens with #10 rebar the failure mode was more plastic consisting of shearing of the reinforcement against the surrounding concrete. The splitting failure is caused by the wedging action of the lugs on the bars (ACI Committee 408, 1966). The wedging produces confining pressure from the surrounding concrete and is balanced by

circumferential tensile stresses around the bar. The shearing failure occurs after the reinforcement lugs shear or crush the concrete (Bažant and Sener, 1988). The splitting failures in SCC specimens were more brittle than the other two mixtures and the crack propagated very quickly during the pullout.

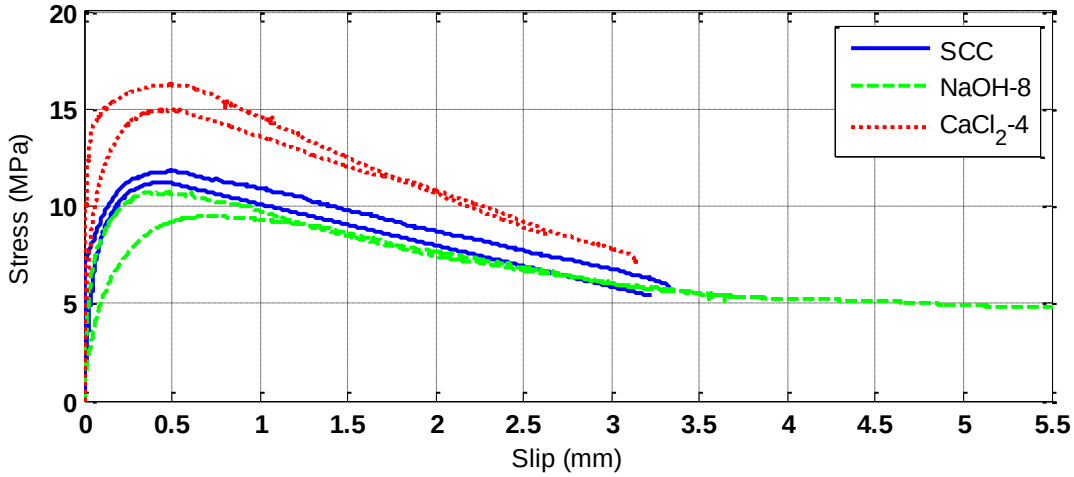

Figure 62 Bond-slip relationship for three concrete mixtures with rebar #10, Phase 1

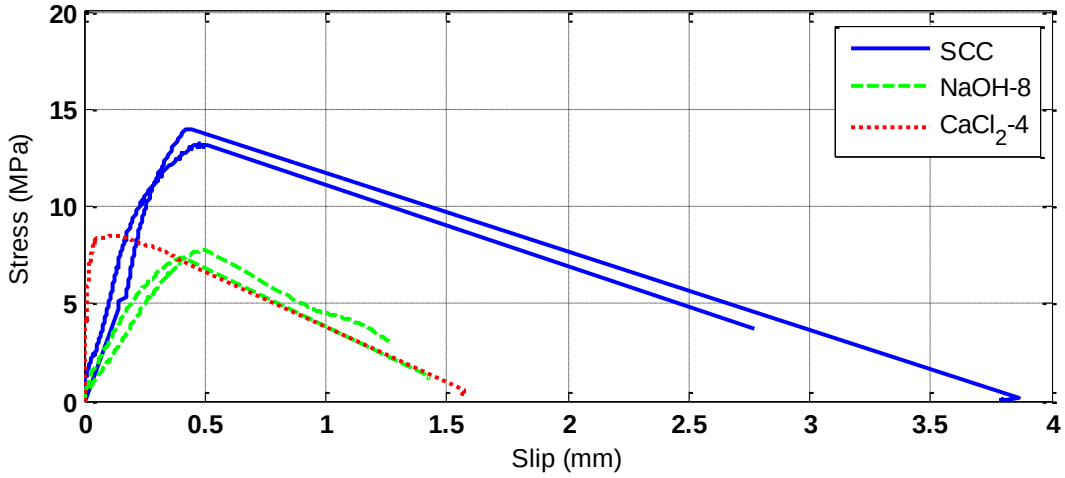

Figure 63 Bond-slip relationship for three concrete mixtures with rebar #19, Phase 1

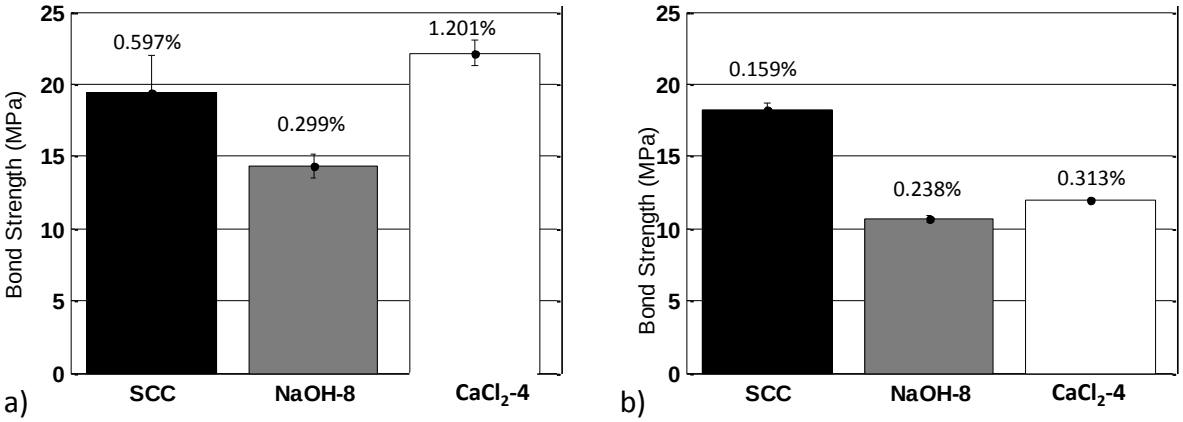

Figure 64 Bond strength of concrete mixtures in phase 1 (a) with #10 rebars (b) with #19 rebars

Figure 65 Failure mode on SCC concrete cube with #19 rebar

4.4 Non-Destructive Testing

A series of non-destructive tests were performed on the specimens including monitoring the cracks, performing a series of electrochemical tests and conducting Schmidt hammer tests. Non-destructive testing such as visual inspection for crack mapping, electrochemical monitoring of the concrete specimens, as well as UPV measurement.

4.4.1 Crack mapping

One of the methods to check the soundness of concrete is visual inspection. When the corrosion progresses and applies pressure on the concrete, the surface will crack and the cracks will grow over time. The crack growth with time indicates that the amount of corrosion product increased and the rebar has corroded further. Similarly, when ASR gel starts to expand and cracks the surface of the concrete, the ASR progression can be measured from crack growth or crack density. To measure crack widths, a magnifier with a scale, as shown in Figure 66 was used. To document the crack growth and propagation, a grid was drawn on the surface of the specimens. A grid and crack width measurement on ASR specimens using a magnifier is shown in Figure 67.

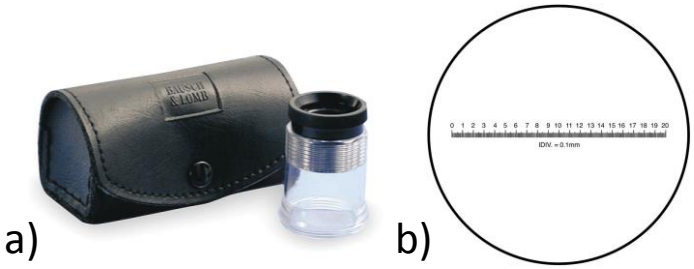

Figure 66 (a) magnifier, (b) 0.1 mm scale (Grainger, 2014)

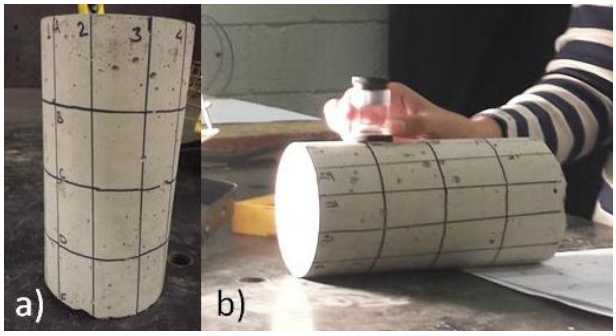

Figure 67 (a) grid on a specimen, (b) crack width measurement using magnifier

In ASR accelerated specimens, when the internal pressure due to the ASR gel expansion exceeded concrete tensile strength, it caused crack formation on the surface of concrete. The cracks were mostly in the form of three branches (Triskele) and increased with age due to the expansion of gel through the time and transformed into honeycomb cracks when they started

interconnecting. After 3 months, cracks were visible in both specimen sizes. Figure 68 and Figure 69 show this crack formation for seven different times (at 114, 171, 225, 276, 342, 432 and 492 days after casting) through the lifetime of two cylinders with dimensions of 75 x 150 mm and 100 x 200 mm. The specimens were prepared with 0.8% NaOH by weight of cement in the mix from the first phase. The comparison of the cracks in the different specimen sizes indicates that geometry plays an important role in the amount of cracking, and the smaller specimen showed more cracks on the surface. The crack width was almost constant and equal to 0.05 or 0.1 mm; however, the amount of cracks increased with aging of the concrete.

Cracks were also observed on the corrosion accelerated specimens. In these specimens with corroding the rebar inside the concrete, corrosion products started expanding and applying a pressure to concrete surrounding the rebar and cracking the surface of concrete. The crack width increased with increasing expansion and eventually resulted in the spalling of the cover concrete.

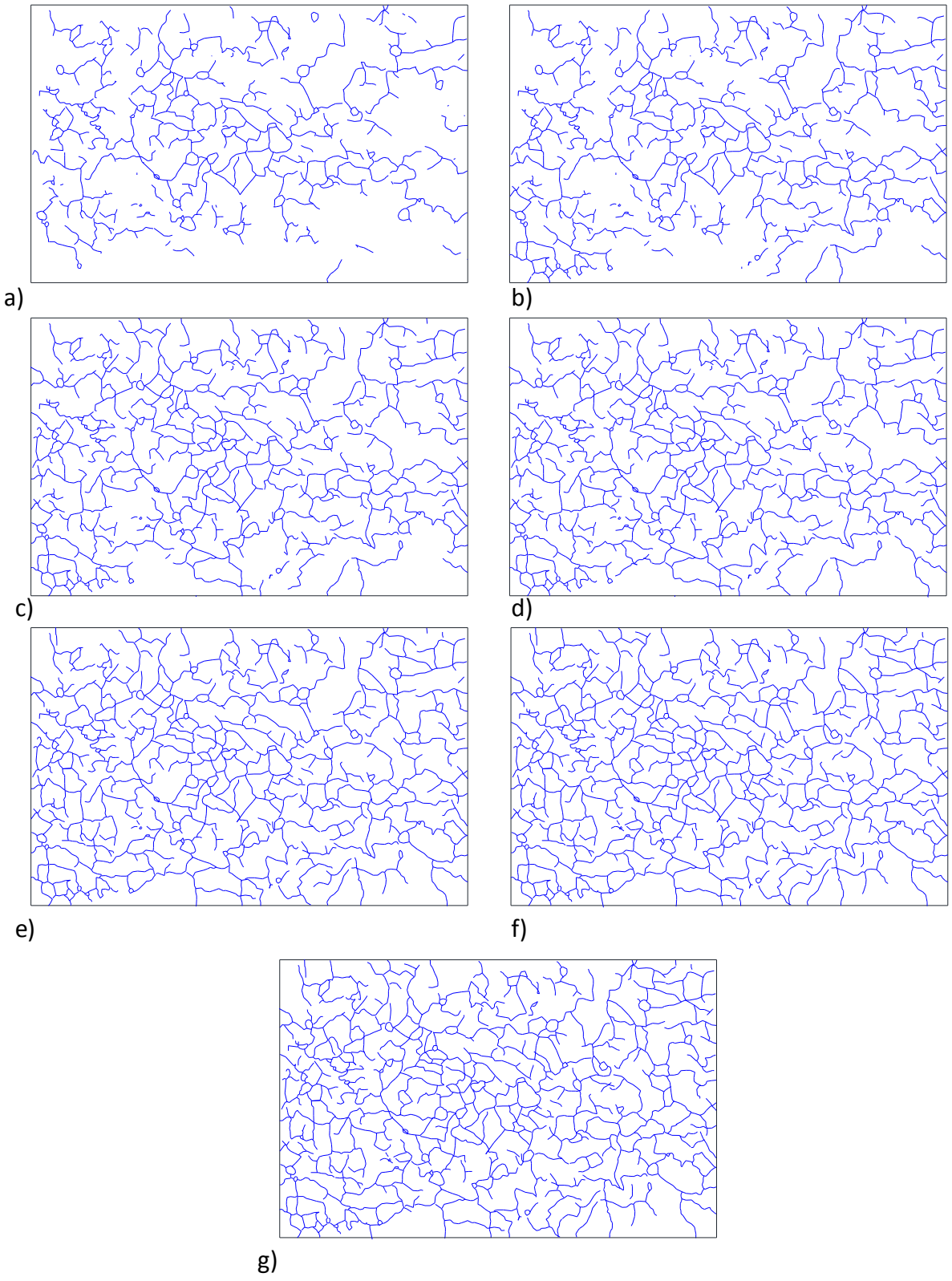

Figure 68 ASR crack mapping on a 75 x 150 mm specimen, (a) 117 (b) 171 (c) 225 (d) 276 (e) 342 (f) 432 (g) 492 days

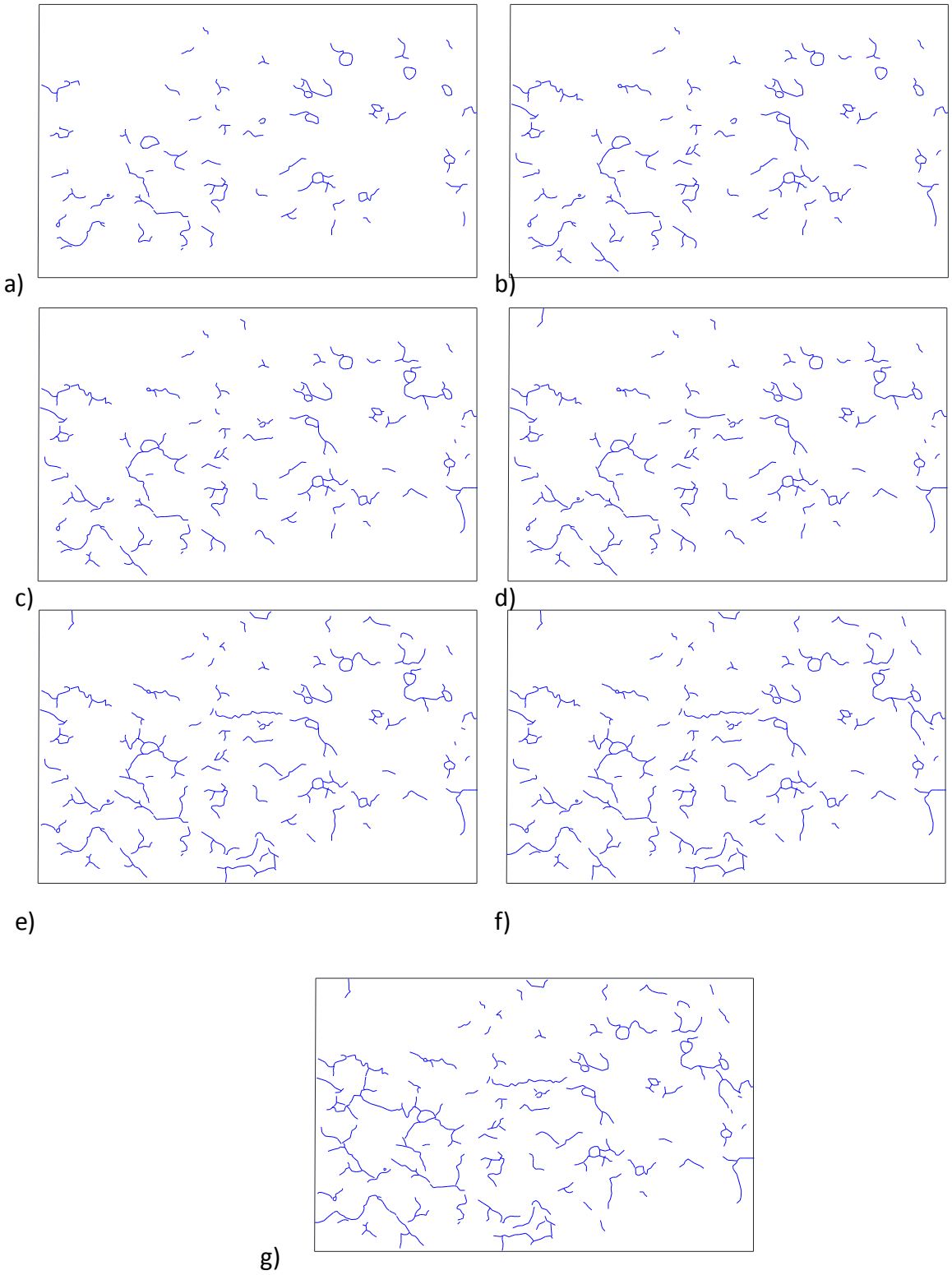

Figure 69 ASR crack mapping on a 100 x 200 mm specimen, (a) 117 (b) 171 (c) 225 (d) 276 (e) 342 (f) 432 (g) 492 days

The lollipop shaped specimens with single embedded rebar with rebar #10 and #19 were prepared for this test. The diameter of the concrete cylinders is chosen based on actual concrete cover inside the dry cask storages. #10 rebar has a cover of 38.1 mm and it is for the scaled down cask. #19 rebar has a cover of 63.5 mm and represents the prototype cask size. The length of all the lollipop specimens is the same and equal to 254 mm. The dimensions of the specimens and the molds are shown in Figure 70. Cracks on lollipop specimens with #10 rebar, containing 4% chloride ion per weight of cement cracked after approximately 3 months in the outdoor environmental conditions mentioned previously. The results from monitoring the crack widths over a fourteen month period are provided in Figure 71 and Figure 72 for two separate specimens with #10 rebar and in Figure 73 and Figure 74 for two separate specimens with #19 rebar. The crack growth continued during the aging process and the width of some of these cracks increased from 0.1 mm to 0.4 mm; in some cases, spalling could be seen on these specimens(The crack widths for these specimens are shown in Table A 24 and Table A 25 in the appendix).

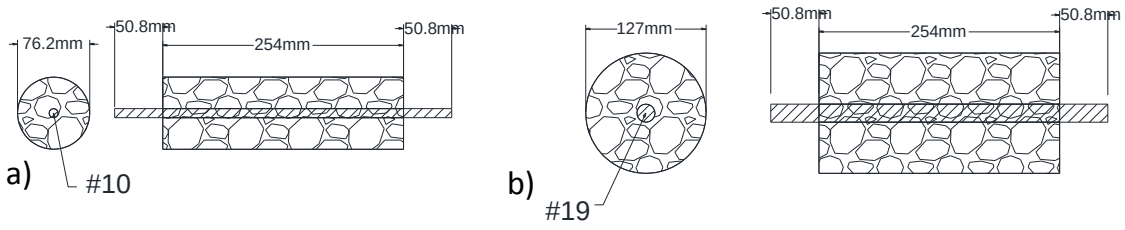

Figure 70 Corrosion/mass loss specimen dimension, (a) bar #10 (corresponds to #3 in US system) (b) bar #19 (corresponds to #6 in US system)

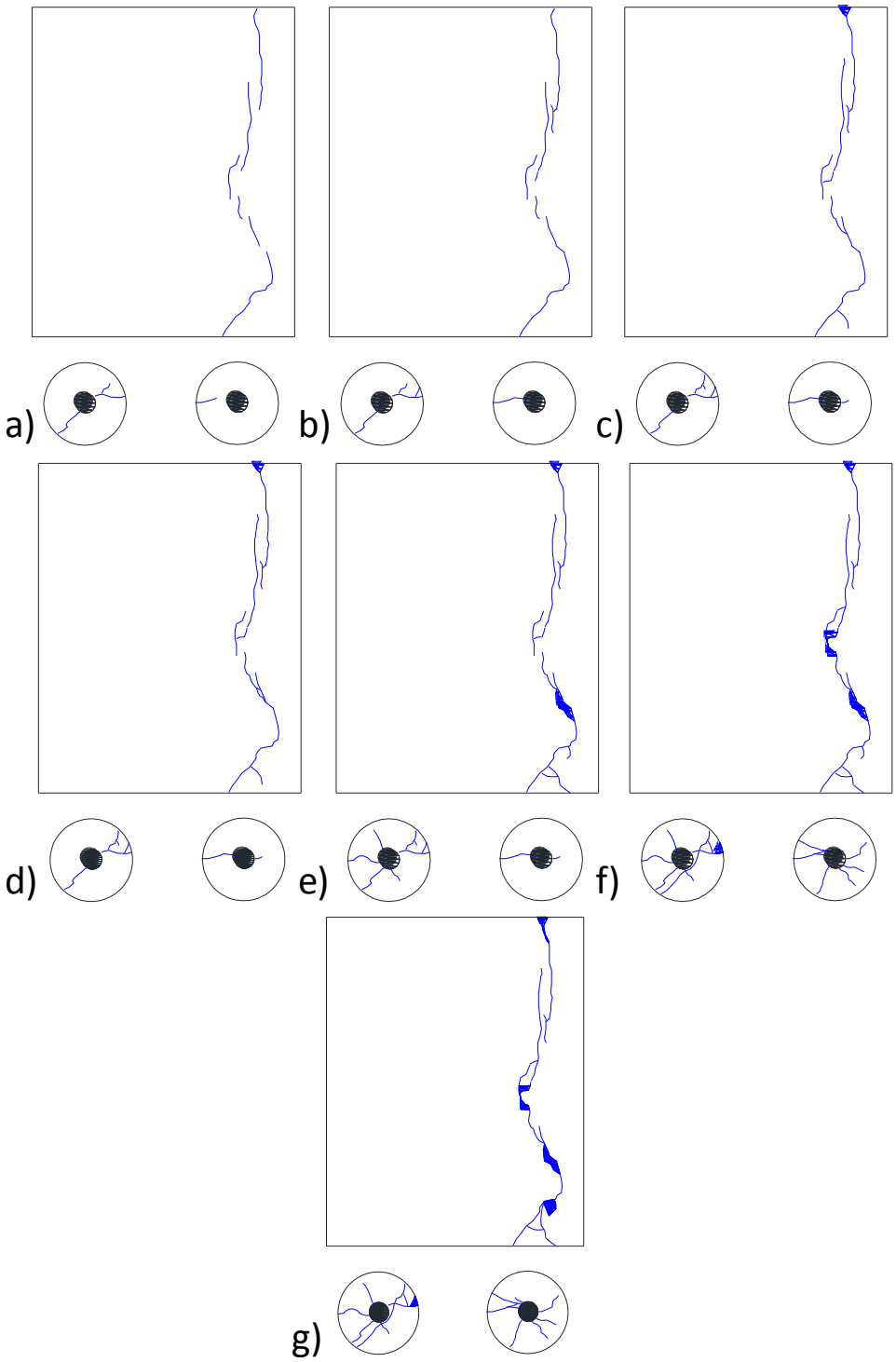

Figure 71 Crack maps on lollipop specimen no. 4 with #10 rebar at (a) 117 days (b) 171 days (c) 225 days (d) 276 days (e) 342 days (f) 432 days (g) 492 days.

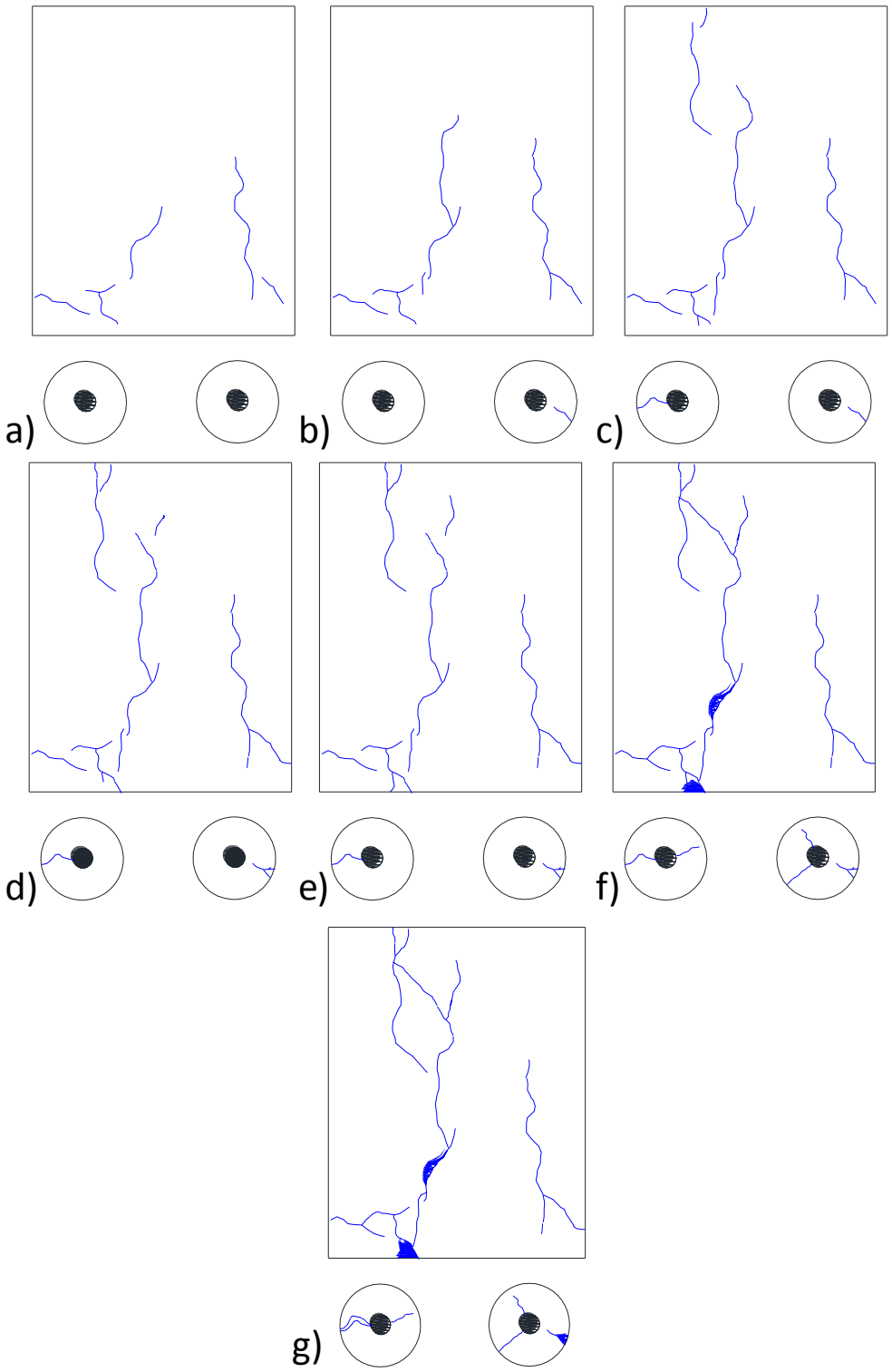

Figure 72 Crack maps on lollipop specimen no. 5 with #10 rebar at (a) 117 days (b) 171 days (c) 225 days (d) 276 days (e) 342 days (f) 432 days (g) 492 days.

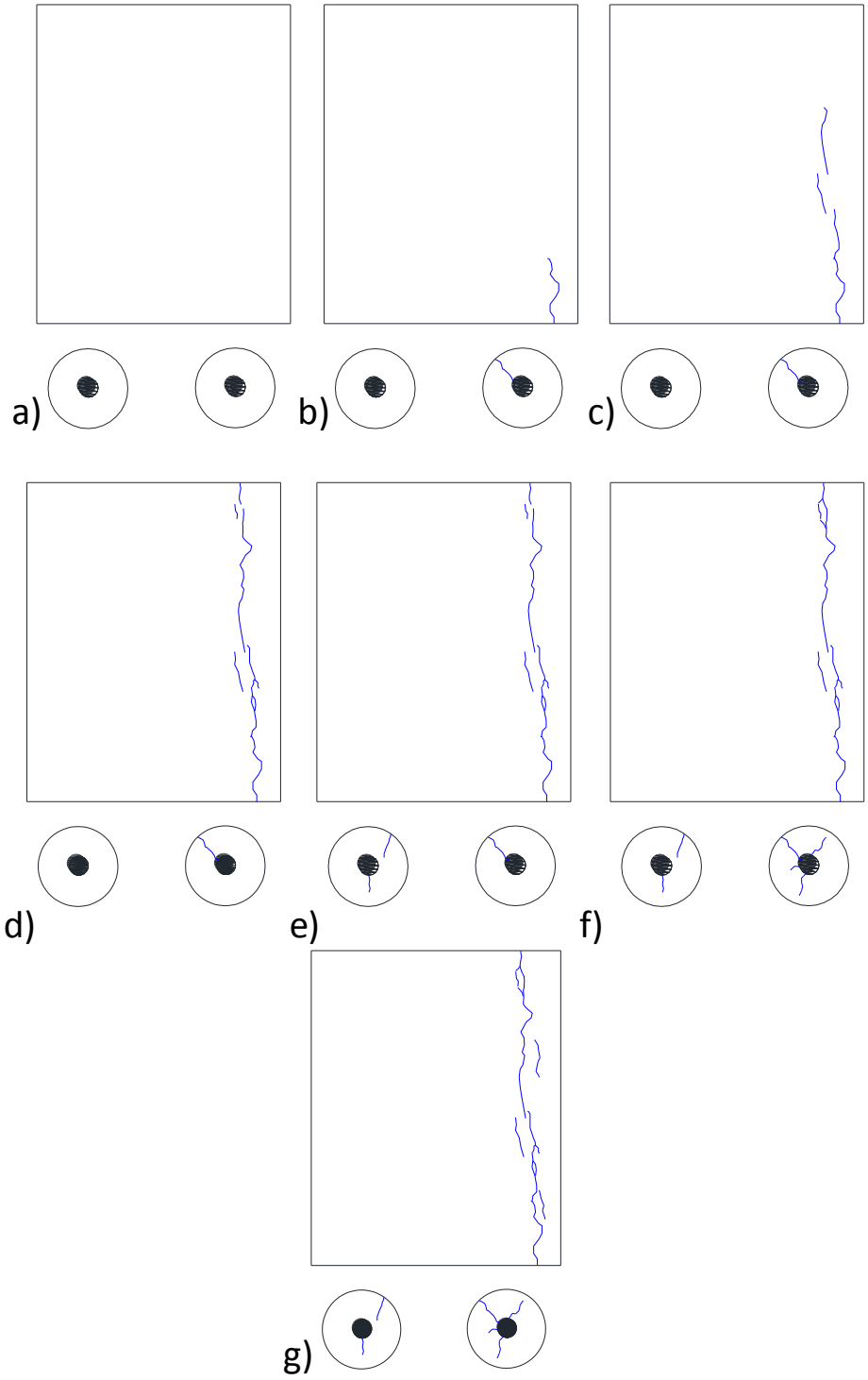

Figure 73 Crack maps on lollipop specimen no. 14 with #19 rebar at (a) 117 days (b) 171 days (c) 225 days (d) 276 days (e) 342 days (f) 432 days (g) 492days.

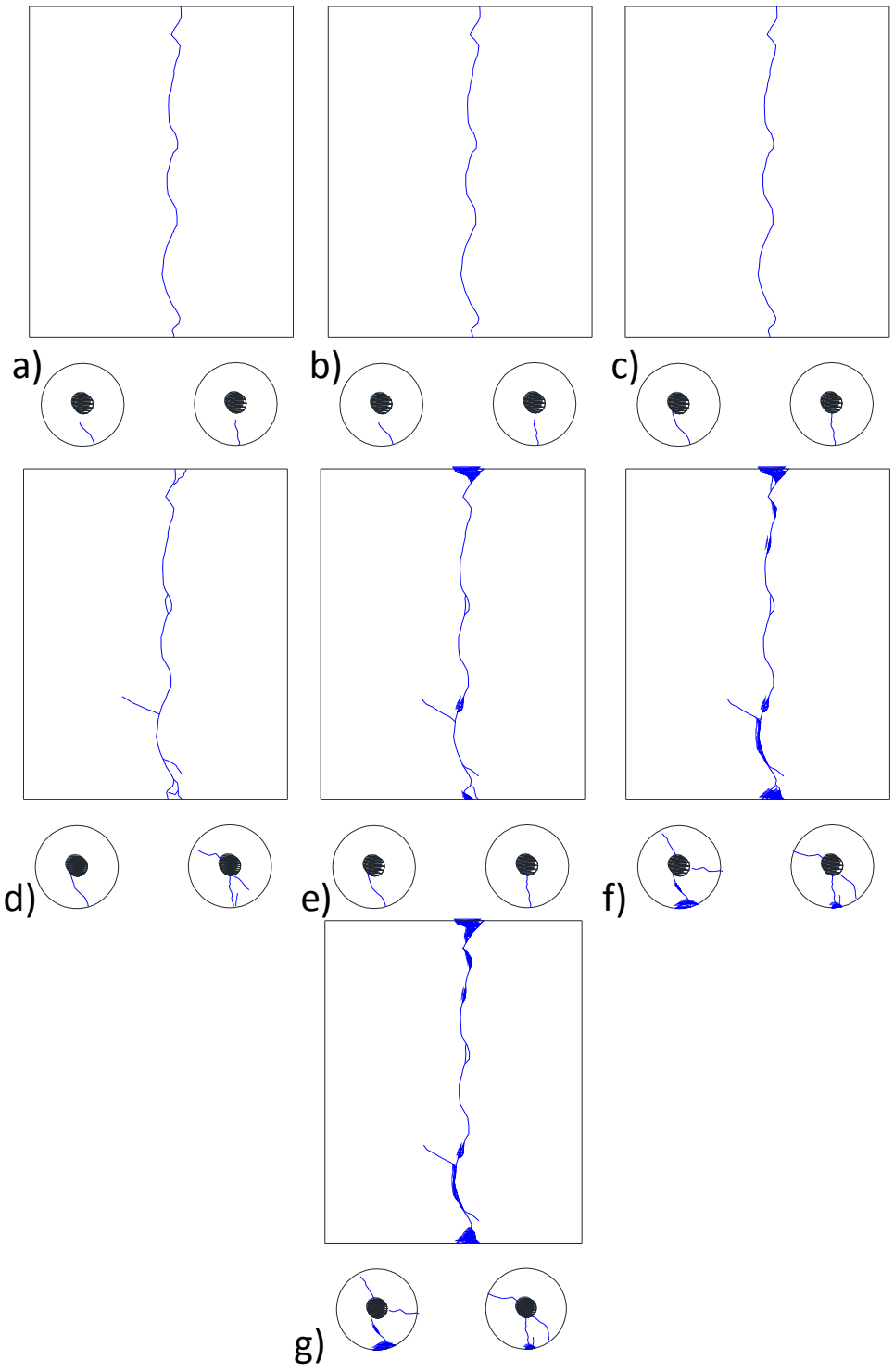

Figure 74 Crack maps on lollipop specimen no. 17 with #19 rebar at (a) 117 days (b) 171 days (c) 225 days (d) 276 days (e) 342 days (f) 432 days (g) 492 days

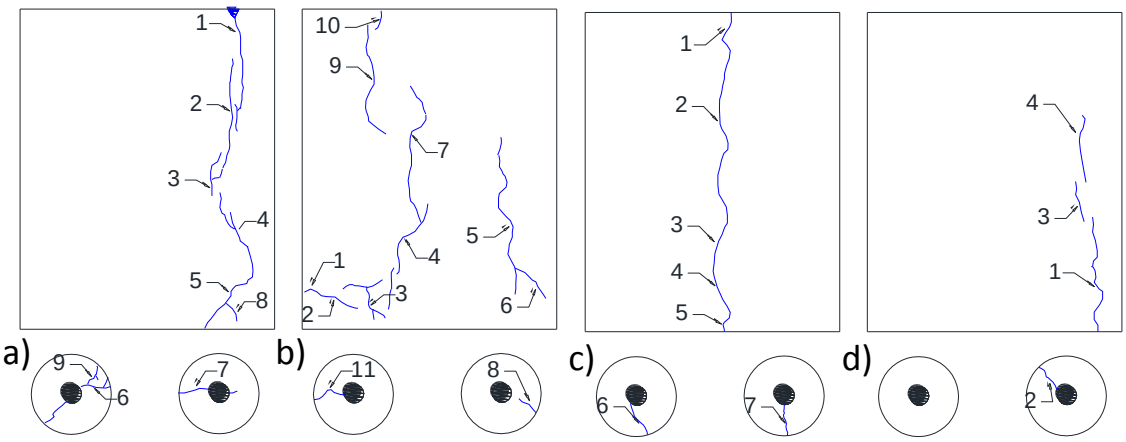

Figure 75 Crack numbers on (a) bar #10, No.4 (b) bar #10, No.5 (c) bar #19, No. 17, (d) bar #19, No. 14

4.4.2 Electrochemical tests

The effect of the addition of chloride ions was investigated by means of electrochemical monitoring of concrete and the corrosion behavior of steel embedded in concrete through two different tests: half-cell potential and surface resistivity.

4.4.2.1 Half-cell potential measurements

Half-cell potential measurement is one of the non-destructive methods that can help researchers understand the progress of corrosion with time. The device, as shown in Figure 76, measures the potentials on the surface of the concrete with respect to an arbitrary reference point on the reinforcement. The measured value is dependent on several factors such as temperature, type of reference electrode and pre-wetting time. These factors are explained below (NEA, 2002):

- *Concrete moisture content.* Depending on the moisture condition of concrete, its resistivity varies by as much as ±200 mV. It should be noted that moisture conditions of the whole structure affects the measurement, not only that of the determined point. Potential values become more negative as concrete moisture increases.

- *Cover thickness.* Increase in cover thickness makes locating the small corrosion spots harder by diminishing the difference between active and passive potential values which cause a uniform potential value at infinity.

- *Concrete carbonation*. As the carbonation process leads to an increase of concrete resistivity, potential measurements show more positive values on both passive and corroding bars.

- *Oxygen content.* Low oxygen content leads to a pronounced decrease of the rest potential. In wet concrete, due to a very low oxygen diffusivity coefficient, conditions may arise in a shift of potential to comparably negative values, so passive steel may show negative potentials similar to those of the corroding steel. This leads to the risk that passive areas under low aeration conditions could be considered corroding areas.

- *Chloride content.* There is a positive correlation between chloride content of concrete and potential values; the higher potentials indicate the area with higher chloride content.

Since concrete cover and chloride content are the same, the other four parameters, temperature, moisture, oxygen content and carbonation, should be considered during the measurement. Moisture and oxygen content are related to each other; when the moisture content of the specimens increases, the oxygen content decreases. In the case of observing carbonation, a note should be made for the measurement and the recording should be corrected accordingly. In this study, since the carbonation was not observed on the specimens, the temperature and humidity of the specimens are recorded alongside the half-cell potential. The half-cell potential measurements were repeated once a month.

Figure 76 Half Cell potential device (Giatec, 2014)

Table 47 shows the relationship between the potential values and corrosion probability based on ASTM C876 (2009a). Three points were measured and averaged.

Table 47 Relationship between the Potential Values and Corrosion Probability Based on ASTM C876 (2009a). (Note, CSE= Copper Sulfate Electrode)

Measured Potential (mV/CSE)	Probability of Steel Corrosion Activity
> -200	Less than 10%
-200 to -350	Uncertain
< -350	More than 90%

The dimensions of the test specimens are described in Section 0 and Figure 70. The measurement was performed at three different locations along the length of the rebar embedded in the concrete. The temperature effect was considered in these measurements and the value converted to measurement at 25 ˚C based on the JSCE-E 601-2000 (2002) using the following equation for the copper/copper sulfate electrode

$$P = 0.9 \times (T - 25) + P_0, \quad (62)$$

where *P* is the potential after correction, *T* is the temperature measured in Celsius and P_0 is the initial potential.

Figure 77 and Figure 78 show the potential measurement in specimens of first phase with #10 rebar and #19 rebar, respectively (see also Table A 26 and Table A 27 in the appendix). Potential

values more than -200mV/CSE indicate the probability of steel corrosion is less than 10%; when this value is less than -350mV/CSE, the probability of corrosion is more than 90%. It is clear from these results that for both rebar sizes in SCC and NaOH mixtures, the half-cell potential is higher than -200mV/CSE, which indicates little to no corrosion in these specimens. But in $CaCl_2$ mixtures, there is a high corrosion potential. It is also observed that specimens with #10 rebar have a higher amount of corrosion compared to the specimens with #19 rebar.

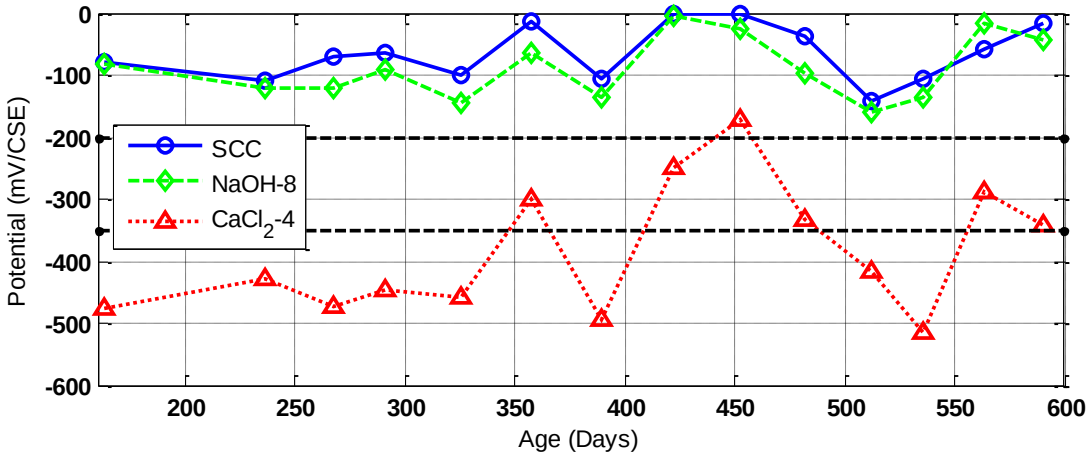

Figure 77 Half-cell potential measurements in specimens with #10 rebar (corresponds to #3 in the US system), phase 1

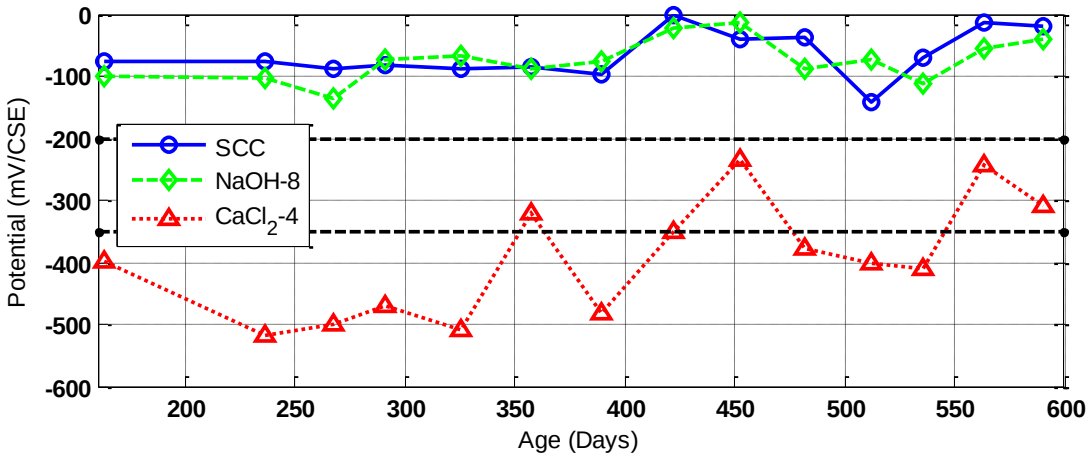

Figure 78 Half-cell potential measurements in specimens with #19 rebar (corresponds to #6 in the US system), phase 1

The specimens from the second phase with addition of different percentage of $CaCl_2$ showed a similar trend. Figure 79 shows that the probability of steel corrosion increased with the increasing amount of chloride (see also Table A 28 in appendix). It was also found that the effect of adding

1% and 2% chloride ion by weight of cement to the mixture was almost the same. However, 4% chloride drastically increased the probability of corrosion to more than 90%.

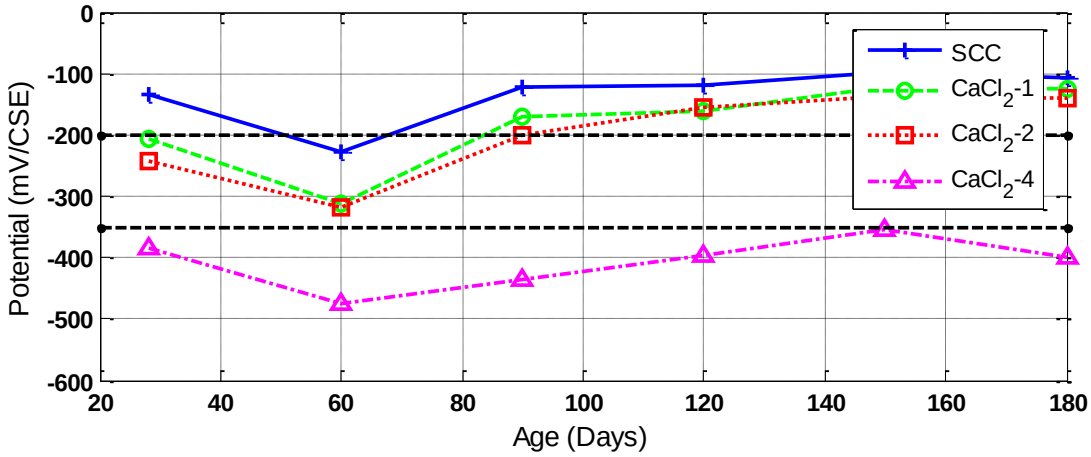

Figure 79 Half-cell potential measurements in $CaCl_2$ specimens with #10 rebar (corresponds to #3 in the US system), phase 2

4.4.2.2 Surface resistivity

Surface resistivity is a noninvasive and non-destructive test that gives information regarding the concrete's ability to resist chloride ion diffusivity, permeability, and properties of its pore water solution in water-saturated conditions (Streicher and Alexander, 1995; Morris et al., 1996). This test is performed directly on the surface of the structure. According to previous studies (Kessler et al., 2008; Rupnow and Icenogle, 2011; Ardani, 2012; Ghosh and Tran, 2015), this test has a good correlation with bulk diffusivity and rapid chloride penetration test (RCPT) and can be a reliable replacement for these tests. The measurement of concrete resistivity varies based on different factors such as (NEA, 2002):

- *Humidity content.* The surface resistivity (ρ) decreases when concrete moisture increases and vice versa. The ρ is an indirect measure of saturation of the concrete.

- *Temperature*. The effect of temperature is controversial, as its effect on ρ depends on whether the concrete is shielded or not, i.e. whether the water can evaporate or condensate. Thus, an increase of *T* will decrease the ρ unless the opposite occurs due to drying induced by increasing T. The opposite happens when *T* decreases, but only until a certain *T* (around 5 °C), below which the *ρ* increases so much that the condensation cannot compensate for this dramatic increase.

- *Chloride content*. The presence of chlorides induces a certain decrease of the *ρ*.

- *Carbonation*. Carbonation increases ρ due to the densification that the formation of calcium carbonates usually induces.

- *Type of cement*. Blending agents (fly ashes, slags or silica fume) in general induce an increase of ρ when compared with ordinary Portland cement.

- *Porosity*. The porosity is a consequence of the w/c ratio and the compaction and curing. An increase in w/c leads to a decrease of ρ.

- *Type of aggregate*. The effect of the aggregate type cannot be generically predicted. It will depend on their nature and porosity, but for the same grading, the concrete resistivity is influenced by the nature of the aggregate.

To reduce these effects and obtain similar conditions of specimens, the electrical resistivity of water-saturated concrete is measured based on AASHTO TP 95 (2014). To obtain the saturated concrete cylinders, specimens must remain in a 100% humidity condition for at least 7 days before testing; therefore, the specimens of all three mixtures were immersed in water and kept inside the lab during this time period. Additionally, to see the difference and make sure that the specimens with NaOH and $CaCl_2$ content were not losing some of their free ions because of

immersion, they were also stored in solutions with 1.3 g/l NaOH and 6.85 g/l $CaCl_2$ respectively as shown in Figure 80. After the specimens were removed from the water, the excess water was blotted off and they were placed inside the surface resistivity measurement device as shown in Figure 81. This test repeated once a month.

Figure 80 Immersing specimens inside water, NaOH or $CaCl_2$ solutions

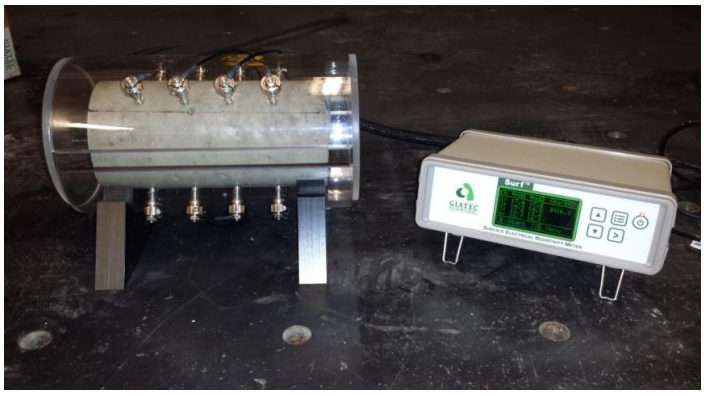

Figure 81 surface resistivity measurement device

AASHTO TP 95-14 (2014) present a table that shows the chloride ion penetrability based on the surface resistivity test, shown in Table 48 for 100 x 200 mm cylinder specimens.

Table 48 Relationship between the Surface Resistivity and Chloride Ion Penetrability Based on AASHTO TP 95-14 (2014)

Chloride Ion Penetrability	Surface Resistivity Test
	100 x 200 mm Cylinder (kOhm-cm)
High	< 12
Moderate	12 -21
Low	21- 37
Very Low	37 – 254
Negligible	> 254

Results of surface resistivity measurements on first phase specimens are shown in Figure 82 (see also Table A 29 in the appendix). The results indicate that SCC has moderate chloride ion permeability and the other two mixtures (NaOH and $CaCl_2$) have high chloride ion permeability based on AASHTO TP 95-14 (2014). Figure 83 (see also Table A 35 in the appendix) show the surface resistivity for NaOH specimens, in the second phase. The specimens without sodium hydroxide showed the lowest surface resistivity and the specimens with the highest amounts of sodium hydroxide (0.8%) show the highest resistivity. The other two mixtures have almost the same resistivity. The resistivity in all cases increases with aging. Figure 84 (see also Table A 31 in the appendix) shows the surface resistivity for $CaCl_2$ mixtures. In this series of specimens, the addition of calcium chloride decreased the resistivity, except in the case of addition of 2% chloride ion to the mixture. The surface resistivity of already aged specimens of the TRIGA reactor was measured using the same method and the results are shown in Table 49 These results show high chloride ion permeability for this aged concrete which can lead to corrosion of rebars inside the concrete and decrease the serviceability of the structure. The surface resistivity of TRIGA specimens was 75%, 41%, and 58% less than SCC, NaOH-8 and $CaCl_2$-4 specimens from the first phase, respectively.

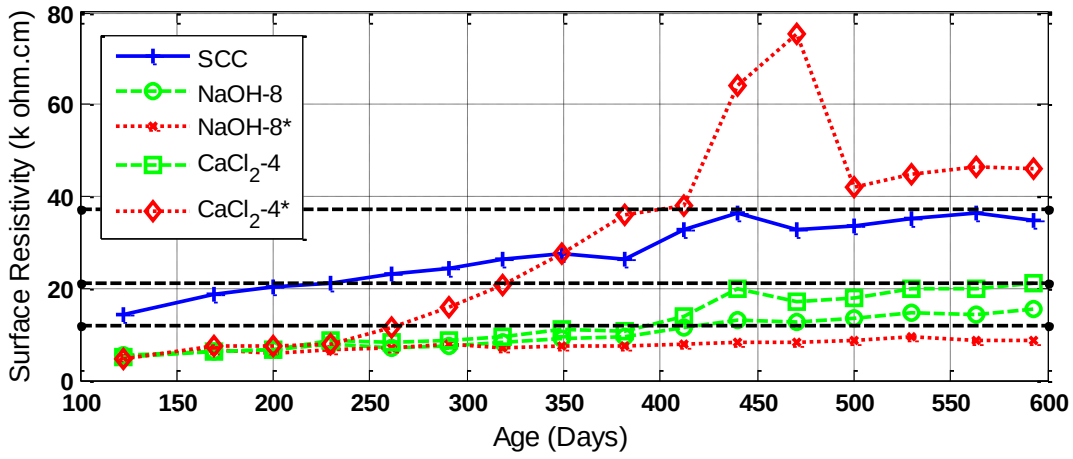

Figure 82 Surface resistivity of three concrete mixtures at different ages (*: indicate specimens in solution NaOH-8 in 1.3 g/l NaOH solution and $CaCl_2$-4 in 6.85 g/l CaCl2 solution), phase 1

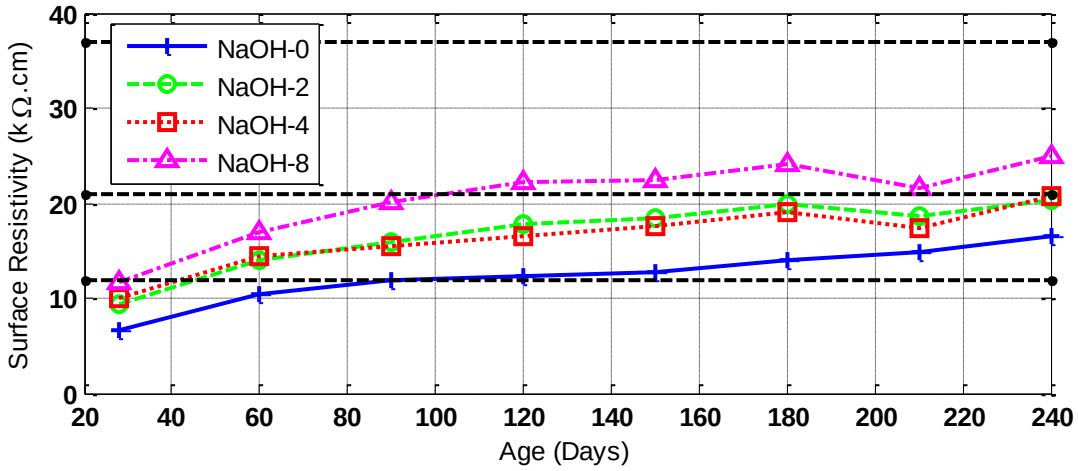

Figure 83 Surface resistivity of NaOH mixtures at different ages, phase 2

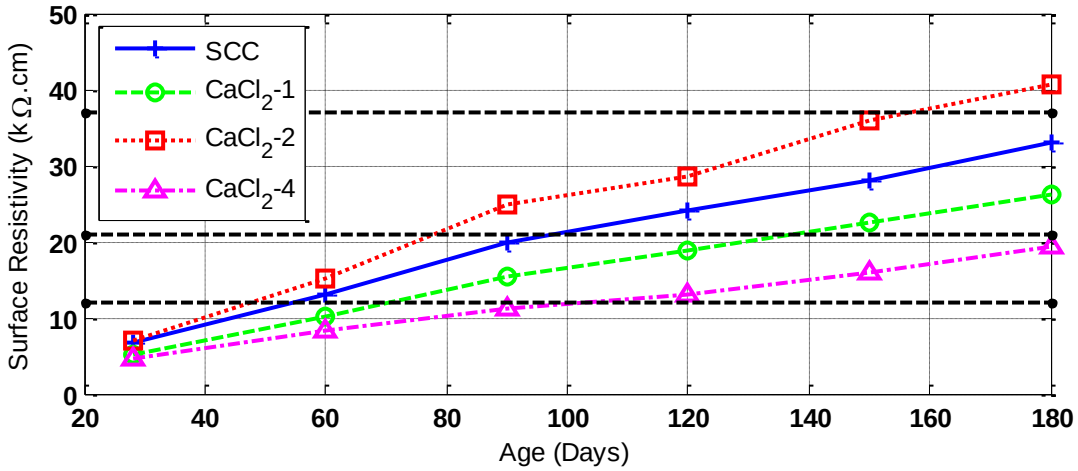

Figure 84 Surface resistivity of $CaCl_2$ mixtures at different ages, phase 2

Table 49 Surface Resistivity of TRIGA Specimens

No.	ρ (KΩ.com)
1	9.8
2	9.8
3	7.5

4.4.3 Ultrasonic Pulse Velocity (UPV)

UPV is a non-destructive test to estimate flaws and uniformity inside the concrete by measuring the propagation velocity of an ultrasonic pulse that travels through the material (Ohdaira and Masazawa, 2000). The velocity primarily depends on the elastic properties of the materials and is almost independent of the geometry. For concrete, because of the high scattering that occurs at matrix/aggregate interfaces as well as at micro cracks, the velocity is measured using through-transmission techniques (Bungey and Millard, 1996). UPV can give information regarding quality of concrete. Higher velocities are obtained when density, homogeneity and uniformity are good and low velocity indicates poor quality. Based on this knowledge, BS 1881 (1983) classifies the concrete quality based on UPV as shown in Table 50. Therefore, UPV not only can be used for quality control, such as identification of cracks and voids, but also allows the evaluation of aging and deterioration of reinforced concrete structures.

Table 50 Quality of Concrete Based on BS 1881 (2005)

UPV (m/s)	Concrete Quality
Above 4500	Excellent
3500 to 4500	Good
3000 to 3500	Medium
Below 3000	Doubtful

The wave velocity inside the specimens was measured by using a UPV system based on ASTM C597M (1997b); see Figure 86. The ultrasonic equipment consists of a pair of transducers, one is for transmitting and the other one for receiving the ultrasonic pulses. To perform this test, a conductive gel is applied on the surface of the transducers (here, 54 kHz transducers that

measure the P-wave were used). Afterwards, they are placed on the sides of the specimens along the same line and the wave velocity is recorded. There are three basic ways in which the transducers may be arranged, opposite faces (direct transmission), adjacent faces (semi-direct transmission) and same face (indirect transmission), as shown in Figure 85. The most reliable method is the direct reading and the least satisfactory method is the indirect reading since the received signal amplitude might be less than 3% of that for a comparable direct transmission (Bungey and Millard, 1996). For this study the direct reading is used for the material level tests.

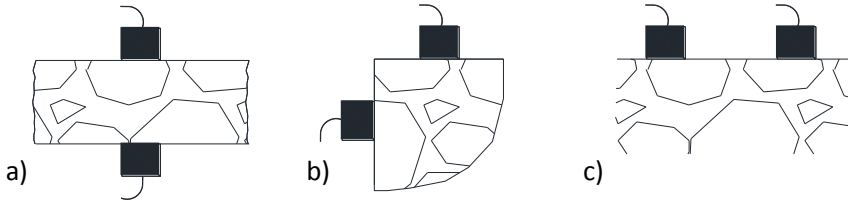

Figure 85 Types of reading, (a) direct (b) semi-direct (c) indirect

The velocity of sound is calculated according the following formula

$$V = \frac{L}{t}, \tag{63}$$

where V is wave velocity (m/s), L is length of specimen (m), and t is the transit time (s). The UPV measurement was repeated once a month.

Figure 86 Ultrasonic pulse velocity system

Figure 87 (see also Table A 29 in the appendix) shows the velocity measurements in NaOH and SCC specimens of first phase at different ages. The temperature and relative humidity of the

storage environment are also included in Figure 87. The higher UPV measurements between 129 days and 261 days is due to an increase in the water content of specimens and lower temperatures, which reduce the loss of moisture. This is in accordance with the findings of Ohdaira and Masazwa (2000) and Panzera et al. (2011) that UPV increases with an increase in the specimen's water content. UPV is also related to the strength of concrete; therefore, when temperature and relative humidity are almost the same, it can be said that according to the results, the compressive strength did not change substantially.

UPV was measured on the cores taken from TRIGA reactor. These cores did not contain rebar and the direct measurement was performed in a manner similar to the method used for specimens in the first and second phases of the project. Table 51 shows the UPV measurement on 6 different concrete specimens from this structure. The average UPV measurement shows that the quality of concrete in the harsh environment of a reactor with high temperature and nuclear radiation after 33 years is good and in the acceptable range. The results from these specimens were close to the mixtures prepared in the lab. The difference can be explained due to the water content of specimens at the time of testing as well as the type of aggregate used in TRIGA. TRIGA specimens were completely dry during the testing; therefore, moisture content had little to no effect on the results. Furthermore, magnetite was mixed with concrete of the TRIGA reactor to provide extra shielding, which can affect the wave speed inside the concrete matrix.

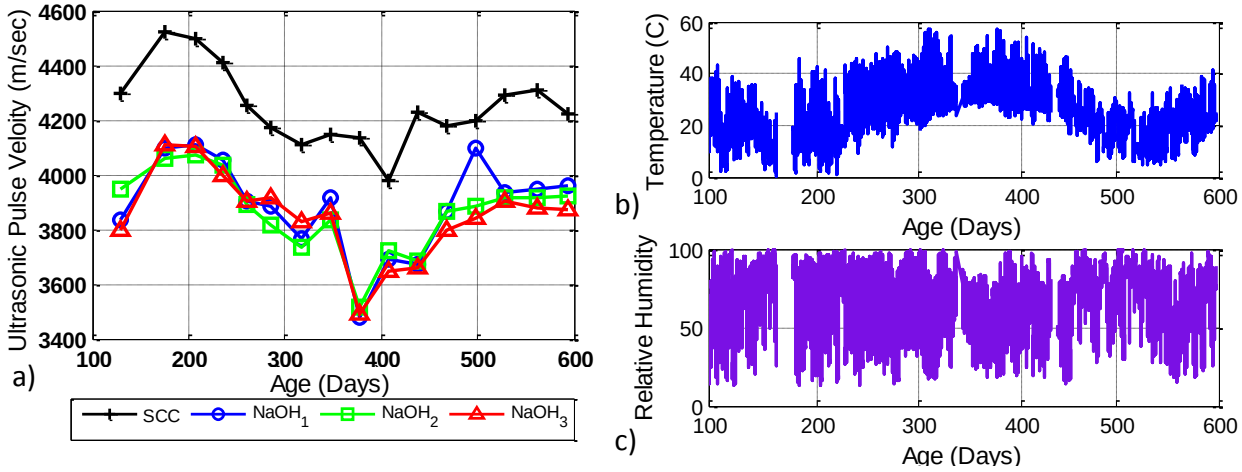

Figure 87 (a) UPV measurement of specimens in phase 1 (b) ambient temperature from 100 to 600 days (c) relative humidity from 100 to 600 days

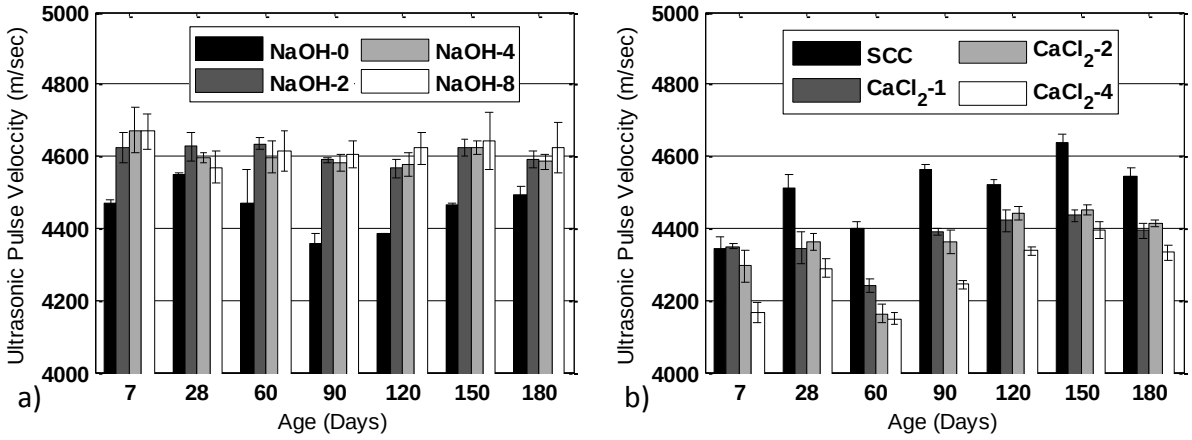

Figure 88 UPV measurement on prisms (a) NaOH concrete mixture, phase 2(b) $CaCl_2$ concrete mixture, phase 2

Table 51 UPV Measurement Results of TRIGA Specimens

No.	V_{avg} (m/sec)	Average
1	4027	3962
2	4352	
3	4100	
4	3909	
5	3771	
6	3612	

4.4.4 Schmidt hammer

Schmidt hammer is one of the non-destructive testing methods used to estimate the relative strength of concrete in structures. However, it can provide only an estimate of strength; it cannot be considered a substitute for a compressive strength test. According to ASTM C805 (2013e), the concrete members for this test shall be at least 100 mm thick and the distance between each impact point shall be at least 25 mm. Also this test should not be performed on frozen concrete. In this study, Schmidt rebound hammer is used on the specimens of NaOH and $CaCl_2$ mixtures prepared in the second phase at ages of 7, 28, 90 and 180 days. Figure 89 shows the Schmidt hammer used in testing. The results of these tests are shown in Figure 90 (see also Table A 35 and Table A 36 in the appendix).

Figure 89 Silver Schmidt hammer (Humboldt, 2015)

The results indicate an increase in the strength of NaOH concrete mixtures of phase 2 until 28 days; at later ages, the strength is almost similar in all the mixtures. It should be noted that a high percentage of sodium hydroxide (NaOH-8) reduces the concrete strength at both early ages and later ages. The results of $CaCl_2$ addition to the second phase showed a higher strength for concrete with 2% percent ($CaCl_2$-2) due to the higher hydration amount and lower strength in CaCl2-4 mixtures caused by the excessive amount of calcium chloride inside the mixture. The

results of testing on all the specimens in the second phase are similar to compressive strength obtained from destructive testing.

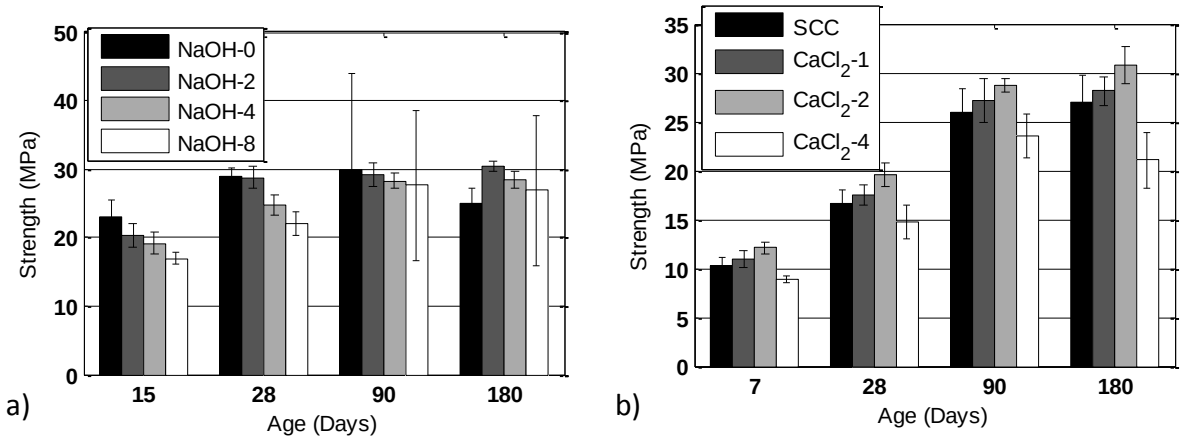

Figure 90 Schmidt hammer (a) NaOH concrete mixture, phase 2 (b) $CaCl_2$ concrete mixture, phase 2

4.5 Other Measurements

4.5.1 Mass loss

Corrosion (through half-cell potential) and mass loss, as a function of age, are measured for both #10 and #19 rebar. The specifications of these specimens are discussed in Section 0 and Figure 70. To measure the mass loss, the rebar is cleaned with the use of a soft brush in a solution that contains hydrochloric acid, antimony trioxide and stannous chloride. Because of the high amount of acid vapor, this cleaning is performed inside a fume hood with carbon filters. After the rebar is cleaned, the mass loss is measured using a gravimetric method and through a direct comparison to the mass that was measured and recorded prior to the rebar being placed inside the concrete cylinders.

The level of corrosion in the lollipop specimens was determined through mass loss tests. The results of tests at 28, 210 and 365 days are shown in Table 52. From the results it is seen that the mass loss of $CaCl_2$ specimens with both #10 and #19 rebar increased with the age of the concrete.

Additionally, the corrosion rate at 28 days was higher than at the later age, which indicates that the rate of corrosion is higher at the beginning and it decreases with aging.

Table 52 Mass Loss and Corrosion Rate of Lollipop Specimens of Phase 1

Bar Size	Mix	28 Days		210 Days		365 Days	
		Mass loss (%)	Corrosion rate (mm/year)	Mass loss (%)	Corrosion rate (mm/year)	Mass loss (%)	Corrosion rate (mm/year)
#10	SCC-PH1	0.51	0.076	0.51	0.009	0	0
	NaOH-8-PH1	0.51	0.076	0.26	0.005	0	0
	$CaCl_2$-4-PH1	1.27	0.19	1.27	0.023	2.02	0.036
#19	SCC-PH1	0.132	0.037	0.26	0.009	0.13	0.004
	NaOH--PH18	0	0	0.13	0.004	0.13	0.004
	$CaCl_2$-4-PH1	0.652	0.185	1.81	0.039	1.19	0.037

5. CASE STUDY AT THE STRUCTURAL LEVEL

5.1 Geometry

The concrete cask is a reinforced concrete structure with a structural steel inner liner and base, see Figure 91. The reinforced concrete wall and steel liner provide the neutron and gamma radiation shielding for the stored spent fuel. The reinforced concrete wall provides the structural strength to protect the test shipping cask (TSC) and its contents in natural phenomena such as tornado wind loading and wind-driven missiles, and during a non-mechanistic tip-over event. The concrete cask provides an annular air passage to allow the natural circulation of air around the TSC to remove the decay heat from the contents. The concrete portion of the cask is constructed by placing concrete between a reusable, exterior form and the steel liner. Reinforcing bars are used near the inner and outer concrete surfaces to provide structural integrity. Table 53 summarizes the main dimensions (relevant to this study) of the common vertical concrete casks in United States. As one can see, the dimensions are similar for the different concrete versions. A scale factor of 2.83 was used in construction of the physical models. The scaled dimensions for the average of the casks under consideration and the dimensions used in the physical cask models are further discussed in Section 5.2.

Table 53 Main Dimensions of Most Common Vertical Concrete Casks in the US (Dimensions in mm, Note: Hi-Storm Concrete Section is enclosed by Two Steel Liners)

Vertical Concrete Cask	Height	Outer Dia.	Liner Thick.	Concrete Thick.
MAGNASTOR CC1&CC2	5723	3454	44.5	673
MAGNASTOR CC3	5545	3454	76.2	643
VSC-24	5718, 5410, 5000	3353	44.5	737
Hi-Storm	5867	3353	51	699
NAC-UMS	5309-5740	3454	63.5	711
VSC-17	5740	2667	89	508
Average	5607	3416	56	692
Scaled Average	1979	1206	19.8	244
Physical Model	2032	1219	16	238

5.2 Selection of Cask Dimensions and Similitude

According to the design specifications of the casks mentioned in Section 5.1, average values of dimensions were used for the scale model. It is obvious that results of the test are more consistent with reality as the scaling factor decreases. Three specimens with a scaling factor of 2.83 were fabricated, one for each of the normal, corrosive and alkali-silica reactive concrete mixtures. The scaling factor was mostly governed by availability of plate thickness on the market. The dimensions of the prototype and scaled model are provided in Table 54. The prototype cask information is based on a review of most commonly used commercial cask designs with an exposed reinforced concrete (RC) overpack. The cask geometry is shown in Figure 91, where the main components are identified. Note that the rebar cage is removed from the drawings for clarity and it is shown separately in Figure 92.

Table 54 Dimensions of the Prototype and Scaled Models

Property	Prototype Size (mm)	Scaled Size (mm)	Final Dimension (mm)
VCC length (standard)	5722.6	2019.7	2032.0
VCC outer diameter	3454.4	1219.2	1219.2
Concrete thickness	673.1	237.6	238.1
Liner length	5557.5	1961.5	1968.5
Liner inner diameter	2019.3	712.7	711.2
Liner thickness	44.5	15.7	15.9
Air outlet	1300 × 114	459.5 × 40.4	457.2 × 44.5
Air outlet plate thickness	6.35	2.11	3.2
Air inlet	1300 × 114.0	459.5 × 40.4	457 × 38.1
Air inlet top thickness	50.8	18.0	19.1
Air inlet side thickness	19.1	6.35	6.35

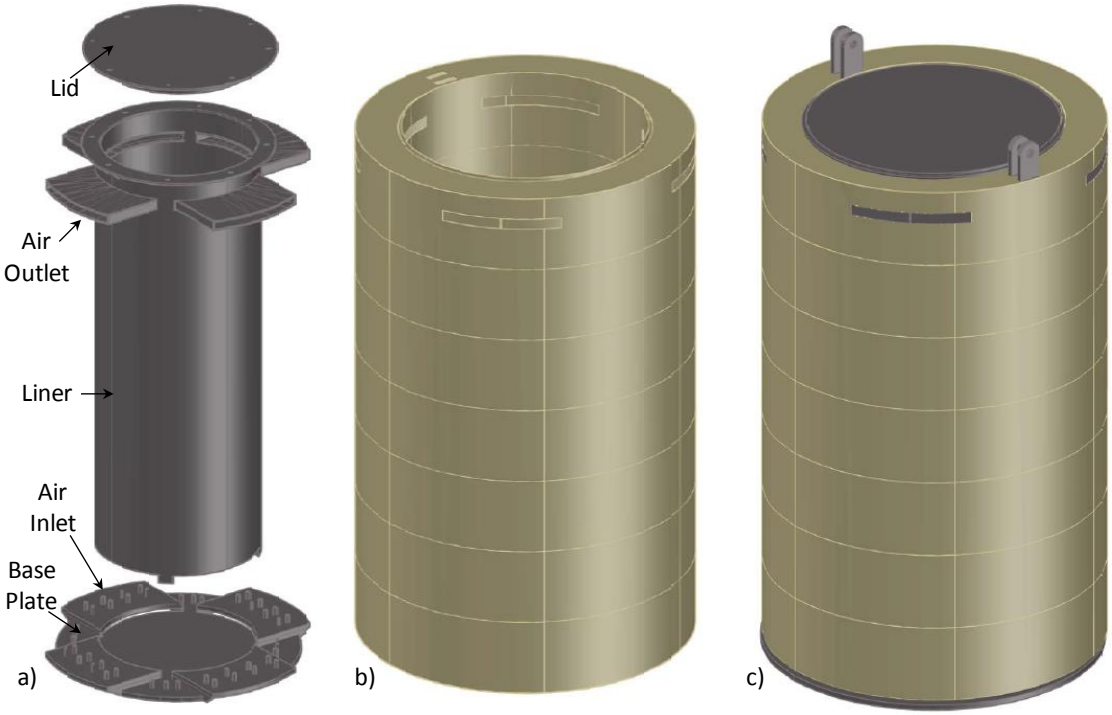

Figure 91 Cask model (a) steel components, (b) concrete shield, and (c) cask

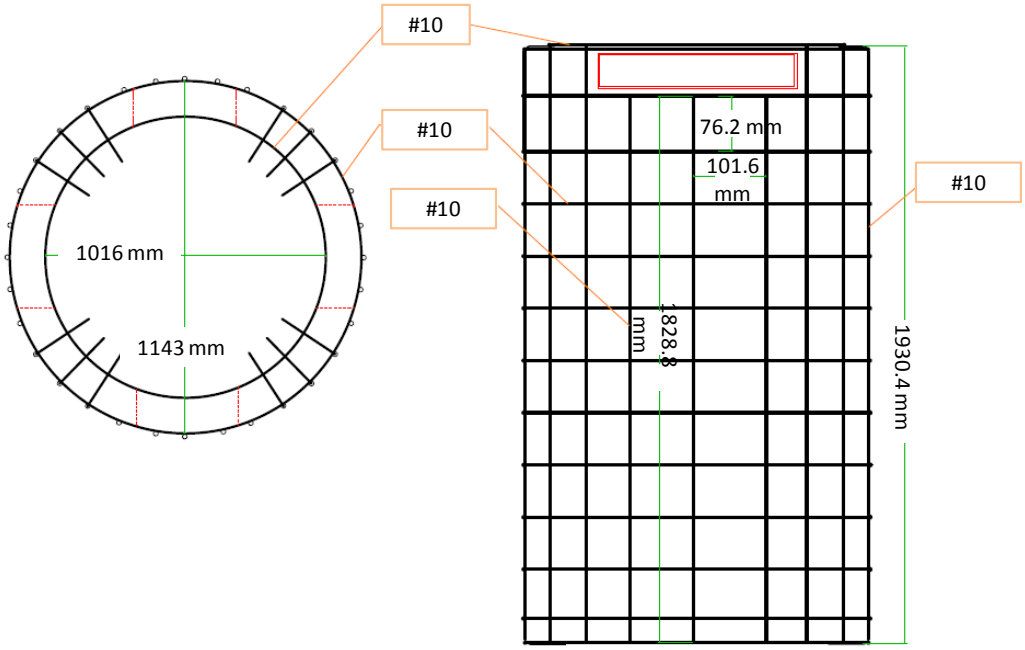

Figure 92 Rebar cage

The concrete cover was equal to 40 mm in the scaled casks and #10 rebar (9.5 mm diameter) was used as both vertical and horizontal reinforcement. The yield strength of the rebar was found to be 551.4 MPa, as shown in Section 3.1. The rebar were fabricated at a precast concrete plant

and shipped to the University of Houston Structural Research Laboratory. They were placed around the steel liner in the laboratory—see Figure 94(a)—before the concrete molds were assembled as shown in Figure 94(b). The three concrete mixtures, two identical SCC mixtures with 25% fly ash replacement of cement and one SCC mixture with no fly ash replacement of cement, were delivered separately in three ready-mix trucks. NaOH powder was added to the fresh SCC mixture with no fly ash to accelerate ASR and mixed inside the truck for 15 min before casting. The concrete mixtures for the cask were provided along with the first phase concrete. Similarly, $CaCl_2$ flakes were added to one of the SCC mixtures with fly ash to accelerate corrosion. Thereafter, casks were poured as shown in Figure 93, and formwork was sealed with plywood and plastic sheets to prevent rapid loss of moisture. After 28 days of casting, the formwork was removed. A picture of the three cask models is shown in Figure 94(c).

Figure 93 Casting three concrete casks

Figure 94 (a) steel parts and rebar cage, (b) mold for concrete casting, and (c) three concrete casks

5.3 Results

A series of non-destructive testing, such as UPV, half-cell potential, visual inspection and Schmidt hammer, was performed on the three casks, SCC, NaOH-8, and $CaCl_2$-4, to see the effect of the addition of chemicals at the structural level to check the validity of proposed method in this study. The results are presented in the following sections.

5.3.1 Schmidt hammer

Schmidt hammer was used to estimate the compressive strength distribution of the casks along their height at 370 days. The Schmidt hammer measurements were calibrated using the actual compressive strengths obtained from material testing such that the mean value along the height was the same as the average of the material test results at 365 days. The strength was measured using a Schmidt hammer at ten equally spaced locations along the height of the cask. Ten measurements were collected around each location and averaged. The results of these measurements are shown in Figure 95. Before calibration, the SCC cask showed the highest strength and the NaOH-8 cask showed the lowest strength, which was in line with the material tests presented in Section 4. In all three casks, the strength was found to decrease along the height of the casks from bottom to top. This is attributed to the settlement of the coarse aggregate towards the bottom of the casks, since the casting was done from the top and a self-consolidating mixture was used. Although some variation along the height is observed, the strengths at the bottom were approximately 17%, 28% and 30% higher than those at the top for the SCC, NaOH-8 and $CaCl_2$-4 casks, respectively.

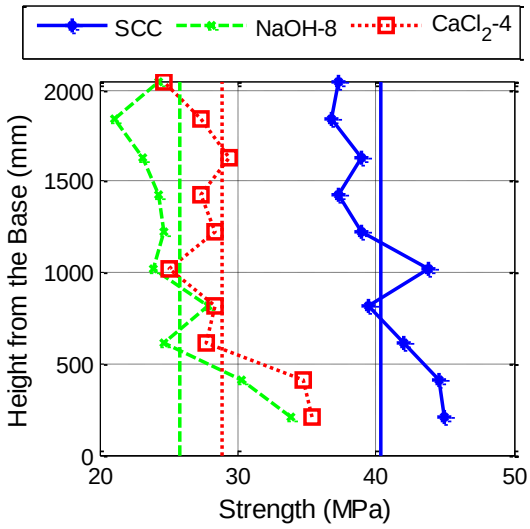

Height from the base (mm)	SCC Cask (MPa)	NaOH-8 Cask (MPa)	$CaCl_2$-4 Cask (MPa)
2042	37.3	24.3	24.7
1838	36.8	21.1	27.4
1634	38.9	23.1	29.4
1430	37.3	24.3	27.4
1225	38.9	24.7	28.4
1021	43.8	23.9	25.0
817	39.5	27.9	28.4
613	42.0	24.7	27.7
408	44.6	30.3	34.7
204	45.0	33.9	35.4
Avg.	40.42	25.82	28.9

Figure 95 Schmidt hammer measurement. Note that the vertical dashed lines in the figure shows the average compressive strength measurements at 365 days from material tests.

5.3.2 Visual inspection

Cracks were observed in the NaOH cask approximately 90 days after casting. This indicates that the ASR process was accelerated considerably, given that in regular structures it takes approximately 10 years until the first appearance of cracks (IStructE, 2010). The crack maps for ASR accelerated casks at 517 and 591 days are shown in Figure 96(a) and (b), respectively. Comparing the time of appearance of cracks on the casks and small NaOH-8 specimens of prepared in phase 1, it is clear that ASR cracks were observed around the same time at both levels; however, the density of the cracks was different due to the differences in geometry. The density of cracking increased with time and higher crack density was observed towards the top of the cask, potentially due to lower concrete strength in that region as explained above. Similar to the results of material specimens presented in Section 0, the crack widths remained between 0.05 mm and 0.1 mm over the measurement period.

On the $CaCl_2$-4 cask, the first cracks were visually observed after around 120 days. Comparing the time frame of the appearance of cracks on the surface of the specimens at the material level,

prepared in the first phase, there is a one month period difference, which shows the effect of geometry of structure on the speed of the corrosion reaction and propagation of cracks. The crack propagation over time on the $CaCl_2$-4 cask is shown in Figure 97. After less than a year, there was extensive cracking on the casks and several of the cracks had coalesced. The crack width was measured at 23 randomly chosen points on the casks, and the change over time in the average crack width is shown in Figure 98 (see also Table A 37 in the appendix). It is seen that at 569 days (i.e., the last measurement) the cracks were 0.33 mm wide on average with the largest and smallest measurements being 0.1 mm and 1.0 mm.

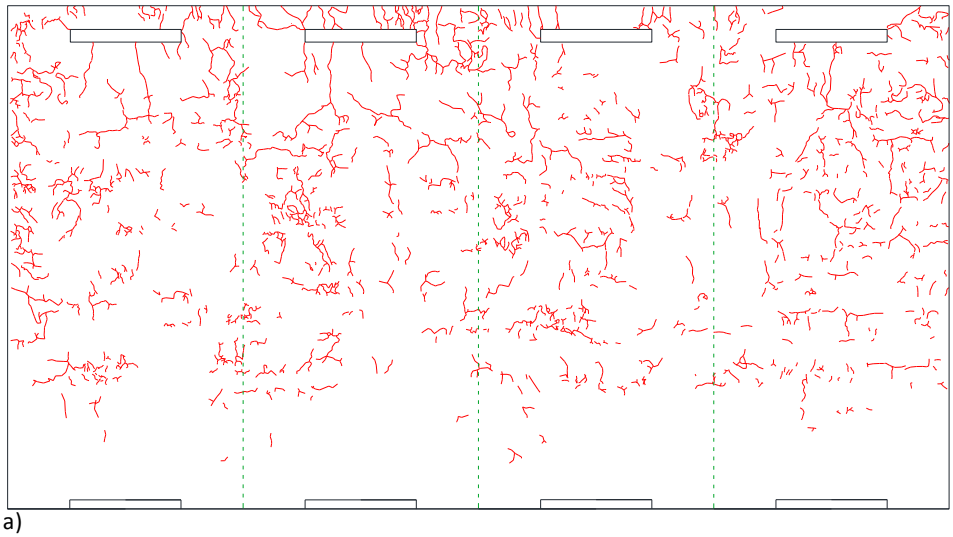

a)

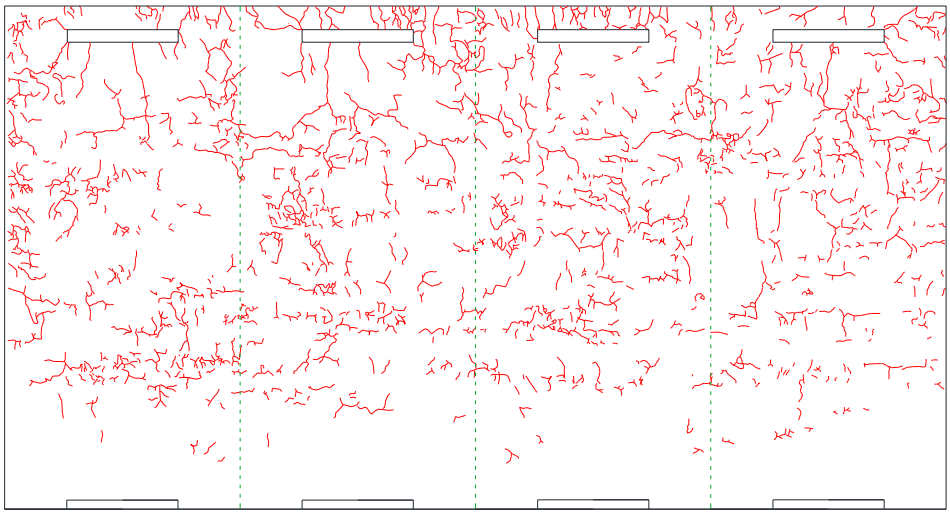

b)

Figure 96 Crack propagation on cask with NaOH-8 mixture (a) 517 days (b) 591 days

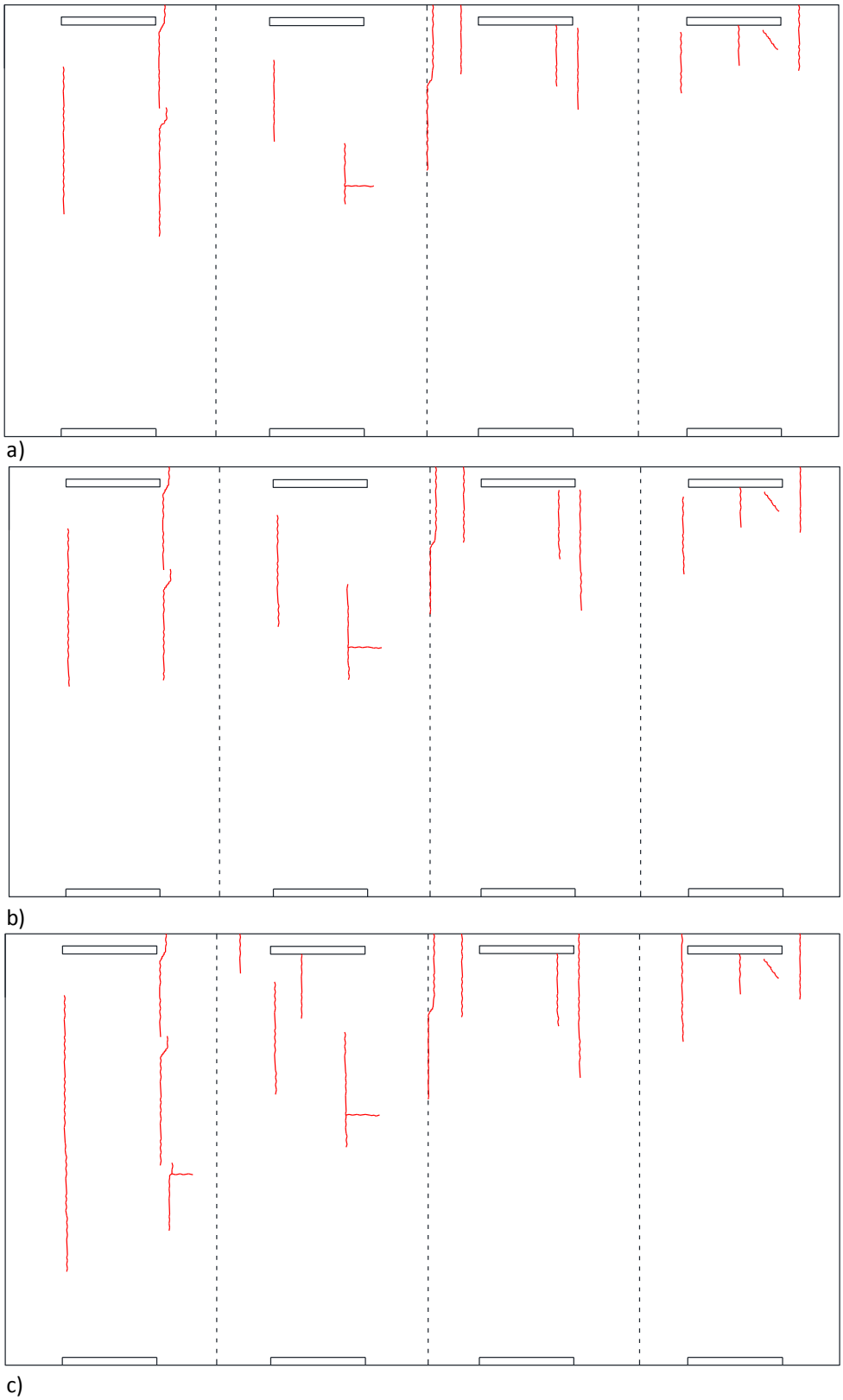

Figure 97 Crack propagation on cask with $CaCl_2$-4 mixture (a) 163 days (b) 186 days (c) 225 days (d) 295 days (e) 512 days (f) 569 days

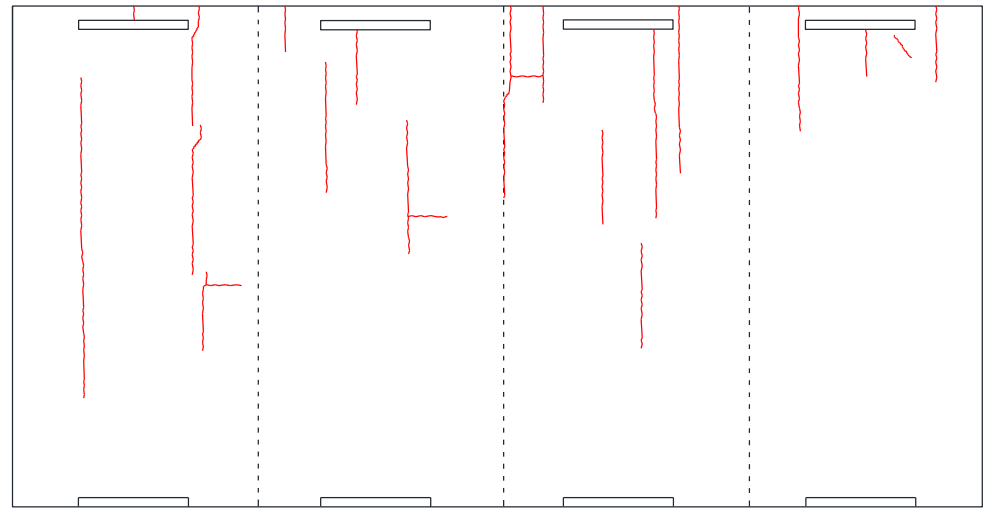

d)

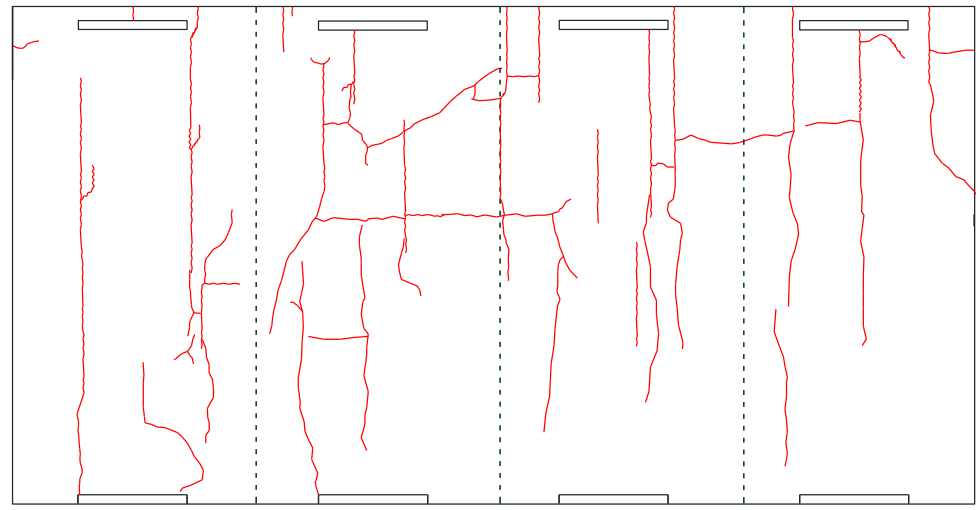

e)

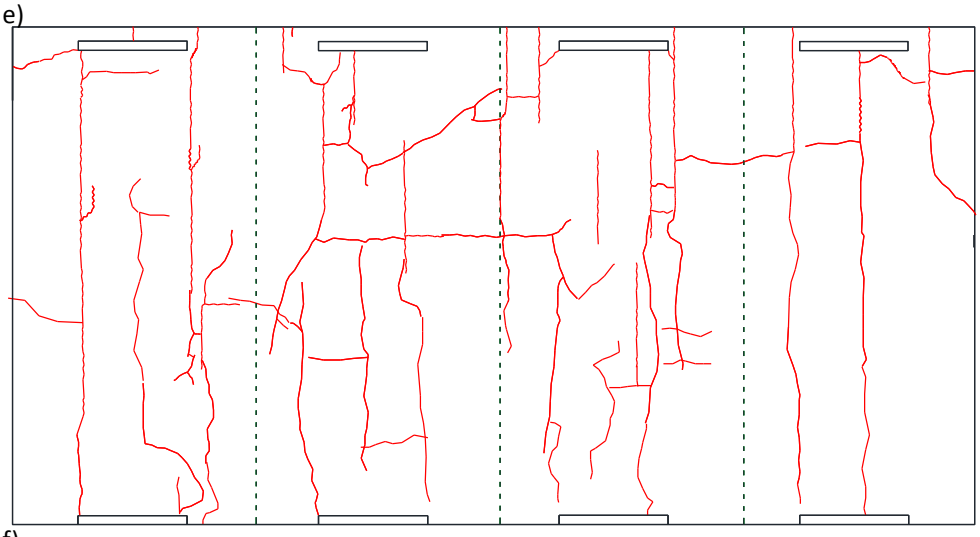

f)

Figure 97 (continued). Crack propagation on cask with $CaCl_2$-4 mixture (a) 163 days (b) 186 days (c) 225 days (d) 295 days (e) 512 days (f) 569 days

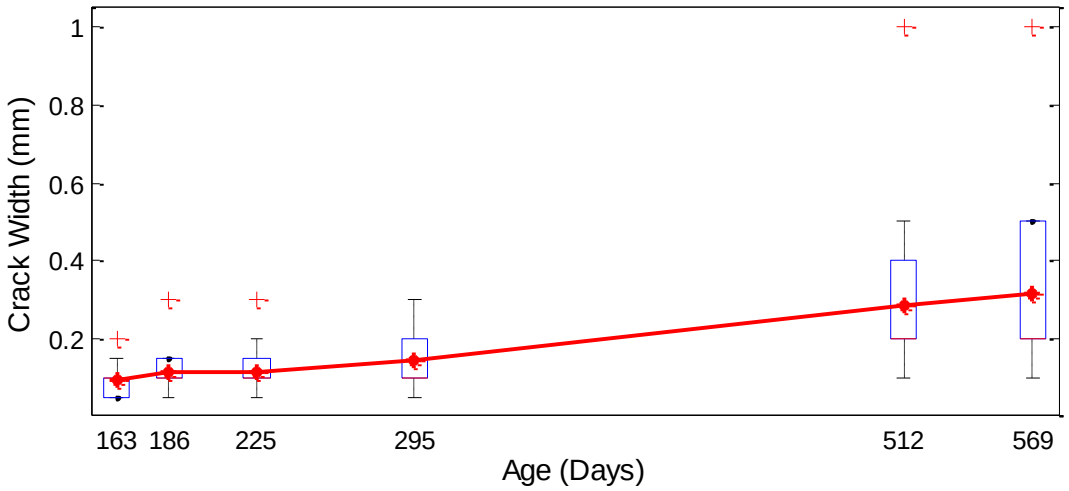

Figure 98 Crack width growth on $CaCl_2$ cask

5.3.3 UPV

The UPV was measured at three different levels and on two sides of each cask as shown in Figure 99. Since it was not possible to measure the UPV on the casks by the direct method, a series of readings were performed with a fixed transmitter and incremental movement of the receiver as shown in Figure 99. The average of UPV measurements over time is shown in Figure 100. These results indicated a higher velocity in the SCC cask compared to NaOH-8 and $CaCl_2$-4 casks, which had similar UPV values. These findings were consistent with the material testing and Schmidt hammer measurements. Small differences in the measured values between material testing and the structural level can be explained due to the existence of rebar inside the casks as well as not being able to measure the UPV with a direct method approach. Contrary to what was initially thought, the UPV results were not able to capture any degradation in concrete properties due to aging at this scale because of their sensitivity to moisture content, temperature and the presence of rebar and other minor defects inside the concrete around the measurement locations.

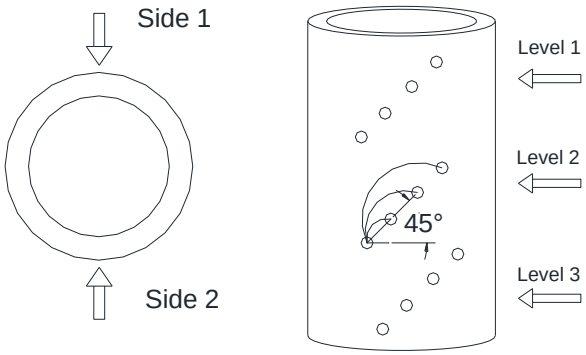

Figure 99 Level of UPV measurement on casks

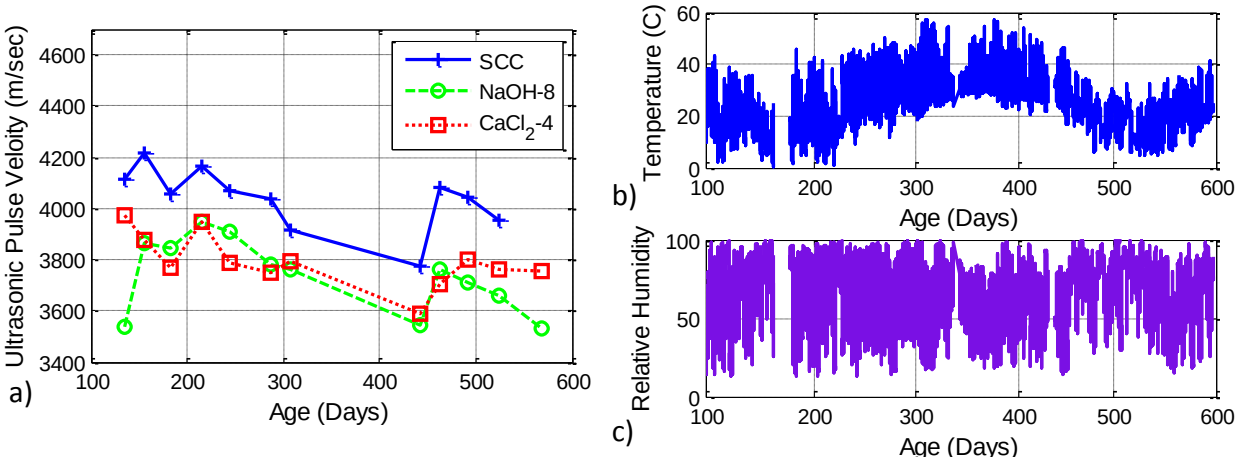

Figure 100 (a) UPV measurement on casks (b) temperature from 100 to 600 days (c) relative humidity from 100 to 600 days

5.3.4 Half-cell potential

The half-cell potential was measured to evaluate the probability of corrosion in each of the casks. At each measurement date, more than 150 points were read on one half of the cask along a grid of lines. The measurements were consistent at different locations on the casks; therefore, in Figure 101, only the average of these measurements in an eighteen-month period is shown. Half-cell potentials in SCC and NaOH-8 casks were similar and always higher than -100mV/CSE, which indicates that the probability of corrosion is less than 10%. On the other hand, the measurement for $CaCl_2$-4 cask was always lower than -350mV/CSE, which shows that the probability of corrosion is more than 90%. As an overall trend, the half-cell potential decreased over time, which is an

indicator of increased corrosion activity in the $CaCl_2$-4 cask. The measurement on the casks was similar to the measurement at the material level specimens of first phase.

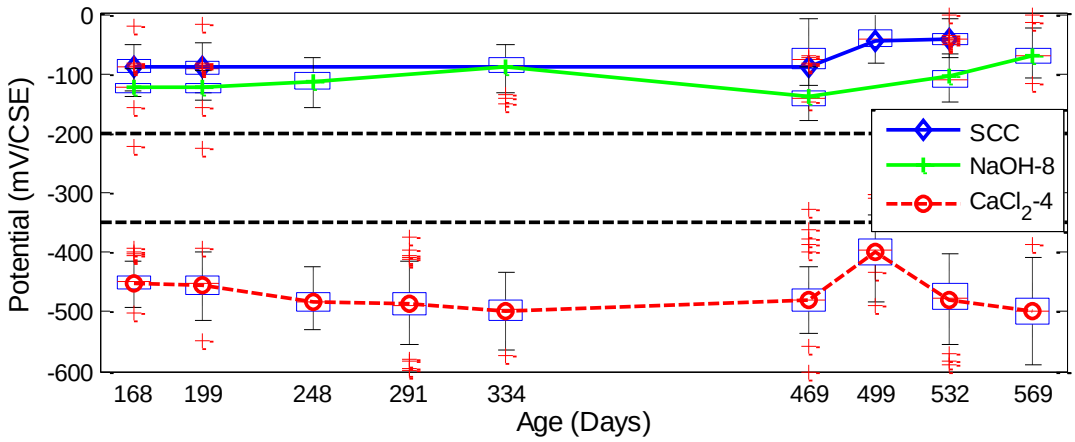

Figure 101 Half-cell potential in three casks

5.4 Estimating the In-Service Age of the Cask Subjected to Accelerated Corrosion

To correlate the rate of deterioration under accelerated conditions and compare to the real field conditions, the environmental exposure should be considered. Based on the location, the environmental parameters that affect the speed of this process vary substantially. For this study, three locations around the United States are considered: Seabrook Station at New Hampshire, St. Lucie Power Plant at Florida, and Rancho Seco Nuclear Generating Station at California. These locations were chosen based on the locations of the existing nuclear power plants accommodating concrete dry cask storage and the amount of chloride ion deposition in that area. Since most of the independent spent fuel storage installations (ISFSIs) are located near a marine setting, most of the salts and chloride ions in dust and aerosols originate from sea water (Enos et al., 2013). Figure 102 shows the three chosen locations in addition to the chloride ion

concentration in different areas of the US as taken from the National Atmospheric Deposition Program/National Trends Network (NADP, 2016).

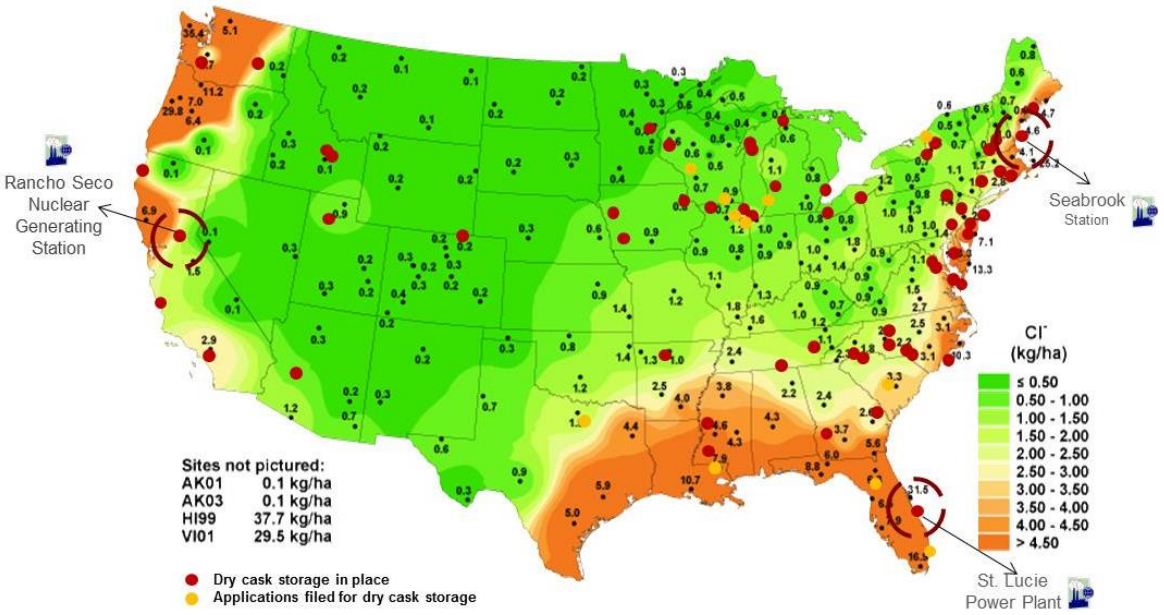

Figure 102 Location of three chosen power station (NADP, 2016).

Placing the heat pipes on the air inlet and outlet on the outside of the steel liner makes the liner act like a cooling compartment for the hot basket. This system prevents large temperature gradients in the concrete. Childress et al. (1989) performed an analysis for fire conditions to predict the warmest rod cladding in the concrete, and in this condition they found the highest temperature in concrete close to the basket to be equal to 107°C and on the surface to be equal to 63°C. However, under normal conditions this temperature is lower and considering that the temperature of the fuel basket decreases over the years, the temperature of the concrete was assumed to be 60°C on the inside surface. Furthermore, since the basket located inside the dry cask is the source of heat and the temperature is higher than the ambient temperature, it is considered that the temperature on the inside surface in all three locations is the same regardless of the physical location of the dry cask.

The chloride concentration on the surface of casks in these locations was chosen based on extrapolation of the results taken from Shill (2014) and based on the average of chloride ion amounts in these locations. Shill (2014) measured the chloride concentration on the surface of the concrete specimens placed close to Dania Beach, FL, for over a year; these results are shown in Table 55. The chloride concentration on the surface of the casks in each station was estimated by extrapolating these data based on chloride ion concentration at Dania Beach through proportional scaling using the data in Figure 102 and each of these three stations; the results are shown in Figure 103. Furthermore, this extrapolation was performed over different time intervals and a linear fit was considered for these data with time.

Table 55 Chloride Concentration at Surface of Specimens Close to Dania Beach, FL (Shill, 2014)

C_s (% weight of cement)				
Time	6 month	10 month	18 month	24 month
Spec01	0.679%	1.752%	0.996%	1.233%
Spec02	1.005%	0.909%	1.483%	1.233%
Spec03	0.574%	0.606%	0.782%	0.939%
Spec04	1.199%	0.545%	1.139%	1.087%
Spec05	0.863%	0.684%	0.848%	1.188%
Spec06	0.714%	0.643%	0.863%	1.509%
Spec07	0.762%	0.534%	0.493%	0.819%
Avg.	0.828%	0.810%	0.943%	1.144%

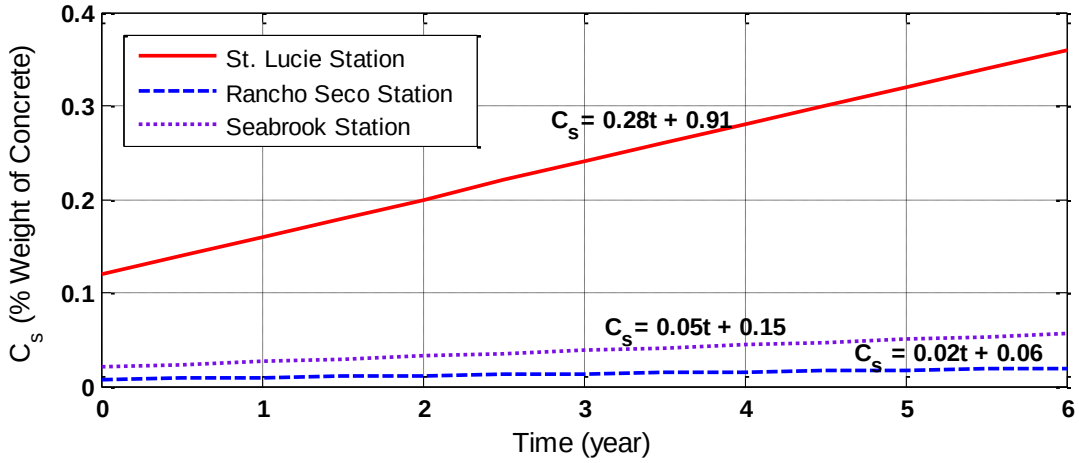

Figure 103 Assumed chloride concentration on the surface of DCSS

With these data, corrosion initiation can be found from equation (14) presented in Section 2.5.1.1. The concrete cover was considered to be equal to 38.1 mm. The effective chloride transport coefficient used in this equation was equal to the average of measured values for SCC specimens in the first phase of the project in all three intervals and equal to 1.048e-11 m^2/sec. Initial chloride content was considered similar to the value of SCC mixture prepared in first phase and equal to 0.0143% weight of concrete. Critical chloride concentration was chosen based on the value presented in the previous study of DuraCrete (1998). Table 56 summarizes the values assigned to the parameters used in this calculation. The results are presented in Table 57. The high chloride concentration at the St. Lucie station area, which led to the highest value of chloride concentration on the surface of the cask in this region, led to having the shortest time span compared to the other two locations for initiation of corrosion. The low chloride concentration also leads to the longest time period for corrosion initiation in the cask located in the Rancho Seco station area.

Table 56 Assumed Parameter for Corrosion Initiation Measurement

Parameter	Value
$x_{cr:}$ Concrete cover (mm)	38.1
D_i: Diameter of steel bar (mm)	9.5
D_e: Diffusion coefficient (m^2/sec)	1.048e-11
C_{cr}: Critical chloride concentration (% weight of concrete)	0.1
C_i: Initial chloride content (% weight of concrete)	0.0143

Table 57 Corrosion Initiation Time at Different Locations

Station	Corrosion Initiation Time (years)
St. Lucie	2.92
Rancho Seco	56.60
Seabrook	18.59

After corrosion initiation, it will only take a few years until the concrete starts to crack and reach the end of its service life. To estimate this time, different models are presented in the

literature, several of which were discussed in Section 2.5.1.2. The parameters needed for estimating the concrete cover cracking is shown in Table 58. These parameters were chosen based on parameters measured in this study such as concrete cover, diameter of steel bar, modulus of elasticity of concrete, compressive and tensile strength of concrete, water-cement ratio as well as bar spacing in the casks. The time from corrosion to concrete cover cracking can be estimated from the different models presented in 2.5.1.2 as shown in Table 59.

Table 58 Assumed Parameter for Concrete Cover Cracking Measurement

Parameter	Value
C: Concrete cover (mm)	38.1
D_i: Diameter of steel bar (mm)	9.5
d_0: Porous zone around the steel-concrete interface (mm)	1.048e-11
φ_c: creep coefficient	0.2
E_c: Elastic modulus of concrete (MPa)	23503.39
E_s: Young modulus of steel (MPa)	210000
υ_c: Poisson ratio of concrete	0.29
υ_s: Poisson ratio of steel	0.3
f_c: Compressive strength of concrete (MPa)	40.42
f_t: Tensile strength of concrete (MPa)	4.38
S: Bar spacing (mm)	106
ρ_{st}: Mass density of steel (kg/m^3)	7850
α is the molecular weight corrosion products	Between 0.523 and 0.622; here 0.5725
α_1: Volume expansion ratio	0.3
R_c: Resistivity of Concrete (Ohm)	1450
w/c: water cement ratio	0.5
T: Temperature on steel (˚K)	331
t: Time when chloride concentration measured (years)	1

Table 59 Time from Corrosion to Concrete Cover Cracking at Different Locations

	Time from Corrosion to Concrete Cover Cracking (years)		
Model	St. Lucie	Rancho Seco	Seabrook
Beaton and Stratfull (1963)	1.41	3.60	2.62
Clear and Hay (1976)	1.51	4.71	3.20
Morinaga (1990)	0.05	0.28	0.23
Bazant (1979)	0.03	0.14	0.11
Liu (1996)	2.83	15.20	12.65
Bhargva et al (2006)	2.20	11.78	9.80
Maaddawy (2007)	6.19	33.19	27.63

The results show the wide range of estimation for different locations. The differences in the results of each model are due to the different parameters considered in the modeling. The empirical modeling of Beaton and Straful (1963), Clear and Hay (1976) and Morinaga (1990) were based on limited test data and could not consider all the parameters. In mathematical modeling it is true that all of the models presented here used elastic mechanics and a thick walled cylinder model; however, only one model, Bhargava (2006), considers the rust, and the models have other differences in their assumptions and modeling, which results in different estimated values. However, similar to corrosion initiation, the specimens located in the St. Lucie station showed a shorter time span until the concrete cover cracking and Rancho Seco Station showed the highest interval. Among the seven presented models, the results of two models, those of Liu (1996) and Bhargva et al. (2006), were close to each other. The time averages of these models were chosen as the time from corrosion to concrete cover cracking in these three stations as shown in Table 60.

Table 60 Average Time from Corrosion to Concrete Cover Cracking at Different Locations

Station	Time from Corrosion to Concrete Cover Cracking (years)
St. Lucie	2.52
Rancho Seco	13.49
Seabrook	11.22

Service life of a structure is defined from the time it was built until concrete cover cracks, which means it can be found from the addition of corrosion initiation time and time from corrosion to concrete cover cracking. The range of service life of the cask can be estimated as shown in Table 61. Considering cracks were observed on the corrosion accelerated cask at 4 months (0.33 year), the acceleration factor compared to real life can be estimated as shown in Table 61. Having a high percentage of chloride on the surface of the structure in the St. Lucie station as well as having only 38.1 mm of concrete cover led to the very short life span for the cask located in this area. The acceleration factor in each station compared to the corrosion accelerated cask is 16.5, 213.4, and 90.3 years for St. Luce, Rancho Seco, and Seabrook station respectively. It should be noted that the service lifes for casks with real dimension are higher, since the concrete cover is 3 times larger, and this delays corrosion initiation time considerably (increase the time by 71%, 24%, 42% for St. Lucie, Rancho Seco and Seabrook station, respectively).

Table 61 Service Life of Casks at Three Locations

Station	Scaled Casks		Prototype Casks
	Service life (years)	Acceleration factor	Service life (years)
St. Lucie	5.4	16.5	72.3
Rancho Seco	70.1	213.4	294.9
Seabrook	29.8	90.3	195.6

The second method to estimate the acceleration factor, as mentioned in Section 0, is through the area loss. Area loss of the rebar of the corrosion accelerated casks was measured by removing rebar from different locations of the casks after 2 years. For removing the rebar, the locations were first investigated using a rebar detector and thereafter the concrete cover was removed and the rebar was cut from the cask; see Figure 104. Afterwards, the rebar was washed in hydrochloric acid based on ASTM G1 (2011a) and the area loss was measured. Figure 105 shows the rebar after removing the corrosion products and rust from the rebar and the corrosion

damage is visible on them. The diameter of the rebar was measured using calipers with a precision of 0.0001 mm, in twenty different locations on two rebar and the smallest diameter was about 9.07 mm, which compare to the original diameter of 9.52 mm, it shows 4.7% decrease in the diameter (also see Table A 38 in the appendix for detailed measurement).

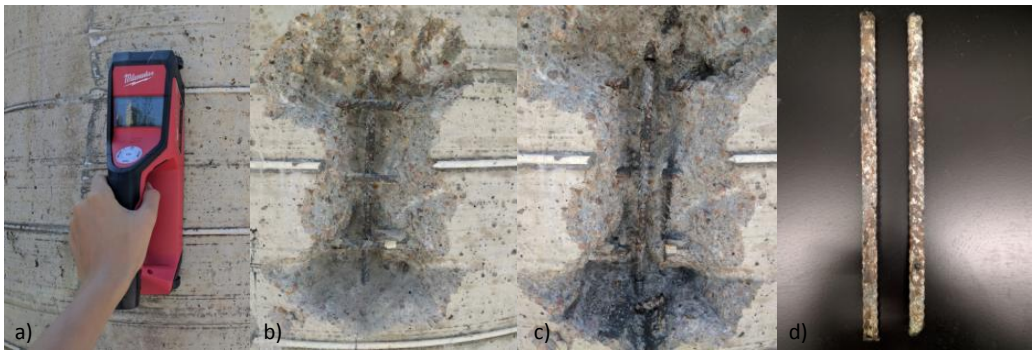

Figure 104 (a) rebar detection (b) removing concrete cover (c) cutting rebar from the cask (d) corroded rebar

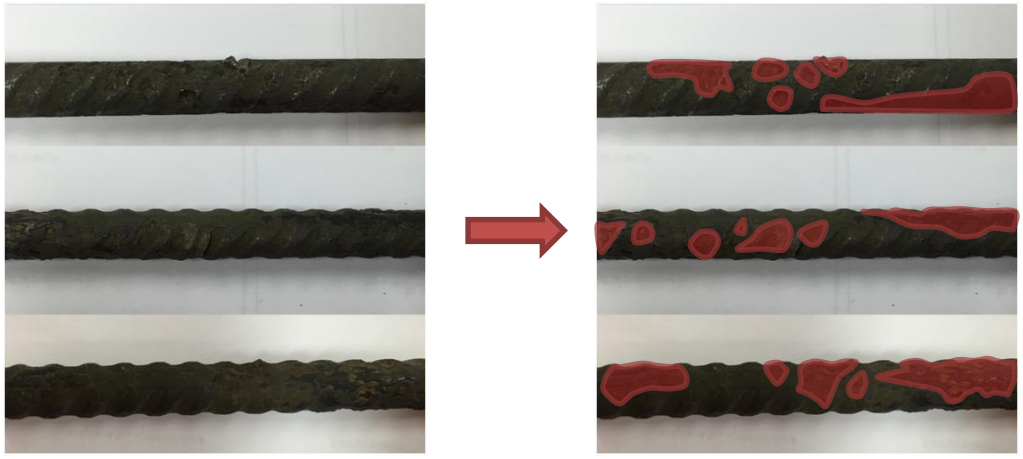

Figure 105 Effect of corrosion on the rebar after removing the rust

From the measured diameter, the area of the rebar can be estimated to be about 64.58 mm^2. This number indicates that the rebar had 9% reduction in its surface area.

Table 62 shows the parameters used to model the area loss based on the methods of Thoft-Christensen (1996) and the corrosion rate model presented by Liu (1996), presented in Section 2.5.2 and Section 2.5.3, respectively. The area loss of the rebar based on this model for

the three locations is shown Figure 106. In these graphs, the constant area showing the corrosion initiation time. Similar to the previous models, area loss in St. Lucie station is more critical and the slope of area loss is much higher than at the other two locations. From the graph, the age that rebar reaches on suffering to the same area loss to that measured from the casks subjected to accelerated aging was estimated as shown in Table 63.

Table 62 Assumed Parameter for Concrete Cover Cracking Measurement

Parameter	Value
D_i: Diameter of steel bar (mm)	9.5
R_c : Corrosion time (year)	1.048e-11
w/c: water cement ratio	0.5
T: Temperature on steel (˚K)	331
t: Time when chloride concentration measured (years)	1

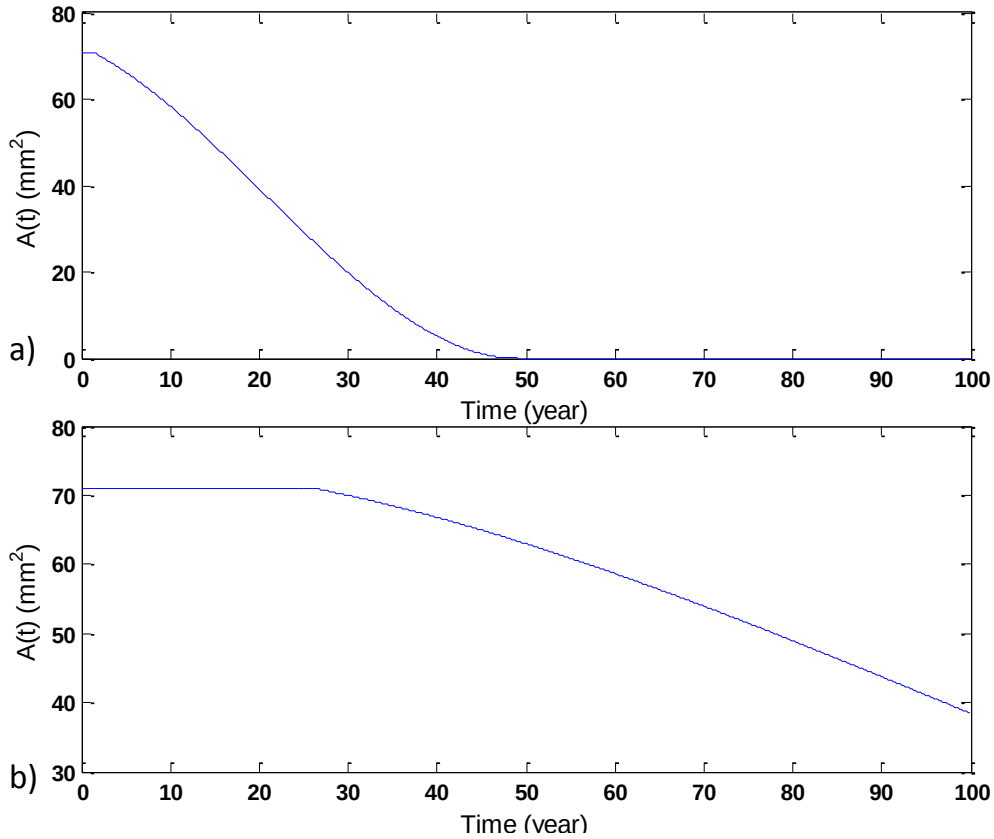

Figure 106 Area loss estimation in three power stations (a) St.Lucie station, (b) Rancho Seco station, (c) Seabrook Station

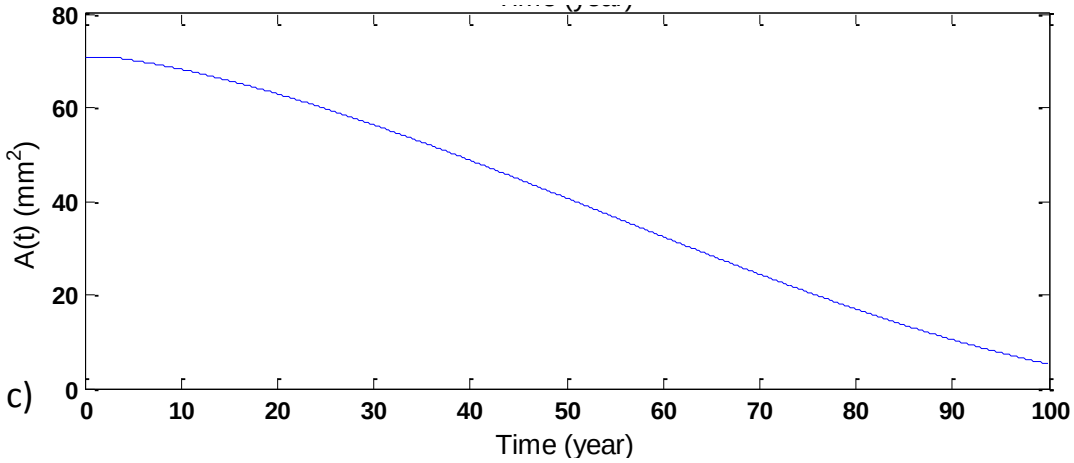

Figure 106 (continued) Area loss estimation in three power stations (a) St.Lucie station, (b) Rancho Seco station, (c) Seabrook Station

Table 63 Age estimate of casks in different station when rebar area become equal to 64.6 mm^2

Station	Age (years)	Acceleration factor
St. Lucie	6.21	3.1
Rancho Seco	46.03	23.0
Seabrook	42.79	21.4

The results show that placing the cask in real conditions in each station would cause 9% area loss in 6.21, 46.03, and 42.79 years in St Lucie, Rancho Seco, and Seabrook stations, respectively. It was also found that the acceleration factor of the proposed method in this study 3.1, 23.0 and 21.4 for St Lucie, Rancho Seco, and Seabrook stations, respectively. It should be noted that this method mainly considers the corrosion rate based on limited parameters, which may be one of the main reasons for the difference between the acceleration factor obtained from this method and the service life method. However, results of both methods indicate the importance of the location and show that the proposed method in this study can considerably accelerate the aging in the structure, from 16 to 200 times depending on their location.

6. CONCLUSIONS AND RECOMMENDATIONS FOR FUTURE RESEARCH

The following conclusions were drawn from the findings of this research:

- Using reactive fine aggregate, not using fly ash and adding alkalis in the form of NaOH directly into the fresh concrete paste was found to be an effective method for accelerating alkali-silica reactivity (ASR) of specimens kept in ambient outdoor conditions. 0.2% and 0.4% addition of NaOH by weight of cement were found to result in acceptable changes in mechanical properties of concrete, while the changes were more drastic for 0.8% NaOH addition and the ensuing concrete mixture may not be considered a good representation of the original concrete design.
- The first ASR cracks on specimens with 8% NaOH addition by weight of cement were observed after around 90 days and the crack intensity increased over time during the 432 days measurement period. While the crack intensity on the surface increased and the cracks coalesced, the crack widths remained between 0.05 mm and 0.1 mm throughout.
- Similarly, addition of chloride to the fresh concrete paste in the form of $CaCl_2$ flakes substantially accelerated the rebar corrosion. Addition of 1% and 2% chloride by weight of cement resulted in acceptable differences in the physical and mechanical properties of the concretes, while the effects of 4% chloride addition were more drastic and deemed not representative of the control mixture.
- Cracks due to corrosion on specimens with 4% chloride by weight of cement were first observed after approximately 90 days of casting. The crack lengths and widths increased during the course of measurements. The average crack width increased by about 82%

within a year and spalling was seen occasionally. Approximately 2% mass loss of rebar was observed within one year.

- Adding NaOH to the concrete mixture, removing any supplementary cementitious materials with alkali-silica reactivity (ASR) suppression characteristics (e.g., fly ash) and using reactive fine aggregate could be used as an effective method to accelerate ASR at the structural level. A 0.8% addition of NaOH by weight of cement into the fresh concrete reduced the time to first observation of ASR distress from tens of years to approximately 90 days. However, the concrete strength with this special mixture reduced by approximately 36% at 28 days compared to the control self-consolidating concrete (SCC).
- Similarly, it was observed that the direct addition of $CaCl_2$ is an effective way of accelerating the corrosion-induced aging. In this study, corrosion cracks were observed at approximately 120 days of age with 4% addition of $CaCl_2$ by weight of cement into the fresh concrete. However, it was seen that the concrete strength reduced by 24% at 28 days in comparison to the control SCC mixture. The $CaCl_2$ and SCC mixtures were identical except for the addition of chloride; therefore, all of this reduction was due to the presence of chloride. The impact of the addition of a lower amount of $CaCl_2$ was studied and the results are presented in Part I of the paper.
- The average width of cracks in the $CaCl_2$ cask increased from about 0.1 mm to 0.3 mm in approximately 1 year, and the maximum crack width reached 1.0 mm.
- Adding chloride and alkali to the mixture decreased the setting time of the concrete by 37% and 16%, respectively. Addition of chloride also increased the hydration temperature by 5%.

- Comparing the predicted service life of dry cask storage for three different locations showed the effect of salt contamination on service life and corrosion initiation. This calculation also showed approximately how much the selected approach accelerates the aging of cask due to corrosion, with an estimated acceleration factor of 16.5, 213.4 and 90.3 for St. Lucie, Rancho Seco, and Seabrook stations respectively.

Recommendations for future research:

- Further investigation is required for the effect of addition of different percentages of NaOH and $CaCl_2$ to the mixtures. Since it is known that each of these chemicals will cause changes to concrete chemical composition, how each of these chemicals in different percentages affect the hydration process and chemical bonding in concrete should be studied.
- Addition of sodium hydroxide and calcium chloride to the mixture has an effect on creep and shrinkage of concrete. Further investigation on these two properties is recommended.
- In this study, bonding effect was investigated for a certain day. For future study, it is recommended to look at these effects extensively with the beam end test method.
- For the ASR case, a model for crack propagation which can estimate the time that cracks will show on the surface to the time it gets to the critical level should be developed considering the mix properties and environmental conditions. This model will be helpful in predicting the service life of ASR affected structures.

REFERENCES

AASHTO (1980). *Standard Method of Test for Resistance of Concrete to Chloride Ion Penetration,* AASHTO T259-80, American Association of State Highway and Tranportation Officials, Washington, DC.

AASHTO (1996). *Standard Method of Test for Accelerated Detection of Potentially Deleterious Expansion of Mortar Bars Due to Alkali-Silica Reaction,* AASHTO T 303, American Association of State Highway and Transportation Officials (AASHTO), Washington, DC.

AASHTO (2004). *Standard Method of Test for Rapid Identification of Alkali-Silica Reaction Products in Concrete,* AASHTO T 299-93, American Association of State and Highway Transportation Officials (AASHTO), Washington, DC.

AASHTO (2011a). *Electrical Indication of Concrete's Ability to Resist Chloride Ion Penetration (ASTM C1202-05),* AASHTO T277-07, American Assocition of State Highway and Transportation Officials (AASHTO), Washington, DC.

AASHTO (2011b). *Standard Specification for Coal Fly Ash and Raw or Calcined Natural Pozzolan for Use in Concrete,* AASHTO M 295, American Association of State Highway and Transportation Officials (AASHTO), Washington, DC.

AASHTO (2014). *Standard Method of Test for Surface Resistivity Indication of Concrete's Ability to Resist Chloride Ion Penetration,* AASHTO TP 95-14, American Assocition of State Highway and Transportation Officials (AASHTO), Washington, DC.

Abalaka, A. E. and Babalaga, A. D. (2011). "Effects of Sodium Chloride Solutions on Compressive Strength Development of Concrete Containing Rice Husk Ash," ATBU Journal of Environmental Technology, 4(1), 33-40.

Abd El-Salam, S., Shehab Eldin, H. and Shawky, S. M. M. (2012). "Effect of High Percentage of Sodium Chloride (Nacl) on the Behavior of Reinforced Concrete Beams," Life Science Journal, 9(3), 315-320.

ACI Committee 221 (1998). *Report on Alkali-Aggregate Reactivity,* ACI 221.1R, American Concrete Institute, Farmington Hills, MI.

ACI Committee 222 (2001). *Protection of metals in Concrete Against Corrosion,* ACI 222-01, American Concrete Institute, Farmington Hills, MI.

ACI Committee 318 (2011). *Building Code Requirements for Structural Concrete and Commentary (ACI 318-11)*, American Concrete Institute, Farmington Hills, MI.

ACI Committee 349 (2013). *Code Requirements for Nuclear Safety-Related Concrete Structures and Commentary (ACI 349-13)*, American Concrete Institute, Farmington Hills, MI.

ACI Committee 408 (1966). "Bond Stress-The State of the Art," ACI Journal Proceedings, 63(11), 1161-1191, DOI: 10.14359/7665.

Ahmed, T., Burley, E. and Ridgen, S. (1998). "Effect of Alkali-Silica Reaction on Tensile Bond Strength of Reinforcement in Concrete Tested under Static and Fatigue Loading," ACI Material Journal, 96(4), 419-428.

Al-Attar, T. S. and Abdul-Kareem, M. S. (2011). "Effect of Chloride Ions Source on Corrosion of Reinforced Normal and High Performance Concrete," Buletinul AGIR, 2, 107-112.

Al-Bakri, A. M. M., Kamarudin, H., Bnhussain, M., Khairul Nizar, I., Rafiza, A. R. and Zarina, Y. (2011). "Microstructure of Different NaOH Molarity of Fly Ash Based Green Polymeric Cement," Journal of Engineering and Technology Research, 3(2), 44-49.

Allahverdi, A. and Ghorbani, J. (2006). "Chemical Activation and Set Acceleration of Lime-Natural Pozzolan Cement," Ceramics-Silikaty, 50(4), 193-199.

Almusallam, A. A., Al-Gahtani, A. S., Aziz, A. R. and Rasheeduzzafar (1996). "Effect of Reinforcement Corrosion on Bond Strength," Construction and Building Materials, 10(2), 123-129.

Amleh, L. and Ghosh, A. (2006). "Modeling the Effect of Corrosion on Bond Strength at the Steel-Concrete Interface with Finite-Element Analysis," Canadian Journal of Civil Engineering, 33(6), 673-682.

Anacta, E. T. (2013). "Effect of Salt-Contaminated Mixing Water and Aggregates on Time-to-Initiate Rebar Corrosion in Concrete," International Journal of Scientific & Engineering Research, 4(4), 1524-1527.

Anantharaman, S. (2008). "Sulfate and Alkali Silica Resistance of Class C & F Fly Ash Replaced Blended Cements," School of Sustainable Engneering and Built Environment, Arizona State University, Tuscon, AZ.

Ardani, A. (2012). *Surface Resistivity Test Evaluation as an Indicator of the Chloride Permeability of Concrete,* FHWA-HRT-13-024, US Department of Transportation, Federal Highway Administration (FHWA), McLean, VA.

ASTM (1996). *Standard Practice for Developing Accelerated Tests to Aid Prediction of the Serice Life of Building Componenets and Materials (Withdrawn 2005),* ASTM E632-82, American Society of Testing and Materials Academic & Science (ASTM), West Conshohocken, PA.

ASTM (1997a). *Standard Test Method for Potential Volume Change of Cement-Aggregate Combinations,* ASTM C342-97, American Society of Testing and Materials Academic & Science (ASTM), West Conshohocken, PA.

ASTM (1997b). *Standard Test Method for Pulse Velocity Through Concrete,* ASTM C597-97, American Society of Testing and Materials Academic & Science (ASTM), West Conshohocken, PA.

ASTM (2007a). *Standard Test Method for Potential Alkali-Silica Reactivity of Aggregates (Chemical Method),* ASTM C289-07, American Society of Testing and Materials Academic & Science (ASTM), West Conshohocken, PA.

ASTM (2007b). *Standard Test Methods for Potential Alkali Reactivity of Aggregates,* ASTM C1260-07, American Society of Testing and Materials Academic & Science (ASTM), West Conshohocken, PA.

ASTM (2008a). *Standard Test Method for Time of Setting of Concrete Mixtures by Penetration Resistance,* ASTM C403/C403M-08, American Society of Testing and Materials Academic & Science (ASTM), West Conshohocken, PA.

ASTM (2008b). *Standard Test Methods for Determination of Length Change of Concrete Due to Alkali-Silica Reaction,* ASTM C1293-08b, American Society of Testing and Materials Academic & Science (ASTM), West Conshohocken, PA.

ASTM (2009a). *Standard Test Method for Corrosion Potentials of Uncoated Reinforcing Steel in Concrete,* ASTM C876-09, American Society of Testing and Materials Academic & Science (ASTM), West Conshohocken, PA.

ASTM (2009b). *Standard Test Method for Slump Flow of Self-Consolidating Concrete,* ASTM C1611/C1611M-09b, American Society of Testing and Materials Academic & Science (ASTM), West Conshohocken, PA.

ASTM (2010a). *Standard Guide for Examination of Hardened Concrete Using Scanning Electron Microscopy,* ASTM C1723, American Society of Testing and Materials Academic & Science (ASTM), West Conshohocken, PA.

ASTM (2010b). *Standard Test Method for Determining the Penetration of Chloride Ion into Concrete by Ponding,* ASTM C1543-10a, American Society of Testing and Materials Academic & Science (ASTM), West Conshohocken, PA.

ASTM (2010c). *Standard Test Method for Flexural Strength of Concrete (Using Simple Beam with Third-Point Loading,* ASTM C78-10, American Society of Testing and Materials Academic & Science (ASTM), West Conshohocken, PA.

ASTM (2010d). *Standard Test Method for Potential Alkali Reactivity of Cement-Aggregate Combinations (Mortar-Bar Method),* ASTM C227-10, American Society of Testing and Materials Academic & Science (ASTM), West Conshohocken, PA.

ASTM (2011a). *Standard Practice for Preparing, Cleaning, and Evaluating Corrosion Test Specimens,* ASTM G1-03, American Society of Testing and Materials Academic & Science (ASTM), West Conshohocken, PA.

ASTM (2011b). *Standard Test Method for Splitting Tensile Strength of Cylindrical Concrete Specimens,* ASTM C496-11, American Society of Testing and Materials Academic & Science (ASTM), West Conshohocken, PA.

ASTM (2012a). *Standard Guide for Petrographic Examination of Aggregates for Concrete,* ASTM C295/C295M-12, American Society of Testing and Materials Academic & Science (ASTM), West Conshohocken, PA.

ASTM (2012b). *Standard Specification for Coal Fly Ash and Raw or Calcined Natural Pozzolan for Use in Concrete,* ASTM C618, American Society of Testing and Materials Academic & Science (ASTM), West Conshohocken, PA.

ASTM (2012c). *Standard Specification for Portland Cement,* ASTM C150/C150M, American Society of Testing and Materials Academic & Science (ASTM), West Conshohocken, PA.

ASTM (2012d). *Standard Test Method for Compressive Strength of Cylindrical Concrete Specimens,* ASTM C39-12, American Society of Testing and Materials Academic & Science (ASTM), West Conshohocken, PA.

ASTM (2012e). *Standard Test Method for Density, Relative Density (Specific Gravity), and Absorption of Coarse Aggregate,* ASTM C127-12, American Society of Testing and Materials Academic & Science (ASTM), West Conshohocken, PA.

ASTM (2012f). *Standard Test Method for Density, Relative Density (Specific Gravity), and Absorption of Fine Aggregate1,* ASTM C128-12, American Society of Testing and Materials Academic & Science (ASTM), West Conshohocken, PA.

ASTM (2012g). *Standard Test Method for Electrical Indication of Concrete's Ability to Resist Chloride Ion Penetration,* ASTM C1202-12, American Society of Testing and Materials Academic & Science (ASTM), West Conshohocken, PA.

ASTM (2012h). *Standard Test Methods and Definitions for Mechanical Testing of Steel Products,* ASTM A370-12, American Society of Testing and Materials Academic & Science (ASTM), West Conshohocken, PA.

ASTM (2013a). *Density and Void Content of Freshly Mixed Pervious Concrete,* ASTM C1688/C1688M-13, American Society of Testing and Materials Academic & Science (ASTM), West Conshohocken, PA.

ASTM (2013b). *Standard Test Method for Density, Absorption, and Voids in Hardened Concrete,* ASTM C642, American Society of Testing and Materials Academic & Science (ASTM), West Conshohocken, PA.

ASTM (2013c). *Standard Test Method for Determining the Potential Alkali-Silica Reactivity of Combinations of Cementitious Materials and Aggregate (Accelerated Mortar-Bar*

Method), ASTM C1567-13, American Society of Testing and Materials Academic & Science (ASTM), West Conshohocken, PA.

ASTM (2013d). *Standard Test Method for Measurement of Rate of Absorption of Water by Hydraulic-Cement Concretes,* ASTM C1585-13, American Society of Testing and Materials Academic & Science (ASTM), West Conshohocken, PA.

ASTM (2013e). *Standard Test Method for Rebound Number of Hardened Concrete,* ASTM C805/C805M-13a, American Society of Testing and Materials Academic & Science (ASTM), West Conshohocken, PA.

ASTM (2013f). *Standard Test Method for Total Evaporable Moisture Content of Aggregate by Dryin,* ASTM C566, American Society of Testing and Materials Academic & Science (ASTM), West Conshohocken, PA.

ASTM (2014a). *Standard Practice for Petrographic Examination of Hardened Concrete,* ASTM C856-14, American Society of Testing and Materials Academic & Science (ASTM), West Conshohocken, PA.

ASTM (2014b). *Standard Test Method for Static Modulus of Elasticity and Poisson's Ratio of Concrete in Compression,* ASTM C469/C469M - 14, American Society of Testing and Materials Academic & Science (ASTM), West Conshohocken, PA.

Attar, A., Gencturk, B., Hanifehzadeh, M. and Willam, K. (2016). "Accelerated Aging of Concrete Dry Cask Storage System Nuclear Waste," Journal of Advanced Concrete Technology, 14(Special Issue), 299-310.

Attoh-Okine, N. and Atique, F. (2006). *Service Life Assessment of Concrete with ASR and Possible Mitigation,* DCT 172, Delaware Center for Transportation, Newark, Delaware.

Bahadure, B. M. and Naik, N. S. (2013). "Effect of Alkaline Activator on Workability and Compressive Strength of Cement Concrete with RHA " International Journal of Computational Engineering Research, 3(5), 15-20.

Bargaheiser, K. and Butalia, T. S. (2007). *Prevention of Corrosion in Concrete Using Fly Ash Concrete Mixes*.

Bassam, S. A., Yu, B.-J. and Ansari, F. (2007). "Fracture Energy of Concrete by Maturity Method," Materials Journal, 104(1), 77-85, DOI: 10.14359/18498.

Bažant, Z. P. (1979). "Physical Model for Steel Corrosion in Concrete Sea Structures - Application," Journal of the Structural Division, ASCE, 105(ST6), 1155-1166.

Bažant, Z. P. and Sener, S. (1988). "Size Effect in Pullout Tests," Materials Journal, 85(5), 347-351, DOI: 10.14359/2257.

Beaton, J. L. and Stratfull, R. F. (1963). *Environmental Influence on Corrosion of Reinforcing in Concrete Bridge Substructures,* HRR 14 HRB, Concrete Bridge Decks and Pavement Surfaces, Washington, DC.

Bentur, A., Diamond, S. and Berke, N. S. (1997). *Steel Corrosion in Concrete*, E & FN Spon, New York, NY.

Bertolini, L., Elsener, B., Pedeferri, P., Redaelli, E. and Polder, R. (2013). *Corrosion of Steel in Concrete; Prevention, Diagnosis, Repair*, Wiley-VCH, Singapore, Singapore.

Berube, M.-A. and Fournier, B. (1993). "Canadian Experience with Testing for Alkali-Aggregate Reactiity in Concrete," Cement & Concrete Composites, 15(1-2), 27-47.

Bérubé, M. A. and Frenette, J. (1994). "Testing Concrete for AAR in NaOH and NaCl Solutions at 38°C and 80°C," Cement & Concrete Composites, 16(3), 189-198.

Bhargava, K., Ghosh, A. K., Mori, Y. and Ramanujam, S. (2006). "Model for Cover Cracking due to Rebar Corrosion in RC Structures," Engineering Structures, 28(8), 1093-1109.

Bilodeau, A. and Malhotral, V. M. (1992). "Concretes Incorporating High Volume of ASTM Class F Fly Ashes: Mechanical Properties and Resistance to De-icing Salt Scaling and to Chloride-ion Penetration." *Fourth International Conference on the Use of Fly Ash, Silica Fume, Slag and Natural Pozzolans in Concrete*, ed Malhotra, V. M., May 1, Istanbul, Turkey, SP-132, 319-349.

Blackwell, B. Q., Thomas, M. D. A., Nixon, P. J. and Pettifer, K. (1992). "The Use of Fly Ash to Suppress Deleterious Expansion due to AAR in Concrete Containing Greywacke Aggregates." *9th International Conference on AAR in Concrete*, July 27-31, London, UK, 102-109.

Blight, G. E. and Alexander, M. G. (2011). *Alkali-Aggregate Reaction and Structural Damage to Concrete, Engineering Assessment, Repair and Management*, Taylor & Francis Group, Leiden, The Netherlands.

Broomfield, J. P. (1997). *Corrosion of Steel in Concrete, Understanding, Investigation and Repair*, E & FN Spon, London, UK.

Broomfield, J. P. (2007). *Corrosion of Steel in Concrete, Understanding, Investigation and Repair*, Taylor & Francis, New York, NY.

Brown, P. W. (2013). *Commentary on "Seabrook Station: Impact of Alkali-Silica Reaction on Concrete Structures and Attachements"*, The Union of Concerned Scientists.

Brown, P. W. and Doerr, A. (2000). "Chemical Changes in Concrete Due To the Ingress of Aggressive Species," Cement and Concrete Research, 30(3), 411-418.

BSI (1983). *Method for Determination of Compressive Strength of Concrete Cubes* BS 1881: Part 116, British Standards Institution (BSI), London,UK.

BSI (2000). *Concrete Specification, Performance, Production and Conformity,* BS EN-206, British Standards Institute (BSI), London,UK.

BSI (2005). *Structural Use of Concrete,* BS 8110, British Standards Institute (BSI), London, UK.

Bungey, J. H. and Millard, S. G. (1996). *Testing of Concrete in Structures*, Blackie Academic & Professional, London, UK.

CEFRACOR (2014). *Steel in the Sound Concrete,* Available from: http://www.concretecorrosion.net/html_en/mecanism/cadre.htm, Accessed on November 20, 2014.

Charlwood, R. G. (1994). "A Review of Alkali Aggregate Reactions in Hydroelectric Plants and Dams," The International Journal on Hydropower & Dams, 1(3), 73-80.

Chatterji, S. (1978). "Mechanism of the $CaCl_2$ Attack on Portland Cement Concrete," Cement and Concrete Research, 8(4), 461-468.

Childress, P., Matheson, J. and McGuinn, E. (1989). *Constar-A Family of Concrete Spent Fuel Dry Storage Casks,* 1.

Clear, K. C. and Hay, R. E. (1976). *Time-to-Corrosion of Reinforcing Steel in Concrete Slabs,* FHWA-RD-76-70, Federal Highway Administration (FHWA), Washington, DC.

COE (2010). *Determining the Potential Alkali-Silica Reactivity of Combinations of Cementitious Materials, Lithium Nitrate Admixture and Aggregate (Accelerated Mortar-Bar Method),* COE CRD-C 662-10, US Army Corps of Engineers (COE), Los Angeles, CA.

COWI, DuraCrete and Brite EuRam III (1998). *Mini-Project Chloride Induced Corrosion: DuraCrete, Performance Based Durability Design of Concrete Structures,* BRPR-CT95-0132, Project BE95-1347, The European Union

Brite EuRam III, Gouda, Netherlands.

CSA (2014). *Concrete Materials and Methods of Concrete Construction/Test Methods and Standard Practice for Concrete,* CSA A23.1-14/A23.2-14, Canadian Standards Association (CSA), Toronto, ON.

Darwin, D., Browning, J., Gong, L. and Hughes, S. R. (2007). *Effects of Deicers on Concrete Deterioration,* SL Report 07-3, Structural Engineering and Materials Laboratory University of Kansas, Lawrence, KS.

Davis, G. and Oberholster, R. E. (1988). "Alkali-Silica Reaction Products and Their Development," Cement and Concrete Research, 18(4), 621-635, DOI: 10.1016/0008-8846(88)90055-5.

Deschenes, D. J., Bayrak, O. and Folliard, K. J. (2009). *ASR/DEF-Damaged Bent Caps: Shear Tests and Field Implications,* Report No. 12-8XXIA006, Texas Department of Transportation (TxDOT), Austin, TX.

Detwiler, R. (1997). *The Role of Fly Ash Composition in Reducing Alkali-Silica Reaction,* Report No. 2092, Portland Cement Association (PCA), Skokie, Illinois.

Diamond, S. (1986). "Chloride Concentrations in Concrete Pore Solutions Resulting from Calcium and Sodium Chloride Admixtures," Cement, Concrete and Aggregates, 8(2), 97-102.

Diamond, S. and Ong, S. (1994). "Effects of Added Alkali Hydroxides in Mix Water on Long-Term SO_4^{2-} Concentration in Pore Solution," Cement & Concrete Composites, 16(3), 219-226, DOI: 10.1016/0958-9465(94)90019-1.

Enos, D. G., Bryan, C. R. and Norman, K. M. (2013). *Data Report on Corrosion Testing of Stainless Steel SNF Storage Canisters,* FCRD-UFD-2013-000324, SAND2013-8314P, Sandia National Laboratory (SNL), US Department of Energy Used Fuel Disposition Campaign, Albuquerque, NM.

Enright, M. P. and Frangopol, D. M. (1998). "Probabilistic Analysis of Resistance Degradation of Reinforced Concrete Bridge Beams under Corrosion," Engineering Structures, 20(11), 960-971.

FAA (2005). *Engineering Brief No. 70, Accelerated Alkali-SIlica Reactivity in Portland Cemet Concrete Pavements Exposed to Runway Deicing Chemicals,* FAA EB-70, Federal Aviation Administration (FAA).

Fan, S. and Hanson, J. M. (1998a). "Effect of Alkali Silica Reaction Expansion and Cracking on Structural Behavior of Reinforced Concrete Beams," Structural Journal, 95(5), 498-505, DOI: 10.14359/564.

Fan, S. and Hanson, J. M. (1998b). "Length Expansion and Cracking of Plain and Reinforced Concrete Prisms Due to Alkali-Silica Reaction," ACI Materials Journal, 95(5), 480-487.

Farny, J. A. and Kosmatka, S. H. (1997). *Diagnosis and Control of Alkali-Aggregate Reactions in Concrete* Portland Cement Association.

Ferraris, C. F. (1995). *Alkali-Silica Reaction and High Performance Concrete,* NISTIR 5742, National Institute of Standards and Technology (NIST), Gaithersburg, MD.

FHWA (2013). *Alkali-Silica Reaction (ASR)*.

Figg, J. (1983). *An Attempt to Provide an Explanation for Engineers of the Expansive Reaction between Alkalis and Siliceous Aggregates in Concrete*, Copenhagen, Denmark.

FMC (1985). "Determination of the Fracture Energy of Mortar and Concrete by Means of Three-Point Bend Tests on Notched Beams," Materials and Structures, 18(4), 287-290.

Folliard, K. J., Barborak, R., Drimalas, T., Du, L., Garber, S., Ideker, J., Ley, T., Williams, S., Juenger, M., Fournier, B. and Thomas, M. D. A. (2006). *Preventing ASR/DEF in New Concrete: Final Report,* FHWA/TX-06/0-4085-5, Center for Transportation Research at The University of Texas at Austin, Austin, TX.

Folliard, K. J., Ideker, J., Thomas, M. D. and Fournier, B. (2004). "Assessing Aggregate Reactivity Using the Accelerated Concrete Prism Tests." *7th CANMET/ACI International Conference on Recent Advances in Concrete Technology*, Las Vegas, NV, 269-283.

Folliard, K. J., Thomas, M. D. A. and Kurtis, K. E. (2003). *Guidelines for the Use of Lithium to Mitigate or Prevent Alkali-Silica Reaction (ASR),* FHWA-RD-03-047, Federal Highway Administration Research and Technology (FHWA), Austin, TX, http://www.fhwa.dot.gov/publications/research/.../pavements/.../research/infrastructure/pavements/pccp/03047/index.cfm.

Fournier, B. and Bérubé, M. A. (1993). "Recent Applications of a Modified Gel Pat Test to Determine the Potential Alkali-Silica Reactivity of Carbonate Aggregates," Cement & Concrete Composits, 15(1-2), 49-73, DOI: 10.1016/0958-9465(93)90038-B.

Freskakis, G. N. (1979). "Strength Properties of Concrete at Elevated Temperature." *Civil Engineering Nuclear Power*, April 12th, 1979, Boston, MA, 1.

Gao, X. X., Multon, S., Cyr, M. and Sellier, A. (2013). "Alkali-Silica Reaction (ASR) Expansion: Pessimum Effect versus Scale Effect," Cement and Concrete Research, 44, 25-33.

Garci Juenger, M. C. and Jennings, H. M. (2011). "Effects of High Alkalinity on Cement Pastes," ACI Materials Journal, 98(3), 251-255.

Ghosh, P. and Tran, Q. (2015). "Correlation between Bulk and Surface Resistivity of Concrete," International Journal of Concrete Structures and Materials, 9(1), 119-132.

Gillott, J. E. and Soles, J. A. (1993). "Petrography of Concrete Cores from New Brunswick, Relating to the Durability Problem," Cement and Concrete Composits, 15(1-2), 101-114, DOI: 10.1016/0958-9465(93)90041-7.

Hansson, C. M., Frølund, T. and Markussen, J. B. (1985). "The Effect of Chloride Cation Type on the Corrosion of Steel in Concrete by Chloride Salts," Cement and Concrete Research, 15(1), 65-73.

Hansson, C. M., Poursaee, A. and Laurent, A. (2006). "Macrocell and Microcell Corrosion of Steel in Ordinary Portland Cement and High Performance Concrete," Cement and Concrete Research, 36(11), 2098-2102, DOI: 10.1016/j.cemconres.2006.07.005.

Harrisson, A. M., Varma, S. P. and Winter, N. B. (1987). "Alkali-Silica Gel Formation at an Early Age through Solution," ACI Special Publication, SP 100-89, 1743-1758.

Hausmann, D. A. (1967). "Steel Corrosion in Concrete; How Does It Occur?," Materials Protection, 6(11), 19-23.

Helmuth, R., Stark, D., Diamond, S. and Moranville-Regourd, M. (1993). *Alikali-Silica Reactivity: An Overview of Research,* SHRP-C-342, Strategic Highway Research Program (SHRP), Washington, DC.

Hewlett, P. C. (2004). *Lea's Chemistry of Cement and Concrete*, Elsevier Science & Technology Books.

Holder, T. B. (1999). "The Deterioration of Chloride Threshold Concentrations Using Different Supplementary Cementing Materials in Steel-Reinforced Concrete," Department of Civil Engineering, University of Toronto, Toronto, Canada.

Howard, R. and Akker, B. V. d. (2014). "Considerations for Disposition of Dry Cask Storage System Materials at End of Storage System Life." *Symposium on Recycling of Metals arising from Operation and Decommissioning of Nuclear Facilites*, April 8-10, Nyköping, Sweden, D-4.

Idorn, G. M., Johansen, V. and Thaulow, N. (1993). *Assessment of Causes of Cracking in Concrete* Materials Science in Concrete III, American Ceramic Society, New York, NY.

IStructE (2010). *Addendum*, The Institution of Structural Engineers, London, UK.

Jaffer, S. J. and Hansson, C. M. (2009). "Chloride-Induced Corrosion Products of Steel in Cracked-Concrete Subjected to Different Loading Conditions," Cement and Concrete Reseach, 39(2), 116-125.

Jang, J.-W., Iwasaki, Iwao and Weiblen, P. (1995). *Effect of Salt Additives on Concrete Degradation (Phase II),* MN/RC-96/10, Minnesota Department of Transportation (MnDOT), St. Paul, Minnesota.

JCI (2003). *Method of Test for Fracture Energy of Concrete by Use of Notched Beam,* JCI-S-001-2003, Japan Concrete Institute Standard (JCI), Tokyo, Japan.

Johnson, J. B. (2010). "Bond Strength of Corrosion Resistant Steel Reinforcement in Concrete," Department of Civil and Environmental Engineering, Virginia Polytechnic Institute and State University, Charlottesville, Virginia.

Jones, A. E. K. and Clark, L. A. (1998). "The Effects of ASR on the Properties of Concrete and the Implications for Assessment," Engineering Structures, 20(9), 785-791.

Jones, F. E. and Tarleton, R. D. (1958a). *Reaction between Aggregates and Cements, Parts I-IV*, DSIR National Building Studies Research, HMSO, London, UK.

Jones, F. E. and Tarleton, R. D. (1958b). *Reaction between Aggregates and Cements, Parts I-IV*, DSIR National Building Studies Research, HMSO, London, UK.

Jung, W.-Y., Yoon, Y.-S. and Sohn, Y.-M. (2003). "Predicting the Remaining Service Life of Land Concrete by Steel Corrosion," Cement and Concrete Research, 33(5), 663-677.

Kelestemur, O. and Yildiz, S. (2006). "Effect of Various NaCl Concentration on Corrosion of Steel in Concrete Produced by Addition of Styrofoam," Gazi University Journal of Science, 19(3), 163-172.

Kessler, R. J., Powers, R. G., Vivas, E., Paredes, M. A. and Virmani, P. Y. (2008). "Surface Resistivity as an Indicator of Concrete Chloride Penetration Resistance." *Concrete Bridge Conference*, May 4-7, St. Louis, MO.

Kim, D.-G., Cho, M.-S. and Lee, J.-S. (2013). "The Effects of Chloride on Durability of Concrete Mixed With Sea Sand," US-China Education Review A, 3(5), 325-331.

Kishar, E. A., Ahmed, D. A., Mohammed, M. R. and Noury, R. (2013). "Effect of Caclium Chloride on the Hydration Characteristics of Ground Clay Bricks Cement Pastes," Bein-Suef University Journal of Basic and Applied Sciences, 2(1), 20-30.

Koch, G. H., Brongers, M. P. H., Thompson, N. G., Virmani, Y. P. and Payer, J. H. (2002). *Corrosion Costs and Preventive Strategies in the United States,* FHWA-RD-01-156, Federal Highway Administration (FHWA), Washington, DC.

Kropp, J. and Hisldorf, H. K. (1995). *Performance Criteria for Concrete Durability*, E & FN Spon, London, UK.

Kupwade-Patil, K. and Allouche, E. (2013). "Impact of Alkali Silica Reaction on Fly Ash-Based Geopolymer Concrete," Journal of Materials in Civil Engineering, 25(1), 131-139.

Kurdowski, W. (2004). "The Protective Layer and Decalcification of C-S-H in the Mechanism of Chloride Corrosion of Cement Paste," Cement and Concrete Research, 34(9), 1555-1559.

Kurdowski, W. (2014). *Cement and Concrete Chemistry*, Springer Science & Business, Mumbai, India.

Lambert, J. D., Bakhtiari, S., Bondar, I., Kot, C. and Pence, J. (2012). *NRC Job Code V6060: Extended In-Situ and Real Time Monitoring,* ANL/NE-12/18, Argonne National Laboratory (ANL), Lemont, IL.

Lamond, J. F. and Pielert, J. H. (2006). *Significance of Tests and Properties of Concrete and Concrete-Making Materials,* STP 169D, ASTM International, West Conschohocken, PA.

Latifee, E. (2013). "Miniature Concrete Prism Test - A New Test Method for Evaluating the ASR Potential of Aggregates, the Effectiveness of ASR Mitigation and the Job Mixture," Department of Civil Engineering, Clemson University, South Carolina, USA.

Leduc, D. R. (2012). *Dry Storage of Used Fuel Transition to Transport,* FCRD-UFD-2012-000253, Savannah River National Laboratory (SRNL), Aiken, SC.

Lee, H., Cody, R. D., Cody, A. M. and Spry, P. G. (2000). "Effects of Various Deicing Chemicals on Pavement Concrete Deterioration." *Mid-Continent Transporation Symposium*, May 15-16, 2000, Ames, IA, 151-155.

Liu, K. K. and Tam, W. H. (2002). *The Use of Accelerated Mortar Bar Test Methods for Assessment of Alkali-Aggregate Reactivity of Aggregate in Hong Kong,* GEO REPORT No. 145, Public Works Central Laboratory Materials Division (PWL), Hong Kong.

Liu, Y. (1996). "Modeling the Time-to-Corrosion Cracking of the Cover Concrete in Chloride Contaminated Reinforced Concrete Structures," Department of Civil Engineering, Virginia Polytechnic Institute and State University, Blacksbourg, VA.

Lopez, W., Gonzalez, J. A. and Andrade, C. (1993). "Influence of Temperature on the Service Life of Rebars," Cement & Concrete Research, 23(5), 1130-1140.

Maaddawy, T. E. and Soudki, K. (2007). "A Model for Prediction of Time from Corrosion Initiation to Corrosion Cracking," Cement & Concrete Composites, 29(3), 168-175.

Martin, J. W. (1985). "Service-Life Predictions from Accelerated Aging Tests Using Reliability Theory and Life Testing Analysis," in *Problems in Service Life Prediction of Building and Construction Materials,* 5*,* ed Masters, L., Springer Netherlands, Wisconsin, Madison, 95, 191-211.

Memon, F. A., Nuruddin, M. F., Khan, S., Shafiq, N. and Ayub, T. (2013). "Effect of Sodium Hydroxide Concentration on Fresh Properties and Compressive Strength of Self-

Compacting Geopolymer Concrete," Journal of Engineering Science and Technology, 8(1), 44-56.

Mladenovic, A., Šturm, S., Mirtic, B. and Šuput, J. S. (2009). "Alkali Silica Reaction in Mortars Made from Aggregates Having Different Degrees of Crystalinity," Ceramics – Silikáty, 53(1), 31-41.

Monette, L. J. and Gardner, N. J. (2002). "Residual Strength of Reinforced Concrete Beams Damaged by Alkali-Silica Reaction - Examination of Damage Rating Index Method," ACI Material Journal, 99(1), 42-50.

Morinaga, S. (1990). "Prediction of Service Lives of Reinforced Concrete Buildings Based on the Corrosion rate of Reinforcing Steel." *5th International Conference on Durability of Building Materials and Components*, Nov. 7-9, Brighton, UK, 5-16.

Morris, W., Moreno, E. I. and Sagues, A. A. (1996). "Practical Evaluation of Resistivity of Concrete in Test Cylinders Using a Wenner Array Probe," Cement and Concrete Research, 26(12), 1779-1787.

Mukhopadhyay, A. K., Ghanem, H., Shon, C.-S., Gress, D. and Hooton, D. (2009). *Mitigation of ASR in Concrete Pavement - Combined Materials Testing,* IPRF-01-G-002-03-2, Innovative Pavement Research Foundation (IPRF), Skokie, Illinois.

Mukhopadhyay, A. K., Zollinger, D. G. and Shon, C.-S. (2005). *Evaluation of Alkali Silica Reactivity of Mineral and Aggregate Using Dilatometer Method,* PRF-01-G-002-02-5.1, Texas Transportation Institute (TTI), Skokie, Illinois.

NADP (2016). *Chloride Ion Wet Deposition,* National Atmospheric Deposition Program/National Trends Network (NADP), Available from: http://nadp.sws.uiuc.edu, Accessed on May 15, 2016.

Nagataki, S., Ohga, H. and Inquel, T. (1991). "Evaluation of Fly Ash for Controlling Alkali-Aggregate Reaction." *2nd International Conference on Durability of Concrete* June 13-15, Montreal, Canada, 126, 955-972.

Naik, T. R., Ramme, B. W. and Tews, J. H. (1995). "Pavement Construction with High-Volume Class C and Class F Fly Ash Concrete," ACI Materials Journal, 92(2), 200-210.

Naik, T. R., Singh, S. S. and Hossain, M. M. (1994). "Permeability of Concrete Containing Large Amount of Fly Ash," Cement & Concrete Research, 24(5), 913-922.

Naus, D. J. (2007). *Primer of Durability of Nuclear Power Plant Reinforced Concrete Structures - A Review of Pertinent Factors,* NUREG/CR-6927, ORNL/TM-2006/529, Oak Ridge National Laboratory (ONRL), Washington, DC.

Naus, D. J. (2010). *A Compilation of Elevated Temperature Concrete Material Property Data and Information for Use in Assessments of Nuclear Power Plant Reinforced Concrete Structures,* NUREG/CR-7031, ORNL/TM-2009-175, Oak Ridge National Laboratory (ORNL)

United States Nuclear Regulatory Commision (U.S. NRC), Oak Ridge, TN.

Naus, D. J., Oland, C. B. and Ellingwood, B. R. (1996). *Report on Aging of Nuclear Power Plant Reinforced Concrete Structures* NUREG/CR-6424, BNL-NUREG-13148, Oak Ridge National Laboratory (ONRL), Oak Ridge, TN.

Nawy, E. G. (2008). *Reinforced Concrete: A fundamental Approach*, Prentice Hall, Toronto, Canada.

NEA (2002). *Electrochemical Techniques to Detect Corrosion in Concrete Structures in Nuclear Installations - Technical Note,* NEA-CSNI-R-2002-21, Nuclear Energy Agency of the OECD (NEA), Paris, France.

NEI (2014). *Guidance for Operations Based Aging Management for Dry Cask Storage,* Report No. NEI 14-03, Nuclear Energy Institute (NEI), Washington D.C.

Neville, A. (1995). "Chloride Attack of Reinforced Concrete: an Overview," Materials and Structures, 28, 63-70.

NOAA (2016). *Houston Climate; Extremes, Normals and Annual Summaries,* National Oceanic and Atmospheric Administration*,* Available from: http://www.srh.noaa.gov/hgx/?n=climate_iah_normals_summary, Accessed on July 20th, 2016.

Nordson, D. (2014). *3 and 4 Point Flexural Testing, Application Note*

NT-build (1995). *Concrete, Hardened: Accelerated Chloride Penetration,* NT build 443, Nordtest, Esbo, Finland.

NT-build (1996). *Concrete, Hardened: Chloride Content by Volhard Titration,* NT build 208, Nordtest, Esbo, Finland.

NT Build (1985). *Sand: Alkali-Silica Reactivity Accelerated Test,* NT Build 295, Nordtest (NT) Build, Espoo, Finland.

NT Build (1999). *Concrete, Mortar and Cement-Based Repair Materials: Chloride Migration Coeficient from Non-Steady-State Migration Experiments,* NT Build 492, Nordtest (NT) Build, Espoo, Finland.

Nuruddin, M. F., Demie, S., Ahmed, M. F. and Shafiq, N. (2011). "Effect of Superplasticizer and NaOH Molarity on Workability, Compressive Strength and Microstructure Properties of Self-Compacting Geopolymer Concrete " World Academy of Science, Engineering and Technology, 5(3), 187-194.

Ohdaira, E. and Masazawa, N. (2000). "Water Content and Its Effect on Ultrasound Propagation in Concrete - the Possibility of NDE," Ultrasonics, 38(1-8), 546-552.

Okba, S. H., El-Dieb, A. S. and Reda, M. M. (1997). "Evaluation of the Corrosion Resistance of Latex Modified Concrete (LMC)," Cement and Concrete Research, 27(6), 861-868.

Ortega, N. F., Rivas, I. E., Aveldaño, R. R. and Peralta, M. H. (2011). "Beams Affected by Corrosion Influence of Reinforcement Placement in The Cracking," Structural Engineering and Mechanics, 37(2), 163-175.

Pakshir, M. and Esmaili, S. (1998). "The Effect of Chloride Ion Concentration on the Corrosion of Concrete," Scientia Iranica, 4(4), 201-205.

Pan, J. W., Feng, Y. T., Wang, J. T., Sun, Q. C., Zhang, C. H. and Owen, D. R. (2012). "Modeling of Alkali-Silica Reaction in Concrete: A Review," Frontiers of Structures and Civil Engineering, 6(1), 1-18.

Parrott, L. J. (1987). *A Review of Carbonation in Reinforced Concrete*, Cement and Concrete Association, Slough, UK.

Parsons, W. H. and Insley, H. (1944). "Alkali Etching Tests on Concrete Aggregates," Journal of American Concrete Institute, 40, 229-244.

Pesavento, F., Gawin, D., Wyrzykowski, M., Schrefler, B. A. and Simoni, L. (2012). "Modeling alkali-silica reaction in non-isothermal, partially saturated cement based materials," Computer Methods in Applied Mechanics and Engineering, 225-228, 95-115.

Pignatelli, R. (2012). "Modeling of Degradation Induced by Alkali-Silica Reaction in Concrete Structures," Structural Engineering, Politecnico di Milano, Milan, Italy.

Pinto, R., Hobbs, S. and Hover, K. (2002). *Accelerated Aging of Concrete: a Literature Review,* FHWA-RD-01-073, US Department of Transportation, Federal Highway Administration (FHWA), McLean, Virgina.

Pommersheim, J. and Clifton, J. (1985). "Prediction of Concrete Service-Life," Materials and Structures, 18(1), 21-30.

Poole, A. B. (1992). "Introduction to Alkali-Aggregate Reaction in Concrete," in *The Alkali-Silica Reaction in Concrete,* eds. Swamy, R. N. and Van Nostrand, R., New York, NY.

Poole, J. L. (2007). "Modeling Temperature Sensitivity and Heat Evolution of Concrete," Graduate School, The University of Texas at Austin, Austin, TX.

Prezzi, M., Monteiro, P. J. M. and Sposito, G. (1992). "The Alkali-Silica Reaction Part I: Use of the Double-Layer Theory to Explain the Behavior of Reaction-Product Gels," ACI Materials Journal, 94(1), 10-17.

Pruckner, F. and Gjørv, O. E. (2004). "Effect of $CaCl_2$ and NaCl Additions on Concrete Corrosivity," Cement and Concrete Research, 34(7), 1209-1217.

Purvis, R. L., Babaei, K., Clear, K. C. and Markow, M. J. (1994). *Life-Cycle Cost Analysis for Protection and Rehbilitation of Concrete Bridges Relative to Reinforcement Corrosion,* SHRP-S-377, Strategic Highway Research Program (SHRP), Washington, DC.

Rangaraju, P. R. and Olek, J. (2011). *Performance of Concrete in the Presence of Airfield Pavement Deicers and Identification of Induced Distress Mechanisms, Appendix F*, American Concrete Pavement Associatio (ACPA), Rosemont, IL.

Rao, G. A. and Prasad, B. K. R. (2002). "Fracture Energy and Softening Behavior of High-Strength Concrete," Cement and Concrete Research, 32(2), 247-252, DOI: http://dx.doi.org/10.1016/S0008-8846(01)00667-6.

Ricker, R. E., Stoudt, M. R., Dante, J. F., Fink, J. L., Beauchamp, C. R. and Moffat, T. P. (1994). "Corrosion of Metals," in *Evaluation of Alternative In-Flight Fire Suppressants for Full-Scale Testing in Simulated Aircraft Engine Nacelles and Dry Bays,* 7, eds. Grosshandler, W. L., Gann, R. G. and Pitts, W. M., Washington, DC, 669-728.

Rigby, D. B. (2010). *Evaluation of the Technical Basis for Extended Dry Storage and Transportation of Used Nuclear Fuel*, United States Nuclear Waste Technical Review Board (NWTRB), Arlington, VA, http://www.nwtrb.gov/reports/eds_rpt.pdf.

RILEM TC-106-2 (2000). "Alkali-aggregate reaction - Recommendations-B-TC106-2 (now AAR-2) - Detection of Potential Alkali-Reactivity of Aggregates: A - The Ultra-accelerated Mortar-bar Test," Materials and Structures, 33(29), 283-289.

RILEM TC-106-AAR (2000). "Alkali-aggregate reaction - Recommendations-B-TC106-3 (now AAR-3) - Detection of Potential Alkali-Reactivity of Aggregates - Method for Aggregate Comibinations Using Concrete Prisms," Materials and Structures, 33(229), 290-293.

RILEM TC-154-EMC, Andrade, C., Alonso, C., Gulikers, J., Polder, B., Cigna, R., Vennesland, Ø. and Salta, M. (2004). "Recommendations of RILEM TC-154-EMC: "Electrochemical techniques for measuring metallic corrosion," Materials and Structures, 37(273), 623-643.

RILEM TC-191-ARP (2003). "RILEM Recommended Test Method AAR-1 'Detection of potential alkali-reactivity aggregates' Petrographic method," Materials and Structures, 36(261), 480-496.

Roy, D., Malek, R. and Licastro, P. (1987). "Chloride Permeability of Fly Ash-Cement Pastes and Mortars," in *Concrete Durability,* ed Scanlon, J. M., American Concrete Institute (ACI), 100, 1459-1476.

Rupnow, T. D. and Icenogle, P. (2011). *Evaluation of Surface Resistivity Measurements as an Alternative to the Rapid Chloride Permeability Test from Quality Assurance and Acceptance,* FHWA/LA.11/479, Louisiana Department of Transportation and Development (LaDOT), Baton Rouge, LA.

Sarkar, S. L., Zollinger, D. G., Mukhopadhyay, A. K., Seungwook, L. and Shon, C.-S. (2004). *Handbook for Identification of Alkali-Silica Reactivity in Airfield Pavement,* 150/5380-8, US Department of Transportation, Federal Aviation Administration (FAA), College Station, Texas.

Schiessl, P. (1988). *Corrosion of Steel in Concrete*, Reunion Internationale des Laboratoires et Experts des Materiaux (RILEM), New York, NY.

Shafaatian, S. M. H., Akhavan, A., Margaghechi, H. and Rajabpour, F. (2013). "How Does Fly Ash Mitigate Alkali-Silica Reaction (ASR) in Accelerated Mortar Bar Test (ASTM C1567)?," Cement and Concrete Composites, 37(1), 143-153.

Shayanfar, M. A. and Ghalehnovi, M. (2007). "Corrosion Effects on Tension Stiffening Behavior of Reinforced Concrete," Computers and Concrete, 4(5), 403-424.

Shehata, M. H. and Thomas, M. D. A. (2000). "The Effect of Fly Ash Composition on the Expansion of Concrete Due to Alkali-Silica Reacting," Cement and Concrete Reseach, 30(7), 1063-1072, DOI: http://dx.doi.org/10.1016/S0008-8846(01)00680-9.

Shi, X., Xie, N., Dang, Y., Muthumani, A., Huang, J., Hagel, A., Forsythe, S., Selig, E., Falk, D., McVey, E., Kessel, A., Martins, C., Zhang, Y. and Fang, Y. (2014). *Understanding and Mitigating Effects of Chloride Deicer Exposure on Concrete,* FHWA-OR-RD-08, Federal Highway Administration (FHWA), Washington, DC.

Shill, S. T. (2014). "Chloride Penetration into Concrete Structures Exposed to the Marine Atmosphere," Engineering and Computer Science, Florida Atlantic University, Boca Raton, FL.

Silva, N. (2013). "Chloride Induced Corrosion of Reinforcement Steel in Concrete," Department of Civil and Environmental Engineering, Chalmers University of Technology, Göteborg, Sweden

SINTEF (2008). *Modelling of Reinforced Corrosion in Concrete - State of the Art,* COIN Project report 7, SINTEF Research Company, Trondheim, Norway.

Smaoui, N., Bérubé, M. A., Fournier, B., Bissonnette, B. and Durand, B. (2005). "Effects of Alkali Addition on the Mechanical Properties and Durability of Concrete," Cement and Concrete Research, 35(2), 203-212.

Stanish, K. D., Hooton, R. D. and Thomas, M. D. A. (1997). *Testing the Chloride Penetration Resistance of Concrete: A literature Review,* FHWA contract DTFH61-97-R-00022, Department of Civil Engineering, University of Toronto, Toronto, Ontario, Canada.

Stanton, T. E. (1943a). "Studies to Develop an Accelerated Test Procedure for The Detection Of Adversely Reactive Cement-Aggregate Combination." *American Society of Testing and Materials Proceeding*, 43, 875-893.

Stanton, T. E. (1943b). "Studies to Develop an Accelerated Test Procedure for the Detection of Adversley Reactive Cement-Aggregate Combination." *American Society of Testing and Materials Proceeding*, 43, 875-893.

Stark, D. (1994). "Alkali-Silica Reaction in Concrete," in *Significance of Tests and Properties of Concrete and Concrete-Making Materials,* 32*,* eds. Klieger, P. and Lamond, J. F., ASTM, Fredericksburg, VA, STP 169C, 365-371.

Streicher, P. E. and Alexander, M. G. (1995). "A chloride Conduction Test for Concrete," Cement and Concrete Research, 25(6), 1284-1294, DOI: http://dx.doi.org/10.1016/0008-8846(95)00121-R.

Sutter, L., Peterson, K., Julio-Betancourt, G., Hooton, D., Van Dam, T. and Smith, K. (2008). *The Deleterious Chemical Effects of Concentrated Deicing Solutions on Portland Cement Concrete*, Michigan Tech Transportation Institute, Houghton, MI.

Suwito, A. and Xi, Y. (2003). "Service Life of Reinforced Concrete Structures with Corrosion Damage due to Chloride Attack," in *Life-Cycle Performance of Deteriorating Structures:*

Assessment, Design, and Management, eds. Frangopol, D. M., Bruhwiler, E., Faber, M. H. and Adey, B., American Society of Civil Engineers (ASCE), Reston, VA, 207-218.

Talley, K. G., Kapitan, J. G. and Breen, J. E. (2016). "Methods for Approximation of ASR/DEF Damage in Concrete Columns," ACI Structural Journal, 113(1), 105-110.

Temuujin, J., Williams, R. P. and Riessen, A. v. (2009). "Effect of Mechanical Activation of Fly Ash On The Properties Of Geopolymer Cured at Ambient Temperature," Journal of Materials Processing Technology, 209(12-13), 5726-5280.

Thoft-Christensen, P., Jensen, F. M., Middleton, C. R. and Blackmore, A. (1996). "Assessment of the Reliability of Concrete Slab Bridges. Aalborg: Dept. of Building Technology and Structural Engineering," Structural Reliability Theory, R9616(157).

Thomas, M., Dunster, A., Nixon, P. and Blackwell, B. (2011). "Effect of Fly Ash on the Expansion of Concrete due to Alkali-Silica Reaction – Exposure Site Studies," Cement & Concrete Composites, 33(3), 359-367.

Touma, W. E. (2000). "Alkali-Silica Reaction in Portland Cement Concrete: Testing Methods and Mitigation Alternatives," Graduate School, The University of Texas At Austin, Austin, TX.

Tuutti, K. (1982). *Corrosion of Steel in Concrete*, Swedish Cement and Concrete Research Institute, Stockholm, Sweden.

U.S. GAO (2012). *Spent Nuclear Fuel, Accumulating Quantities at Commercial Reactors Present Storage and Other Challenges,* GAO-12-797, United States Government Accountability Office (GAO), Washington, D.C.

U.S. NRC (2015). *Backgrounder on Dry Cask Storage of Spent Nuclear Fuel,* United States Nuclear Regulatory Commission (U.S. NRC), Available from: http://www.nrc.gov/reading-rm/doc-collections/fact-sheets/dry-cask-storage.html, Accessed on February 10, 2016.

U.S. NRC (2016). *NRC Regulations, Title 10 Code of Federal Regulations (10 CFR)*, U.S. Nuclear Regulatory Commission (U.S. NRC), Rockville, MD.

Wang, K., Nelsen, D. E. and Nixon, W. A. (2006). "Damaging Effects of Deicing Chemicals on Concrete Materials," Cement & Concrete Composites, 28(2), 173-188.

Yu, H., Shi, X., Hartt, W. H. and Lu, B. (2010). "laboratory Investigation of Reinforcement Corrosion Initiation and Chloride Threshold Content for Self-Compacting Concrete," Cement and Concrete Research, 40(10), 1507-1516.

Zhou, F. P., Barr, B. I. G. and Lydon, F. D. (1995). "Fracture Properties of High Strength Concrete with Varying Silica Fume Content and Aggregates," Cement and Concrete Research, 25(3), 543-552.

Zollinger, D. G., Mukhopadhyay, A. K., Ghanem, H., Shon, C.-S., Gress, D. and Hooton, D. (2009). *Mitigation of ASR in Concrete Pavement - Combined Materials Testing,* IPRF-01-G-002-03-2, Texas Transportation Institute (TTI), Texas A&M University, College Station, TX.

APPENDIX

Table A 1 Sieve Analysis of Fine Aggregate

Sieve Size (mm)	Weight of fine aggregate retained (g)				Percent Retained	Cumulative Percent Retained	Percent Passing
	Determination No.						
	I	II	III	Avg.			
9.5	0.0	0.0	0.0	0.0	0.0	0.0	100.0
4.75	5.6	4.5	8.2	6.1	0.6	0.6	99.4
2.36	84.5	99.6	122.6	102.2	10.2	10.8	89.2
0.85	270.5	287.7	310.5	289.6	29.0	39.8	60.2
0.6	282.0	250.9	223.9	252.3	25.2	65.0	35.0
0.3	202.3	202.3	201.8	202.1	20.2	85.2	14.8
0.15	130.1	128.4	114.0	124.2	12.4	97.6	2.4
0.075	22.0	23.1	16.1	20.4	2.0	99.7	0.3
Pan	3.0	3.5	2.9	3.1	0.3	100.0	0.0
Total	1000	1000	1000	1000	100	-	-

Table A 2 Sieve Analysis of Coarse Aggregate

Sieve Size (mm)	Weight of Coarse aggregate retained (g)				Percent Retained	Cumulative Percent Retained	Percent Passing	Size Number	Nominal Size
	Determination No.								
	I	II	III	Avg.					
25.4	23.0	25.2	0.0	16.1	1.3	1.3	98.7	6 & 67	3/4 to 3/8" & 3/4" to No.4
19.0	190.8	128.0	128.6	149.1	12.4	13.8	86.2		
12.7	225.4	228.2	187.7	213.8	17.8	31.6	68.4		
9.5	195.2	205.2	211.7	204.0	17.0	48.6	51.4		
4.75	388.3	415.8	421.5	408.5	34.0	82.6	17.4		
2.36	155.0	169.0	185.2	169.7	14.1	96.8	3.2		
Pan	22.3	28.6	65.3	38.7	3.2	100.0	0.0		
Total	1200	1200	1200	1200	100	-	-		

Table A 3 Density of Fresh Concrete, Phase 1

Mix	Density (g/cm^3)	Average Density (g/cm^3)
SCC_PH1	2.339	2.325
	2.344	
	2.297	
NaOH-8_PH1	2.322	2.319
	2.317	
	2.314	
$CaCl_2$-4_PH1	2.355	2.347
	2.338	
	-	

Table A 4 Density of Fresh Concrete, NaOH Mixtures, Phase 2

Mix	Density (g/cm^3)	Average Density (g/cm^3)
NaOH-0_PH2	2.35	2.36
	2.36	
	2.37	
NaOH-2_PH2	2.43	2.41
	2.40	
	2.40	
NaOH-4_PH2	2.42	2.42
	2.42	
	2.42	
NaOH-8_PH2	2.38	2.38
	2.39	
	2.38	

Table A 5 Density of Fresh Concrete, $CaCl_2$ Mixtures, Phase 2

Mix	Density (g/cm^3)	Average Density (g/cm^3)
$CaCl_2$_0_PH2	2.31	2.31
	2.32	
	2.31	
$CaCl_2$_1_PH2	2.35	2.36
	2.38	
	2.34	
$CaCl_2$_2_PH2	2.31	2.33
	2.33	
	2.34	
$CaCl_2$_4_PH2	2.27	2.30

Table A 6 Slump Test Results, Phase 1

Mix	Slump (mm)	Average Slump (mm)
SCC_PH1	279.4	271.8
	254.0	
	241.3	
NaOH-8_PH1	190.5	228.6
	241.3	
	254.0	
$CaCl_2$-4_PH1	266.7	275.1
	266.7	
	292.1	

Table A 7 Density of Hardened Concrete at 28 Days, NaOH Mixtures, Phase 2

Mix	Bulk Density, Dry (g/cm^3)	Bulk Density after Immersion (g/cm^3)	Apparent Density (g/cm^3)
NaOH-0_PH2	1.66	1.74	1.81
NaOH-2_PH2	1.64	1.72	1.78
NaOH-4_PH2	1.64	1.71	1.77
NaOH-8_PH2	1.65	1.73	1.79

Table A 8 Absorption and Voids of Hardened Concrete at 28 Days, NaOH Mixtures, Phase 2

Mix	Absorption after Immersion (%)	Absorption after Immersion and Boiling (%)	Volume of permeable pore space (voids) (%)
NaOH-0_PH2	4.6	4.8	8.0
NaOH-2_PH2	4.5	4.7	7.6
NaOH-4_PH2	4.2	4.4	7.3
NaOH-8_PH2	4.7	4.9	8.1

Table A 9 Density of Hardened Concrete at 28 Days, $CaCl_2$ Mixtures, Phase 2

Mix	Bulk Density, Dry (g/cm^3)	Bulk Density after Immersion (g/cm^3)	Apparent Density (g/cm^3)
$CaCl_2$-0_PH2	1.67	1.75	1.82
$CaCl_2$-1_PH2	1.65	1.73	1.80
$CaCl_2$-2_PH2	1.65	1.73	1.79
$CaCl_2$-4_PH2	1.66	1.74	1.80

Table A 10 Absorption and Voids of Hardened Concrete at 28 Days, $CaCl_2$ Mixtures, Phase 2

Mix	Absorption after Immersion (%)	Absorption after Immersion and Boiling (%)	Volume of permeable pore space (voids) (%)
$CaCl_2$-0_PH2	4.4	4.9	8.1
$CaCl_2$-1_PH2	4.7	5.0	8.3
$CaCl_2$-2_PH2	4.5	4.8	8.0
$CaCl_2$-4_PH2	4.6	4.9	8.1

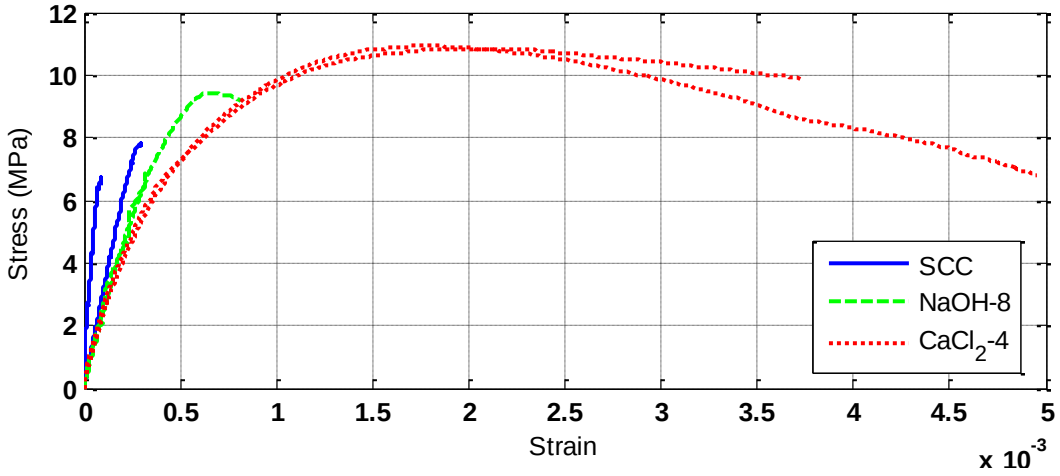

Figure A 1 Compression test, phase 1, 1st day

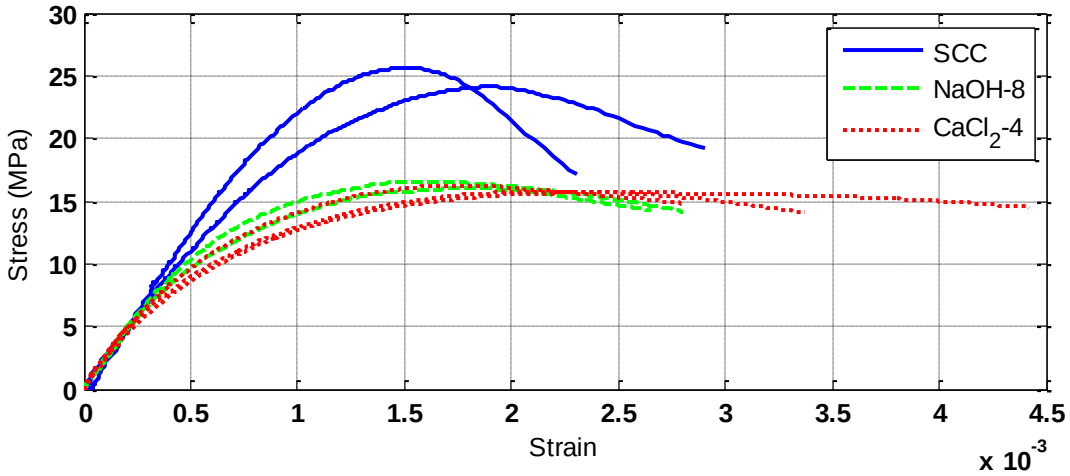

Figure A 2 Compression test, phase 1, 3rd day

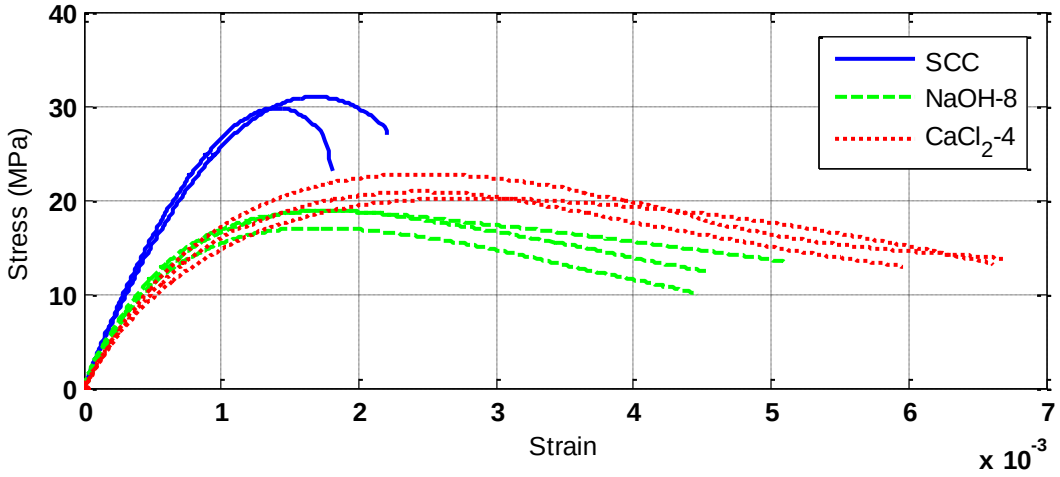

Figure A 3 Compression test, phase 1, 7th day

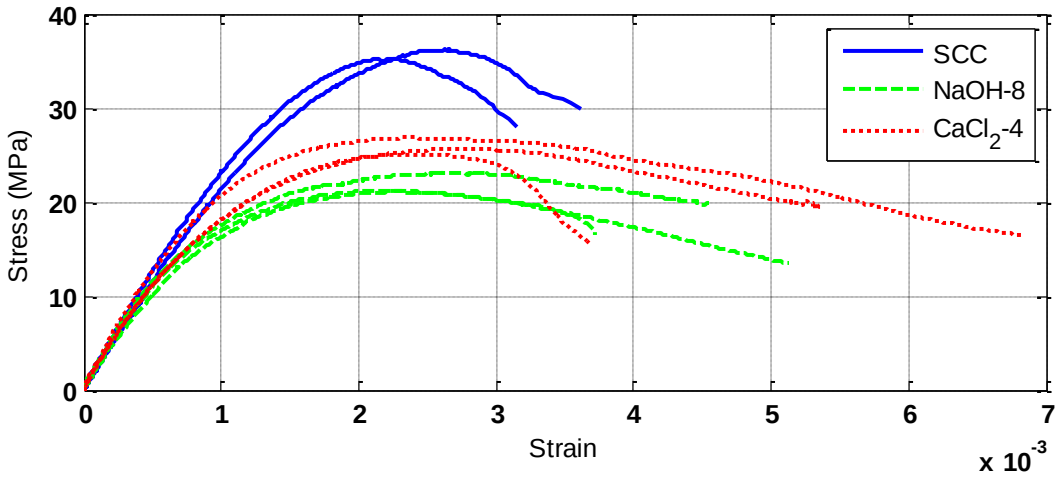

Figure A 4 Compression test, phase 1, 28th day

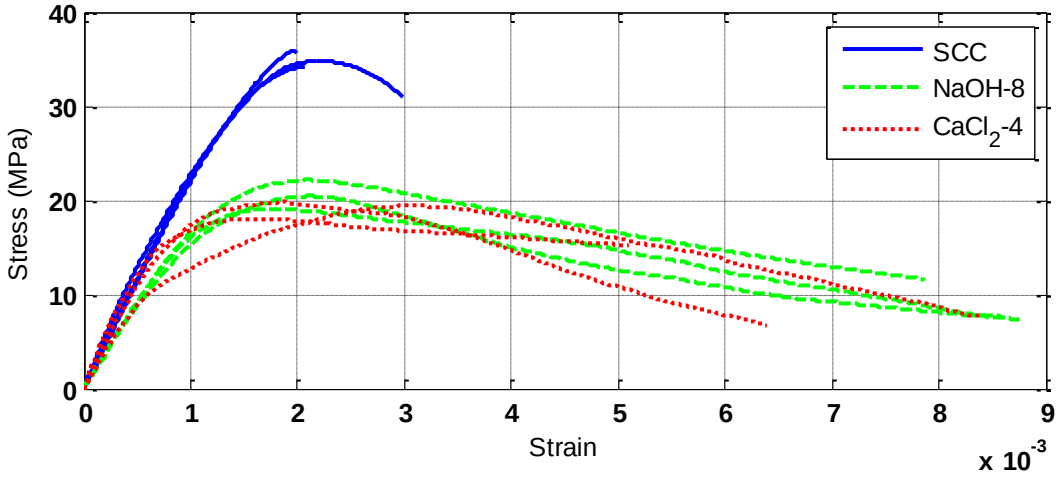

Figure A 5 Compression test, phase 1, 210th day

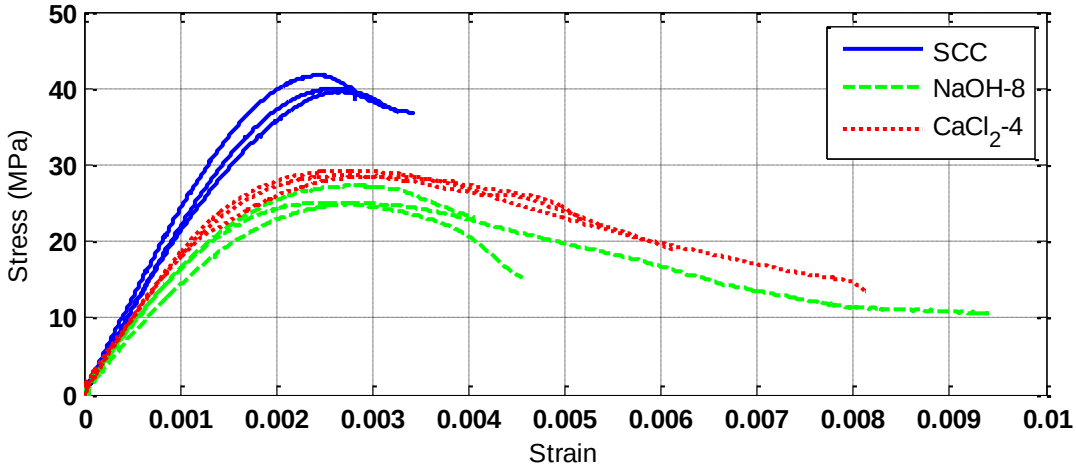

Figure A 6 Compression test, phase 1, 365th day

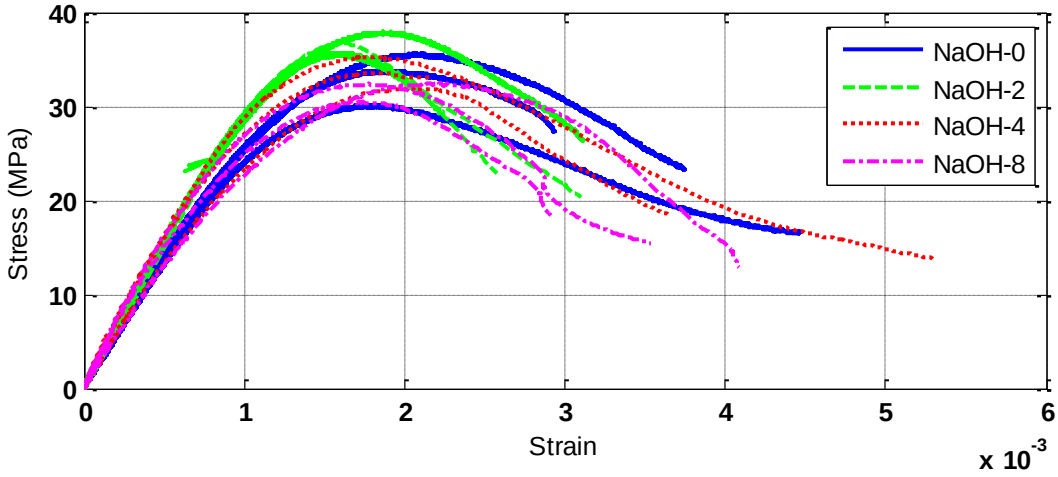

Figure A 7 NaOH compression test, vertical strain, phase 2, 7th day

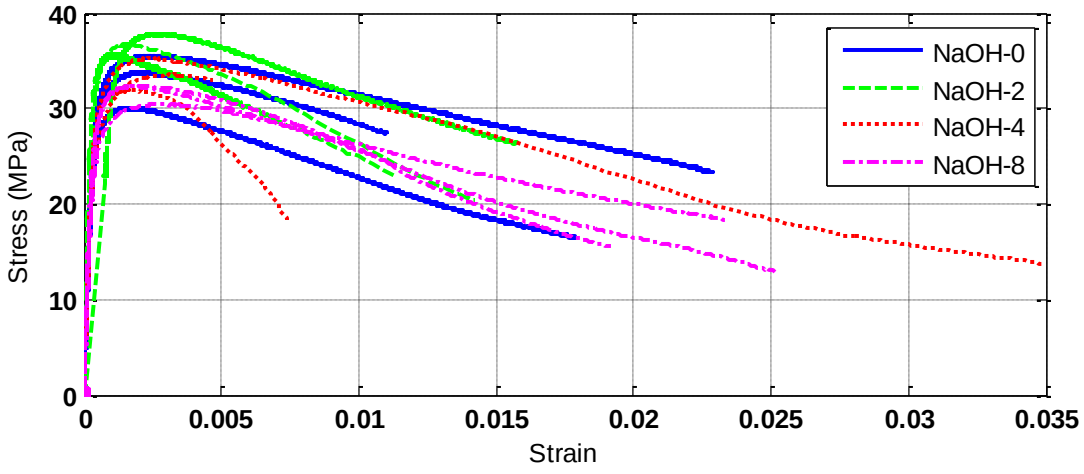

Figure A 8 NaOH compression test, horizontal strain, phase 2, 7th day

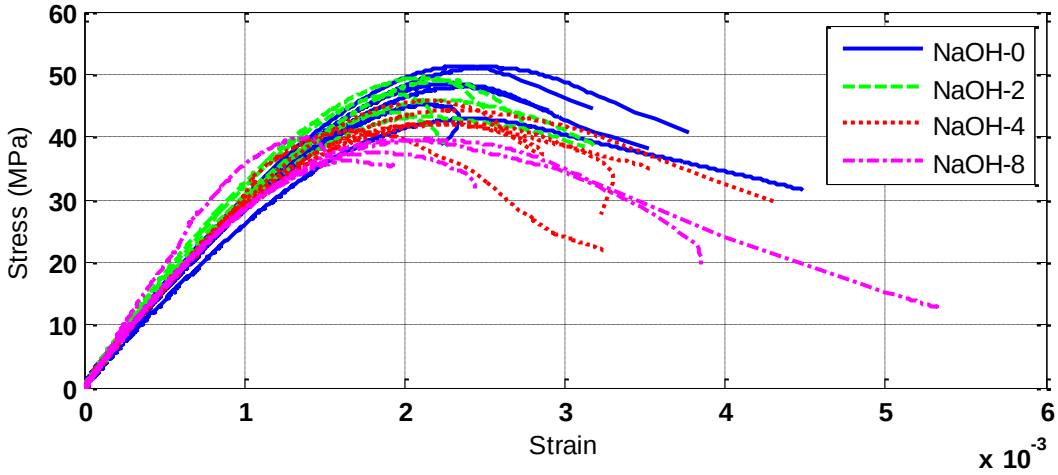

Figure A 9 NaOH compression test, vertical strain, phase 2, 28th day

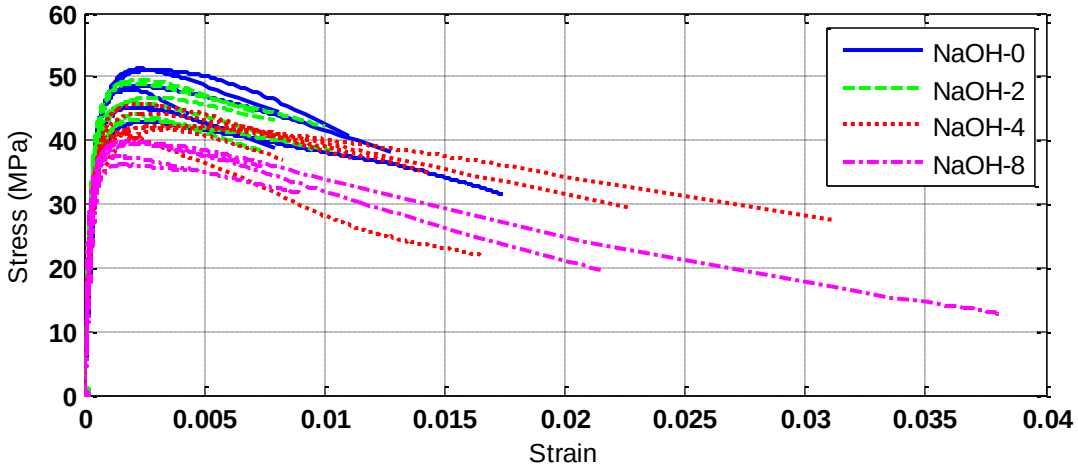

Figure A 10 NaOH compression test, horizontal strain, phase 2, 28th day

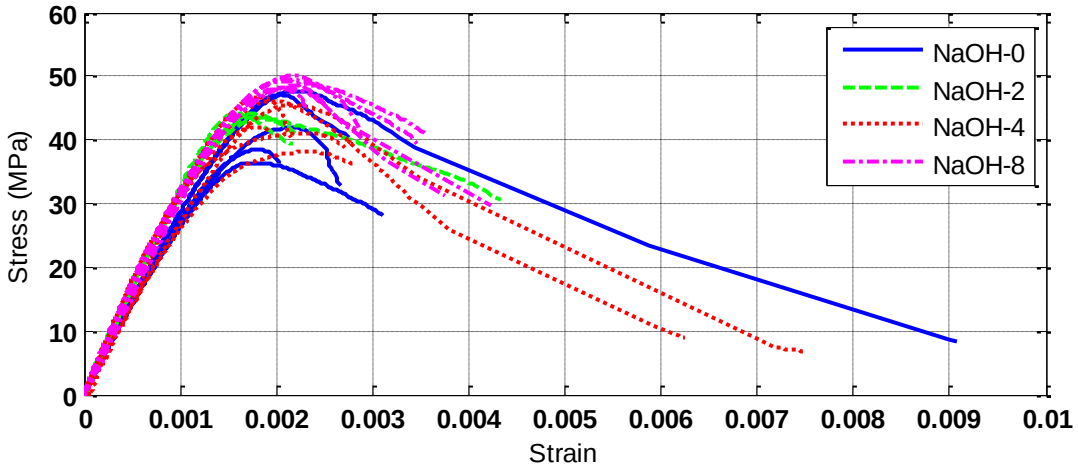

Figure A 11 NaOH compression test, vertical strain, phase 2, 180th day

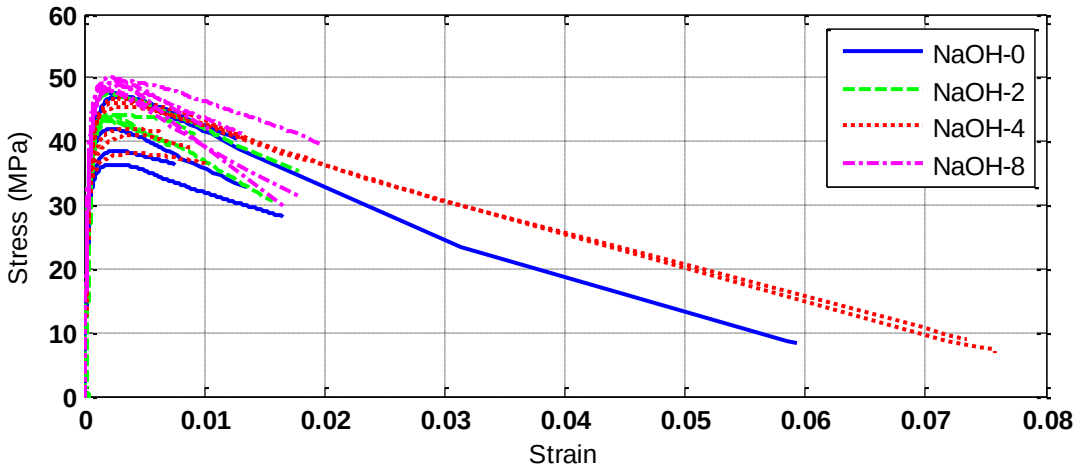

Figure A 12 NaOH compression test, horizontal strain, phase 2, 180th day

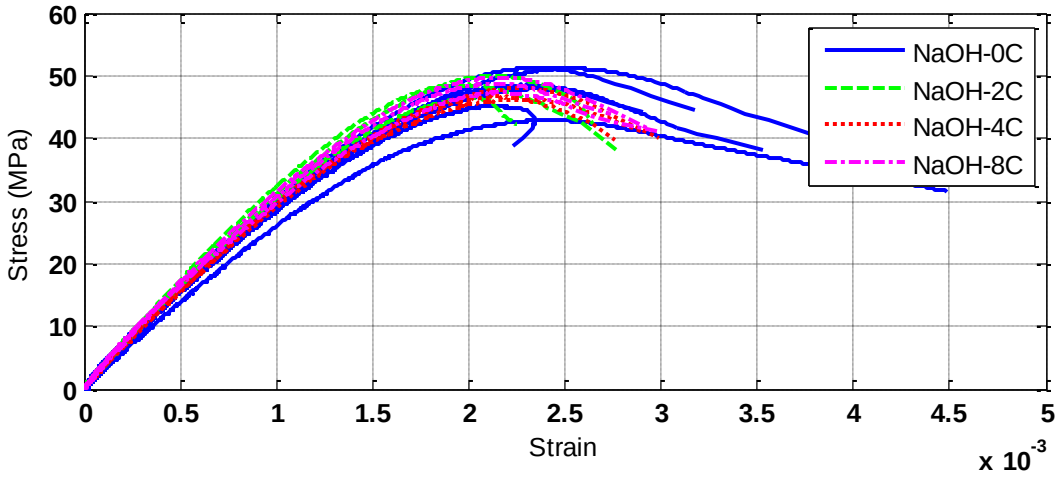

Figure A 13 NaOH control compression test, vertical strain, phase 2, 28th day

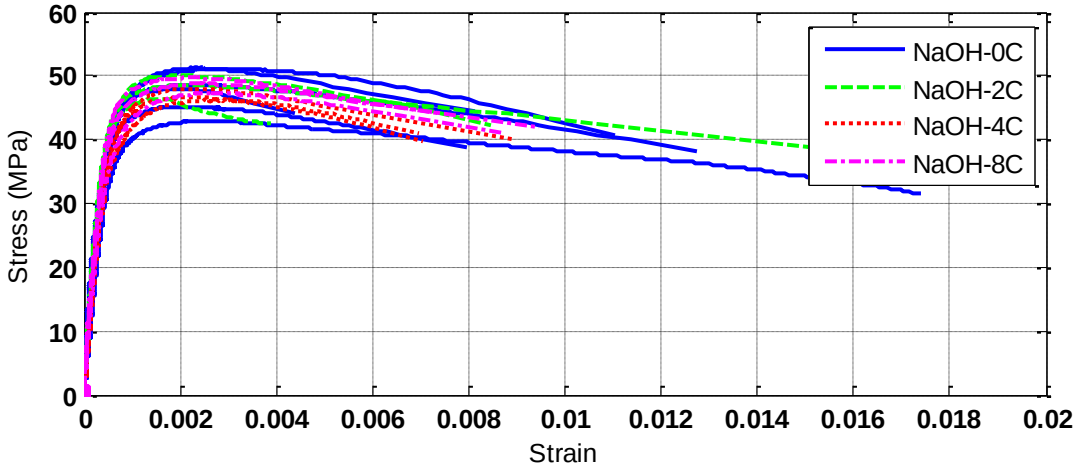

Figure A 14 NaOH control compression test, horizontal strain, phase 2, 28th day

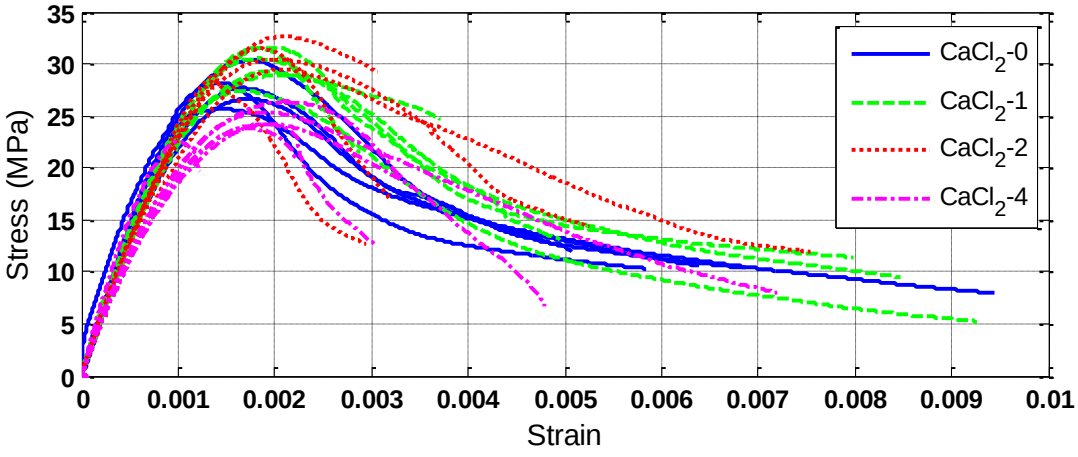

Figure A 15 $CaCl_2$ compression test, vertical strain, phase 2, 7th day

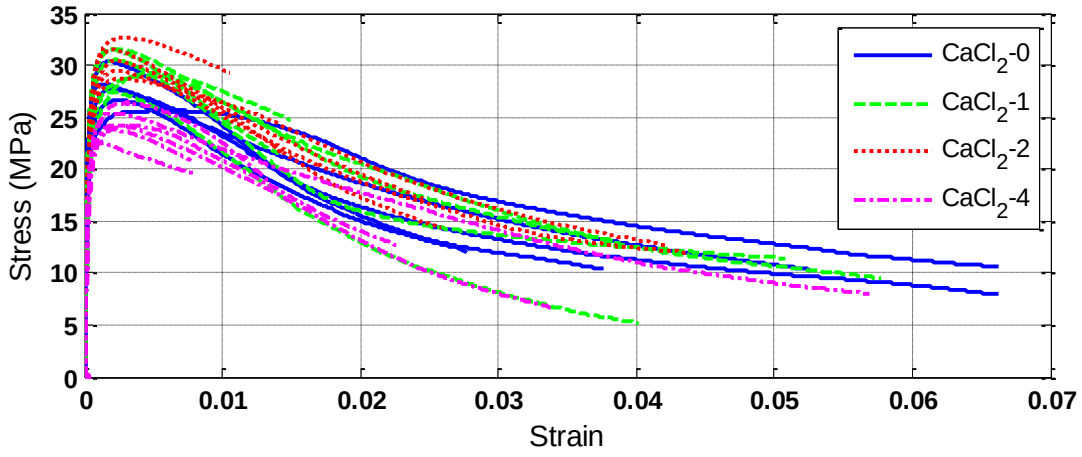

Figure A 16 $CaCl_2$ compression test, horizontal strain, phase 2, 7th day

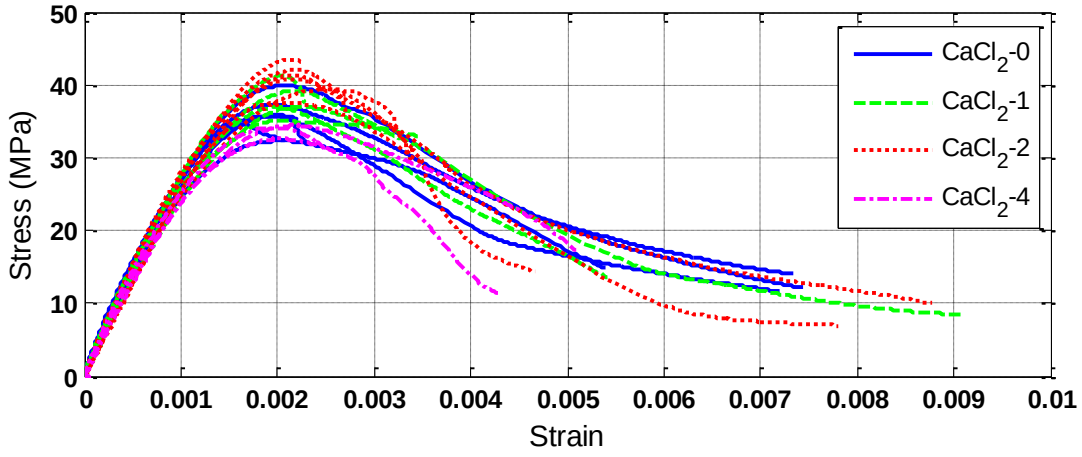

Figure A 17 $CaCl_2$ compression test, vertical strain, phase 2, 28th day

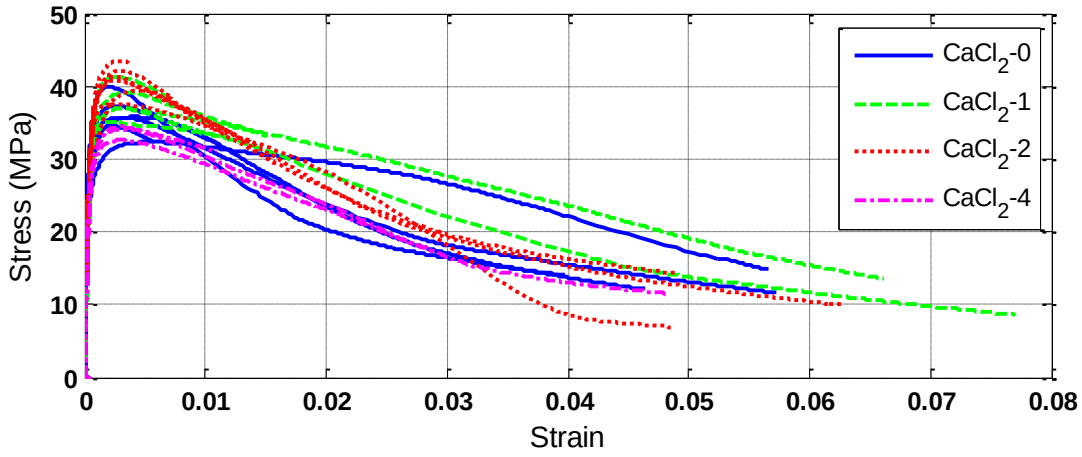

Figure A 18 $CaCl_2$ compression test, horizontal strain, phase 2, 28th day

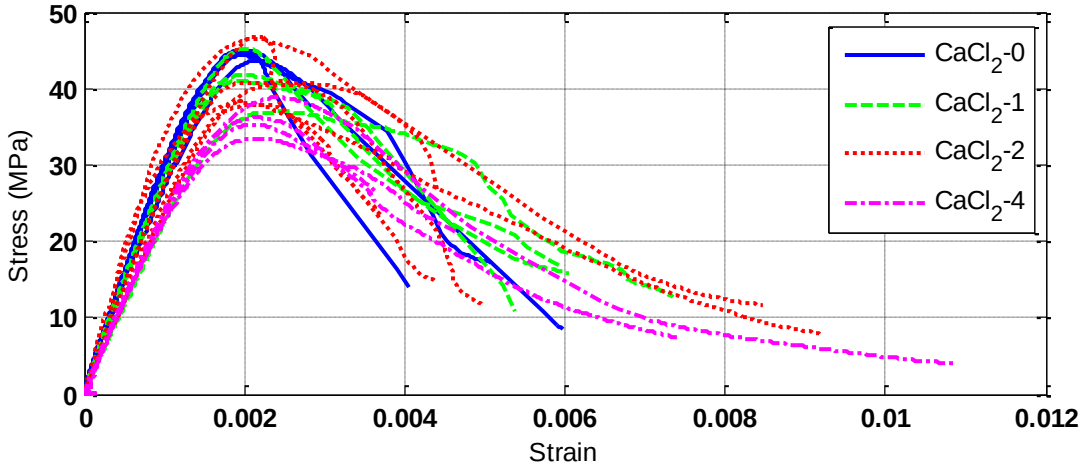

Figure A 19 $CaCl_2$ compression test, vertical strain, phase 2, 90th day

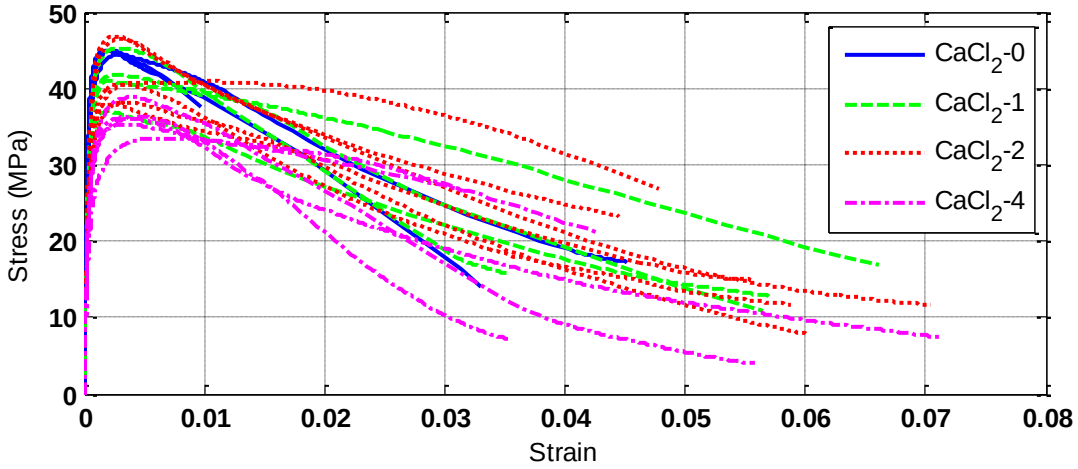

Figure A 20 $CaCl_2$ compression test, horizontal strain, phase 2, 90th day

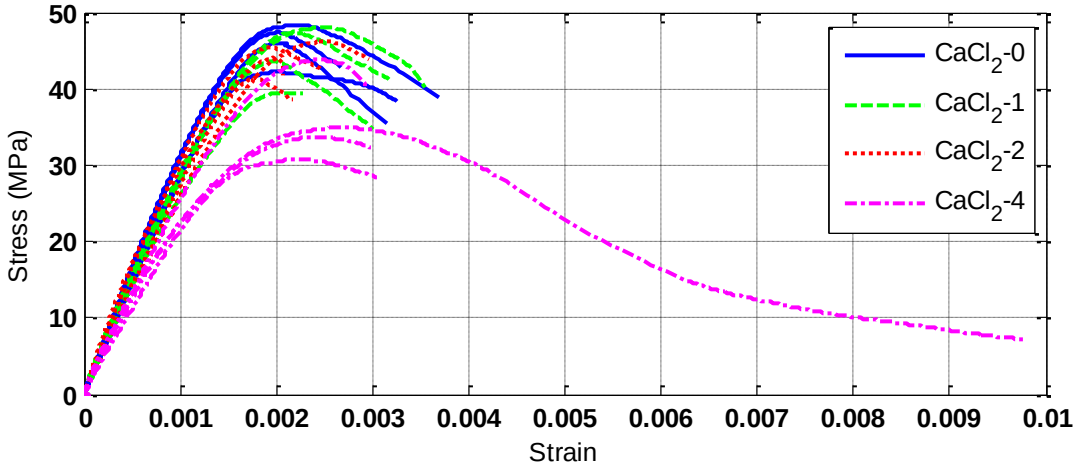

Figure A 21 $CaCl_2$ compression test, vertical strain, phase 2, 180th day

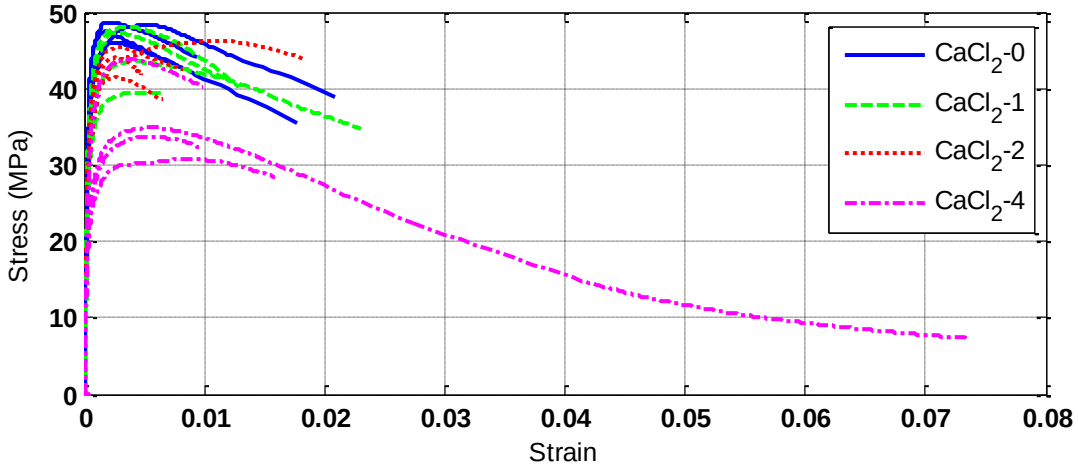

Figure A 22 $CaCl_2$ compression test, horizontal strain, phase 2, 180th day

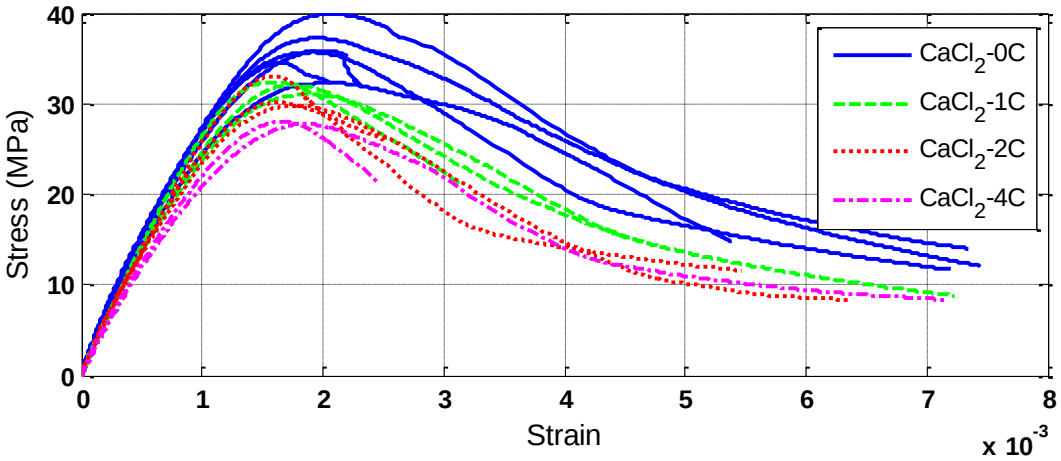

Figure A 23 $CaCl_2$ control compression test, vertical strain, phase 2, 28th day

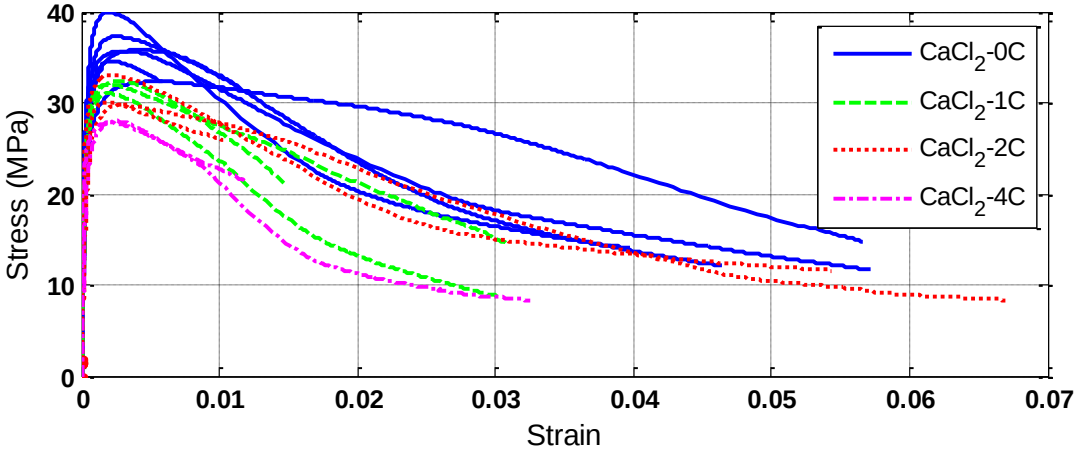

Figure A 24 $CaCl_2$ control compression test, horizontal strain, phase 2, 28th day

Table A 11 Strength of Control Specimens of NaOH Mixtures, Phase 2

Mix	Max Stress (MPa)	Average	MOE (MPa)	Average	Poisson's Ratio	Average
NaOH-0_PH2	45.1	47.8	29722	30042	0.29	0.31
	48.5		30584		0.30	
	51.1		30098		0.35	
	47.9		30622		0.30	
	42.9		27142		0.33	
	51.1		32085		0.32	
NaOH-2_PH2	48.5	48.3	33635	32783	0.32	0.30
	46.3		31938		0.29	
	50.0		32776		0.31	
NaOH-4_PH2	46.2	46.9	30578	30537	0.36	0.34
	46.6		30838		0.31	
	48.0		30194		0.34	
NaOH-8_PH2	49.7	48.6	33209	32207	0.32	0.34
	47.3		31672		0.37	
	48.7		31741		0.32	

Table A 12 Strength of Control Specimens of $CaCl_2$ Mixtures, Phase 2

Mix	Max Stress (MPa)	Average	MOE (MPa)	Average	Poisson's Ratio	Average
$CaCl_2$-0_PH2	32.3	36.0	27748	29593	0.30	0.30
	35.9		29538		0.31	
	37.3		29497		0.32	
	35.7		30879		0.23	
	39.9		29269		0.31	
	34.5		30627		0.34	
$CaCl_2$-1_PH2	32.4	31.8	29117	27869	0.32	0.32
	32.0		27114		0.33	
	31.0		27376		0.31	
$CaCl_2$-2_PH2	29.8	31.0	26832	27025	0.35	0.32
	30.1		27812		0.29	
	33.1		26431		0.31	
$CaCl_2$-4_PH2	28.0	27.9	24492	24266	0.37	0.33
	27.8		24040		0.29	

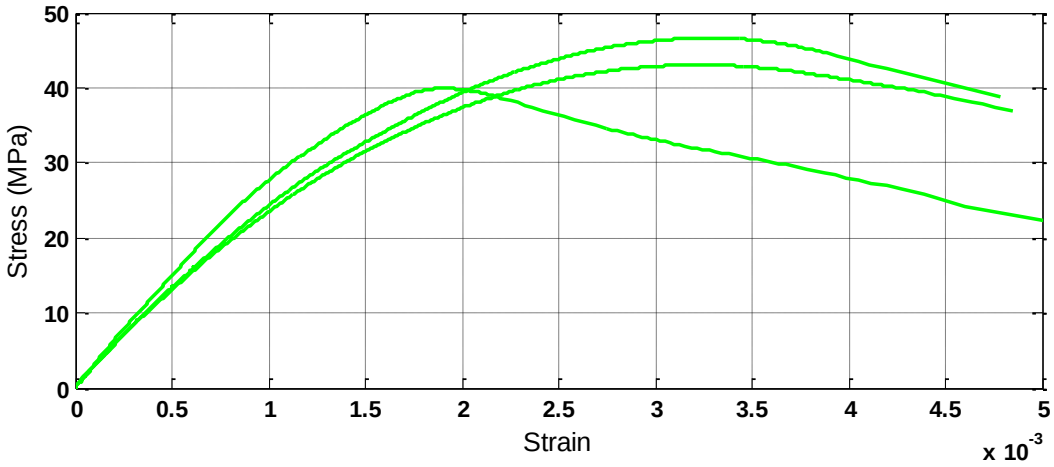

Figure A 25 TRIGA compression test, vertical strain

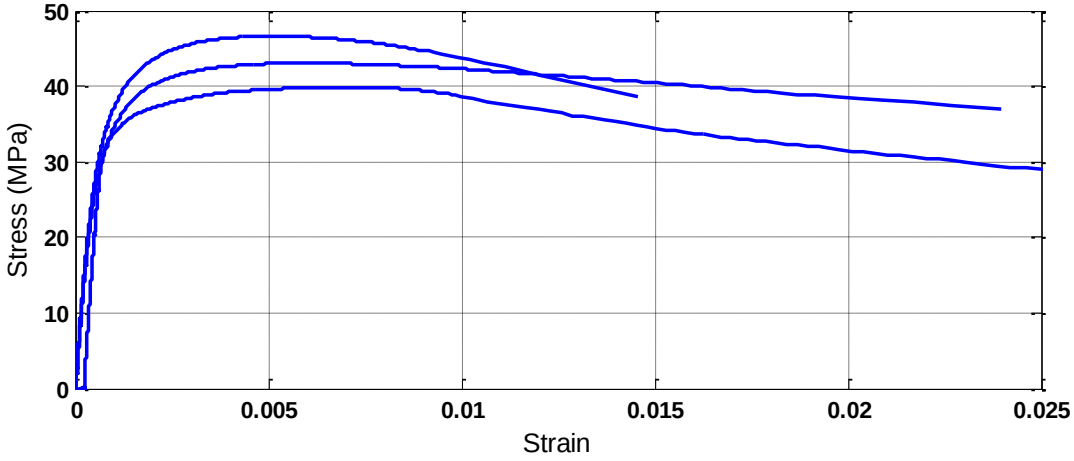

Figure A 26 TRIGA compression test, horizontal strain

Table A 13 Modulus of Elasticity of Concrete Mixtures, Phase 1, at 210 and 365 Days

Mix	210 Days		365 Days	
	E (MPa)	Average	E (MPa)	Average
SCC_PH1	25358.0	25250.9	22099.0	23503.4
	25143.8		24907.8	
	-		22466.7	
NaOH-8_PH1	17397.7	17878.1	15193.7	16549.1
	-		16581.9	
	18358.5		17904.5	
$CaCl_2$-4_PH1	22809.4	20455.3	19102.1	18783.3
	17802.6		19093.4	
			18154.4	

Table A 14 Modulus of Elasticity of NaOH Concrete Mixtures, Phase 2

Mix	7 Days		28 Days		180 Days	
	E (MPa)	Average	E (MPa)	Average	E (MPa)	Average
NaOH-0_PH2	28291	27813	29722	30042	29477	28837
	28560		30584		-	
	26586		30098		27666	
	-		30622		29748	
	-		27142		29303	
	-		32085		27990	
NaOH-2_PH2	31470	31948	35486	32805	33156	34662
	32117		31612		-	
	32258		31039		33771	
	-		31146		38106	
	-		34526		35146	
	-		33020		33132	
NaOH-4_PH2	32613	30768	32403	31231	27930	31710
	32649		30039		36137	
	27042		31257		33369	
	-		30747		27971	
	-		31294		31946	
	-		31647		32906	
NaOH-8_PH2	33138	29971	41597	34195	33495	33057
	30761		31655		31104	
	26012		34981		32065	
	-		32551		35323	
	-		32472		32725	
	-		31912		33633	

Table A 15 Modulus of Elasticity of $CaCl_2$ Concrete Mixtures, Phase 2

Mix	7 Days		28 Days		90 Days		180 Days	
	E (MPa)	Average	E (MPa)	Average	E (MPa)	Average	E (MPa)	Average
$CaCl_2$-0_PH2	-	28417	27748	29593	30805	30057	28627	32768
	27199		29538		27559		31026	
	29688		29497		29777		33271	
	28908		30879		31410		-	
	27539		29269		31263		31845	
	28751		30627		29528		39071	
$CaCl_2$-1_PH2	28171	27082	27248	27822	22645	27564	-	29277
	26554		30740		-		28223	
	25534		-		28660		28410	
	26808		28793		29913		30372	
	26185		25445		-		-	
	29239		26883		29039		30104	
$CaCl_2$-2_PH2	25486	26331	30822	28043	23771	29902	26312	29775
	22669		29638		28428		33490	
	33001		25928		35356		-	
	26154		28717		28082		27451	
	26819		27298		25831		27928	
	23856		25854		37941		33694	
$CaCl_2$-4_PH2	24357	24918	27046	27439	-	25236	-	24745
	23628		28322		26762		22077	
	33684		-		25096		25554	
	22354		28708		24330		-	
	22384		25678		23582		26474	
	23100		-		26411		24875	

Table A 16 Poisson's Ratio of Concrete Mixtures, Phase 1, at 210 and 365 Days

Mix	210 Days		365 Days	
	Poisson's Ratio	Average	Poisson's Ratio	Average
SCC_PH1	0.24	0.27	0.29	0.29
	0.31		0.29	
	-		0.24	
NaOH-8_PH1	0.46	0.38	0.23	0.29
	0.29		0.29	
	0.31		0.34	
$CaCl_2$-4_PH1	0.31	0.353	0.27	0.29
	0.43		0.26	
	-		0.33	

Table A 17 Poisson's Ratio of NaOH Concrete Mixtures, Phase 2

Mix	7 Days		28 Days		180 Days	
	Poisson's Ratio	Average	Poisson's Ratio	Average	Poisson's Ratio	Average
NaOH-0_PH2	0.29	0.31	0.29	0.31	0.29	0.31
	0.31		0.30		0.30	
	0.33		0.35		0.35	
	-		0.30		0.30	
	-		0.33		0.33	
	-		0.32		0.32	
NaOH-2_PH2	0.26	0.30	0.32	0.31	0.38	0.34
	0.32		0.28		-	
	0.32		0.29		0.31	
	-		0.33		0.34	
	-		0.36		0.35	
	-		0.28		0.32	
NaOH-4_PH2	0.39	0.37	0.35	0.33	0.27	0.33
	0.38		0.31		0.35	
	0.35		0.32		0.32	
	-		0.32		0.28	
	-		0.37		0.39	
	-		0.29		0.35	
NaOH-8_PH2	0.39	0.34	0.36	0.34	0.32	0.32
	0.35		0.35		0.31	
	0.27		0.28		0.30	
	-		0.40		0.32	
	-		0.34		0.29	
	-		0.34		0.36	

Table A 18 Poisson's Ratio of $CaCl_2$ Concrete Mixtures, Phase 2

Mix	7 Days		28 Days		90 Days		180 Days	
	Poisson's Ratio	Ave.	Poisson's Ratio	Ave.	Poisson's Ratio	Ave.	Poisson's Ratio	Ave.
$CaCl_2$-0_PH2	-	0.30	0.30	0.30	0.24	0.31	0.32	0.31
	0.29		0.31		-		0.28	
	0.33		0.32		0.26		0.33	
	0.28		0.23		0.28		-	
	0.26		0.31		0.30		0.25	
	0.32		0.34		0.28		0.39	
$CaCl_2$-1_PH2	0.28	0.32	0.31	0.35	0.29	0.34	-	0.29
	0.27		0.35		-		0.26	
	0.28		-		0.28		0.38	
	0.37		0.42		0.33		0.23	
	0.36		0.31		-		-	
	0.37		0.37		0.32		0.30	
$CaCl_2$-2_PH2	0.36	0.35	0.37	0.35	0.28	0.33	0.24	0.29
	0.31		0.36		0.31		0.33	
	0.48		0.31		0.38		-	
	0.27		0.36		0.29		0.30	
	0.38		0.39		0.27		0.24	
	0.32		0.33		0.31		0.31	
$CaCl_2$-4_PH2	0.35	0.37	0.35	0.35	-	0.32	-	0.32
	0.37		0.34		0.44		0.28	
	0.45		-		0.32		0.35	
	0.34		0.36		0.37		-	
	0.34		0.35		0.30		0.31	
	0.38		-		0.35		0.33	

Table A 19 Modulus of Rupture of Concrete Mixtures, Phase 1

Mix	28 Days (MPa)	Average	365 Days (MPa)	Average	455 Days (MPa)	Average
SCC_PH1	3.95	3.95	4.16	4.67	5.86	5.19
	3.26		4.74		5.13	
	4.10		5.11		4.58	
	4.49					
	3.13					
NaOH-8_PH1	2.84	2.92	2.86	2.95	2.44	2.32
	2.91		2.97		2.42	
	2.86		3.02		2.06	
	2.99					
	2.98					
CaCl2-4_PH1	3.69	3.65	3.88	3.89	3.42	3.35
	3.62		3.50		3.67	
	3.62		4.23		2.95	
	3.31					
	4.30					

Table A 20 Modulus of Rupture of NaOH Concrete Mixtures, Phase 2

Mix	28 Days (MPa)	Average
NaOH-0_PH2	5.12	4.57
	4.07	
	4.50	
NaOH-2_PH2	4.53	4.29
	4.52	
	3.81	
NaOH-4_PH2	3.59	3.83
	3.33	
	4.57	
NaOH-8_PH2	4.03	4.24
	4.39	
	4.30	

Table A 21 Modulus of Rupture of $CaCl_2$ Concrete Mixtures, Phase 2

Mix	28 Days (MPa)	Average
$CaCl_2$-0_PH2	3.43	3.68
	4.05	
	3.56	
$CaCl_2$-1_PH2	3.61	3.60
	3.76	
	3.45	
$CaCl_2$-2_PH2	4.36	4.49
	4.35	
	4.76	
$CaCl_2$-4_PH2	3.45	3.43
	3.32	
	3.51	

Table A 22 Bond Strength of Concrete Mixtures with #10 Rebars, Phase 1

Mix	Bond (MPa)	Average Bond (MPa)	Corrosion (%)	Average Corrosion (%)
SCC_PH1	16.733	19.362	0.613	0.597
	21.991		0.581	
NaOH-8_PH1	15.201	14.339	0.602	0.601
	13.476		0.599	
$CaCl_2$-4_PH1	21.236	22.118	1.205	1.201
	23.000		1.198	

Table A 23 Bond Strength of Concrete Mixtures with #19 Rebars, Phase 1

Mix	Bond (MPa)	Average Bond (MPa)	Corrosion (%)	Average Corrosion (%)
SCC_PH1	17.768	18.241	0.159	0.159
	18.714		0.159	
NaOH-8_PH1	10.941	10.690	0.158	0.238
	10.439		0.319	
$CaCl_2$-4_PH1	12.017	11.917	0.313	0.314
	11.816		0.315	

Table A 24 Crack Widths of Specimens with #10 Rebar, Phase 1 (Note that the Crack No. are Indicated in Figure 75)

Bar No.	No.	Crack Width (mm)						
		117 Days	171 Days	225 Days	276 Days	342 Days	432 Days	492 Days
4	1	0.6	0.8	0.8	0.8	1.0	3.0	4.2
	2	0.4	0.5	0.5	0.5	0.8	1.2	1.8
	3	0.2	0.2	0.2	0.3	0.3	Spalling	Spalling
	4	0.2	0.3	0.4	0.5	2.0	4.6	5.1
	5	0.2	0.2	0.4	0.5	0.9	1.3	1.8
	6	0.4	0.5	0.6	0.6	0.8	1.0	1.3
	7	0.1	0.2	0.3	0.5	0.5	0.8	1.0
	8	-	-	0.2	0.3	0.4	0.4	0.7
	9	-	-	0.2	0.2	0.2	0.2	0.3
5	1	0.3	0.4	0.4	0.4	0.4	0.4	0.8
	2	0.1	0.2	0.2	0.2	0.3	0.3	0.5
	3	0.1	0.2	0.2	0.2	0.2	0.5	0.8
	4	0.1	0.2	0.4	0.5	0.5	3.8	4.2
	5	0.2	0.3	0.3	0.3	0.3	0.3	0.3
	6	0.2	0.2	0.2	0.3	0.3	1.0	0.3
	7	-	0.1	0.2	0.3	0.3	0.6	1.3
	8	-	0.1	0.2	0.2	0.3	0.9	0.8
	9	-	-	0.1	0.2	0.3	0.6	0.7
	10	-	-	0.1	0.2	0.3	0.7	0.8
	11	-	-	0.1	0.1	0.1	0.2	0.4

Table A 25 Crack Width of Specimens with #19 Rebar, Phase 1 (Note that the Crack No. are Indicated in Figure 75)

Bar No.	No.	Crack Width (mm)						
		117 Days	171 Days	225 Days	276 Days	342 Days	432 Days	492 Days
14	1	-	0.1	0.2	0.3	0.4	1.3	1.3
	2	-	0.1	0.2	0.3	0.3	0.6	0.8
	3	-	-	0.1	0.2	0.2	0.3	0.4
	4	-	-	0.1	0.2	0.3	0.4	0.7
	5	-	-	-	0.1	0.2	0.4	0.7
17	1	0.2	0.4	0.4	0.5	0.7	0.8	Spalling
	2	0.2	0.2	0.5	0.6	0.7	1.0	2.1
	3	0.3	0.4	0.5	0.6	0.6	0.7	0.9
	4	0.4	0.4	0.5	0.8	1.2	3.4	4.1
	5	0.2	0.4	0.4	1.0	Spalling	Spalling	Spalling
	6	0.1	0.2	0.3	0.4	0.5	0.7	1.5
	7	0.1	0.2	0.3	0.5	0.5	0.5	0.5
	8	-	-	0.2	0.2	0.2	0.4	0.4

Table A 26 Half-Cell Potential Measurements in Specimens with #10 Rebar, Phase 1 (Corresponds to #3 in the US system), Phase 1

Age	163 Days	236 Days		267 Days		291 Days		325 Days		357 Days		389 Days		422 Days		452 Days		482 Days		512 Days		536 Days		563 Days		590 Days		
Mix	Potential (mV/CSE*)	Temp. (˚C)	Potential (mV/CSE)	Temp. (˚C)	Potential (mV/CSE)	Temp. (˚C)	Potential (mV/CSE)	Temp. (˚C)	Potential (mV/CSE)	Temp. (˚C)	Potential (mV/CSE)	Temp. (˚C)	Potential (mV/CSE)	Temp. (˚C)	Potential (mV/CSE)	Temp. (˚C)	Potential (mV/CSE)	Temp. (˚C)	Potential (mV/CSE)	Temp. (˚C)	Potential (mV/CSE)	Temp. (˚C)	Potential (mV/CSE)	Temp. (˚C)	Potential (mV/CSE)	Temp. (˚C)	Potential (mV/CSE)	Temp. (˚C)
SCC_PH1	-80.59**	9.2	-88.30	20.7	-53.11	17.9	-64.23	25.6	-66.10	23.7	-13.80	32.0	-105.40	22.0	-5.11	22.1	-2.38	22.8	-37.44	21.4	-141.09	17.9	-107.23	17.3	-59.70	28	-15.07	26.7
NaOH-8_PH1	-55.41	13.1	-104.19	19.9	-109.25	18.5	-70.56	22.6	-98.57	20.7	-56.83	32.3	-104.44	21.4	-5.60	21.0	-33.81	22.1	-79.01	20.1	-144.74	17.4	-154.5	17	-23.19	27.9	-17.04	26.4
$CaCl_2$-4_PH1	-546.5	7	-424.97	21.7	-462.08	18.8	-423.75	26.5	-439.23	24.3	-254.90	32.0	-494.73	22.3	-204.93	23.3	-157.14	23.4	-308.92	24.2	-435.94	18.4	-512.44	18.4	-280.99	27.9	-374.58	26.8

*CSE: Copper-sulfate electrode

**Measurements shown in this table are corrected based on JSCE-E 601-2000

Table A 27 Half-Cell Potential Measurements in Specimens with #19 Rebar (Corresponds to #6 in the US system), Phase 1

Age	163 Days		236 Days		267 Days		291 Days		325 Days		357 Days		389 Days		422 Days		452 Days		482 Days		512 Days		536 Days		563 Days		590 Days	
Mix	Potential (mV/CSE*)	Temp. (˚C)	Potential (mV/CSE)	Temp. (˚C)	Potential (mV/CSE)	Temp. (˚C)	Potential (mV/CSE)	Temp. (˚C)	Potential (mV/CSE)	Temp. (˚C)	Potential (mV/CSE)	Temp. (˚C)	Potential (mV/CSE)	Temp. (˚C)	Potential (mV/CSE)	Temp. (˚C)	Potential (mV/CSE)	Temp. (˚C)	Potential (mV/CSE)	Temp. (˚C)	Potential (mV/CSE)	Temp. (˚C)	Potential (mV/CSE)	Temp. (˚C)	Potential (mV/CSE)	Temp. (˚C)	Potential (mV/CSE)	Temp. (˚C)
SCC_PH1	-76.99**	5.9	-86.99	23.9	-102.15	18.5	-81.12	26.2	-87.32	25.2	-84.56	33.6	-97.48	22.8	-2.06	25.6	-39.33	24.3	-38.55	26.5	-141.14	20.4	-70.55	20.5	-12.91	26.1	-18.24	24.4
NaOH-8_PH1	-104.03	12.4	-134.8	23	-115.86	18.6	-104.85	26.5	-91.51	25.1	-28.61	35.1	-108.87	22.7	-41.90	25.0	-15.8	24	-119.4	26	-108.53	19.3	-138.96	19.6	-44.68	25.8	-45.34	23.4
$CaCl_2$.4_PH1	-416.29	7	-480.6	24	-491.4	19	-482.27	26.7	-529.32	25.2	-351.36	33.6	-507.18	22.8	-335.90	26.0	-228.05	24.5	-348.75	27.5	-411.23	21.3	-463.93	21.3	-240.06	26.6	-338.36	25.6

*CSE: Copper-sulfate electrode

**Measurements shown in this table are corrected based on JSCE-E 601-2000

Table A 28 Half-Cell Potential Measurements in $CaCl_2$ Specimens with #10 Rebar (Corresponds to #3 in the US system), Phase 2

Age	28 Days		60 Days		90 Days		120 Days		150 Days		180 Days	
Mix	Potential (mV/CSE*)	Temp. (˚C)	Potential (mV/CSE)	Temp. (˚C)	Potential (mV/CSE)	Potential (mV/CSE)	Potential (mV/CSE)	Temp. (˚C)	Potential (mV/CSE)	Temp. (˚C)	Potential (mV/CSE)	Temp. (˚C)
SCC_PH1	-135.6**	17.1	-227.3	19.2	-123.0	17.2	-119.2	19.7	-98.0	14.5	-107.4	18.8
$CaCl_2$-1_PH2	-207.8	17.3	-311.3	19.0	-171.2	17.5	-161.5	21.3	-122.5	14.5	-125.2	21.8
$CaCl_2$-2_PH2	-241.3	17.7	-316.7	18.8	-199.3	17.6	-155.7	22.8	-137.8	14.5	-138.7	20.5
$CaCl_2$-4_PH2	-384.4	17.8	-474.1	18.8	-434.9	17.6	-396.5	23.9	-355.7	14.6	-400.0	19.4

*CSE: Copper-sulfate electrode

**Measurements shown in this table are corrected based on JSCE-E 601-2000

Table A 29 Surface Resistivity of Specimens, Phase 1

		115 Days	171 Days	202 Days	230 Days	261 Days	291 Days	318 Days	349 Days	382 Days	412 Days	440 Days	470 Days	500 Days	530 Days	563 Days	593 Days
Mix	No.	ρ (KΩ.com)	ρ (KΩ.com)	ρ (KΩ.com)	ρ (KΩ.com)	ρ (KΩ.com)	ρ (KΩ.com)	ρ (KΩ.com)	ρ (KΩ.com)	ρ (KΩ.com)	ρ (KΩ.com)	ρ (KΩ.com)	ρ (KΩ.com)	ρ (KΩ.com)	ρ (KΩ.com)	ρ (KΩ.com)	ρ (KΩ.com)
SCC-PH1	1	16.1	21.2	22.3	23.2	25.3	26.1	28.5	29.0	26.4	32.8	35.3	32.9	33.9	34.8	38.1	37.0
	2	14.3	18.6	21.3	21.7	23.8	25.5	27.1	28.7	28.1	34.9	36.5	34.3	34.1	37.3	37.1	35.8
	3	12.1	16.0	16.9	18.2	20.5	21.5	23	25.1	24.5	30.9	37.5	31.2	32.5	33.3	33.9	31.5
NaOH-8-PH1 (in water)	1	5.7	6.3	6.8	8.9	7.5	7.6	8.2	9.2	9.4	12.1	12.3	13.4	14.4	14.0	13.7	15.5
	2	5.4	6.1	6.5	7.1	6.9	7.2	8.1	9.2	9.2	11.1	13.7	12.2	12.3	15.5	14.7	15.2
NaOH-8-PH1 (in NaOH solution)	1	4.7	6.9	5.4	6.0	7.1	6.2	6.4	6.8	6.9	7.1	7.4	7.4	8.6	9.0	8.1	7.7
	2	5.7	6.7	6.4	7.0	7.3	9.3	7.5	7.7	8.0	8.5	8.7	8.9	8.9	10.0	9.5	9.3
$CaCl_2$-4-PH1 (in water)	1	5.2	6.4	6.8	7.4	8.2	8.7	9.7	11.1	11.4	14.5	22.8	17.8	19.8	20.8	21.3	22.0
	2	5.2	6.2	6.7	9.7	8.1	8.4	9.1	10.6	10.2	13.2	16.5	16.3	16.0	18.6	18.8	20.4
$CaCl_2$-4-PH1 (in $CaCl_2$ solution)	1	4.9	9.1	7.3	8.1	12	16.8	21.7	28.7	36.6	38.5	64.3	74.4	41.4	43.4	44.8	44.0
	2	4.6	5.9	7.2	7.6	11.2	14.8	20	26.3	34.9	37.4	64.4	75.9	42.4	46.5	47.9	48.0

Table A 30 Surface Resistivity of NaOH Specimens, Phase 2

		28 Days	60 Days	90 Days	120 Days	150 Days	180 Days	210 Days	240 Days
Mix	No.	ρ (KΩ.com)	ρ (KΩ.com)	ρ (KΩ.com)	ρ (KΩ.com)	ρ (KΩ.com)	ρ (KΩ.com)	ρ (KΩ.com)	ρ (KΩ.com)
NaOH-0_PH2	1	6.5	10.5	12.5	12.1	12.8	14.6	15.0	16.5
	2	6.8	10.5	11.4	12.3	12.6	13.4	15.2	16.9
	3	6.8	10.5	11.9	12.4	12.9	14.1	14.6	16.2
NaOH-0.2_PH2	1	8.5	13.3	16.0	17.9	17.6	19.6	19.5	19.8
	2	9.8	14.3	16.7	18.3	19.5	20.2	19.5	21.1
	3	9.8	14.6	15.4	17.0	18.6	19.9	16.8	20.4
NaOH-0.4_PH2	1	9.8	14.3	15.3	16.2	17.3	18.8	17.3	20.1
	2	11.0	14.8	15.2	17.7	18.5	19.7	19.1	21.3
	3	9.6	14.1	15.6	15.9	17.1	18.6	15.9	21.1
NaOH-0.8_PH2	1	11.5	17.0	21.6	23.3	23.2	25.2	21.9	25.9
	2	11.0	16.7	18.8	21.6	21.9	23.4	22.6	24.4
	3	12.4	17.0	20.2	21.8	22.5	23.7	20.2	24.4

Table A 31 Surface Resistivity of $CaCl_2$ Specimens, Phase 2

		28 Days	60 Days	90 Days	120 Days	150 Days	180 Days
Mix	No.	ρ (KΩ.com)	ρ (KΩ.com)	ρ (KΩ.com)	ρ (KΩ.com)	ρ (KΩ.com)	ρ (KΩ.com)
SCC_PH2	1	6.5	12.3	20.1	22.5	26.2	32.0
	2	7.3	14.2	21.6	26.2	30.3	36.2
	3	6.2	12.7	18.2	23.5	27.6	31.1
$CaCl_2$-1_PH2	1	5.2	9.9	15.6	19.0	22.7	26.0
	2	5.2	10.4	16.0	19.6	23.8	27.4
	3	4.9	10.1	14.8	17.9	21.1	24.8
$CaCl_2$-2_PH2	1	6.3	14.1	23.4	26.9	33.8	37.4
	2	7.3	15.7	25.6	28.8	36.7	42.0
	3	7.2	15.5	26.0	29.7	37.6	42.4
$CaCl_2$-4_PH2	1	4.7	8.1	10.6	12.6	15.0	18.6
	2	4.9	8.0	11.2	12.8	16.0	20.3
	3	4.7	8.4	11.5	13.5	16.7	19.0

Table A 32 UPV Measurement Results, Phase 1

Mix	129 Days	176 Days	207 Days	235 Days	261 Days	286 Days	318 Days	348 Days	378 Days	408 Days	438 Days	468 Days	498 Days	528 Days	561 Days	594 Days
	V_{avg} (m/sec)	V_{avg} (m/sec)	V_{avg} (m/sec)	V_{avg} (m/sec)	V_{avg} (m/sec)	V_{avg} (m/sec)	V_{avg} (m/sec)	V_{avg} (m/sec)	V_{avg} (m/sec)	V_{avg} (m/sec)	V_{avg} (m/sec)	V_{avg} (m/sec)	V_{avg} (m/sec)	V_{avg} (m/sec)	V_{avg} (m/sec)	V_{avg} (m/sec)
SCC_PH1	4294	4520	4495	4412	4255	4171	4109	4146	4134	3977	4229	4176	4196	4291	4309	4225
NaOH-8_PH1 Spec. 1	3837	4098	4109	4052	3904	3886	3768	3914	3480	3691	3671	3864	4099	3934	3946	3957
NaOH-8_PH1 Spec. 2	3944	4062	4070	4033	3888	3814	3732	3835	3516	3723	3684	3864	3886	3916	3916	3924
NaOH-8_PH1 Spec. 3	3799	4109	4102	3998	3901	3916	3828	3859	3493	3649	3660	3797	3842	3906	3881	3874

Table A 33 UPV Measurement Results for NaOH Mixtures on Prisms, Phase 2

Mix	7 Days	28 Days	60 Days	90 Days	120 Days	150 Days	180 Days
	V_{avg} (m/sec)	V_{avg} (m/sec)	V_{avg} (m/sec)	V_{avg} (m/sec)	V_{avg} (m/sec)	V_{avg} (m/sec)	V_{avg} (m/sec)
NaOH-0_PH2	4470	4548	4467	4359	4383	4463	4495
NaOH-0.2_PH2	4623	4627	4635	4589	4566	4624	4592
NaOH-0.4_PH2	4672	4596	4597	4580	4578	4624	4584
NaOH-0.8_PH2	4669	4569	4615	4606	4622	4642	4622

Table A 34 UPV Measurement Results for $CaCl_2$ Mixtures on Prisms, Phase 2

Mix	7 Days	28 Days	60 Days	90 Days	120 Days	150 Days	180 Days
	V_{avg} (m/sec)	V_{avg} (m/sec)	V_{avg} (m/sec)	V_{avg} (m/sec)	V_{avg} (m/sec)	V_{avg} (m/sec)	V_{avg} (m/sec)
$CaCl_2$-0_PH2	4343	4510	4401	4565	4521	4636	4554
$CaCl_2$-1_PH2	4349	4344	4239	4389	4421	4436	4393
$CaCl_2$-2_PH2	4296	4362	4163	4363	4444	4451	4414
$CaCl_2$-4_PH2	4167	4290	4150	4244	4337	4394	4332

Table A 35 Schmidt Hammer Test Results for NaOH Specimens, Phase 2

	15 Days	28 Days	90 Days	180 Days
	Stress (MPa)	Stress (MPa)	Stress (MPa)	Stress (MPa)
NaOH-0_PH2	23.1	29	30.0	25.1
NaOH-0.2_PH2	20.3	28.8	29.3	30.3
NaOH-0.4_PH2	19.2	24.7	28.3	27.7
NaOH-0.8_PH2	17.0	22.1	27.7	26.9

Table A 36 Schmidt Hammer Test Results for $CaCl_2$ Specimens, Phase 2

	7 Days	28 Days	90 Days	180 Days
	Stress (MPa)	Stress (MPa)	Stress (MPa)	Stress (MPa)
$CaCl_2$-0_PH2	10.4	16.6	26.0	26.4
$CaCl_2$-1_PH2	11.2	17.8	27.2	28.1
$CaCl_2$-2_PH2	12.1	19.5	28.7	30.8
$CaCl_2$-4_PH2	8.9	14.7	23.6	21.1

Table A 37 Crack width on $CaCl_2$ cask

No.	Crack Width (mm)					
	163 Days	186 Days	225 Days	295 Days	512 Days	569 Days
1	0.2	0.3	0.3	0.3	0.5	0.5
2	0.1	0.1	0.1	0.1	0.1	0.2
3	0.05	0.05	0.05	0.05	0.1	0.1
4	0.1	0.1	0.1	0.1	0.2	0.3
5	0.15	0.15	0.15	0.25	0.4	0.5
6	0.1	0.1	0.1	0.1	0.2	0.2
7	0.05	0.05	0.05	0.1	0.1	0.1
8	0.05	0.1	0.1	0.1	0.2	0.2
9	0.05	0.05	0.05	0.05	0.1	0.1
10	0.15	0.15	0.15	0.2	0.2	0.2
11	0.1	0.1	0.1	0.1	0.3	0.3
12	0.1	0.1	0.1	0.15	0.2	0.2
13	0.1	0.1	0.1	0.1	0.1	0.2
14	0.1	0.1	0.1	0.15	0.3	0.4
15	0.1	0.15	0.15	0.2	1	1
16	0.15	0.15	0.2	0.2	0.4	0.5
17	0.05	0.1	0.1	0.1	0.2	0.2
18	0.1	0.15	0.15	0.2	0.2	0.2
19	0.1	0.1	0.1	0.15	0.5	0.5
20	0.1	0.15	0.15	0.2	0.4	0.5
21	0.1	0.1	0.1	0.2	0.5	0.5
22	0.05	0.1	0.1	0.1	0.2	0.2
23	0.05	0.1	0.1	0.1	0.2	0.2
Mean	0.10	0.12	0.12	0.14	0.29	0.32

Table A 38 Diameter of Rebar in Corrosion Accelerated Cask

No.	Diameter of Rebar #1 (mm)	Diameter of Rebar #2 (mm)
1	9.3726	9.779
2	9.2964	9.8298
3	9.3218	9.8044
4	9.2964	9.1186
5	9.4488	9.525
6	9.525	9.4996
7	9.4742	9.8298
8	9.4996	9.8298
9	9.2202	9.7536
10	9.144	9.652
11	9.0678	9.4996
12	9.525	9.4488
13	9.4996	9.7536
14	9.1948	9.7282
15	9.2964	9.7536
16	9.144	9.6774
17	9.3472	9.7028
18	9.3726	9.6266
19	9.398	9.5504
20	9.4996	9.779